Modeling of Diblock Copolymers in Selective Solvents

A DISSERTATION
SUBMITTED TO THE FACULTY OF THE GRADUATE SCHOOL
OF THE UNIVERSITY OF MINNESOTA
BY

Raghuram Thiagarajan

IN PARTIAL FULFILLMENT OF THE REQUIREMENTS
FOR THE DEGREE OF
DOCTOR OF PHILOSOPHY

David C. Morse, Adviser

June 2012

Acknowledgment

The research work in this thesis has been conducted under the guidance of my advisor, David Morse. His critical view on carrying out research and writing have improved me as a researcher and have contributed to this thesis significantly. Many of the ideas pursued in this thesis have been identified by him, and wherever "we" appears, it refers to both, David and me.

Along the way, all the research discussions with my colleagues in the Polymer Group has enriched me as a researcher. Especially the collaboration with Prof. Lodge and Dr. Mok, which was an enjoyable experience. I wish to thank all the group members: Jian, Adam, Jun, Drew, Pavani, Jens, Richard, Feng, Sangwoo and many more members for their support of my research and fascinating discussions.

My thesis research has been generously funded by the MRSEC program of the National Science Foundation. I also acknowledge the Minnesota Supercomputing Institute for providing me with computer time for my research.

I received tremendous support outside of school from my family and friends. My siblings, Kartik, Divya, and Tanu have been cheering me on from the sidelines. My friends: Venkat, Damien, Debmitra, Pranjal, Sujit, Srinivas, Ragavendra, Nikhil, Vinay, Nitin, Mohan, Jason, Kathy, Adam, Brad, Shyam, Akshanth, Vamsi, Vivek, Maddy, Swadesh, Jens, Pedro, Jagan, Arvind, Jorge, Srikanth, Kunal, Ray, Monica, Nicole, Anna, Andrea, Pradeep, Sahu, Sreeram, Anudha and many more have made my stay in the twin cities a memorable experience. I will be forever indebted to many of them for all their help and support in time of need.

To Amma and Appa

Abstract

Phase behavior and micellization kinetics of diblock copolymer surfactants in selective solvents influence many processes. We study the driving forces behind the self-assembly of a diblock copolymer AB, consisting of a solvent-philic block (B) and a solvent-phobic block (A), in selective solvents (S). We investigate this system using self-consistent field theory (SCFT), which is a coarse-grained, approximate theory with a proven track record for polymer mixtures. It discards the effects of fluctuations.

Micellar transformations between spherical, cylindrical, and bilayer curvatures are tracked in the dilute regime. We determine thermodynamic and structural properties of these isolated aggregates such as the critical micelle concentration (CMC), the critical micelle temperature (CMT), the solvent penetration of the core, and the core radius of micellar morphologies within the context of SCFT.

We also investigate the morphological variation from ordered phases, found in the concentrated regime, to isolated aggregates upon copolymer depletion. Depleting this blend of surfactant causes these stable structures to swell and ultimately unbind. The unbinding transition of the ordered phases is compared with the morphology transformations observed in the dilute regime. We also delineate two phase coexistence regions between ordered phases, and ordered phases and a solvent rich macrophase.

Furthermore, we quantify the effective interactions between the aggregates themselves. Intriguingly, for spherical micelles, the free energy of BCC, and FCC phases can be described in terms of a single effective pair potential that depends on micellar aggregation number, however, this aggregation number changes significantly with the concentration and temperature.

The kinetic barriers to association and dissociation of diblock copolymers in various selective solvents are calculated. We study the variation of these kinetic barriers for both block copolymers in small molecule solvents and block copolymers in a homopolymer matrix. The kinetic barriers are found to be very sensitive to temperature and surfactant concentration. They also become prohibitive except in a modest range of temperature near the CMT, or in sufficiently highly supersaturated or subsaturated solutions near the equilibrium CMC. The dependence of kinetic barriers upon

the chain lengths and solvent quality is also studied.

Contents

List of Figures

CHAPTER 1

Introduction

Surfactants, which are surface active agents, assemble in solvents to give structures in which a solvent-phobic (solvent hating) core is shielded by a solvent-philic (solvent loving) corona. This field has been widely studied by experiments, theory, and simulation techniques.[4–15] In this thesis I will focus on the case of nonionic diblock copolymer surfactants in a selective solvent. Here one of the two blocks of the diblock copolymer has a solvent-phobic character, and the other has a solvent-philic character.

A polymer is a large molecule made up of many small, chemical units, joined together covalently. Most synthetic polymers are repetitive sequence of a single repeat unit, and take the form (-A-A-A-). The basic unit of the sequence is called the

'structural unit' or 'monomer unit', and the number of units is called the degree of polymerization. A homopolymer consists of a single kind of repeat unit. Block copolymers are made by joining homopolymers of two or more different types. The diblock copolymer AB is two homopolymers joined together by a covalent bond, where each homopolymer A and B represents a block.

Diblock copolymers in a selective solvent form isolated aggregates in the dilute limit, and periodic phases in the concentrated limit. These morphological variations were presented in a general review of the binary system of diblock copolymer AB in a selective solvent S by Sadron and Gallot in 1973.[4] Initial experimental work concentrated on selective solvents rather than neutral ones. According to Shibayama *et al.* [16] this may be partially because the scattering contrast between two coexisting microphases is considerably smaller in neutral solvents than in selective ones. The experimental techniques used to detect different periodic phases were small angle x-ray scattering (SAXS) and electron micrography.

Sadron and Gallot[4] split the isothermal phase diagram of a diblock copolymer AB in a solvent S into three regions of interest as shown in Figure 1.1. The convention used from here on is that block A represents the solvent-phobic block and block B represents the solvent-philic block in the diblock copolymer AB. The first region consists of a solution of diblock copolymers dissolved completely in solvent S. The second region consists of aggregates forming micelles or aggregates with multiple diblock copolymers, and the third region contains periodic structures. In region 3, depending on the block composition of diblock copolymer AB and concentration of diblock copolymer AB in selective solvent S any one of the phases: S_A^{FCC}(face-centered

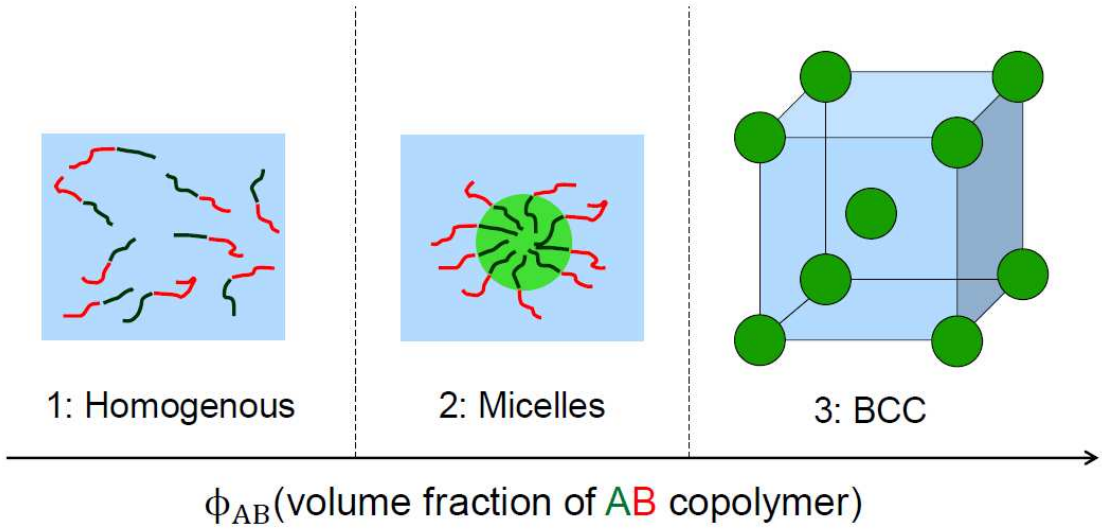

Figure 1.1: Various morphologies found in a binary system of a diblock copolymer AB in a selective solvent S.

cubic), S_A^{BCC}(body-centered cubic), H_A(hexagonal), G_A(gyroid), L (lamellar), G_B, H_B, and S_B^{BCC}, are observed.[3] Here the subscript denotes the monomer type of the core for a particular phase. Sadron and Gallot concluded that the type of structure of a given AB copolymer in a given solvent S is determined mainly by the ratio of the volumes of the phase containing the insoluble sequence and the volume of the phase including the solvent and the solvent-philic block, a fact which can be considered a generalization of the law described in an earlier review by Molau.[17]

Polymers of different types are generally immiscible. Thus, in a melt of diblock copolymer AB, the A blocks tend to cluster together as well as the B blocks, which leads to the formation of a domain structure. The appearance of these domains is called microphase separation. Illustrations of six diblock copolymer microstructures are presented in Figure 1.2. The phase behavior of undiluted diblock copolymers is

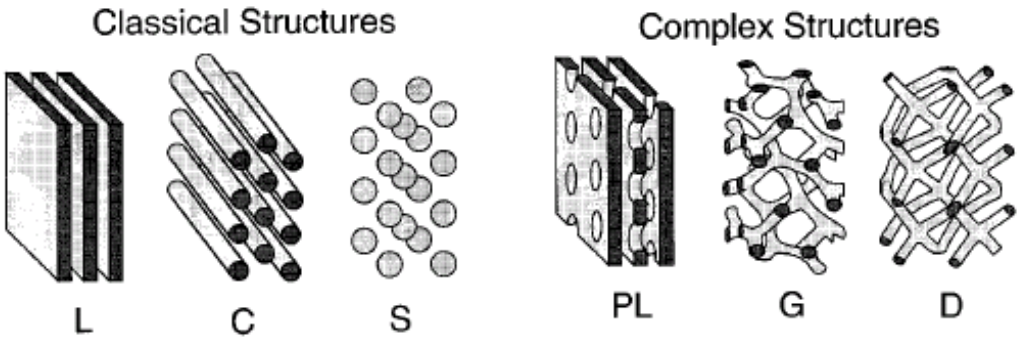

Figure 1.2: Various morphologies found in a AB diblock copolymer melt.

determined by three experimentally controllable factors: the overall degree of polymerization N, the composition f_{B} (overall volume fraction of the B block), and the Flory-Huggins interaction parameter χ_{AB}.[18] The first two factors are regulated through synthesis, whereas the magnitude of χ_{AB} is determined by the choice of the A and B monomer pair.

Small enough values of χ_{AB} and N lead to entropic factors dominating the free energy density and large enough values of the two parameters leads to enthalpic factors dominating it. The entropic and enthalpic contributions to the free energy scale as N^{-1} and χ_{AB}, respectively. Hence, the product $\chi_{\mathrm{AB}}\, N$ dictates the state of block copolymer phase behavior.

Self-consistent field theory (SCFT) is a technique used to study the morphological variations in the binary system of AB/S. The first SCFT model was developed by Helfand and Tagami[19] to study the interface between two homopolymers. SCFT approximates many chain system as a single chain system in a self consistently deter-

mined chemical potential field. The field approximates the interaction between the chains. Helfand and Wasserman used a narrow interface approximation[20] to study lamellar[20] and spherical microdomains[21] in block copolymer melts, but limited the theory to the strong segregation regime ($\chi_{AB}N >> 10$). Leibler[22] studied the opposite extreme which is the weak segregation regime ($\chi_{AB}\,N << 10$) in diblock copolymer melts. He used the random phase approximation (RPA), outlined by de Gennes,[23] to find the limit of stability of an ordered phase. For a symmetric diblock copolymer the order-disorder transition (ODT) was predicted to occur at $\chi_{AB}\,N \approx 10.5$.

1.1 Summary

A summary of literature for phase behavior in the dilute regime as well as in the concentration regime for a diblock copolymer in a solvent is provided in Chapter 2. The description of two formulations of SCFT used in this study, introduction to micelle thermodynamics, and the unbinding transition is provided in Chapter 3. Predictive nature of SCFT aids us to systematically cover the parameter space over ϕ_{AB} , f_B , χ_{AS} , χ_{BS} and χ_{AB} . We study the micellar aggregates bilayers, cylindrical micelles, and spherical micelles in the dilute regime in Chapter 4. A detailed analysis of the phase behavior of AB/S is presented in Chapter 5. Kinetics plays a crucial role in AB/S system when the degree of segregation in the system is large or the components AB and S are polymeric in nature. This leads to large timescales required for equilibration. A SCFT study of micellization kinetics will be discussed later in Chapter 6.

CHAPTER 2

Literature Review

In this chapter, a background of previous research work of self-assembly in the dilute limit for AB in S is presented and a review of previous research work for the concentrated limit of this binary system is also presented. An overview of previous research work using theoretical techniques is presented before presenting an overview of research work utilizing experimental techniques. A separate section is dedicated to the transition between FCC and BCC periodic structures of diblock copolymers in selective solvents. The background of previous research work concludes on the topic of micellization kinetics for AB in small molecule solvent S.

2.1 Isolated Aggregates: Theory

The addition of small amounts of diblock copolymer into a solution consisting of a small molecule selective solvent induces self-assembly in the form of several different morphologies.[24,25] The diblock copolymer AB consisting of a solvent-phobic block A and a solvent-philic block B is observed to self assemble into morphologies in which the selective solvent partitions itself preferentially into the solvent-philic domains. The solvent-phobic block segregates into a solvent poor core to reduce contact with solvent. The driving force behind the formation of these morphologies is in general described in terms of the interplay between three contributions to the free energy: core chain stretching, inter chain corona repulsion, and the core/corona interfacial tension. In general three different morphologies have been observed to form in dilute solutions: bilayers (B), cylinders (C), and spheres (S). One can influence the transition between these morphologies by varying the block composition,[26] solvent selectivity,[27] and length of the copolymer.[26] Other properties of this binary system AB/S which were determined through theoretical predictions are the critical micelle concentration, and concentration profiles.

2.1.1 Polymeric Solvent: AB in B

In the dilute limit the diblock copolymer AB in a homopolymer matrix of B is found to aggregate in the form of bilayers (B), cylindrical micelles (C), and spherical micelles (S). The study of AB in B has influenced the study of diblock copolymers in a small molecule selective solvent.[28–36] For the binary system of diblock copolymer AB/homopolymer B Leibler *et al.* [28] presented an analytic theory for spherical

micelles. The free energy F of a single spherical micelle is expressed as a sum of four individual contributions: core/corona interfacial tension γ, non-uniform stretching of the core chain, stretching of the corona chain, and entropy of mixing of the homopolymer and the corona chain. It is expressed as:

$$F = 4\pi R_{\text{core}}^2 \gamma + F_{\text{core}} + F_{\text{corona}} + F_{\text{mix}}. \tag{2.1.1}$$

Only one block composition with AB diblock copolymer being symmetric was considered and incompressibility was imposed, which yielded simple relations for the radius of the core block R_{core} and the radius of the corona block R_{corona} as a function of the aggregation number M. Leibler *et al.* [28] assumed no penetration of the corona or the core of the spherical micelle by the homopolymer, and did not take into account loss of entropy with the diblock copolymers being localized at the interface of a spherical micelle. The authors utilized the model to determine the critical micelle concentration for spherical micelles.

Initial studies were restricted to the study of critical micelle concentration (CMC) and concentration profiles of spherical micelles. The CMC is the concentration above which the formation of aggregates occurs at a certain temperature. Future scaling theories after Leibler *et al.* [28] expressed the free energy of a spherical micelle as some similar formulation of the contributions described above.[29,31,36–39] The simplest of them was derived by Leibler[37] for the case of a dry brush, where the homopolymer is long enough $N_{\text{h}}^{3/2} > N_{\text{corona}}$ such that it does not penetrate the corona. This leads to $F_{\text{mix}} = 0$ in Equation (2.1.1), where N_{h} is the degree of polymerization of the homopolymer B. The interfacial tension γ was taken to be the value derived by

Helfand and Tagami[40] as $\gamma = (\mathrm{k}T/b^2)(\chi_{\mathrm{AB}}/6)^{1/2}$ expressed in terms monomer length b and Flory-Huggins interaction parameter between monomers A and B χ_{AB}. The Helfand and Tagami[40] expression for γ was calculated for a flat interface in the limit of infinitely long chains of two immiscible homopolymers. The contribution from the core of a spherical micelle F_{core} with the numerical pre-factor is determined by Semenov[41] using a strong stretching limit and is given by

$$\frac{1}{\mathrm{k}T}F_{\mathrm{core}} = (3/4)^{5/3}(\pi^{4/3}/20)M^{5/3}N_{\mathrm{core}}^{-1/3}. \tag{2.1.2}$$

The contribution from elastic corona stretching is estimated by determining the stretching trajectory[37,41,42] which yields

$$\frac{1}{\mathrm{k}T}F_{\mathrm{corona}} \sim \frac{M}{b^2}\int_R^{R_{\mathrm{core}}} dr\frac{dr(n)}{dn}. \tag{2.1.3}$$

The incompressibility condition $(4\pi/3)(R^3 - R_{\mathrm{core}}^3) = MN_{\mathrm{corona}}b^3$ imposed on the system yields the value of $dr(n)/dn$ with n being the index of corona monomer, where R is the radius of the micelle including the core and corona, and R_{core} represents the radius of the core of a spherical micelle. Finally, one arrives at the expression for F_{corona} as

$$\frac{1}{\mathrm{k}T}F_{\mathrm{corona}} = \frac{1}{2}\left(\frac{3}{4\pi}\right)^{2/3} M^{5/3}N_{\mathrm{core}}^{-1/3}(f_{\mathrm{core}}^{-1/3} - 1). \tag{2.1.4}$$

Micelle formation is preferred when the grand canonical free energy of a micelle $\Phi = F - \mu M$ is negative, for a given chemical potential μ. The critical micelle concentration is determined as the concentration at which $\Phi = F - \mu M = 0$. The equilibrium aggregation number of the spherical micelle is obtained by minimizing

the grand canonical free energy Φ relative to the aggregation number M given by $\partial(F/M)/\partial M = 0$. This yields the chemical potential at CMC to be

$$\mu_{\mathrm{CMC}} \sim (\chi_{\mathrm{AB}}\, N)^{1/3} f_{\mathrm{core}}^{4/9} (\alpha f_{\mathrm{core}}^{-1/3} - 1), \tag{2.1.5}$$

where $\alpha \approx 1.74$. The CMC is then given by

$$\phi^{\mathrm{CMC}} \sim \exp(\mu_{\mathrm{CMC}} - \chi_{\mathrm{AB}}\, N_{\mathrm{core}}). \tag{2.1.6}$$

This simple analytical model of Leibler[37] implemented for diblock copolymer AB in homopolymer B for the dry brush condition can not be extended to the case of a small molecule selective solvent. The reasons being: 1. The model does not account for solvent penetration in the core of a spherical micelle, 2. The case of a dry brush does not hold for the corona block as the cost of mixing goes down with the size of the solvent, 3. the Helfand and Tagami expression for γ is no longer valid for this case, and 4. the expression for the free energy of the core needs to take into account the presence of solvent.

Whitmore and Noolandi[29] extended the study performed by Leibler *et al.* [28] by adding an extra term to the free energy due to localizing diblock copolymers to the interface of a spherical micelle, and taking into consideration homopolymer penetrating the core. The authors looked at asymmetric block compositions of the diblock copolymer as well. Whitmore and Noolandi compared the theoretical predictions to experimental observations for the radius of the core R_{core} dependence on the degree of polymerization of the core block N_{core} and the degree of polymerization of

the corona block N_{corona}. The experimental observations are obtained for the PS-PB system studied using small angle neutron scattering (SANS) by Selb *et al.* .[43] Whitmore and Noolandi arrived at $-0.10 \leq \mu \leq -0.07$ and $0.68 \leq \nu \leq 0.70$ for the relation $R_{\text{core}} \sim N_{\text{corona}}^{\mu} N_{\text{core}}^{\nu}$, whereas the experimental study arrived at values of $-0.19 \leq \mu \leq -0.14$ and $0.75 \leq \nu \leq 0.81$. The CMC of the system is derived using the analytical model and is found to scale as $\sim \exp(-\chi_{\text{AB}}\, N_{\text{core}})$ as predicted by Leibler *et al.* [28] as well.

Mayes and Olvera de la Cruz[31] extended the study performed by Leibler *et al.* [28] in order to estimate the transition line between isolated cylindrical (C) and spherical (S) micellar aggregates. They incorporated the free energy contribution due to localization of joints of block copolymer at the interface of the spherical or cylindrical micelle from the previous model. In order to apply Gaussian statistics in the blend they restricted the parameter space they looked at to $N/N_{\text{h}} < N^{1/2}$.[23] This increases the energy of mixing between the corona and the homopolymer and thus, ensuring the corona is surrounded by itself more. The individual analytical contributions to the free energy were calculated for both curvatures C, and S. The CMC is then determined by minimizing the free energy of the system relative aggregation number M, and the fraction of copolymers in the spherical and cylindrical micelles. They determined the CMCs for both aggregate structures and found C to be preferred for lower block compositions of the corona block, and lower values of N/N_{h}. The authors noticed a transition from C to S when the corona block's propensity to stretch increases. The propensity to stretch increases as one starts reducing the block length of the homopolymer and in effect start reducing the cost of entropy due to mixing

of the corona block with the homopolymer solvent. The core block is found to be in a more relaxed state for the cylindrical micelles relative to the spherical micelles simulated using this model due to the additional degree of freedom present in the case of a cylindrical micelle. However, the authors themselves note due to neglecting the effect of free energy contribution of ends of the cylinder the transition between C and S is not exactly determined.

2.1.2 Small Molecule Solvent: AB in S

The most important difference between a polymeric solvent B and small molecule solvent S is the propensity of the solvent S to penetrate the core of an aggregate structure due to it's smaller size. The analytic theory of Noolandi and Hong[30] was used to describe a binary system of diblock copolymer and small molecule solvent which takes into account solvent penetration of the core. It was developed independently around the same time as the analytical model by Leibler *et al.* .[28] Noolandi and Hong split a spherical micelle into three different regions: core, corona, and pure solvent region. The concentrations are assumed to be uniform in all the regions, except at the interface of the spherical micelle where a a linear density profile across the interface of core and corona blocks is assumed. This assumption was used to obtain a reasonably accurate approximation for interfacial tension γ. The interfacial tension in the case of an interface between a polymer and solvent is developed separately[44] and is derived for the case of AB in a small molecule selective solvent S. The authors did not determine the CMC, and rather concentrated on estimating the radius of the core of the spherical micelles. The free energy of the micelle is then expressed relative to the corresponding

free energy of the homogeneous random state. It is split into terms involving polymer interaction energy (which excludes the interfacial tension part), combinatorial entropy of solvent molecules, decrease in entropy of chains due to localization, decrease in entropy due to either stretching or compression of the diblock copolymer, and from the interfacial tension. The model predictions are compared with experimental observations made for the polystyrene(PS)-polybutadiene(PB)/*n*-heptane system using SAXS by Plestil and Baldrian.[45] The interaction parameters used to compare both of them are $\chi_{\text{PS-PB}} = -0.169 + 123/T \approx 0.24$ and $\chi_{\text{PS-Heptane}} = -1.12 + 901/T \approx 2$. $\chi_{\text{PB-Heptane}}$ was obtained by fitting the experimental data to give $\chi_{\text{PB-Heptane}} = 0.53$. The model correctly predicted changes in the radius of gyration, the degree of swelling of the two blocks, and the aggregation number of the micelles. However, it is important to note that the temperatures considered here range from 18 °C to 50 °C, which is a small jump in order to notice any variation in the parameters mentioned earlier. The radius of the core block is found to vary as $\sim N_{\text{core}}^{\frac{2}{3}}$ which concurs with scaling arguments presented by de Gennes.[23]

Munch and Gast[38] investigated the transition between bilayers and spherical aggregates by implementing the analytic theory proposed by Leibler *et al.* [28] to selective solvents. They assumed an athermal solvent for the solvent-philic block B i.e., $\chi_{\text{BS}} = 0$. These authors did not consider the cost of interaction between the blocks A and B. The interfacial tension expression developed by Helfand and Tagami[40] is used, with the interaction parameter in the expression taken as the interaction parameter between the solvent-phobic block A and small molecule solvent S χ_{AS} to yield $\gamma = (\text{k}T\,/b^2)(\chi_{\text{AS}}/6)^{1/2}$. Even though the expression derived by Helfand and Tagami

was derived for two infinitely long immiscible homopolymers. The theory was used to study the variation of CMC relative to the ratio of the size of the polymer and solvent size N/N_S with $20 \leq N/N_S \leq 50$ being the considered range. The authors predict the transition line between bilayer aggregates and spherical micelles using this model. However, a trend observed by the authors where the aggregation number is found to increase with a corresponding decrease in the solvent incompatibility of the core is incorrect. Upon approaching the critical micelle temperature or reducing the solvent selectivity the aggregation number is found to go down, and the solvent penetration of the core is found to go up. The solvent is found to occupy almost half of the volume of the core of a spherical micelle, through our SCFT calculations in chapter 4 as well as by experiments in different systems.[46–53] The authors neglected the presence of solvent in the core of the spherical micelle, which is a good approximation for a polymeric solvent made by Leibler *et al.* .[28] Their treatment of smaller size of the solvent in this aspect and the extension from Leibler *et al.* ,[28] which studied polymeric constituents, is applied incorrectly.

Nagarajan and Ganesh[54] developed an analytic theory for micellization of spherical micelles followed by the work of Leibler *et al.* ,[28] and Noolandi and Hong[30] for a diblock copolymer AB in a selective solvent S. The major distinction of this work is that they described micellization in terms of solvent-philic corona block as well. The approach used by Nagarajan and Ganesh[54] is motivated by the field of small molecule surfactants. The free energy for this model is described in terms of three major terms: the reference state, entropy of mixing of the multiple component system, and the interaction energy which is expressed in terms of a Flory-Huggins

interaction parameter. The last two terms in the free energy model are derived from Flory-Huggins theory. The free energy is then minimized for a given total concentration of a diblock copolymer in the binary system AB/S. The authors do not take into account solvent penetration of the core, and the interfacial tension is derived from the Helfand and Tagami[40] expression. The Helfand and Tagami expression is applicable for a flat interface for a system of two infinitely long homopolymers. The authors developed scaling relations for radius of the core, thickness of the corona shell, and aggregation number of the spherical micelle in terms of N_{core} and N_{corona} using this model.

2.1.3 Scaling Theory of Isolated Aggregates

All the studies described above assumed Gaussian statistics for the corona block. This does not hold true for a sufficiently long corona blocks surrounded by a good small molecule solvent. Incorporating a blob model,[23] other theoretical studies[42,55–57] paid closer attention to this characteristic in the binary system of AB/S. Daoud and Cotton[42] described the conformation of the corona block as well as it's concentration dependence of a star copolymer using a blob model.[23] The blob model involves the size of the correlation blob $\xi(c)$ being dependent on the concentration of corona monomers c. Depending on the solvent quality ν ($\nu = 3/5$ for a good solvent and $\nu = 1/2$ for a Θ solvent) the blob size is found to vary as $\xi \sim c^{-\nu/(3\nu-1)}$. Scaling analysis for the star copolymer[42] was performed where spherical symmetry is assumed for the blobs of corona blocks. For a corona block tethered to spherical micelle it's concentration goes down with increasing distance from the center of the micelle r. Locally, at a

distance r the chain behavior is assumed to be that of a single chain within $\xi(r)$. The blob size $\xi(r)$ is found to increase with r as the concentration of the corona block goes down with increasing r. The blob size can be expressed as a function of r and the swelling parameter $\alpha(r)$ is calculated, where the corona block explores a space for a blob at a distance r with blob size $\xi(r)$: $\alpha(r) = \xi(r)/N^{(1/2)}b$. Daoud and Cotton described three distinct regions for an isolated spherical micelle of a star copolymer: 1. a core region with a constant density, 2. a region where Gaussian statistics are satisfied due to high enough concentration, and 3. a region where excluded volume effects are prominent inside a blob. In order to study the semi-dilute solution or the concentration above which spherical micelles of a star copolymer interact with each other, the authors delineated two regimes based on a certain distance l from the center of the micelle. For $r < l$ it behaves like an isolated micelle, whereas for $r > l$ the behavior is found to be similar to that of linear chains where the size of the blobs are independent of the number of branches of the star copolymer and dependent on the local concentration.

Halperin[55] developed a scaling theory to study the radius of a spherical micelle with long corona blocks i.e., $N_{\text{corona}} >> N_{\text{core}}$. The author used the observation that the spherical micelle should be structurally similar to colloidal particles coated by grafted chains. The Daoud and Cotton[42] treatment of micellar coronas in star copolymers is used to study the structure of the spherical micelle. Instead of assuming a constant concentration profile for the corona, as done by previous theoretical studies, it is assumed to be a decreasing function of radial distance from the center of a spherical micelle. The radii of the spherical micelle were found to scale as $R_{\text{core}} \sim$

$N_{\text{core}}^{\frac{3}{5}}b$, and $R_{\text{micelle}} \sim N_{\text{core}}^{\frac{4}{15}}N_{\text{corona}}^{\frac{3}{5}}b$. For the case of a crew-cut micelle (shorter corona block, $N_{\text{core}} >> N_{\text{corona}}$), Halperin arrived at the relation $R_{\text{core}} \sim N_{\text{core}}^{\frac{2}{3}}b$.

Birshtein and Zhulina[56] have studied the binary system of diblock copolymers in dilute solutions tethered to a flat, cylindrical, or a spherical interface using scaling analysis. They took into consideration the free energy of the system as mentioned earlier in Equation (2.1.1). The incorporation of correlation of polymer densities of the corona into the scaling laws of corona chains tethered to the three types of interfaces is a unique aspect of their study. The difference from the approach used by Leibler *et al.* [28] is that the free energy of the corona F_{corona} incorporates a corona profile derived from the blob model.[23,42] Zhulina *et al.* [57] extended this study and looked at morphological transitions from bilayers $\rightarrow$ cylinders $\rightarrow$ spheres with exact numerical coefficients for their earlier scaling predictions.[56] In general, analytical expressions for the aggregation number M, radius of the core R_{core}, and thickness of the corona shell L_{corona} are derived as well as the free energy of each of the three competing morphologies. The authors notice the crossover between these three morphologies going from B $\rightarrow$ C $\rightarrow$ S with increasing N_{corona} occurs when $L_{\text{corona}}/R_{\text{core}} \sim 1$ in the equilibrium morphology. Upon increasing the block length of the corona block they notice a shift to the spherical morphology because of the increasing propensity of the corona chains to stretch away from each other.

Two numerical prefactors are introduced which take into consideration excluded volume effect in a good solvent and three body interactions in a Θ solvent for the theory proposed by Zhulina *et al.* .[57] These two numerical prefactors, which are dependent on the corona monomer and solvent type, are obtained by fitting experimental

data through their corresponding theoretical predictions. The sizes of the core and corona determined experimentally are used to determine the numerical prefactors involved in F_{corona}.[57–59] Jensen *et al.* ,[59] who studied a PEP-PEO mixture of water/ethanol, emphasized the importance of varying more than one system parameter in experiments in order to obtain a consistent set of numerical prefactors involved in F_{corona}. They arrived at different numerical prefactors for different mixtures of water/ethanol in order to obtain a better fit for the corona profiles and used the same numerical prefactors for a particular mixture of water/ethanol irrespective of different morphologies, C and S, the authors observed. To contrast with the study conducted by Lund *et al.* [58] where the authors used different numerical factors for cylindrical and spherical micelles. The numerical factors should be independent of morphology and the approach followed by Jensen *et al.* seems correct in order to compare the experimental results with the theoretical predictions. The main drawback of the theory is the exact estimation of the numerical factors involved in the free energy of the corona F_{corona}.

The SCFT method implemented by us does not take into account the correlations of the corona block for semi-dilute solutions, which the blob model is used to describe using a scaling argument. However, when you consider the expansion factor α where

$$\alpha = \frac{R_{\text{g}}}{R_{\text{g,0}}}. \tag{2.1.7}$$

Here R_{g} represents the radius of gyration and $R_{\text{g,0}}$ represents the unperturbed dimensions with $R_{\text{g,0}} \sim N^{1/2}b$ or $\nu = 1/2$ for the Θ solvent. In the case of scaling theory the exponent ν is taken as either $\nu = 1/2$ for a Θ solvent or $\nu = 3/5$ for a good solvent.

The good solvent regime is achieved in the limit of $\alpha >> 1$ and the Gaussian limit is true for $\alpha = 1$. Using a simple scaling argument[60] by considering the osmotic drive to swell and entropic drive to coil up we can express α as

$$f(\alpha) \propto \frac{b^3}{v} B(T) N^{\frac{1}{2}}, \tag{2.1.8}$$

where $B(T) = (1/2 - \chi)$. The case considered in this study corresponds to the degree of polymerization of the diblock copolymer being = 100. In this case the corona block degree of polymerization < 100. For the case of a Θ solvent $B(T) = 0$, in which case SCFT is appropriate. For the case of the good solvent considered here $\chi = 0.4$ $B(T) = 0.1$, $N = 100$ which yields $B(T)N^{1/2} \approx 1$, where N represents the degree of polymerization of the corona block. The exponent $\nu = 3/5$ is achieved either when N is large or $(1/2 - \chi)$ is large. Hence, we expect the exponent ν to be somewhere in between the range of $1/2 \leq \nu \leq 3/5$ and maybe ν being closer to $1/2$ because of the smaller degree of polymerization considered with $B(T) = 0.1$. Whereas, scaling theory exponent ν can take only two values, either $\nu = 1/2$ or $\nu = 3/5$. SCFT has an added advantage due to its predictive nature using which we can explore the parameter space for the AB/S system very systematically. Even though there are drawbacks to SCFT we expect most of the results to be at least qualitatively correct.

2.1.4 SCFT Studies of Isolated Aggregates

Scheutjens and Leermakers studied the formation of spherical micelles of block copolymers in aqueous solutions in a series of articles[61–64] They extended the lattice for-

mulation of SCFT developed by Scheutjens and Fleer[65] by incorporating a rotational isomeric state scheme for linear as well as branched copolymers.[61] This extended theory was used to capture systems having a lower critical solution temperature. A pure lattice formulation of SCFT[65] could not have captured this behavior. Micelle formation was studied using a thermodynamic description[62] which involved a translationally restricted excess free energy. This excess free energy is used to determine the critical micelle volume fraction. First, they looked at small molecule surfactant systems of the form $A_{12}B_3$.[63] The interaction parameters used to determine the critical micelle volume fraction are derived from solubility data and known CMC values. The following set was used in the article: $\chi_{\mathrm{AS}} = 1.6$, $\chi_{\mathrm{BS}} = -0.5$, and $\chi_{\mathrm{AB}} = 1.5$, where S represents a small molecule solvent. Stability domains for the formation of micelles are also delineated from the excess free energy of micelle formation which was plotted *vs.* the aggregation number. The domains are split into three regions: micelles, an unstable region, and vesicles.[32,62] Utilizing the same model, Leermakers *et al.* [64] studied the variation in the corona profile by varying the interaction of the solvent and corona block from $\chi_{\mathrm{BS}} = 0$ to $\chi_{\mathrm{BS}} = 0.5$ with $\chi_{\mathrm{AB}} = 0.5$ and $\chi_{\mathrm{AS}} = 2.0$, as well as calculated the critical micelle volume fractions for all the parameters considered. The maximum pile up of the corona monomer volume fraction at the interface the authors notice is of the order of ~ 0.3, which is low for a selective solvent with $\chi_{\mathrm{AS}} = 2.0$.

This model is used to study the interplay between cylindrical and spherical aggregate structures in the dilute limit by Linse[66] for pluronic ($\mathrm{EO}_n\mathrm{PO}_m\mathrm{EO}_n$) copolymers in aqueous solutions. For pluronics in aqueous solutions micelles are found to form upon increasing temperature as water becomes a poor solvent for PPO. This effect

of temperature on the interaction parameters as well as concentration dependence of the interaction parameters were taken into account in this model. Linse noticed the transformation from isolated spherical micelles to isolated cylindrical micelles leads to $\sim 10\%$ reduction for the PEO corona block,[66] which agrees with theoretical and experimental observations where corona stretching leads to preference towards isolated spherical micelles over isolated cylindrical micelles. In a separate study Linse[67] determined CMCs, aggregation number, and concentration profiles for spherical micelles formed by pluronics in aqueous solutions. The CMCs calculated theoretically were found to be at least an order of magnitude higher than the CMCs estimated using surface tension measurements by Linse and Malmsten.[68]

Patricia *et al.* [32] implemented the lattice formulation of SCFT developed by Scheutjens and Fleer[65] to study the partition coefficient of naphthalene dependence on the block length of PPO for pluronic ($EO_nPO_mEO_n$) and tetronic block copolymers and compared them with experimental observations. Naphthalene is an organic compound and has very low solubility in water and hence partitions itself preferentially into PPO domains. The CMC of linear pluronic polymers was found to be lower than that of tetronic polymers having the same overall molecular weight and composition.[32] Patricia *et al.* [69] calculated the critical micelle volume fractions as well as the enthalpy of mixing ΔH_{m} and ΔS_{m} for $EO_{30}PO_{61}EO_{30}$ in aqueous solutions. However, the studies carried out by Patricia *et al.* [32,69] only looked at spherical micelles and did not look at other isolated aggregates such as bilayers and cylinders.

Greenall *et al.* [36,39] studied the micelle formation for the binary system of a diblock copolymer AB in homopolymer B using continuum formulation of SCFT and com-

pared with experimental results of Kinning *et al.* [70] carried out for poly(styrene)(PS)-poly(butadiene)PB in PS. In the first article[39] the authors studied micelle formation and compared it with experimental data as well as analytic theory proposed by Leibler *et al.* .[28] They found that SCFT overestimates the radius by 20-30%, whereas for the CMC, the agreement worsens as the core block increases in length. The authors speculated that this could be due to kinetic effects in the system. Three data points of CMC obtained using experimental techniques were used to compare with SCFT calculations. In their second article Greenall *et al.* [36] investigated the transitions between B, C and S in the same system. The reason for the transition from a spherical to a cylinder to a bilayer structure is given as the swelling of the corona block which is offset by increase in the core radius. This was noted by studying the concentration profiles of the spherical curvature. Their SCFT calculations also predict that the CMC increases when the homopolymer weight increases. This increases the cost of mixing for the corona and the solvent thereby reducing the stretching of the corona block. Reduction in stretching in the corona block leads to the transformation from a spherical micelle to a cylindrical micelle and finally to a bilayer.[36]

Zhou and Shi[71] implemented SCFT for AB in B in the grand canonical ensemble to study the transitions between B, C, and S as well as study the micellar dimensions R_{core} and R_{corona} of different micellar structures. Zhou and Shi[71] noticed a transition from B $\rightarrow$ C $\rightarrow$ S upon increasing the length of the corona block as noted previously by other studies.

SCFT is also used to study the micellization behavior of diblock copolymers in small molecule selective solvents by Yuan *et al.* .[72] The enthalpy change and Gibbs

free energy change upon micellization compare favorably with previous experimental studies for the PS-PI in n-hexadecane system.

2.2 Periodic Phases: Theory and Simulations

In the concentrated limit of diblock copolymer AB in a selective solvent S periodic phases are observed.[3,4] The phase behavior of an AB diblock copolymer melt is, to a good approximation, determined by the product $\chi_{AB}\,N$, and the composition of the molecule f_B , where N is the degree of polymerization of the diblock copolymer and f_B is the volume fraction of the B block.[73] The addition of a selective solvent adds more dimensions to the phase portrait which can be characterized by the volume fraction of the solvent ϕ_S or $1-\phi_{AB}$, as well as the interaction parameters χ_{AS} and χ_{BS} . The selective solvent partitions itself preferentially into one microdomain which leads to a shift in the phase boundaries relative to the diblock copolymer melt phase diagram.

Firstly, the case of neutral solvent diluting an interface between two immiscible homopolymers was first studied theoretically using the dilution approximation by Helfand and Tagami.[19] The approximation involved an interaction parameter called χ_{eff}, which takes into consideration the screening due to the neutral solvent species at the interface. Neutral solvent is characterized by the condition $\chi_{AS} \approx \chi_{BS}$. For a neutral solvent it was suggested that for a given volume fraction of the copolymer ϕ_{AB} behaves equivalently to a neat diblock copolymer melt with χ_{AB} replaced by χ_{eff}, where

$$\chi_{eff} = \phi_{AB}\,\chi_{AB}\,. \tag{2.2.1}$$

Fredrickson and Leibler[74] studied the dilution approximation of a non-selective, good solvent added to a diblock copolymer melt. Two regimes, the weak segregation limit and the semi-dilute regime are analyzed. Concentrated mixtures were modeled using the standard fluctuation-corrected theory of Fredrickson and Helfand,[75] and semi-dilute mixtures were treated by supplementing this with the blob model.[23] According to their model, two phase coexistence regions will be too small to have any experimental significance, and the location of the order-disorder transition (ODT) will follow the dilution approximation in the concentrated regime but not in the semi-dilute regime.

Olvera de la Cruz[76] and Fredrickson and Leibler[74] predicted ODT to scale as $(\phi_{\rm AB}^{1.59}\chi_{\rm AB}N)_{\rm ODT} = F(f_{\rm B})$ in the semi-dilute regime, and $(\phi_{\rm AB}\chi_{\rm AB}N)_{\rm ODT} = F(f_{\rm B})$ for concentrated solutions in the limit $\phi_{\rm AB} \rightarrow 1$, where N is the degree of polymerization of the diblock copolymer and $F(0.5) \approx 21$, and is a weak function of $f_{\rm B}$ in the range $0.4 \leq f_{\rm B} \leq 0.6$.[22]

Whitmore *et al.* [77,78] used SCFT to examine concentrated solutions in the strong segregation regime with a good neutral solvent. They found that the dilution approximation was valid for such cases, and that in particular follow the predicted dependence of the order-order transitions (OOTs) on $\phi_{\rm AB}$, consistent with experimental results.[2,79] The limitations of the dilution approximation were further studied by Naughton and Matsen[80] using SCFT. They concluded that the dilution approximation requires the solvent quality to be good to prevent macrophase separation of the solvent from the copolymer. They also observed stronger segregation regime between the two polymers leads to stronger inhomogeneities in the solvent composition,

which leads to failure of the dilution approximation.

Hong and Noolandi[44,81,82] published a series of articles on phase equilibria of binary systems containing homopolymers/small molecule solvents, block copolymers/small molecule solvents, and block copolymers/homopolymers. They showed the existence of eutectic points, similar to those studied in metallurgy, in the calculated phase diagrams. Their first article[44] concentrated on the homopolymer/small molecule solvent system, which was extended to study diblock copolymer/small molecule solvent system. SCFT is represented in the form of a functional integral and the free energy is minimized by the saddle function method for an incompressible system with a fixed number of species of each component in the system. Binodals, concentration profiles, and interfacial tension are determined for the homopolymer/small molecule solvent system. In their second[81] and third articles[82] the authors implemented the theory developed earlier to the weak segregation limit for block copolymer/neutral small molecule solvent and block copolymer/homopolymer binary systems. They generated phase diagrams consisting of solvent rich homogeneous phase, polymer rich homogeneous phase, and periodic lamellar phase.

Matsen,[33] and Janert *et al.* [34,35] calculated phase diagrams of block copolymer and homopolymer mixtures using SCFT. They found that homopolymers with comparable length to the diblock copolymer swelled the microstructure to a large extent while addition of very short homopolymers induced disordered solution, attributed to a higher mixing entropy for these shorter homopolymers. An unbinding transition for homopolymer lengths comparable to the diblock copolymer is shown in the phase diagrams[33–35] where the spacing of the interface between microdomains diverges to

infinity.

The phase behavior of pluronic block copolymers in aqueous solutions are determined separately using a continuum model and a lattice model[65] of SCFT by Noolandi *et al.* .[83] Water becomes increasingly a poor solvent for PEO and PPO as one increases the temperature, which is taken into account in both formulations of SCFT.[83] The phase diagrams are found to be similar for both models except that the lattice formulation does not work well for small chains which are found to aggregate into micellar structures by experiments and the continuum model.[83,84] The agreement with experiments[85] is qualitatively good, but two phase regions found in experiments between periodic phases is not present for the theoretical phase portraits. Svensson *et al.* [86,87] studied the binary system of pluronics/water[86] and ternary system of pluronics/water/oil[87] using the lattice model described by Noolandi *et al.* .[83] Two block compositions are considered, one with a majority of EO and another with a minority of EO, in order to obtain the whole range of periodic phases in the phase portraits for the binary system where experimental observations are compared with theoretical predictions.[86] For both systems the authors found that at low concentration block copolymers form micelles consisting of a core dominated by the hydrophobic PPO surrounded by a water swollen PEO-rich corona. Whereas, at high polymer concentration lyotropic liquid crystalline phases are found, which are in the weakly segregated regime.[86,87] Large two phase regions are predicted for the case of the binary system,[86] but not for the ternary system.[87]

Huang and Lodge[88,89] utilized SCFT to study the phase behavior and variation of domain size for the AB/S system. In their first article[88] they used RPA to gen-

erate spinodals of the disordered phase, and used SCFT to generate OOTs between homogeneous phase, L, hexagonal cylinders, and BCC spheres with a core of the solvent-philic block B or the solvent-phobic block A. They did not consider the Gyroid phase. They considered only neutral solvents and slightly selective solvents with $\chi_{AS} = 0.6$ and $\chi_{BS} = 0.4$. The dilution approximation is found to hold true for the neutral solvent. The increase in selectivity of the solvent is found to increase the area of periodic phases in the phase portraits as seen for lamellar phases for slightly selective solvents by Banaszak and Whitmore.[78] Their analysis did not consider the regime in which isolated aggregates are expected. In the second article,[89] domain size d and concentration profiles of the lamellar phase with interaction parameters and structural parameters similar to those used in experiments of Hanley for PS-PI in dialkyl phthalates are presented. They noticed the variation of the exponent α where $d \sim \phi_{AB}^{\alpha}$ to go from -0.20 to 0.31 when you start reducing the selectivity of the solvent from $\chi_{AS} = 1$ to a neutral solvent.

Suo *et al.* [90] studied the phase behavior of block copolymer AB in a selective solvent S using a continuum model of SCFT. They generated phase diagrams for concentrations $\phi_{AB} > 0.2$, and in a few cases $\phi_{AB} > 0.1$. They do not notice any large two phase regions between periodic phases with solvent-phobic core except for the gyroid phase, where it is replaced by two phase coexistence of lamellar and hexagonal phase. The phase diagrams are dominated by periodic phases with core consisting of the solvent-phobic block. They do not notice "compound" micelles or micelles with solvent-philic core coexisting with a solvent rich homogeneous phase as observed by Zhang and Eisenberg[24] using experimental techniques.

Here we have developed a real space implementation of SCFT to relate micellar aggregate morphologies in the dilute regime to periodic phases present at higher concentrations of the diblock copolymer. This has not been pursued before. The presence of large two phase regions for periodic phases with solvent-phobic core block and presence of large two phase regions between a solvent rich homogeneous phase and periodic phases with solvent-philic corona block are also unique features observed by us. These results are presented in later chapters.

2.3 Isolated Aggregates: Experimental Studies

In this section a description of experimental results in the dilute limit of diblock copolymer AB in a selective solvent S is presented first which is followed by a discussion of phase behavior of block copolymer solutions. Transition between bilayers, cylindrical micelles, and spherical micelles have been observed in various systems.[24,25,57,91]

Eisenberg and coworkers[24,26,27,92,93] studied PS-poly(acrylic acid)(PAA) in aqueous solutions as well as non-polar solvents where they report the transition between bilayers, cylinders and spheres by utilizing transmission electron microscopy(TEM). The authors recognized the fact that the experiments have been performed well below glass transition temperature of PS and hence, expect the system to be in a non-equilibrium state as the organic solvent used to facilitate dissolution of PS-PAA in water is removed from the system. The transition from bilayers to cylindrical micelles to spherical micelles was found to occur upon increasing the block composition of the corona block.[26] Zhang and Eisenberg noticed a new morphology in the dilute

limit in the form of "compound" micelles which have a solvent-philic core.[92]

The interplay between different morphologies B, C, and S is studied in ternary systems of PS-PAA/dioxane/water by Shen and Eisenberg using TEM and turbidity measurements.[93] Turbidity measurements[93] show that transformation between the morphologies occurs in a matter of minutes. The reversibility of transformations make the authors conclude the system to be in equilibrium.[93] The jumps in turbidity were used as a sign of morphology transformation, and TEM was used to confirm the observation. For a particular block composition upon increasing the water content the authors noticed a transformation from dissolved block copolymers $\rightarrow$S $\rightarrow$C $\rightarrow$B. There are large two phase coexistence regimes noticed between regions of S and C as well as B and C on the morphology diagrams in the plane of block copolymer wt% *vs.* water wt % as well as for dioxane wt % *vs.* water wt%. Shen and Eisenberg[26] found vesicle formation to be favored over open bilayers for short chain lengths and at low values of water wt% in the system.

Bates and coworkers[25,94–96] utilized cryo-TEM and SAXS measurements to study these multiple morphologies in the dilute system for PB-PEO in water. Won *et al.* [94] found the formation of giant worm like micelles for $< 5\%$ by weight of PB-PEO. In a later article Won *et al.* [95] determined transitions between B, C, and S for PB-PEO, poly(ethyl ethylene) PEE-PEO, and PEO-PEE-PEO in aqueous solutions using cryo-TEM in the plane of N_{core} *vs.* f_{EO}. Large two phase coexistence regions are found for B and C as well C and S morphologies which is a common occurrence in other systems as well.[86,91] Jain and Bates[25] extended the study to higher molecular weight of block copolymers of the diblock copolymer PB-PEO in aqueous solutions, where they found

the aforementioned morphologies. In addition a new morphology the network phase was found to occur between bilayers and cylinders. A phase portrait is determined using cryo-TEM and SAXS for PB-PEO in water in the plane of weight fraction of PEO in the diblock copolymer *vs.* concentration of the diblock copolymer in the binary system.[96] In this phase portrait they show the complete transformation from an aggregate morphology such as B, C, and S to ordered phases found in the pure diblock copolymer limit.

Lodge and coworkers[91] studied the formation of multiple morphologies in dilute solutions of diblock copolymer poly(styrene)-poly(isoprene)(PS-PI) in dialkyl phthalate.[91] The sequence of three basic structures - spherical micelles, cylindrical micelles and vesicles was observed as the volume fraction of the solvophilic block is decreased in all of these experimental studies. The study by Bang *et al.* [91] involved studying one block composition (a minority of the styrene block) of PS-PI in dialkyl phthalates. By varying the type of alkyl chains in the solvent they influenced solvent selectivity and studied different morphologies in binary mixtures of dibutyl phthalate and diethyl phthalate as well as in diethyl phthalate and dimethyl phthalate. TEM and SAXS data were utilized to determine the type of morphology and noticed a transformation from S $\rightarrow$ C $\rightarrow$ B $\rightarrow$ phase separation upon increasing selectivity of the solvent.

LaRue and coworkers studied micelle formation of PS-PI in n-heptane.[53,57,97] LaRue *et al.* noticed the formation of wormlike micelles and found the size of these micelles to go down with increase in temperature utilizing light scattering and atomic force microscopy (AFM).[97] The transformation from B $\rightarrow$ C $\rightarrow$ S with increasing length of corona block is observed.[57] The structural properties of the micelles, aggre-

gation number and radii, are determined using static light scattering, dynamic light scattering, SAXS, and small angle neutron scattering (SANS).[57]

2.3.1 Estimates of CMC

The critical micelle concentration is the concentration at which either one of the morphologies B, C, and S are first observed. The volume fraction ϕ^{CMC} is generally represented as ϕ^{CAC} to take into consideration bilayers and micelles, where CAC represents the critical aggregation concentration. ϕ^{CAC} is theoretically predicted to be a function of both the interaction parameter between the solvent S and the core (made up of solvophobic block A) of an aggregate χ_{AS} and core block length N_{A} of the form $\phi^{\mathrm{CAC}} \sim \exp(-\chi_{\mathrm{AS}} N_{\mathrm{A}})$ for $\chi_{\mathrm{AS}} >> 1$. [28,29] Earlier theoretical estimates of ϕ^{CAC} have been performed for block copolymer/homopolymer blends where the size of the polymers leads to very low solubility of solvent in the core relative to small molecule solvents. In the case of experimental studies of diblock copolymers in small molecule selective solvents ϕ^{CAC} was found to have a change in variation, relative to core block length N_{A} , as one increases N_{A} . ϕ^{CAC} dependence on N_{A} was found to go from $\phi^{\mathrm{CAC}} \sim N_{\mathrm{A}}^{-1}$ dependence to $\phi^{\mathrm{CAC}} \sim N_{\mathrm{A}}^{-1/3}$.[98–103]

Eisenberg and coworkers[104–106] studied the critical micelle concentration for PS-poly(sodium acrylate) (PANa) diblock copolymers in organic as well as aqueous solutions. In a review paper by Moffitt *et al.* ,[106] the CACs of various linear block copolymers in organic as well as aqueous systems are discussed. They also condense results of other CAC calculations on a master plot of CAC *vs.* core block length for organic and aqueous solvents. The techniques used to determine the CAC are

fluorescence, osmometry, viscometry, and static light scattering. Khougaz *et al.* [98] determined aggregation number and CAC of PS-PANa and PS-PAA in organic solvents. They noticed a weak dependence of CAC on core block length of the form $\sim N_{\mathrm{A}}^{-1/3}$. All the previous results are put in perspective with regards to weaker dependence of ϕ^{CAC} on N_{A} . Similar weaker dependence of ϕ^{CAC} on N_{A} is reported for PS-PMMA(polymethylmethacralate) in ionic solvents by Mok *et al.* .[107]

The weaker dependence of ϕ^{CAC} on N_{A} is reported by Booth and coworkers as well.[100–103] Booth and coworkers studied the association behavior in dilute aqueous solution of block copoly(oxyalkylene)s in which hydrophilic PEO is combined with hydrophobic polymer. Three kinds of linear block copolymers are studied, i.e. copolymers of type $\mathrm{E_mA_n}$, $\mathrm{E_mA_nE_m}$ and $\mathrm{A_nE_mA_n}$, where E denotes a PEO unit, A denotes a hydrophobic oxyalkylene unit. Three kinds of hydrophobic oxyalkylene chains are used with the notation: P as oxypropylene, B as oxybutylene, and S as oxyphenyethylene. The measure of hydrophobicity of the oxyalkylene group increases with number of carbon atoms. The authors renormalized block lengths of oxyalkylene blocks in the ratio of 1:2:6[108] for P:B:S, respectively. This transformation helped them to collate all the CAC values, for different oxyalkylene blocks, into one master plot. In essence, the authors plotted CAC values relative to $\chi_{\mathrm{AS}}\, N_{\mathrm{A}}$ on a master plot for all types of oxyalkylene molecules. They noticed a variation in slope at a certain value of renormalized block length for the different types of block copolymers as well as architectures they studied. Unimolecular micellization was attributed to a sudden change in the slope of CAC relative to renormalized block length. By unimolecular micellization they imply the diblock copolymers are kinetically trapped in the form

of single surfactant molecules as described by Sadron and Gallot,[4] and Chu.[109] SCFT studies have been suggested by the authors to resolve this issue. The measurements were expected to be equilibrium measurements by the authors because of the T_g being low for the hydrophobic blocks. Booth and coworkers[100–103] also studied the enthalpy of micellization using temperature dependence of CAC. Kelarakis *et al.* [99] found that the CAC variation of E_mA_n type of diblock copolymers relative to temperature to be close to athermal behavior.

This behavior is explained by the formation of unimolecular micelle where core block A exists in a tightly coiled state. The presence of unimolecular micelle is attributed to almost negligible change in the enthalpy of micellization for the diblock copolymers which results in negligible cost of transferring unimolecular micelle to a multi-molecular micelle. The same behavior for enthalpy of micellization is shown by Booth and coworkers as well.[100–103]

2.3.2 Estimates of CMT

In some systems, micellization can be induced or suppressed by changing temperature, and micelles first appear at a critical micelle temperature (CMT). Experimental techniques used to estimate the CMT have included dynamic light scattering (DLS)[3,52,89] and small angle neutron scattering (SANS).[46–52] In particular, two systems have been studied extensively. Pluronics (PEO-PPO-PEO) in aqueous solutions[46–51] was studied using SANS, and PS-PI in dialkyl phthalates[3,52,89] was studied using DLS and SANS. The two systems are distinct because CMT is found upon cooling in the case of pluronics, as water is a good solvent for PPO below 288 K, and CMT is found upon

heating in the case of PS-PI in dialkyl phthalates, as in this case solvent selectivity decreases with increase in temperature. DLS measurements are used to determine the CMT and SANS measurements are used to determine details of the micellar structure such as aggregation number M, volume fraction of solvent in the core of a micelle $\phi_{\text{core-solvent}}$, and core radius R_{core}. The consistent general trends presented in the literature, upon approaching the CMT from a micellar aggregate, are that the aggregation number M decreases, the solvent increasingly penetrates the core, and the core radius of the micelle goes down.[46–52]

2.4 Periodic Phases: Experimental Studies

Pioneering experimental studies of block copolymer solutions in neutral and selective solvent systems from the concentrated to the dilute limit were carried out by Hashimoto and coworkers.[16,110–114] The authors fit their data of domain spacing for different concentration regimes in terms of power law expressions of volume fraction of the diblock copolymer ϕ_{AB} and temperature T. The experimental results were compared with theoretical predictions of domain spacings made by Hong and Noolandi.[115] The first two articles[110,111] concentrated on the PS-PB block copolymer in a selective solvent (n-tetradecane) that is a good solvent for PB but a poor solvent for PS. The rest of the articles in the series concentrated on the behavior of the PS-PB block copolymers and PS-PI (polyisoprene) diblock copolymers in neutral solvents toluene and dioctyl phthalate (DOP).[2,16] Microdomain structure in these solutions was investigated by small-angle X-ray scattering (SAXS).

In their first article, Shibayama *et al.*[110] showed a transition from a periodic lattice

of spheres to isolated spherical micelles on increasing the temperature of the system. Upon further increase in temperature the isolated spheres were found to melt into a homogeneous solvent rich phase. The variation of the domain spacing (D) with respect to the concentration of the diblock copolymer $\phi_{\rm AB}$ was studied by Shibayama *et al.*.[16] In a wide composition window they found $D \sim \phi_{\rm AB}^{1/3}$. However, they noticed a decrease in the domain spacing with an increase in the concentration of the diblock copolymer in the high-concentration regime, $\phi_{\rm AB} \gtrsim 0.7$. The authors found this last observation to be counter intuitive, because they expected an increase in the domain size when the segregation power increases with decrease in amount of neutral solvent in the binary system. The authors hypothesized that the observation was due to the slow kinetics in the high concentration regime, whereas the lower concentrations are thermodynamically controlled and attain equilibrium within the timescale of the measurements. The behavior in the higher concentration regimes was further studied in their future work.[113,114]

In their next article Hashimoto *et al.*[112] studied the dependence of the domain spacing D on temperature T, concentration of the diblock copolymer $\phi_{\rm AB}$, and the degree of polymerization of the diblock copolymer N. The authors plotted a master curve as a function of $(\phi_{\rm AB}\,/T)$ to look at the temperature dependence. Combining the results from their earlier studies[116] $(D \approx N^{\frac{2}{3}})$ they obtained a scaling relation,

$$D \approx N^{\frac{2}{3}} \left(\frac{\phi_{\rm AB}}{T} \right)^{\frac{1}{3}} \tag{2.4.1}$$

for the ordered state (lamellar microdomains) where the microdomains exist in solution.

Lodge *et al.*[2] tested the accuracy of the dilution approximation in block copolymer solutions. They studied PS-PI diblock copolymers with toluene and DOP as the neutral solvents and poly(ethylenepropylene-b-ethylethylene) (PEP-PEE) diblock copolymers with squalene as the neutral solvent. The authors calculated the ODT (ϕ_{ODT}) for varying volume fractions of the diblock copolymers. They considered nearly symmetric diblock copolymers, which exhibit a transition between the lamellar and disordered states. The transition is detected using static birefringence.

Lodge *et al.* found that the results for PEP-PEE system are much closer to the dilution approximation, whereas in PS-PI system there is no concentration regime in which the dilution approximation is applicable. The authors noted that because PEP-PEE has a much smaller χ_{AB} than PS-PI, the values of N (degree of polymerization of the diblocks) are considerably greater; hence, chain stretching and fluctuations in the diblock concentration should be diminished. The non-universality of the scaling of ϕ_{ODT} with respect to $\chi_{\mathrm{AB}}\, N$ was made evident.[2]

Hanley and Lodge[117] studied the phase behavior of SI block copolymer in the neutral solvent DOP. They found that χ_{ODT} scales as $\phi_{\mathrm{AB}}^{-1.4}$ and the χ_{OOT} scales as ϕ^{-1}. This implies the failure of the dilution approximation for ODT, but success in predicting the OOT. The authors, suggest that the shortcomings of the mean field theory might cancel each other out when comparing the free energies of the ordered phases. The scaling of domain spacings with respect to ϕ_{AB} and χ_{AB} was determined. The results are that the domain spacing scales as $\sim \phi_{\mathrm{AB}}^{\frac{1}{3}}\chi_{\mathrm{AB}}^{\alpha}$, with $\alpha \approx 0.3$. The scaling were found to match with the results obtained by Hashimoto and coworkers[16,112] and SCFT calculations by Whitmore and Noolandi.[77]

2.4.1 Pluronics in Aqueous Solutions

Phase behavior of block copolymers in a selective solvent is widely studied for pluronics in aqueous solutions.[46,86,118–120] Mortensen and Pedersen[46] constructed temperature *vs.* concentration phase diagram for a particular pluronic block composition of $EO_{25}PO_{40}EO_{25}$ in water determined using SANS. For a particular concentration, with increasing temperature or increasing selectivity of the solvent they found transformation between morphologies to go from S $\rightarrow$ C $\rightarrow$ B.[46] Wanka *et al.* [118] determined phase diagram in the temperature *vs.* concentration plane for a range of pluronic block compositions in a detailed study that used several experimental techniques. Surface tension measurements, DSC, light scattering and SANS were used to study the micellization transformation from a dissolved state of pluronics in water. DSC, and polarization microscopy was used to detect the periodic phases in the phase space. The authors noticed a transformation from S $\rightarrow$ C $\rightarrow$ B for a certain composition of the pluronic block copolymer with increasing temperature. The same transformation was also observed upon decreasing the corona length or the length of the EO block. Large two-phase coexistence regions were noticed between the cubic, hexagonal, and lamellar phases. Alexandridis *et al.* [119] and Svensson *et al.* [86] also noticed the formation of periodic phases upon increasing the concentration of pluronic in aqueous solutions using ^{1}H-NMR and SAXS. Alexandridis[120] utilizing SAXS determined periodic phases of pluronic block copolymers in formamide and determined the phase transformation from $S_A^{BCC} \rightarrow H_A \rightarrow G_A \rightarrow L$, where A represents the core block monomer PO in this case, with increasing concentration of the block copolymer for a particular block composition. The periodic phase transformation represents all the

different types of periodic phases one can expect for a pure diblock copolymer melt with the majority component in the block copolymer being the solvent-philic block.

2.4.2 PA-PEO in Aqueous Solutions

Other experimental studies involving polymeric amphiphiles polyalkane (PA)-PEO in aqueous systems have been carried out by Bates and coworkers[25,95,96,121] over the complete concentration regime of the diblock, i.e. from $\phi_{AB} = 0.01$ to $\phi_{AB} = 1$. In contrast to pluronics, the PA systems considered here show a much higher degree of hydrophobic character than PPO. Hajduk *et al.* [121] studied the phase behavior of pure poly(ethylethylene) (PEE)-PEO diblock with $0.29 < f_{EO} < 0.72$. Phase diagrams were generated for solutions using SAXS with temperature as the y-axis and wt% polymer on the x-axis. The phase behavior was shown to be driven by solvent partitioning itself favorably into EO domains. The authors found that the gyroid phase is restricted to regions close to pure diblock copolymer melt. In the dilute regime they noticed large two phase coexistence region between L and $H_A$in regions where one would expect $G_A$to be present.

Jain *et al.* [96] constructed a similar phase diagram for PB-PEO in water and found the network phase (which resembles a network morphology (N)) to be stable over a large region. They found the morphology to coexist with water in the at low concentrations of the diblock copolymer. They noticed $S_B^{BCC} \rightarrow H_B \rightarrow L \rightarrow N \rightarrow H_A \rightarrow S_A^{FCC}$with decreasing concentration of the diblock copolymer in the binary system. The most striking observation was the formation 'Y-junctions', which assemble into a dense three dimensional network morphology. The authors noted that the

closest structural analogue to the N phase is the ordered network morphology the gyroid phase. They noticed that the tendency to form threefold branches extends to all levels of hydration, but with long range order frustrated in the presence of large amount of water in the dilute limit. However, they did not rule out the possibility that the N phase might be an extraordinary metastable state as the kinetics in the system is very slow.[122]

2.4.3 PS-PI in Dialkyl Phthalates

Lodge and coworkers studied the phase behavior of the diblock copolymer PS-PI in solvent thoroughly with solvents of varying degrees of selectivity. They considered toluene[2] and DOP[2,79,89,117] as the neutral solvents. The experimental techniques used to determine the order-disorder transition (ODT) and order-order transition (OOT) were SAXS, rheological measurements, and static birefringence. Static birefringence was used to find the boundaries between birefringent phases (lamellar and cylindrical) and non-birefringent phases (cubic, gyroid, and disordered). The appearance (or disappearance) of birefringence is used to determine the phase boundaries. The experimental protocol, following Balsara *et al.*,[123] consisted of measuring the depolarized transmitted intensity from a HeNe laser, during a sequence of incremental increases in temperature.

Lodge and coworkers[3,89,117] also studied how the phase behavior of PS-PI diblock copolymer in dialkyl phthalate solutions depends on the concentration of the diblock, solvent selectivity, and block composition of PS-PI for the selective solvents case. The solvent quality was varied by using solvents with different alkyl groups with

the longer alkyl groups having lower solvent selectivity towards styrene monomer. They qualitatively compared their results with SCFT calculations.[78,88] The authors found in the concentrated regime,[3] the phase boundaries tend to curve depending on how the solvent partitions itself in the micro-domains of styrene and isoprene. The more selective the solvent gets, more of the area in the phase portraits is covered by phases having solvent-phobic isoprene core in order to reduce contact between isoprene and the solvent. Lodge and coworkers observed phase transformations from $S_A^{BCC} \rightarrow H_A \rightarrow G_A \rightarrow L \rightarrow G_B \rightarrow H_B \rightarrow S_B^{BCC}$, where A represents the solvent-phobic block PI and B the solvent-philic block PS. The $G_A$phase is found to be replaced by two phase coexistence between L and $H_A$as the solvent segregation increases either with decreasing temperature or increasing fraction of the solvent. Large regions of S_A^{FCC}were found in the dilute limit.

2.4.4 Phase Behavior in Ionic Solvents

In recent years phase behavior of block copolymers in ionic solvents have also been explored.[124–129] Ionic solvents have desirable properties such as a wide accessible liquid range as high as 300 °C, low vapor pressure, thermally stable up to 200 °C, and are relatively cheap.[130] The phase behavior of PS-PEO and PB-PEO in 1-ethyl-3-methylimidazolium bis(trifluoromethylsulfonyl)imide ([EMI][TFSI]) and phase behavior of PB-PEO in 1-butyl-3-methylimidazolium hexafluorophosphate ([BMI][PF6]) was studied by Simone and Lodge.[125,126] The phase behavior of PB-PEO was studied in [EMI][TFSI] and [BMI][PF6] in the plane of wt% of PB-PEO *vs.* f_{EO} by utilizing SAXS and cryo-TEM.[125] Phase behavior similar to that described earlier for different

diblock copolymers in selective solvents was found for these binary systems. Segalman and coworkers[127,128] studied the phase behavior of PS-poly(2-vinylpyridine)(P2VP) in imidazolium bis(trifluoromethane)sulfonamide ([Im][TFSI]) in the plane wt% of PS-P2VP *vs.* f_S utilizing SAXS and optical transmission characterization, which also showed similar phase behavior.

2.5 FCC to BCC Transition

The interplay between isolated spherical micelles and two spherical phases $S_A^{FCC}$and S_A^{BCC}in the dilute limit[3,52,89,131–141] has been widely studied. Starting with pioneering studies of this morphological transition by McConnell and Gast.[131–135] McConnell and Gast studied PS-PI in decane. They looked at the transition from a disordered solution of spherical micelles to an ordered structure, which can either be a face-centered cubic (FCC) lattice or a body-centered cubic (BCC) lattice. They concluded that the thickness of the corona layer determined the transition. If the corona was layer was thick or "hairy" the spherical micellar suspension would crystallize onto a BCC lattice and if the corona layer was thin or "crew-cut" it would crystallize onto a FCC lattice.[131–135] Small angle neutron scattering (SANS), small angle x-ray scattering (SAXS), and dynamic light scattering (DLS) were used by the authors to study the structural properties of these solutions.

Also, the authors determined the transition between FCC and BCC lattices using a liquid-state theory.[134] The liquid-state theory required pair-wise interactions between spherical micelles as an input. Gast and coworkers estimated pair-wise interactions using a self-consistent field theory calculation of brushes tethered to a flat

surface interacting with each other.[132,133,135] The SCFT calculations were used under the assumption that the radius of the spherical micelle was much larger than the distance between interacting micellar aggregates. The structure factor from SANS measurements compare favorably with the results obtained using SCFT calculations, which validated their SCFT calculations.

Hamley and coworkers studied the same phase transitions for poly(oxyethylene)-poly(oxybutylene) (POE-POB) in aqueous solutions.[136–138] They also noticed a transition from a BCC lattice to a FCC lattice upon reducing the length of the corona block.[136–138] Furthermore, they noticed a large two phase region between periodic spherical lattices and a periodic hexagonal lattice.[137] Even for shorter corona block lengths, Hamley and coworkers noticed a transformation from a FCC lattice to a BCC lattice upon increasing the concentration of the diblock copolymer POE-POB.

Lodge and coworkers[52,139–141] payed close attention to how the spherical micellar aggregates condense onto a lattice and what drives them to choose a FCC lattice or a BCC lattice. They studied PS-PI in several different dialkyl phthalate solvents. Structural properties were determined using SANS measurements. In particular, the authors determined the aggregation number M of the spherical micellar aggregates, and correlated M to interaction between these spherical micellar aggregates. They concluded that decreasing M leads to dilution of the corona brush and hence, leads to a softer micellar potential leading to the formation of BCC phase.[140] Lodge and coworkers also studied the transition between FCC and BCC lattices with varying concentration of PS-PI in DBP as well.[3,52,89]

Grason[142] proposed a mean field model in order to describe condensation of spher-

ical micelles onto a periodic structure of either FCC or BCC for the binary system of AB/S. Grason implemented the model developed by Zhulina[57] for determining competing terms in the free energy for an individual micelle, and used a pair-wise potential developed by Likos *et al.* [143] in order capture the interactions between individual spherical micelles. BCC is found to be stable when entropic factors (low ϕ_{AB} , and high T) or long range inter-micellar potential (high ϕ_{AB}) dominates. The aggregation number is found to initially increase with increasing volume fraction of diblock copolymer AB ϕ_{AB} and found to achieve a maximum before dropping down with increasing ϕ_{AB} . This follows the re-entrant BCC transition where upon increasing ϕ_{AB} one notices the transition from a homogeneous solution $\rightarrow$ BCC $\rightarrow$ FCC $\rightarrow$ BCC for the phase map generated using this model. This process leads to fission of the spherical micelles thereby reducing the aggregation number with increasing ϕ_{AB} . Grason also showed upon changing the character of the diblock copolymer from "hairy" to "crew-cut" leads to an increase in the presence of FCC phase in the morphology diagrams. However, the assumption that there is no small molecule solvent penetration in the core of micelles limits the model as it is known through SANS measurements that the solvent penetrates the core of micellar aggregates significantly. Grason did not consider other competing periodic structures in his study as well.

Suo *et al.* [90] used continuum formulation of SCFT in order to determine which spherical periodic phase, FCC or BCC, is stable over a particular concentration range. They split the free energy contributions into interactions between diblock copolymer AB and solvent S, blocks A and B, and translational entropy of the solvent. They observed the interaction between AB and S to drive the transition. However, their

analysis was limited. This is due to absence of any information regarding structural properties of isolated spherical micellar aggregates. The studies presented above studied both, the isolated spherical aggregates and periodic phases $S_A^{BCC}$and S_A^{FCC}.

Here we utilize real space implementation of SCFT to study isolated spherical micellar aggregates. The periodic formulation of SCFT is used to study swollen BCC and FCC phases to understand this transition in a binary system of AB/S. Simulating isolated aggregates gives us information about aggregation number and radius of the spherical micelles. Combining this with results for $S_A^{FCC}$and S_A^{BCC}, one can obtain the pair-wise interactions between micelles as they assemble on a spherical lattice. The aggregation number of the spherical aggregates on $S_A^{FCC}$and S_A^{BCC}can also be obtained. The results of this analysis are presented later in Section 5.5.

2.6 Micellization Kinetics: Experimental studies

Kinetics plays a crucial role in the binary system AB/S when the degree of segregation in the system is large, or the components AB and S are polymeric in nature which leads to large time scales required for equilibration. In this section I provide a summary of previous research work on micellization kinetics pursued through experiments.

In their pioneering work, Hashimoto and coworkers[113,114] noticed a hysteresis in mixtures of block copolymers in selective solvents. In the concentrated regime of di-block copolymers, domain sizes were found to differ at a particular temperature upon heating and cooling. This was seen for both for the lamellar and spherical periodic phases of a PS-PI surfactant in a non-selective solvent dioctyl phthalate(DOP) or toluene.

Correspondingly, in the dilute regime, light-scattering stop flow measurements have been used to study micellar association and dissociation of diblock copolymers by Bednar *et al.* .[144] The difference in scattering power between single block copolymers dissolved in solution (unimers) and micelles is large, which makes this technique very useful in the study of block copolymer micellization. The authors studied PS-PB diblock copolymer and PS-PB-PS triblock copolymer in a mixture of dioxane and heptane. Micellar association and dissociation is studied by analyzing the exponential decay in the intensity. Using a double exponential of the form $I(t) = a_1 e^{\frac{t}{\tau_1}} + a_2 e^{\frac{t}{\tau_2}} + a_3$, where τ_1 and τ_2 represent two relaxation times, which possibly do not correspond to real relaxation processes. The mean value of τ_1 and τ_2 is then taken as the relaxation times for either association or dissociation timescales depending on whether one is forming or dissolving micelles. The two timescales determined by the authors were found to be of the same order of magnitude.

A similar procedure for estimating the time scales of association and dissociation has been used in several articles[145–148] in press, for a variety of block copolymers in selective solvents. Mattice and coworkers[145,149] studied the micellization kinetics for PS-poly(oxyethylene)(POE) in mixture of water/ethanol with these flouroscence techniques and DLS. This micellar system has a glassy core, with PS having a high $T_g = 105\,^{\circ}\mathrm{C}$. They find τ_1 and τ_2 to be of the same order of magnitude. It is however important to note that the kinetics are essentially frozen due to the glassy PS core of the micelles.

Michels *et al.* [150] studied two Pluronic triblock copolymers of the form $\mathrm{EO_n} - \mathrm{PO_m} - \mathrm{EO_n}$, with $m > n$ for one case and $m < n$ for the other, in aqueous solu-

tions. According to previous measurements[118] they expect the cost of dissolving PO in water to be lower than dissolving PS in water, and observe that the CMC of this system varies over 3 orders of magnitude,[151] through a temperature range of 20 °C. This behavior made it an excellent system to study the dynamics of micelle formation and dissolution. Micellar dynamics were measured using an ultrasonic relaxation and intensity measurement corresponding to a temperature jump. Two relaxation timescales are observed where they associate the faster process with unimer insertion/expulsion, and the slower process to micelle fusion and fission. The first one is associated with micelle formation while the second is important for the system to achieve equilibrium micelle size.

Eisenberg and coworkers[152,153] have studied some kinetic aspects of morphology transformations in the dilute limit for PS-PAA in mixtures of dioxane/water[152] and dimethylformamide (DMF)/water.[153] PS is strongly hydrophobic and these mixtures are often kinetically trapped. A mixture of solvents with a small concentration of water $< 10\%$ was varied to influence the kinetic barrier and study the relaxation kinetics. In their first article,[152] turbidity measurements (by measuring the optical density of transmitted light) coupled with TEM were employed to study the kinetics of the rod to vesicle transformation at room temperature. These turbidity measurements are fit with exponentials describing relaxation on two timescales, as described earlier. They found the fast and slow process timescales to differ by a factor of 4 rather than an order of magnitude as seen from these other micellization studies. They describe the mechanism for the rod to vesicle transformation as a two step process, a first fast step of the rod-lamella transition followed by the relatively slower process of the

lamellae to vesicles transformation.

In their second study, Zhang and Eisenberg[153] analyzed the kinetics of morphology transformation between spherical micelles, cylindrical micelles, and vesicles for PS-PAA in DMF/water mixture using TEM for two preparation procedures. The first one involved dissolving the diblock copolymer in DMF and then adding small amount of water, whereas the second one involved dissolving the diblock copolymer directly in a mixture of DMF/water. The structures were frozen after 5 days of mixing by the addition of more water to the system, and finally DMF is removed from the mixture using dialysis. A 5.5 wt% water concentration mixture was found to change morphology in a matter of minutes, whereas the case of 8.5 wt% water concentration mixture the authors observed that it took days to notice a morphological transition. With the direct dissolution method thermodynamics were credited to dictate the morphology even for high water content, as opposed to the case of water addition where the system appeared to be kinetically frozen. The authors hypothesize the high concentration of unimers reduce the barrier to micelle formation in the direct dissolution method.

Along similar lines, Jain and Bates[122] observed the non-ergodic mixing behavior of blends of various block lengths of PB-PEO in water with two preparation schemes. The experimental technique used to determine the morphologies was primarily cryo-TEM, and the morphologies were observed over time. They prepare one way by mixing the diblocks of different block compositions before dissolving them in water, and separately by adding each block copolymer individually to water. By comparing these two schemes they found no unimer exchange to occur, and observed frozen

morphologies for PB-PEO in water. This can be expected because of a high degree of hydrophobic character of PB.

Meli and Lodge have studied diblock copolymer PB-PEO in the ionic solvents [EMI][TFSI] and [BMI][TFSI].[154,155] Using DLS and cryo-TEM the observed the relaxation of micellar size at high temperatures ($> 120\,^{\circ}\mathrm{C}$), studied from three different preparation procedures.[154] All the preparation procedures yielded a wide range of hydrodynamic radii. Annealing temperatures $120\,^{\circ}\mathrm{C} < T < 180\,^{\circ}\mathrm{C}$ are used, which yielded the same final size for a particular temperature and preparation protocol.

Another experimental technique used to study micelle dynamics is time-resolved small angled neutron scattering (SANS), developed by Willner *et al.* .[156] They investigated kinetics of system of poly(ethylene-alt-propylene) (PEP)-PEO/DMF by exploiting the large difference in the scattering lengths of protonated and deuterated species. Since the glass transition temperature of PEP is very low ($-56\,^{\circ}\mathrm{C}$) compared to that of PS ($105\,^{\circ}\mathrm{C}$), this copolymer is ideal for eliminating the influence of glassy dynamics. The authors used a double exponential fit of the form $I(t) = a_1\, e^{\frac{t}{\tau_1}} + a_2\, e^{\frac{t}{\tau_2}} + a_3$ as discussed before. In this case, they noticed that the two relaxation times to differ by two orders of magnitude (if not by at least one order of magnitude), and thus, predict presence of two different mechanisms for the formation or dissolution of micelles. They hypothesize the faster process corresponds to unimer exchange and were unable to attribute the slower process to a physical mechanism.

This technique of time-resolved SANS was also used by Lund and coworkers,[157–160] and they further investigate micellization kinetics of PEP-PEO/DMF system. Two studies[157,158] investigate star copolymers of PEP-PEO in a solvent mixture of wa-

ter/DMF. The micellar interfacial tension is tuned by varying concentration of DMF in the system. Water has been found to have an interfacial tension five times higher relative to DMF so that higher water content is expected to slow kinetics exchange of the surfactant. The authors noticed the kinetics to be frozen when the solvent is pure water but also found observable kinetics when they added moderate amounts of DMF to the system. In a separate study utilizing synchroton x-ray scattering, the authors[160] were able to describe the micellization process in the system with an elemental kinetics process driven by unimer insertion and expulsion.

Iyama and Nose[161] utilized time-resolved static and dynamic light scattering to analyze the association processes of micelle formation. In this investigation, the aggregation number was found to initially increase but then begin to decrease over time at a certain temperature. The authors also noticed the formation of cylindrical micelles, which then evolves to a vesicle morphology on heating to a unimer state which was then quenched from a higher temperature to room temperature. The cylindrical morphology was however not found on cooling slowly to room temperature from above the critical micelle temperature. This morphology at room temperature was found to be path dependent.

2.7 Summary and Perspective

A summary of literature for the phase behavior in the dilute regime as well as in the concentration regime has been provided here. The behavior in these two regimes are intertwined and a comprehensive theoretical study is missing. Using two formulations of SCFT we simulate the micellar aggregates B, C, and S in the dilute regime, and

periodic phases in the concentrated regime.

A real space implementation of SCFT is used to determine the states of aggregation i.e., regions where B, C, and S are stable. This method is used to determine the critical aggregation concentration (CAC) and the critical micelle temperature (CMT). A SCFT method to estimate CMT has not been pursued before. The solvent selectivity χ_{AS} required to completely collapse the corona brush at the interface is also investigated. The analysis of isolated aggregates is presented in chapter 4.

We notice unique features in phase diagrams by combining two formulations of SCFT over the complete concentration regime $0 \leq \phi_{AB} \leq 1$. We systematically sweep through the phase cube encompassing f_B , χ_{AS} , and ϕ_{AB} to determine the stable ordered phases. In this phase cube, the network morphology[25] should occur between B and C transition. Another goal is to determine if the gyroid phase $G_A$coexists with the solvent rich homogeneous phase. Suo *et al.* [90] have studied the phase behavior of AB/S, but their analysis is found lacking in certain areas. They do not consider the morphology variation of isolated aggregates B, C, and S. This behavior should be intertwined with the phase behavior in the concentrated regime. The periodic phases are found to require higher degree of numerical accuracy in the dilute limit. The number of basis functions (described in the next chapter) required to generate accurate calculations is almost five times of those used by Suo *et al.* .[90] The accuracy in our case is verified by comparing independent calculations obtained from the periodic and real space implementations of SCFT. They do not notice any two phase regions between periodic phases in the dilute limit, whereas we observe otherwise. We have also considered solvent selectivities which are 50% higher.

Also, we describe the region of low ϕ_{AB} and low f_B , where we expect the periodic phases with solvent-philic core to coexist with pure solvent. A theoretical study of this region is missing. RPA and Flory-Huggins theory are used to gain further insight into the phase behavior of AB/S. By combining results obtained from the dilute regime and the concentrated regime, we analyze the FCC to BCC transition in the dilute limit.

CHAPTER 3

Self-Consistent Field Theory

In the remainder of this thesis, SCFT is used to simulate both isolated aggregates and periodic phases in solutions of AB diblock copolymers in a selective solvent S. In this chapter, I review the SCFT formalism and discuss our numerical implementation of the theory. A general introduction of micelle thermodynamics with a corresponding implementation in the real space formulation of SCFT is discussed, which is used to determine morphologies in the dilute limit. Finally, the unbinding transition noticed in blends of AB and homopolymer B is studied for the binary system of AB in small molecule solvent S by combining results from two different formulations of SCFT.

3.1 Notation

The nomenclature used throughout the thesis is that A represents the solvent phobic block of the diblock copolymer, B represents the solvent philic block, and S represents a small molecule selective solvent. The Flory-Huggins interaction parameters between these species are represented by χ_{AB} , χ_{AS} , and χ_{BS} . In most of this thesis, I will be concerned with a binary system containing an AB diblock copolymer in small molecule solvent S. The degree of polymerization of the diblock copolymer is represented by N, which is defined as the ratio of the volume of the copolymer to a reference volume ν. In general, the volume of the small molecule solvent is given by $N_{\mathrm{S}}\nu$. By convention, the reference volume in this system is taken to be equal to the solvent volume, taking $N_S = 1$, so that N is the ratio of the polymer volume to the solvent volume. The block composition of the diblock is given by f_{B} , which is the volume fraction of the solvent philic block B within the diblock copolymer AB.

We consider a binary system containing M_{AB} copolymer molecules and M_{S} solvent molecules in a total volume V. Let

$$\bar{\phi}_{\mathrm{AB}} = \left(\frac{\nu}{V}\right) M_{\mathrm{AB}} N \tag{3.1.1}$$

$$\bar{\phi}_{\mathrm{S}} = \left(\frac{\nu}{V}\right) M_{\mathrm{S}} N_{\mathrm{S}} \tag{3.1.2}$$

denote the average volume fractions of AB copolymer and solvent in this system, respectively.

In an incompressible system we have

$$M_{\mathrm{AB}} N \nu + N_{\mathrm{S}} M_{\mathrm{S}} \nu = V. \tag{3.1.3}$$

The Gibbs free energy G for this binary system can be expressed as a function of pressure P and M_{AB}, for which

$$\frac{\partial G(P, M_{\mathrm{AB}})}{\partial M_{\mathrm{AB}}} = \Delta\mu. \tag{3.1.4}$$

In the above equation $\Delta\mu$ represents the exchange chemical potential, which is defined as

$$\Delta\mu \equiv \mu_{\mathrm{AB}} - \frac{N}{N_{\mathrm{S}}}\mu_{\mathrm{S}}. \tag{3.1.5}$$

Correspondingly, the total Helmholtz free energy for an incompressible system ($\delta V = 0$) under constant pressure ($\delta P = 0$) can be expressed as a function of volume V and M_{AB}. This is given by

$$\left.\frac{\partial F(V, M_{\mathrm{AB}})}{\partial M_{\mathrm{AB}}}\right|_V = \Delta\mu. \tag{3.1.6}$$

Let f denote the corresponding Helmholtz free energy per monomer, which satisfies

$$\frac{\partial f}{\partial \phi_{\mathrm{AB}}} = \frac{1}{N}\frac{\partial F}{\partial M_{\mathrm{AB}}} \tag{3.1.7}$$

$$= \frac{1}{N}\Delta\mu. \tag{3.1.8}$$

3.2 Self-Consistent Field Theory

SCFT is based on exact treatment of the statistical mechanics of individual molecules in a self-consistently determined set of chemical potential fields. The required information about the statistics of the AB diblock copolymer in the systems of interest is given by a statistical weight $q_{\mathrm{AB}}(\mathbf{r}, n)$. This quantity is proportional to the constrained partition function of a subchain containing monomers 0 to n of a diblock copolymer with a degree of polymerization N, when monomer n is constrained to point $\mathbf{r}$, in a specific set of chemical potential field.

The function $q_{\mathrm{AB}}(\mathbf{r}, n)$ satisfies a modified diffusion equation (MDE)

$$\frac{\partial q_{\mathrm{AB}}(\mathbf{r}, n)}{\partial n} = -\left[-\frac{{b_{\alpha(n)}}^2}{6}\nabla^2 + \omega_{\alpha(n)}(\mathbf{r})\right] q_{\mathrm{AB}}(\mathbf{r}, n) \tag{3.2.1}$$

with an initial condition $q_{\mathrm{AB}}(\mathbf{r}, 0) = 1$ for all $\mathbf{r}$. Here, b_α is the statistical segment length, $\omega_\alpha(\mathbf{r})$ is the chemical potential field for α monomers, divided by kT. The quantity $\alpha(n)$ is the type index for monomer n, which is equal to A within A block and B within the B block of the copolymer. An analogous function ${q_{\mathrm{AB}}}^\dagger(\mathbf{r}, n)$ is defined for the subchain containing monomers n to N. The function ${q_{\mathrm{AB}}}^\dagger(\mathbf{r}, n)$ satisfies a similar diffusion equation with the left hand side multiplied by -1, with a final condition ${q_{\mathrm{AB}}}^\dagger(\mathbf{r}, N) = 1$.

The chemical potential field $\omega_\alpha(\mathbf{r})$ expressed on a per monomer basis in units of kT is given by

$$\omega_\alpha(\mathbf{r}) = \sum_\beta \chi_{\alpha\beta}\phi_\beta(\mathbf{r}) + \xi(\mathbf{r}) \tag{3.2.2}$$

where $\chi_{\alpha\beta}$ is the Flory-Huggins interaction parameter for binary interaction between α and β monomers, for which $\chi_{\alpha\beta} = \chi_{\beta\alpha}$. By convention, $\chi_{\alpha\alpha} = \chi_{\beta\beta} = 0$. The form of interaction considered here is same as the one used in Flory-Huggins theory. The local volume fractions of α monomers, which can either be A or B or S, is represented by $\phi_\alpha(\mathbf{r})$. The field $\xi(\mathbf{r})$ is a Lagrange multiplier field, which is chosen to satisfy the incompressibility constraint

$$\sum_\alpha \phi_\alpha(\mathbf{r}) = 1. \tag{3.2.3}$$

The local volume fraction $\phi_{\mathrm{A}}(\mathbf{r})$ of A monomers that are part of an AB diblock copolymer is given by

$$\phi_{\mathrm{A}}(\mathbf{r}) = \frac{\bar{\phi}_{\mathrm{AB}}}{Q_{\mathrm{AB}}} \int_0^{f_{\mathrm{A}}N} \frac{dn}{N}\, q_{\mathrm{AB}}(\mathbf{r}, n) {q_{\mathrm{AB}}}^\dagger(\mathbf{r}, n). \tag{3.2.4}$$

Here, $\bar{\phi}_{\mathrm{AB}}$ is the average volume fraction defined in Equation (3.1.2) and Q_{AB} is unconstrained partition function defined by an integral

$$Q_{\mathrm{AB}} \equiv \frac{1}{V} \int \mathrm{d}\mathbf{r}\; q_{\mathrm{AB}}(\mathbf{r}, N). \tag{3.2.5}$$

The n in integral from Equation (3.2.4) is constrained to blocks of monomer type β by the Kronecker δ function $\delta_{\beta,\alpha(n)}$.

For the binary system of diblock copolymer AB in homopolymer B considered in Chapter 6 the corresponding q_{B} can be calculated by setting $f_{\mathrm{A}} = 0$ in the equations presented above. Once q_{B} is determined we estimate the contribution from the homopolymer to $\phi_{\mathrm{B}}(\mathbf{r})$ using Equation (3.2.4) with $f_{\mathrm{A}} = 0$.

The small molecule solvent can be considered as a special case of polymeric species

in which the Laplacian ∇^2 is neglected in the MDE presented in Equation (3.2.1), as a result of the small size of the solvent. In this case, statistical weight q is a function of $\mathbf{r}$ alone, and is given (for an arbitrary reference volume) by the Boltzmann factor $q_S(\mathbf{r}) = \exp\left(-N_{\mathrm{S}}\omega_{\mathrm{S}}(\mathbf{r})\right)$. The volume fraction of solvent is then

$$\phi_{\mathrm{S}}(\mathbf{r}) = \frac{\bar{\phi}_{\mathrm{S}}}{Q_{\mathrm{S}}} \exp\left(-N_{\mathrm{S}}\omega_{\mathrm{S}}(\mathbf{r})\right), \tag{3.2.6}$$

where

$$q_{\mathrm{S}}(\mathbf{r}) = \exp\left(-\omega_{\mathrm{S}}(\mathbf{r})\right). \tag{3.2.7}$$

The unconstrained partition function of the solvent Q_{S} is given by

$$Q_{\mathrm{S}} \equiv \frac{1}{V} \int \mathrm{d}\mathbf{r} \ \exp\left(-N_{\mathrm{S}}\omega_{\mathrm{S}}(\mathbf{r})\right). \tag{3.2.8}$$

As already noted, by convention, we take the reference volume equal to the solvent volume, thus yielding $N_{\mathrm{S}} = 1$.

The chemical potential of the AB copolymer is related to average volume fraction $\bar{\phi}_{\mathrm{AB}}$ and Q_{AB} through:

$$\mu_{\mathrm{AB}} = \mathrm{k}T \ln\left(\frac{\bar{\phi}_{\mathrm{AB}}}{Q_{\mathrm{AB}}}\right). \tag{3.2.9}$$

Similarly,

$$\mu_{\mathrm{S}} = \mathrm{k}T \ln\left(\frac{\bar{\phi}_{\mathrm{S}}}{Q_{\mathrm{S}}}\right) \tag{3.2.10}$$

is the chemical potential for the small molecule solvent.

Self-consistent field theory may be formulated in either the canonical or grand canonical ensemble. In the canonical ensemble we explicitly specify a value for the

average volume fraction $\bar{\phi}_i$ for each molecule type i, where i denotes AB or S. In grand-canonical ensemble, we instead specify values for the chemical potential μ_i for each species. To formulate SCFT calculation in grand-canonical ensemble, we use Equations (3.2.9) and (3.2.10) to calculate for the ratios $\bar{\phi}_{\mathrm{AB}}/Q_{\mathrm{AB}}$ and $\bar{\phi}_{\mathrm{S}}/Q_{\mathrm{S}}$ that appear as prefactors in Equations (3.2.4) and (3.2.6) for the local volume fractions. This is accomplished by simply making the replacement

$$\bar{\phi}_i/Q_i \rightarrow e^{\mu_i/\mathrm{k}T} \tag{3.2.11}$$

in these two equations.

To study the phase behavior, one must compare free energies of competing structures. The total Helmholtz free energy F of a simulation volume is given in SCFT by

$$\begin{aligned}\frac{F}{\mathrm{k}T} &= M_{\mathrm{AB}} \ln\left(\frac{\bar{\phi}_{\mathrm{AB}}}{eQ_{\mathrm{AB}}}\right) + M_{\mathrm{S}} \ln\left(\frac{\bar{\phi}_{\mathrm{S}}}{eQ_{\mathrm{S}}}\right) \\ &\quad + \frac{1}{2}\sum_{\alpha,\beta}\chi_{\alpha\beta}\int \mathrm{d}\mathbf{r}\, \phi_\alpha(\mathbf{r})\,\phi_\beta(\mathbf{r}) - \sum_\alpha \int \mathrm{d}\mathbf{r}\, \omega_\alpha(\mathbf{r})\,\phi_\alpha(\mathbf{r})\end{aligned} \tag{3.2.12}$$

where α and β are of the monomer type A, B, or S. The grand canonical free energy Φ is given by the definition

$$\Phi = F - \mu_{\mathrm{AB}} M_{\mathrm{AB}} - \mu_{\mathrm{S}} M_{\mathrm{S}}. \tag{3.2.13}$$

The pressure P of a macroscopically homogeneous system related to Φ by the thermodynamic identity $\Phi = -PV$.

3.3 Stress in SCFT

When using SCFT to treat periodic phases, the equilibrium structure must minimize the free energy per volume with respect to variations in dimensions of the periodic unit cell, corresponding to a stress free crystal. The code used by our group for periodic phases uses a method that was implemented by Tyler[162,163] to calculate derivatives of the Helmholtz free energy, and to find the unit cell dimensions for which these derivatives vanish.

The unit cell for any periodic structure can be characterized by a set of independent parameters, where the number of parameters depends upon the crystal system e.g., length of any one edge of a cubic system, or three independent lengths for an orthorhombic crystal. In a periodic structure characterized by d independent parameters, denoted by θ_i with $i = 1, \ldots, d$, we require that

$$\frac{\partial F}{\partial \theta_i} = 0 \tag{3.3.1}$$

for all i. The general expression for the stress for an incompressible melt of multi-block copolymers was derived by Tyler and Morse[162,163] as

$$\frac{1}{\mathrm{k}T}\frac{\partial F}{\partial \theta_i} = -M_{AB}\frac{\partial \ln Q}{\partial \theta_i}. \tag{3.3.2}$$

A straightforward generalization to the case of a binary mixture of copolymer and solvent of interest here yields

$$\frac{1}{\mathrm{k}T}\frac{\partial F}{\partial \theta_i} = -M_{AB}\frac{\partial \ln Q_{\mathrm{AB}}}{\partial \theta_i} - M_S\frac{\partial \ln Q_{\mathrm{S}}}{\partial \theta_i}. \tag{3.3.3}$$

It is straightforward to show, however, by considering the expressions given by Tyler and Morse for $\partial \ln Q/\partial\theta_i$ for chain molecules, that

$$\frac{\partial \ln Q_{\mathrm{S}}}{\partial \theta_i} = 0 \tag{3.3.4}$$

in the special case of a point-like solvent species. As a result, the stress is given by the contribution arising from the polymeric species alone, which gives the same contribution per polymer molecule as that used by Tyler and Morse.

3.4 Numerical Implementations

SCFT has been implemented in two types of formulations. The first formulation of SCFT is implemented in real space and the governing equations are solved numerically utilizing a pure Newton Raphson method. This formulation is used to study the isolated dilute morphologies B, C, and S in a binary system consisting of AB/S. The second one is a periodic formulation of SCFT (PSCF), where a particular periodic lattice is represented in the form of basis functions using the pseudo-spectral method implemented by Qin and Morse.[164] Both implementations are discussed in the following subsections.

3.4.1 Real Space Implementation

The real space formulation of SCFT is used to study isolated aggregate structures present in the form of spheres, cylinders, and bilayers. One needs to obtain the statistical weights $q_{\mathrm{AB}}(\mathbf{r}, n)$ and $q_{\mathrm{S}}(\mathbf{r}, n)$ from which the thermodynamic properties of

each morphology can be obtained. The statistical weight for the species AB and S are determined by numerically solving the MDE, presented earlier in Equation (3.2.1), in real space using the Crank-Nicolson scheme with mirror boundary conditions. From the initial omega field we determine the statistical weights $q_{\mathrm{AB}}(\mathbf{r}, n)$ and $q_{\mathrm{S}}(\mathbf{r}, n)$, using which the concentration profiles and thermodynamic properties of the system can be determined. After solving the MDE a Newton-Raphson iteration scheme is used to self-consistently determine the final solution according to certain criteria described later.

Utilizing the initial condition $q_{\mathrm{AB}}(\mathbf{r}, 0) = 1$ for all $\mathbf{r}$ and zero flux boundary condition we calculate the values of $q_{\mathrm{AB}}(\mathbf{r}, n)$ for values $n > 0$ using the Crank-Nicolson scheme. Upon comparison with a diffusion equation, this translates to constructing the concentration profile by utilizing the relation between the concentration at a given time t and at time $t - \Delta t$ given the initial concentration profile at $t = 0$. In the MDE monomer index n can be considered similar to time t in the diffusion equation. The Crank-Nicolson scheme is an implicit method where in order to determine the statistical weight of monomer n along the diblock copolymer AB a system of algebraic equations have to be solved numerically. The individual values of the $q_{\mathrm{AB}}(\mathbf{r}, n)$ at each value of $\mathbf{r}$ and n are related to each other by

$$q_{\mathrm{AB}}(\mathbf{r}, n+1) = q_{\mathrm{AB}}(\mathbf{r}, n) \; + \frac{\Delta n}{2} \left[K(\mathbf{r}, n+1) + K(\mathbf{r}, n) \right], \tag{3.4.1}$$

where $K(\mathbf{r}, n)$ represents the right hand side of the modified diffusion equation (3.2.1), in which the Laplacian is discretized using a central difference scheme in $\mathbf{r}$. The algebraic problem is tridiagonal in nature, or the solution of $q_{\mathrm{AB}}(\mathbf{r}, n)$ for the index

n and a particular $\mathbf{r}$ is implicitly dependent on its values at indices $n-1$, n, and $n+1$. This tridiagonal matrix is solved numerically using a LAPACK routine whose convergence scales as $\mathcal{O}(N/\mathrm{d}s)$, where $\mathrm{d}s$ is the step size for discretization along the contour of the diblock copolymer AB. A similar procedure is used to obtain value of $q_{\mathrm{S}}(\mathbf{r}, n)$ or value of $q_{\mathrm{B}}(\mathbf{r}, n)$ depending on whether the binary system is AB/S or AB/B.

Once the MDE has been solved, the residual is calculated and if it is not within the specified tolerance, a Newton-Raphson scheme is used to satisfy the tolerance. The residual comprises two criteria. The first one is incompressibility imposed by the Lagrange multiplier field $\xi(\mathbf{r})$ and the second one is related to the chemical potential fields $\omega_\alpha(\mathbf{r}) = \sum_\beta \chi_{\alpha\beta}\phi_\beta(\mathbf{r}) + \xi(\mathbf{r})$. $\xi(\mathbf{r})$ is calculated using the equation for chemical potential field of monomer A $\omega_{\mathrm{A}}(\mathbf{r})$, i.e. $\xi(\mathbf{r}) = \sum_\beta \chi_{A\beta}\phi_\beta(\mathbf{r}) - \omega_{\mathrm{A}}(\mathbf{r})$. The size of the residual matrix is $N_{\mathrm{monomer}} * N_{\mathrm{grid}}$, where N_{monomer} represents the number of monomers and N_{grid} represents the grid size, as the constraints have to be satisfied for each monomer at each grid point. The incompressibility constraint is implemented in the corresponding row of $\omega_{\mathrm{A}}(\mathbf{r})$ in the residual vector as the condition $\omega_{\mathrm{A}}(\mathbf{r}) = \sum_\beta \chi_{A\beta}\phi_\beta(\mathbf{r}) + \xi(\mathbf{r})$ is already satisfied in the calculation of $\xi(\mathbf{r})$. The residual R, where monomer A contributes to row 1 of the residual, for a particular grid point n

can be calculated from the following relations

$$\xi(n) = \omega_{\mathrm{A}}(n) - \sum_{\beta} \chi_{A\beta}\phi_{\beta}(n) \tag{3.4.2}$$

$$R(1) = \sum_{\alpha} \phi_{\alpha}(n) - 1 \tag{3.4.3}$$

$$R(\gamma) = \omega_{\gamma}(n) - \sum_{\beta} \chi_{\gamma\beta}\phi_{\beta}(n) - \xi(n) \tag{3.4.4}$$

where γ, which ranges from from 2 to N_{monomer}, represents contributions to the residual from the rest of monomers other than A. The chemical potential fields are tweaked after each iteration till the required tolerance is achieved.

If the sufficient tolerance is not achieved for iteration step i, for the next iteration chemical potential fields and the Lagrange multiplier field represented by X are updated according to the Newton-Raphson method by

$$X_{\alpha}^{i+1} = X_{\alpha}^{i} - {J_{\alpha\beta}^{i}}^{-1} R_{\beta}, \tag{3.4.5}$$

where the matrix J represents the Jacobian $J_{\alpha\beta}^{i} \equiv (\partial R_{\alpha}^{i}/\partial X_{\beta}^{i})$. The iterations are continued till the residual goes to zero with the required tolerance. One needs to calculate the inverse of Jacobian ${J_{\alpha\beta}^{i}}^{-1}$ for each iteration step i in this formulation of SCFT and is the most time consuming step of the simulation.

The definition of the residual involves a subtlety as the concentration profiles calculated using the canonical ensemble are invariant under constant shifts of the Lagrangian field $\xi(\mathbf{r})$. Hence, in the canonical ensemble one has to specify a reference value of $\xi(\mathbf{r})$ but in the case of the grand canonical ensemble, where one specifies the

chemical potential μ_i for each specie i, it automatically results in a reference value for the Lagrange field $\xi(\mathbf{r})$. Thus, in the canonical ensemble the number of degrees of freedom is reduced by the number of monomers N_{monomer} as a homogeneous shift in the omega fields leads to the same final solution of the concentration profiles of each monomer, which results in an infinite number of possible solutions. This issue is overcome by enforcing the Lagrange field at the last grid point M to be zero i.e., $\xi(M) = 0$.

3.4.2 Pseudo-Spectral Method

Matsen and Schick[165] developed a spectral method in order to solve the MDE which involved symmetry adapted basis functions, and successfully simulated the three dimensional BCC sphere and gyroid phases. The governing MDE is reduced to the form of

$$\frac{\partial q_{\text{AB}}(\mathbf{r}, n)}{\partial n} = -H_{\text{AB}} q_{\text{AB}}(\mathbf{r}, n)\,, \tag{3.4.6}$$

where H_{AB} corresponds to the operator

$$\left[-\frac{{b_{\alpha(n)}}^2}{6}\nabla^2 + \omega_{\alpha(n)}(\mathbf{r})\right]. \tag{3.4.7}$$

The solution for the MDE in their case is obtained by propagating from the initial condition of $q_{\text{AB}}(\mathbf{r}, 0) = 1$ for a given set of chemical potentials for each monomer $\omega_{\alpha(n)}(\mathbf{r})$ through the relation

$$q_{\text{AB}}(r, n + \delta n) = \exp(-H_{\text{AB}}\Delta n) q_{\text{AB}}(\mathbf{r}, n)\,. \tag{3.4.8}$$

The time taken to solve the MDE is found to scale as $\sim M^3$, where M is the number of symmetry adapted basis functions used to resolve the space group of the periodic phase. In comparison, the pseudo-spectral formulation developed by Rasmussen and Kalosakas[166] scales as $MN_{\text{grid}}\log(N_{\text{grid}})$, where M is the number of grid points involved in the discretization of the contour variable s and N_{grid} is the number of grid points for spatial discretization. The pseudo-spectral formalism has been implemented by Qin and Morse[164] and a more detailed description of this method can be found in Qin's thesis.[164] Here we summarize the pseudo-spectral formalism used to simulate periodic phases.

The propagator in this case is complicated to evaluate as $\omega_\alpha(\mathbf{r}, n)$ is diagonal in real space and ∇^2 is diagonal in reciprocal space. In the case of the pseudo-spectral formalism the propagator $\exp(-H_{\text{AB}})$ is given by the approximation[166]

$$q_{\text{AB}}(\mathbf{r}, n+\Delta n) \simeq \exp\left(-\frac{N\omega_\alpha(\mathbf{r},n)}{2}dn\right)\exp\left(\frac{Nb^2\nabla^2}{6}dn\right)\exp\left(-\frac{N\omega_\alpha(\mathbf{r},n)}{2}dn\right)q_{\text{AB}}(\mathbf{r},n)\,.$$

In the pseudo-spectral algorithm the $\omega_\alpha(\mathbf{r}, n)$ operating on $q_{\text{AB}}(\mathbf{r}, n)$ is calculated in real space and $\nabla^2 q_{\text{AB}}(\mathbf{r}, n)$ is calculated in Fourier space with the help of fast Fourier transforms.

Iteration scheme with Broyden's Method

A set of symmetry adapted basis functions which capture the symmetry of the particular space group are generated in order to calculate the residual. The generation

of symmetry adapted basis functions is implemented for the spectral formalism by Tyler and Morse,[162] and for the pseudo-spectral formalism was extended by Qin and Morse[164] in our group. One needs to specify a reference state for the canonical ensemble as mentioned previously for the real space formulation of SCFT. In the case of PSCF, the Lagrange field of the homogeneous component of PSCF is set to zero $\xi(\mathbf{G}=0)=0$ in order to take care of homogeneous shifts in $\xi(\mathbf{r})$ yielding the same solution. For the grand canonical ensemble the Lagrange field $\xi(\mathbf{r})$ is uniquely determined for each grid point or basis function.

Once the MDE has been solved for the periodic phases the solution has to be iterated to get the required tolerance under the constraints mentioned earlier for the real space formulation of SCFT. For the case of PSCF same convention is used to generate the residual, however there are extra terms in the residual incorporating stress or minimization of free energy relative to lattice parameters of the unit cell θ_i. The additional term in the residual is represented by

$$R = \frac{\partial F}{\partial \theta_i}, \tag{3.4.9}$$

with i being the number of number of independent lattice parameters for the periodic lattice.

The residual generated is minimized using a quasi-Newton-Raphson method called the Broyden's method implemented by Qin and Morse.[164] This method reduces the simulation time by generating the Jacobian only once at the start of the iteration algorithm instead of generating a completely new Jacobian for each iteration step in a pure Newton-Raphson implementation. Broyden's method starts with a rough

estimate of the Jacobian and improves the estimate of the Jacobian as the number of iterations go up. This speeds up the calculation as one does not have to calculate the Jacobian at each iterative step.

SCFT calculations are carried out at constant ϕ_{AB} as well as at constant f_{B} for different phases. In the canonical ensemble, the phase having the lowest Helmholtz free energy F in a particular region of the phase diagram is determined to be the stable phase in that region. In the grand canonical ensemble, the grand canonical free energy Φ is a function of chemical potential of the diblock copolymer μ_{AB}, and chemical potential of the solvent μ_{S}. In order to compare the free energies between candidate phases, the chemical potential of the solvent is set to zero, $\mu_{\mathrm{S}} = 0$. This aids in condensing the values of Φ for different phases in a single plot relative to the exchange chemical potential $\Delta\mu = \mu_{\mathrm{AB}} - N\mu_{\mathrm{S}}$. This procedure is carried out by taking into account that SCFT predictions for volume fraction fields and the Helmholtz free energy are invariant under a spatially homogeneous shift of the Lagrange multiplier field.[167] The chemical potentials at which Φ of both phases cross is the chemical potential for phase coexistence from which we calculate the two phase coexistence boundaries.

3.5 Numerical Accuracy

Numerical accuracy plays an important role in any simulation technique. Here, I describe the accuracy limits of the pseudo-spectral method and compare it with the spectral method. Also, I discuss accuracy issues related to SCFT calculations of strongly selective solvents later on in this section.

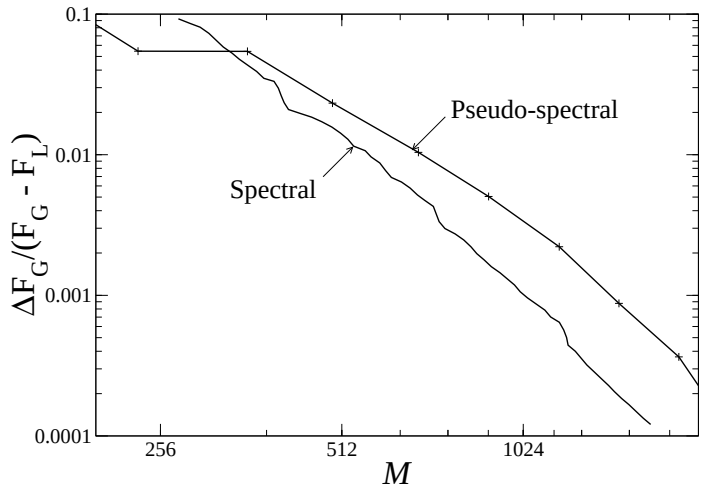

Figure 3.1: The error, ΔF_{G} difference in Helmholtz free energy of gyroid phase (G) with respect to an accurate calculation, relative to the number of basis functions M for a value of $\chi_{\mathrm{AB}}\, N = 30$. The error is tracked along the metastable hexagonal (H)/ lamellar (L) phase boundary and is divided by $\Delta F_{\mathrm{G}} - \Delta F_{\mathrm{L}}$. The data for spectral method with Anderson mixing is obtained from the article by Matsen.[1]

3.5.1 Pseudo-Spectral *vs.* Spectral Algorithms

Here we compare the accuracy of the pseudo-spectral method with Broyden's method with the spectral formulation of SCFT combined with Anderson mixing implemented by Matsen.[1] In Figure 3.1 these two different formulations of SCFT are compared for a diblock copolymer AB melt. This figure represents the variation of the inaccuracy or the error, ΔF_{G} which is the difference in Helmholtz free energy of gyroid phase (G) with respect to an accurate calculation, relative to the number of basis functions M for a value of $\chi_{\mathrm{AB}}\, N = 30$. The error is measured relative to a highly accurate gyroid phase (G) calculation carried out with $M \approx 3000$ and error tolerance for the PSCF simulation of $< 10^{-8}$ for the pseudo-spectral method. This error is tracked along the metastable hexagonal (H)/ lamellar (L) phase boundary, where H and L

have the same Helmholtz free energy. The error, ΔF_{G}, is divided by $\Delta F_{\mathrm{G}} - \Delta F_{\mathrm{L}}$ as it approximates the relative error in the width of the gyroid channel.

The pseudo-spectral method with Broyden's competes favorably relative to the spectral formulation used by Matsen.[1] The rate of convergence, which is the slope of lines in Figure 3.1, is found to be similar for both schemes of SCFT.

3.5.2 Accuracy Issues in Selective Solvent

In order to simulate any periodic phase accurately one requires enough number of grid points to discretize the interface between the core block A and the selective solvent S. If the number of grid points in the interface are low, or equivalently the resolution of interface is low this will lead to numerical errors in the thermodynamic properties of the system. Hence, the dependence of interfacial width is studied relative to the interaction parameter χ_{AS}. The concentration profiles of a lamellar phase can be used to study the numerical cost of simulating three dimensional periodic phases such as face-centered cubic $\mathrm{S}_{\mathrm{A}}^{\mathrm{FCC}}$, body centered cubic $\mathrm{S}_{\mathrm{A}}^{\mathrm{BCC}}$, and gyroid G_{A}. The assumption in this case is that the interfacial width for a particular χ_{AS} is similar in a lamellar phase, hexagonal phase H_{A}, gyroid phase G_{A}, spherical FCC $\mathrm{S}_{\mathrm{A}}^{\mathrm{FCC}}$and spherical BCC $\mathrm{S}_{\mathrm{A}}^{\mathrm{BCC}}$. The ratio of the domain size d and the interfacial width w relative to the solvent selectivity will give a qualitative estimate of why simulations at higher values of χ_{AS} are numerically intractable for phases with three dimensional symmetry.

The concentration profiles of the lamellar phase for $\phi_{\mathrm{AB}} = 0.5$ and $f_{\mathrm{B}} = 0.5$ is studied here. These parameters are chosen right at the center of the parameter space

in a f_{B} *vs.* ϕ_{AB} cut of the phase cube encompassing f_{B} , ϕ_{AB} , and χ_{AS} . The definition of interfacial width w used here is presented in Figure 3.2.

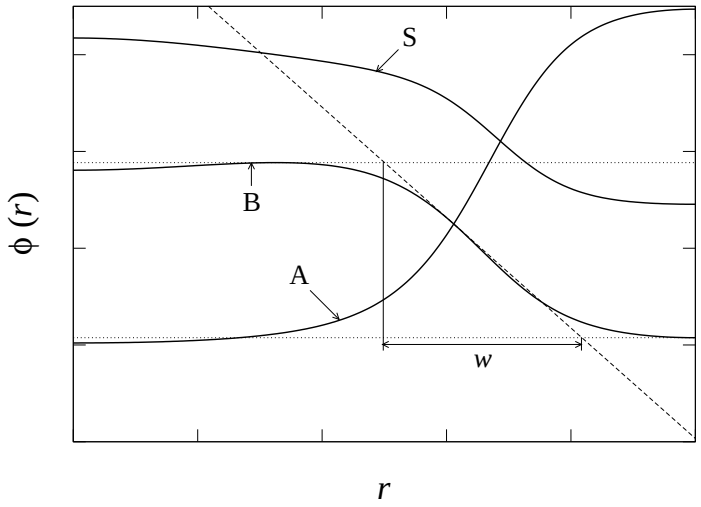

Figure 3.2: Definition of interfacial width w is shown here. Volume fraction ϕ of monomers A, B, and S is plotted against position r. The dashed line represents the linear fit of $\phi_{\mathrm{B}}(r)$ close where $\phi_{\mathrm{A}}(r)$, and $\phi_{\mathrm{B}}(r)$ intersect each other.

Interfacial width w is calculated by fitting a line for the concentration of solvent-philic monomer B at the intersection of volume fraction monomers A, and B. This line is represented by the dashed line in Figure 3.2 with the assumption being that the concentration profile at the interface to be wedge-shaped for various concentration profiles at different χ_{AS} . The dotted lines represent the maximum and minimum in the concentration of solvent philic monomer B. The distance between where the linear fit intersects the maximum and the minimum in concentration of B is defined as the interfacial width w.

The ratio of domain size d relative to interfacial width w is calculated and is presented in Figure 3.3 for a lamellar phase with $\phi_{\mathrm{AB}} = 0.5$, $f_{\mathrm{B}} = 0.5$, $\chi_{\mathrm{BS}} = 0.4$,

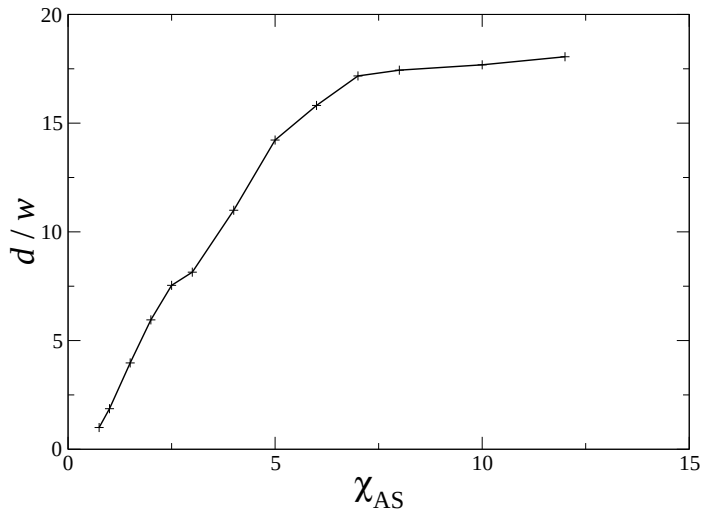

Figure 3.3: The ratio of the domain size d relative to the interfacial width w for a lamellar phase at $\phi_{\mathrm{AB}} = 0.5$ and $f_{\mathrm{B}} = 0.5$ is shown here. The calculations are carried out using a periodic formulation of SCFT and the parameters used are $N = 100$, $\chi_{\mathrm{BS}} = 0.4$, $\chi_{\mathrm{AB}} = 0.2$, and $b_{\mathrm{A}}/b_{\mathrm{B}} = 1$. The values of d/w is normalized relative to the value at $\chi_{\mathrm{AS}} = 0.75$ which yields a value of $d/w = 1$ for $\chi_{\mathrm{AS}} = 0.75$.

and $\chi_{\mathrm{AB}} = 0.2$. The values of d/w is normalized relative to the value at $\chi_{\mathrm{AS}} = 0.75$, which yields $d/w = 1$ for $\chi_{\mathrm{AS}} = 0.75$. The ratio of d relative to w is about an order of magnitude larger for $\chi_{\mathrm{AS}} = 4$ relative to the value of d/w at $\chi_{\mathrm{AS}} = 0.75$ as seen from Figure 3.3. Similarly, the value of d/w at $\chi_{\mathrm{AS}} = 2$ and $\chi_{\mathrm{AS}} = 12$ are about six times and eighteen times larger respectively, the value of d/w at $\chi_{\mathrm{AS}} = 0.75$. The number of basis functions needed to resolve an interface is proportional to the value of $(d/w)^n$ for an n-dimensional phase. Let us assume the number of basis functions needed to resolve the interface for $\chi_{\mathrm{AS}} = 0.75$ be $N_{0.75}$. Hence, we can reasonably expect the number of basis functions required to resolve the interface for values of χ_{AS} being 2, 4, 8, and 12 require basis functions $(6N_{0.75})^n$, $(10N_{0.75})^n$, $(17N_{0.75})^n$, and $(18N_{0.75})^n$, respectively, for an n-dimensional phase. This analysis gives us an idea about why it is

tough to simulate the three dimensional phases S_A^{FCC}, S_A^{BCC}, and G_A when the solvent selectivity χ_{AS} is taken to be $\chi_{AS} = 1.5$ or higher. At this value of χ_{AS} one would require around $\sim 50N_{0.75}^3$ basis functions to resolve a phase with three dimensional symmetry. This is prohibitive due to the upper limit on the memory available on the MSI cluster Calhoun as well as the iteration and MDE solver in the PSCF code slows down considerably because of the large number of basis functions required. Thus, we restrict the highest value of χ_{AS} to $\chi_{AS} = 1.3$ for the current PSCF code for all the three dimensional periodic phases presented later on.

3.6 Isolated Aggregates

The selective nature of the solvent causes the copolymers to form aggregate structures, with core as solvent-phobic block A, in order to avoid unfavorable contact between A and the small molecule selective solvent S. Diblock copolymers in selective solvents form three kinds of aggregate structures: bilayers (B), cylinders (C), and spheres (S). The stable curvature out of the three is determined by using the real space formulation of SCFT. The competition between the three morphologies B, C, and S is studied relative to the solvent selectivity χ_{AS} and good solvent characteristic χ_{BS} for this two-component system in the next chapter.

For a system of a diblock copolymer AB in a solvent S, we consider a spherical simulation cell of radius R, locating a single micelle at the center. In order to overcome finite size effects the concentration outside the region of the micelle should decay to a constant value, one which coexists with the micelle at the center. This balance is determined by the condition of equal chemical potentials for the two coexisting

phases.

From such a simulation, an excess Helmholtz free energy $F^{\rm ex}$ can be defined as the difference between the total Helmholtz free energy of the simulation cell with one micelle and that of a homogeneous system of the same volume and chemical potentials for all species as those in the matrix region of the micelle simulation. The excess free energy that we obtain by this method is an excess Helmholtz free energy, but for systems with equal pressures, inside and outside the micelle, this is also equal to the corresponding excess Gibbs free energy. The difference in free energy of two systems with the same total volume and the same bulk pressure is the same free energy excess. Similarly, an excess number of molecules M_i for each species may be defined as the number difference of molecules of species i in the simulation with one micelle and that of a corresponding homogeneous system. We will refer to M_i as the aggregation number for species i, and use $M \equiv \{M_{\rm AB}, M_{\rm S}\}$ as shorthand for the set of relevant aggregation numbers. Generally, $M_{\rm AB} > 0$ for the surfactant AB, but $M_{\rm S} < 0$ (remember it is an excess and is defined relative to the corresponding homogeneous system) for the matrix solvent S. Let $\mu_i^{\rm m}(M)$ denote the equilibrium chemical potential of species i for a micelle with specified values for M_i. These chemical potentials also describe the coexisting homogeneous solution background for the SCFT simulation. The excess grand-canonical free energy is given by the difference

$$\Phi^{\rm ex}(\mu^{\rm m}) = F^{\rm ex}(M) - \sum_i \mu_i^{\rm m}(M) M_i, \tag{3.6.1}$$

and obeys the identity

$$M_i = \frac{\partial \Phi^{\mathrm{ex}}(\mu^{\mathrm{m}})}{\partial \mu_i^{\mathrm{m}}}. \tag{3.6.2}$$

In an incompressible system, the excess aggregation numbers must satisfy the constraint

$$0 = M_{\mathrm{AB}} N_{\mathrm{AB}} + M_{\mathrm{S}} N_{\mathrm{S}}. \tag{3.6.3}$$

This is simply a statement of the fact that the systems of equal volume with and without the micelle must contain the same total number of monomers. The incompressibility condition is used to express Φ^{ex} (see Equation (3.6.1)) in terms of the exchange chemical potential $\Delta\mu$ (see Equation (3.1.5)) as

$$\Phi^{\mathrm{ex}} = F^{\mathrm{ex}} - \Delta\mu M_{\mathrm{AB}}^{\mathrm{ex}}. \tag{3.6.4}$$

Utilizing the above definitions, the stable structure is determined by calculating the critical aggregation concentration. The critical aggregation concentration (CAC) is the concentration above which the diblock copolymers start to aggregate in the form of B, C, and S. For a particular aggregate structure the definition used is the point at which the grand canonical excess free energy goes to zero,[168] i.e.,

$$\Phi^{\mathrm{ex}} = 0. \tag{3.6.5}$$

This occurs when the free energies of an isolated aggregate and that of a homogeneous mixture become equal, or above the concentration at which $\Phi^{\mathrm{ex}}(T, \Delta\mu) = 0$.

To study the morphology transformation between B, C, and S using SCFT, one

must calculate excess grand canonical free energies of the isolated aggregates involved as described earlier by Chang and Morse.[168] The grand canonical free energy of isolated aggregates Φ at a specified set of chemical potentials and a specified number density ρ_{m} of nearly mono-disperse micelles can be expressed as

$$\frac{\Phi}{V} = -P^{\mathrm{h}}(T,\mu) + \rho_{\mathrm{m}}[\Phi^{\mathrm{ex}}(T,\mu) + \mathrm{k}T\ln(\frac{\rho_m}{e\rho_{\mathrm{m}}^0})]. \tag{3.6.6}$$

Here P^{h} is the pressure of a hypothetical homogeneous phase at a specified set of chemical potentials, determined using Flory-Huggins theory.[167] $\Phi^{\mathrm{ex}}(T,\mu)$ is the extrapolated excess grand canonical free energy of a hypothetical micellar solution with a standard micellar concentration ρ_{m}^0. Ignoring the translational entropy of micelles, which is represented by the logarithmic term in Equation (3.6.6), and considering an isolated micelle then the equation reduces to $\Phi = -P^{\mathrm{h}}(T,\mu)V + \Phi^{\mathrm{ex}}(T,\mu)$, as $\rho_{\mathrm{m}} = V^{-1}$ for a single aggregate in a simulation cell of volume V.

The point at which Φ/V and P^{h} cross over is where $\Phi^{\mathrm{ex}} = 0$ and the concentration of AB at which it occurs yields the CAC. From SCFT calculations we arrive at the volume fraction at CAC ϕ^{CAC} , and the CAC will be represented as a volume fraction ϕ^{CAC} from here on.

The volume fraction of AB ϕ_{AB} is varied while maintaining a constant block length, with constant degree of polymerization of AB N and block composition of solvent-philic block B f_{B} . For each isolated aggregate structure the exchange chemical potential at the CAC $\Delta\mu^{\mathrm{CAC}}$ is determined using the canonical or the grand canonical ensemble. The morphology having the lowest $\Delta\mu^{\mathrm{CAC}}$ is determined as the stable structure for a particular f_{B} . The exchange chemical potential $\Delta\mu^{\mathrm{CAC}}$ and CAC are

directly proportional to each other and thus, the isolated aggregate structure with lower $\Delta\mu^{\mathrm{CAC}}$ will have a lower CAC.

A typical calculation for a cylindrical micellar aggregate with a block composition of $f_{\mathrm{B}} = 0.26$ and $N = 100$ is shown in Figure 3.4. Similar procedure yields ϕ^{CAC} for the other competing aggregates (spherical micelles and bilayers) by determining the exchange chemical potential $\Delta\mu$ for both curvatures. The morphology having a lower ϕ^{CAC} will be the stable structure for that particular f_{B} .

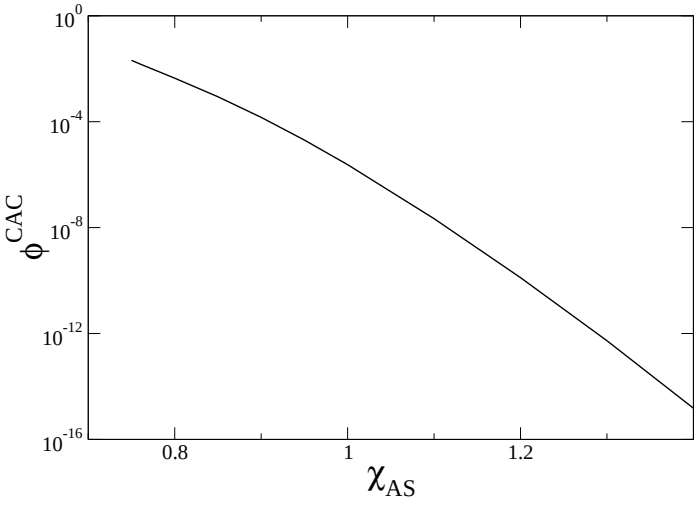

Figure 3.4: Volume fraction of the diblock AB for a cylindrical aggregate at the CAC ϕ^{CAC} plotted *vs.* the selectivity of the solvent χ_{AS} . The calculation was carried out for AB/S system with $f_{\mathrm{B}} = 0.26$, $N = 100$, $\chi_{\mathrm{BS}} = 0.4$, $\chi_{\mathrm{AB}} = 0.2$, and $b_{\mathrm{A}}/b_{\mathrm{B}} = 1$.

3.7 Swollen Ordered Phases

The ordered phases lamellar L, hexagonal phase $\mathrm{H_A}$, body-centered cubic phase $\mathrm{S_A^{BCC}}$, and face-centered cubic phase $\mathrm{S_A^{FCC}}$swell indefinitely upon dilution. Here the subscript represents type of the core block monomer, and A is the solvent-phobic block. Upon

diluting a pure diblock copolymer AB with solvent S eventually leads to a phenomenon called unbinding, where isolated aggregates are observed as addition of solvent to a pure diblock copolymer melt leads to divergence of the domain spacing $d \to \infty$ due to S preferentially partitioning itself into domains of the solvent-philic block B. L phase unbinds to bilayers (B), $H_A$unbinds to cylindrical micellar aggregates (C) and the spherical phases $S_A^{BCC}$and S_A^{FCC}unbind to spherical micellar aggregates (S).

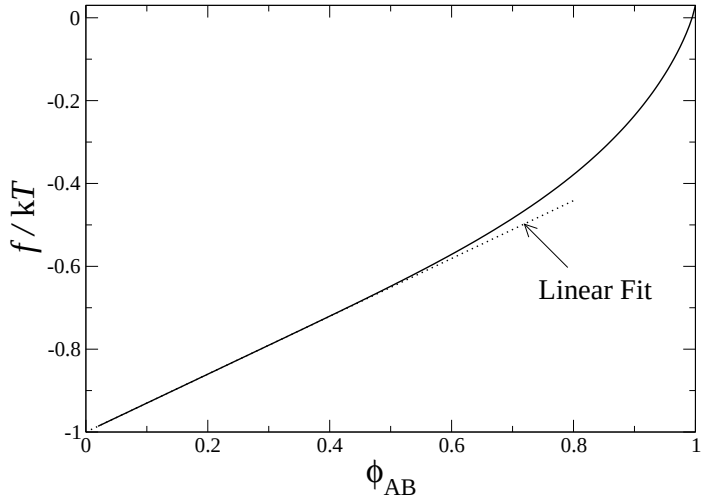

Figure 3.5: Variation of Helmholtz free energy per monomer f with respect to the concentration of the diblock AB ϕ_{AB}. The simulation is carried out for a diblock in a Θ solvent $\chi_{BS} = 0.5$ with lamellar symmetry. The parameters used for the simulation being $\chi_{AS} = 1$, $\chi_{AB} = 0.2$, $N = 100$, $f_B = 0.4$, and $b_A/b_B = 1$. The dotted line represents a linear fit in the dilute limit, and the slope of the linear fit corresponds to the constant exchange chemical potential at ϕ^{CAC} i.e., slope $= \Delta\mu^{CAC}$.

The phenomenon of unbinding is described for a lamellar phase L with $f_B = 0.4$ in a theta (Θ) solvent by plotting the Helmholtz free energy per monomer f *vs.* volume fraction of AB ϕ_{AB} in Figure 3.5. The vanishing interaction between individual bilayers is evident as the system maintains a constant slope or a constant exchange chemical potential $\Delta\mu^{CAC}$ calculated with $\phi_{AB} = \phi^{CAC}$ in the dilute limit. The

exchange chemical potential represents the cost of removing a single copolymer from a sea of dissolved copolymers AB in solvent S with chemical potentials μ_{AB} and μ_{S} , respectively. The concentration of copolymers dissolved in the solvent remains constant at ϕ^{CAC} for $\phi_{\mathrm{AB}} \geq \phi^{\mathrm{CAC}}$ and the rest of diblock copolymers $\phi_{\mathrm{AB}} - \phi^{\mathrm{CAC}}$ are present in the form of isolated aggregates in the dilute limit. This implies, for a system of isolated aggregates having any volume fraction of copolymers above ϕ^{CAC} the cost of removing the copolymers from the solvent remains pinned at $\Delta\mu^{\mathrm{CAC}}$.

In the case of a moderately selective solvent $\chi_{\mathrm{AS}} \approx 1$, ϕ^{CAC} is $\approx 10^{-8}$ which is extremely low as seen from data presented in Figure 3.4. Hence, in the dilute limit one can expect the formation of aggregates in the AB/S even at very low volume fractions of ϕ_{AB} for moderately selective solvents. This morphological transformation can also be seen by a simple scaling argument presented by de Gennes,[23] where the cost of dissolving a homopolymer of A in solvent S is found to scale as $\sim \exp(-\chi_{\mathrm{AS}} N_{\mathrm{A}})$, where N_{A} is the length of homopolymer A.

In swollen ordered phases there is no interaction between individual aggregates arranged on an ordered lattice. This is due to the exchange chemical potential $\Delta\mu$ is constant in this regime at $\Delta\mu^{\mathrm{CAC}}$. The free energy on a per monomer basis of this dilute phase f^{dil} is then given by

$$f^{\mathrm{dil}} = f^{\mathrm{CAC}} + \frac{1}{N}\Delta\mu^{\mathrm{CAC}} (\phi_{\mathrm{AB}} - \phi^{\mathrm{CAC}}). \tag{3.7.1}$$

Notice the constant slope $\Delta\mu^{\mathrm{CAC}}$ in the plot of f *vs.* ϕ_{AB} in Figure 3.5, which can also be calculated from Equations (3.1.6) and (3.1.7). In the above equation, the Helmholtz free energy of the homogeneous phase is represented by f^{CAC}. We are

considering the case where $\phi_{\mathrm{AB}} > \phi^{\mathrm{CAC}}$, and expect the volume fraction of dissolved AB to be ϕ^{CAC}. The intercept in Figure 3.6 is given by $f^{\mathrm{CAC}} - \phi^{\mathrm{CAC}} \Delta\mu^{\mathrm{CAC}}$. Note that we have considered the reference volume to be the volume occupied by a single solvent molecule which leads to $N_{\mathrm{S}} = 1$.

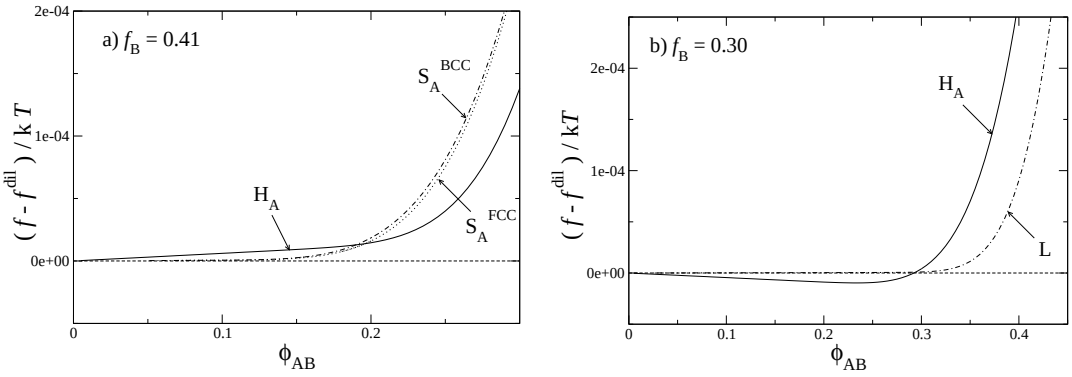

Figure 3.6: The unbinding transition is demonstrated in Figures (a) and (b). The Helmholtz free energy per monomer f is linearly dependent on ϕ_{AB}, as shown earlier in Figure 3.5, and the linear dependent part f^{dil}, presented in Equation (3.7.1), is subtracted from f in order to make the unbinding transition clear. In Figure (a) f^{dil} is calculated using $\Delta\mu^{\mathrm{CAC}}$ of the spherical micellar aggregates and in Figure (b) f^{dil} is calculated using $\Delta\mu^{\mathrm{CAC}}$ of bilayers. The simulation is carried out for a diblock in a Θ solvent $\chi_{\mathrm{BS}} = 0.5$. The parameters being $\chi_{\mathrm{AS}} = 1$, $\chi_{\mathrm{AB}} = 0.2$, $N = 100$, and $b_{\mathrm{A}}/b_{\mathrm{B}} = 1$.

The Helmholtz free energy per monomer of aggregates f^{dil} is used to determine the unbinding transition with the help of Helmholtz free energy per monomer of a periodic phase determined using PSCF. The point where the interactions between the individual bilayers B, cylindrical micellar aggregates C, or spherical micellar aggregates S in the periodic phases becomes non-existent is where one enters the regime of isolated aggregates B, C, or S. This transition from a concentrated periodic regime $\phi_{\mathrm{AB}} \sim 1$, where one expects periodic phases to exist, to a dilute regime $\phi_{\mathrm{AB}} << 1$,

where one expects isolated aggregates to exist, is termed as the unbinding transition.

The absence of interaction between individual micellar aggregates or bilayers leads to the linear dependence of f^{dil} on ϕ_{AB} with the slope proportional to the exchange chemical potential at CAC $\Delta\mu^{\mathrm{CAC}}$. Figures 3.6 (a) and (b) show that the periodic phases unbind continuously to their corresponding isolated aggregates counterparts. The core of the periodic structure determines the type of transition as one moves towards to the dilute regime upon the addition of solvent. One will expect an unbinding transition for phases having a solvent-philic corona or a solvent-phobic core.

In order to determine the unbinding transition for phases L, $\mathrm{H_A}$, $\mathrm{S_A^{BCC}}$, and $\mathrm{S_A^{FCC}}$the free energy of an aggregate morphology f^{dil} is subtracted from the Helmholtz free energy f of the respective periodic phases. The point at which the Helmholtz free energy f of a periodic phase is equal to that of the corresponding isolated aggregate phase f^{dil} is when the periodic phases transition into isolated aggregate phases. When the free energy difference $f - f^{\mathrm{dil}} = 0$ the periodic phases are highly swollen and can be described in terms of isolated aggregates. Figure 3.6 shows the lamellar phase in (b) unbinds at a higher value of volume fraction of AB ϕ_{AB} than the spherical phases presented in (a).

For even lower values of solvent-philic block composition f_{B} , we expect two-phase coexistence between a solvent-rich phase and a periodic structure with $\phi_{\mathrm{AB}} \sim 1$ with a solvent-phobic corona as the ordered phase can not swell indefinitely. This would lead to two-phase coexistence regimes between a homogeneous solvent-rich phase and a periodic phase with B block as the core. In the case of Figure 3.7 the subtraction of f^{dil} from f helps delineate the two phase coexistence for $f_{\mathrm{B}} = 0.16$ between the

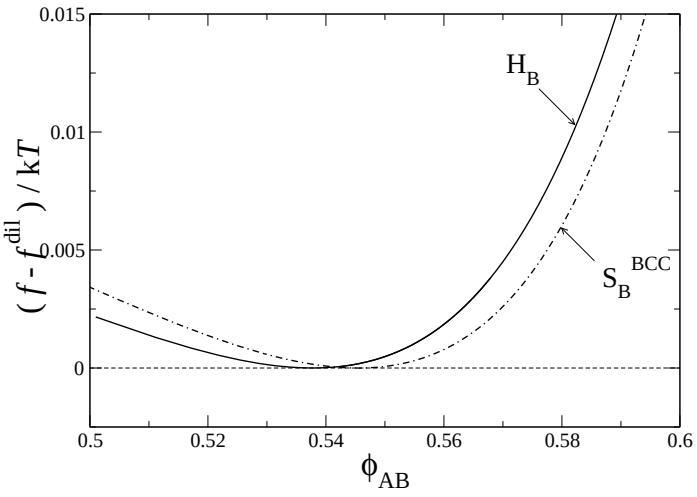

Figure 3.7: This figure shows the tendency of a diblock copolymer AB with low block composition of the solvent-philic block $f_{\mathrm{B}} = 0.16$ to macro phase separate into two phases. The simulation is carried out for a diblock in a Θ solvent $\chi_{\mathrm{BS}} = 0.5$. The parameters being $\chi_{\mathrm{AS}} = 1$, $\chi_{\mathrm{AB}} = 0.2$, $N = 100$, and $b_{\mathrm{A}}/b_{\mathrm{B}} = 1$.

disordered phase and the ordered phase $\mathrm{H_B}$, as well as two-phase coexistence between $\mathrm{H_B}$and $\mathrm{S_B^{BCC}}$. $\Delta\mu^{\mathrm{CAC}}$ of the bilayer phase is used to calculate f^{dil} with $\phi_{\mathrm{AB}} = \phi^{\mathrm{CAC}}$ and the line $f - f^{\mathrm{dil}} = 0$ in Figure 3.7 represents the common tangent construction with $f - f^{\mathrm{dil}} = 0$ representing the solvent rich homogeneous phase.

The phenomenon of unbinding can be captured by keeping track of the variation in the exchange chemical potential $\Delta\mu$ as a periodic phase begins to swell. The $\Delta\mu$ obtained for the periodic phases should tend towards the $\Delta\mu^{\mathrm{CAC}}$ obtained for their respective isolated aggregates counterparts for a particular block composition f_{B} . The aforementioned behavior is observed in all the periodic phases which can swell as seen in Figure 3.8, which are for the same parameters presented for $f_{\mathrm{B}} = 0.41$ in Figure 3.6 (a). In the spherical case, the $\Delta\mu$ obtained from periodic FCC and BCC lattices tend to the spherical micellar aggregate $\Delta\mu^{\mathrm{CAC}}$ as both $\mathrm{S_A^{FCC}}$and

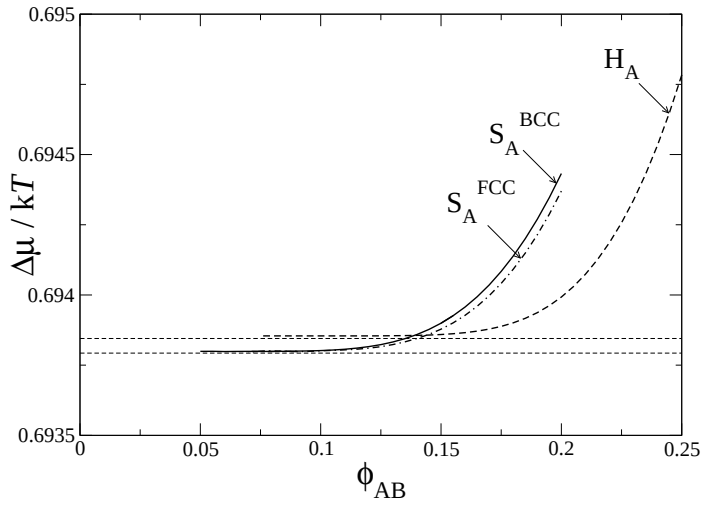

Figure 3.8: Comparison of SCFT calculations of isolated spherical and cylindrical micellar aggregates with their periodic swollen counterparts H_A, S_A^{BCC}, and S_A^{FCC}. The symbol dashed line represents results from the real space formulation of SCFT and other lines represents results from periodic formulation of SCFT. The calculation was carried out for AB/S system with $f_B = 0.41$, $N = 100$, $\chi_{AS} = 1.0$, $\chi_{BS} = 0.5$, $\chi_{AB} = 0.2$, and $b_A/b_B = 1$.

S_A^{BCC}lattices are indistinguishable when their lattice parameters begin to diverge. The agreement shown for the PSCF calculations with the real space formulation SCFT calculations, as seen in Figures 3.5, 3.6, and 3.8, demonstrates the accuracy of calculations performed using PSCF down to dilute solutions of AB even for $\phi_{AB} \approx 0.05$.

3.8 RPA Formalism

The random phase approximation (RPA) is a mean field theory used to determine the correlation functions for the concentration fluctuations in polymeric solutions. Consider the AB/S system with dimensionless number densities given for each monomer

as $\phi_{\rm A}(\mathbf{r})$, $\phi_{\rm B}(\mathbf{r})$, and $\phi_{\rm S}(\mathbf{r})$ at a certain position $\mathbf{r}$. The fluctuations of these number densities $\delta\phi_{\rm A}(\mathbf{r})$, $\delta\phi_{\rm B}(\mathbf{r})$, and $\delta\phi_{\rm S}(\mathbf{r})$ are characterized by the structure factor $\underline{\mathbf{S}}(\mathbf{r}, T)$ which is a three by three matrix. A symbol represented in bold corresponds to a vector, and a symbol represented in bold and underlined corresponds to a matrix in this section. Each element of the matrix is:

$$S_{\rm ij}(\mathbf{r} - \mathbf{r}', T) = \langle \delta\phi_i(\mathbf{r}) \delta\phi_j(\mathbf{r}') \rangle \,, \tag{3.8.1}$$

where i and j represent any one of the monomers A, B, or S. An incompressibility condition is imposed, which yields $\delta\phi_{\rm A}(\mathbf{r}) + \delta\phi_{\rm B}(\mathbf{r}) + \delta\phi_{\rm S}(\mathbf{r}) = 0$.

RPA is used to calculate the spinodal or the stability limit of the homogeneous solution for AB/S. The spinodal calculated using RPA corresponds to divergence of the structure factor $\underline{\mathbf{S}}(q, T)$. The structure factor is inversely proportional to the second derivative $\partial^2 f / \partial \phi_{\rm AB}^2$ of the free energy f . Hence, the spinodal is obtained when $\underline{\mathbf{S}}(q^*, T) \rightarrow \infty$, which occurs at some critical wave vector of modulus q^*.

This divergence of $\underline{\mathbf{S}}(q, T)$ is calculated by determining the divergence of the response function $\underline{\mathbf{R}}(q, T)$, which is related to $\underline{\mathbf{S}}(q, T)$ through

$$\underline{\mathbf{S}}(q, T) = {\rm k}T \, \underline{\mathbf{R}}(q, T). \tag{3.8.2}$$

$\underline{\mathbf{R}}(q, T)$ for a multi-block copolymer was determined by Cochran *et al.* .[169] We use the same method to determine the response function for the diblock copolymer for AB/S.

For a certain temperature, let $\boldsymbol{\phi}(\mathbf{r})$ denote the column vector consisting of dimen-

sionless number densities for each monomer as $\phi_{\mathrm{A}}(\mathbf{r})$, $\phi_{\mathrm{B}}(\mathbf{r})$, and $\phi_{\mathrm{S}}(\mathbf{r})$. Define an order parameter $\psi_i(\mathbf{r}) = \langle \phi_i(\mathbf{r}) - \langle \phi_i(\mathbf{r}) \rangle \rangle$. The linear response of $\boldsymbol{\psi}(\mathbf{r})$ to an external chemical potential $\boldsymbol{\mu}^{\mathrm{e}}(\mathbf{r})$ for a non-interacting ideal gas of chains can be expressed in terms of the response function $\underline{\mathbf{R}}(\mathbf{r} - \mathbf{r}')$[22] as

$$\boldsymbol{\psi}(\mathbf{r}) = -\int \mathrm{d}\mathbf{r}' \underline{\mathbf{R}}(\mathbf{r} - \mathbf{r}') \boldsymbol{\mu}^{\mathrm{e}}(\mathbf{r}). \tag{3.8.3}$$

The interactions are expressed at mean-field level with the use of an effective potential $\boldsymbol{\mu}^{\mathrm{eff}}(\mathbf{r})$. The domain is shifted to q space or the Fourier domain as $\underline{\mathbf{R}}(\mathbf{q})$ is directly related to the light scattering intensity. The order parameter can be expressed as

$$\boldsymbol{\psi}(\mathbf{q}) = \underline{\mathbf{R}}(\mathbf{q}) \boldsymbol{\mu}^{\mathrm{eff}}(\mathbf{r}). \tag{3.8.4}$$

$\boldsymbol{\mu}^{\mathrm{eff}}(\mathbf{r})$ is expressed in terms of the interaction potential $\mathrm{k}T\, \underline{\boldsymbol{\chi}} \psi(\mathbf{q})$, and the Lagrange multiplier field $\boldsymbol{\xi}$. It is given by

$$\boldsymbol{\mu}^{\mathrm{eff}}(\mathbf{q}) = \boldsymbol{\mu}^{\mathrm{e}}(\mathbf{q}) + \mathrm{k}T\, \underline{\boldsymbol{\chi}} \boldsymbol{\psi}(\mathbf{q}) + \boldsymbol{\xi}. \tag{3.8.5}$$

The Lagrange multiplier field is introduced to enforce incompressibility. $\boldsymbol{\xi}$ has the form $\lambda\epsilon$, where λ is a scalar quantity and ϵ is a column vector $[1, 1, 1]^{\mathrm{T}}$. λ is determined from the incompressibility constraint $\delta\phi_{\mathrm{A}}(\mathbf{r}) + \delta\phi_{\mathrm{B}}(\mathbf{r}) + \delta\phi_{\mathrm{S}}(\mathbf{r}) = 0$. This yields

$$\lambda = -\frac{\epsilon^{\mathrm{T}} \underline{\mathbf{R}} \left(\boldsymbol{\mu}^{\mathrm{e}} + \mathrm{k}T\, \underline{\boldsymbol{\chi}} \boldsymbol{\phi} \right)}{\epsilon^{\mathrm{T}} \underline{\mathbf{R}} \epsilon}. \tag{3.8.6}$$

Inserting the value of λ into Equation (3.8.4) for any temperature T, we obtain

$$\boldsymbol{\psi}(\mathbf{q},T) = -\left(\left(\underline{\tilde{\mathbf{R}}}^{0}(\mathbf{q},T)\right)^{-1} + \mathrm{k}T\,\underline{\boldsymbol{\chi}}(T)\right)^{-1}\boldsymbol{\mu}^{\mathrm{e}}(\mathbf{q}). \tag{3.8.7}$$

Here, $\underline{\tilde{\mathbf{R}}}^{0}(\mathbf{q},T)$ represents the response function of an incompressible melt with $\underline{\boldsymbol{\chi}}(T)$ being a null matrix. It is given by $\underline{\tilde{\mathbf{R}}}^{0}(\mathbf{q},T) = \underline{\tilde{\mathbf{R}}}(\mathbf{q},T)(\underline{\mathbf{I}}-(\epsilon\epsilon^{\mathrm{T}}\underline{\tilde{\mathbf{R}}}(\mathbf{q},T)))/(\epsilon^{\mathrm{T}}\underline{\tilde{\mathbf{R}}}(\mathbf{q},T)\epsilon)$. By comparing Equations (3.8.4) and (3.8.7) Cochran *et al.* [169] arrived at the response function as

$$\underline{\tilde{\mathbf{R}}}(\mathbf{q},T) = \left(\left(\underline{\tilde{\mathbf{R}}}^{0}(\mathbf{q},T)\right)^{-1} + \mathrm{k}T\,\underline{\boldsymbol{\chi}}(T)\right)^{-1}. \tag{3.8.8}$$

Using the relation between $\underline{\tilde{\mathbf{R}}}(\mathbf{q},T)$ and $\underline{\tilde{\mathbf{S}}}(\mathbf{q},T)$ presented earlier in Equation (3.8.2) to yield

$$\underline{\tilde{\mathbf{S}}}(\mathbf{q},T) = \left(\left(\underline{\tilde{\mathbf{S}}}^{0}(\mathbf{q},T)\right)^{-1} + \underline{\boldsymbol{\chi}}(T)\right)^{-1}. \tag{3.8.9}$$

In our RPA algorithm we determine $\left(\underline{\tilde{\mathbf{S}}}^{0}(\mathbf{q},T)\right)^{-1} + \underline{\boldsymbol{\chi}}(T)$. This matrix has to be singular or the determinant must be zero so that $\underline{\tilde{\mathbf{S}}}(\mathbf{q},T)$ diverges. This condition is determined by calculating the value of q^{*} that yields an eigenvalue of zero. This leads to the second derivative of free energy being zero.

In order to obtain the spinodal, we first estimate the structure factor by calculating $\underline{\tilde{\mathbf{S}}}^{0}(\mathbf{q},T)$. This requires the calculation of the structure factor of non-interacting Gaussian chains for each block of AB. This is obtained from expressions given by Cochran *et al.* [169] for the diblock AB. For the solvent S, we treated it as a point particle with $qR_{\mathrm{g}} \rightarrow 0$ yielding

$$S_{ii}(\mathbf{q}) = \frac{\bar{\phi}_{\mathrm{S}}N_{\mathrm{S}}}{v}, \tag{3.8.10}$$

where $\bar{\phi}_{\mathrm{S}}$ is the average volume fraction of the solvent, N_{S} is the size of the solvent S, and v is the reference volume.

After enforcing incompressibility $\left(\underline{\tilde{\mathbf{S}}}^{0}(\mathbf{q},T)\right)^{-1}$ is determined with $\underline{\boldsymbol{\chi}}(T)$ being a null matrix. The interaction potential matrix $\underline{\boldsymbol{\chi}}(T)$ is added in order to calculate $\underline{\tilde{\mathbf{S}}}(\mathbf{q},T)$, and the eigenvalues are determined in a sweep of q. The value of q^{*} is determined when the eigenvalue of $\left(\underline{\tilde{\mathbf{S}}}^{0}(\mathbf{q},T)\right)^{-1}+\underline{\boldsymbol{\chi}}(T)$ is zero.

Upon imposing incompressibility the structure factor matrix $\underline{\tilde{\mathbf{S}}}(\mathbf{q},T)$ is singular in nature. One of the eigenvectors x_0 is a vector of the form $[1,1,1]^{\mathrm{T}}$. This yields $\left(\underline{\tilde{\mathbf{S}}}(\mathbf{q},T)\right)^{-1}x_0 = Bx_0$, which diverges as $B \rightarrow \infty$ due to incompressibility. The eigenvalue related to incompressibility is neglected during the calculation of q^{*}.

3.9 Flory-Huggins Theory

The Flory-Huggins theory of homogeneous mixtures is a special case of SCFT, which can be recovered by using SCFT to calculate the free energy of homogeneous phase. Some aspects of both phase behavior and self-assembly in the systems of interest can be understood by considering an appropriate form of Flory-Huggins.

In Chapter 5, we consider the phase behavior of non-dilute solutions of AB diblock copolymers in selective solvent. Flory-Huggins theory can describe parts of the phase diagram in which the system phase separates into two homogeneous phases. This behavior is expected for copolymers containing a very small solvent-philic block, since the copolymer becomes a solvent-phobic homopolymer in the limit $f_{\mathrm{B}} \rightarrow 0$ of a vanishingly small solvent-philic block.

The Helmholtz or Gibbs free energy of mixing per monomer for a homogeneous

solution of AB diblock copolymer in solvent S may be written as a sum

$$\frac{f}{\mathrm{k}T} = \phi_{\mathrm{S}}\ \ln(\phi_{\mathrm{S}}\ ) + \frac{\phi_{\mathrm{AB}}}{N}\ln(\phi_{\mathrm{AB}}\ ) + \chi_{\mathrm{eff}}\phi_{\mathrm{AB}}\ \phi_{\mathrm{S}} \tag{3.9.1}$$

in which

$$\chi_{\mathrm{eff}} \equiv \chi_{\mathrm{AS}}\ f_{\mathrm{A}}\ + \chi_{\mathrm{BS}}\ f_{\mathrm{B}}\ - \chi_{\mathrm{AB}}\ f_{\mathrm{A}}\ f_{\mathrm{B}} \tag{3.9.2}$$

is an effective interaction parameter that takes into account interactions among all three monomer types. The limit of stability with respect to phase separation into homogeneous phases (the Flory-Huggins spinodal) is given by using χ_{eff} in the classical Flory-Huggins expression for the spinodal

$$\chi_{\mathrm{eff}}(\ \phi_{\mathrm{AB}}\ ) = \frac{1}{2}\left(\frac{1}{\phi_{\mathrm{AB}}\ N} + \frac{1}{\phi_{\mathrm{S}}}\right). \tag{3.9.3}$$

The critical point occurs at a composition

$$\phi^{\mathrm{c}}_{\mathrm{AB}} = \frac{1}{\sqrt{N}+1}, \tag{3.9.4}$$

exactly as in a solution of homopolymer in poor solvent. In Chapter 5, we present phase portraits for systems with fixed values for the χ parameters and overall chain length N, but variable values of f_{B} and ϕ_{AB}, in the f_{B} - ϕ_{AB} plane. The above expressions can be solved for f_{B} to locate the critical point in this plane.

A somewhat different form of Flory-Huggins theory is used in Section 4.2 as a highly simplified theory of micellization. There, we consider an approximation in which micellization is treated as coexistence of two phases, one of which represents

the core of the micelle and the other of which represents the solvent-rich phase outside of each micelle.

3.10 Summary

In this chapter we have described the two formulations of SCFT used in the study of phase behavior of the binary system of AB/S. The numerical accuracy of PSCF is compared with a spectral formulation with Anderson mixing developed by Matsen.[1] The rate of convergence of both schemes are found to be similar. An analysis of the ratio of the domain size relative to the interfacial width points to PSCF simulation becoming intractable for values of $\chi_{\mathrm{AS}} > 1.5$. An introduction to micelle thermodynamics is provided with the procedure to estimate ϕ^{CAC}, and the unbinding transformation noticed in AB/B blends is found to occur in AB/S system as well.

The unbinding transition is studied by combining both formulations of SCFT, with PSCF being found to be accurate even for low volume fractions of diblock copolymer AB $\phi_{\mathrm{AB}} \approx 0.05$. From independent SCFT calculations using both formulations of SCFT we test the numerical accuracy of our approach. To obtain numerically accurate calculations in the dilute regime ($\phi_{\mathrm{AB}} \lesssim 0.3$) using PSCF, the number of basis functions required are at least 5 times larger than those used by Suo *et al.* .[90] Utilizing both formulations of SCFT we study how the morphological transitions of isolated aggregates are intertwined with phase transitions of the ordered phases which has not been studied before.

RPA is a powerful tool to estimate the stability domains of the disordered phase. The spinodals generated by RPA, with the information of critical wave vector of

modulus q^*, adds further insight to the phase diagrams generated using SCFT.

We have implemented a wide array of tools to systematically study the phase behavior of the binary system of AB/S. Real space formulation of SCFT is used to study morphology transformations between isolated aggregates, a pseudo-spectral formulation of SCFT is used to simulate ordered phases, and spinodals for the disordered phase are generated using RPA. The real space formulation of SCFT is also used to study micellization kinetics of AB/S later in Chapter 6.

CHAPTER 4

Self-Assembly in Dilute Solution

In this chapter, I use SCFT to study equilibrium properties of isolated aggregates in dilute solutions of diblock copolymers in a small-molecule solvent. Section 4.1 examines the regions of stability of spherical micelle, cylindrical micelle and bilayer aggregate in systems with varying copolymer composition and varying solvent-polymer interaction parameters. Section 4.2 presents a highly simplified model of micellization that is useful for interpreting subsequent results. Section 4.3 examines how the critical aggregation concentration (CAC) depends upon the length of the solvent-phobic block and the solvent selectivity. Section 4.4 discusses the penetration of solvent into the micelle core. In Section 4.5, I discuss the dependence of micelle size on solvent selectivity, and show how SCFT can be used to identify a critical value of the solvent-

core interaction required to form micelles, corresponding to the experimental critical micelle temperature (CMT). Section 4.6 discusses how changes in solvent selectivity change the structure of the solvent-philic corona. All of the SCFT results presented in this chapter were obtained using the real space implementation of SCFT discussed in Section 3.4. Cartesian, cylindrical and spherical coordinate systems are used to describe bilayers, cylindrical micelles, and spherical micelles, respectively.

Throughout this chapter, as elsewhere in this thesis, we use a subscript S to denote solvent, A to denote the solvent-phobic (core) block, and B to denote the solvent-philic (or corona) block of the diblock copolymer. The model studied here is controlled by 5 independent chemical parameters: three Flory-Huggins interaction parameters, χ_{AB} , χ_{AS} , χ_{BS} , the volume fraction f_{B} of the corona block and the diblock copolymer length N. We use a convention in which the volume of a solvent molecule is taken to be the reference volume used to define the interaction parameters. The parameter N is thus more precisely described as the ratio of polymer volume to solvent volume.

This full parameter space is too large to be exhaustively studied. To reduce the problem to a more manageable size, we focus in this and following chapters primarily on systems in which χ_{BS} is usually assigned a value $\chi_{\mathrm{BS}} = 0.4$ that is typical of many a polymer in good solvent.[170] Much of the data shown in this chapter uses a fixed chain length of $N = 100$ and a fixed value $\chi_{\mathrm{AB}} = 0.2$, giving $\chi_{\mathrm{AB}} N = 20$. For longer chain lengths, the value of $\chi_{\mathrm{AB}} N$ is maintained at a constant value of $\chi_{\mathrm{AB}} N = 20$. This choice yields copolymers that would be modestly segregated in the absence of solvent in the case of nearly symmetric diblock copolymers. We focus in this chapter primarily upon how behavior varies with changes in the interaction

χ_{AS} between the solvent and solvent-phobic block, which is the driving force for the formation of aggregates, and on the volume fraction f_B of the solvent-philic block.

4.1 Spheres, Cylinders and Bilayers

SCFT can be used to locate transitions between regions in which spherical micelles (S), cylindrical micelles (S), and bilayers (B) are stable in dilute solution, as discussed in Section 3.6. For each set of values for the chemical parameters (of the interaction parameters, f_B and N), we calculate values of the CAC for each type of aggregate, and identify the most stable state as the one with the lowest CAC.

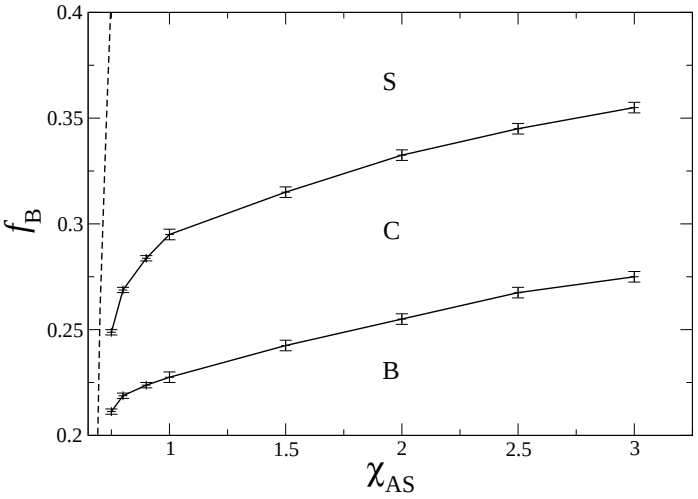

Figure 4.1: Regions of stability of bilayer B, cylinder C, and spherical S morphologies for dilute solutions of diblock copolymer AB in selective solvent S for various block compositions f_B plotted *vs.* the interaction parameter χ_{AS} that controls solvent selectivity. The other parameters used for these simulations are $\chi_{BS} = 0.4$, $\chi_{AB} = 0.2$, and $N = 100$. The dashed line represents the critical value of χ_{AS}, corresponding to the experimental critical micelle temperature, below which no aggregates form.

Figure 4.1 shows the resulting regions of stability of spherical (S), cylindrical (C)

and bilayer (B) aggregates in systems with varying values of f_B = 0.2 - 0.4 (corona block fraction) and χ_{AS} but fixed values of $\chi_{BS} = 0.4$, $N = 100$ and $\chi_{AB} = 0.2$. A few trends are immediately obvious. The B $\rightarrow$ C and C $\rightarrow$ S transitions occur at much lower values of f_B in a selective solvent than in the neat diblock copolymer. In a pure diblock copolymer, the bilayer (lamellar) phase would be centered around at $f_B = 0.5$, and the relevant $H_A$hexagonal cylinder and S_A^{BCC}BCC sphere phases would occur at $f_B > 0.5$. This shift to smaller values of f_B in solvent compared to neat copolymer is an easily understandable result of the asymmetry induced by selective swelling of the solvent-philic corona block. We also note, however, that the boundaries shift to lower values of f_B as χ_{AS} decreases (decreasing solvent selectivity), with a particularly sharp downward shift in the region of modestly selective solvent between $\chi_{AS} = 0.5$ (Θ solvent for A) and $\chi_{AS} = 1$.

For each value of f_B , there is a minimum value of χ_{AS} below which no aggregates can form. This critical value, which corresponds to the experimental critical micelle temperature, is shown by a dashed line in the figure. The C $\rightarrow$ S transition exhibit a particularly sharp downward shift near the CMT, yielding a much larger region of stability for spheres and a shrunken region of stability for cylinders near the CMT.

Figure 4.2 shows the dependence of the B $\rightarrow$ C and C $\rightarrow$ S transitions upon the solvent-corona interaction parameter χ_{BS} over a range of values that range from a unusually good solvent ($\chi_{BS} = 0.2$) to a Θ solvent ($\chi_{BS} = 0.5$), for systems with $\chi_{AS} = 1.0$, $N = 100$ and $\chi_{AB} = 0.2$. Both boundaries shift to lower values of f_B with increasing solvent quality, or decreasing χ_{BS} . This shift is presumably a result of the increased stretching of the corona blocks with increasing solvent quality, which

tends to favor structures with a larger interfacial curvature in order to increase the space available to the corona block. The results obtained for transitions between periodic lamellar and cylindrical phases in the dilute limit match the B $\rightarrow$ C transitions observed in Figure 4.2.

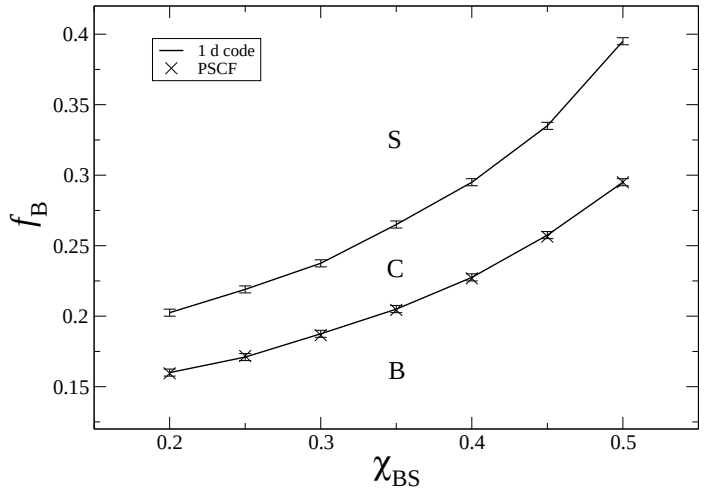

Figure 4.2: The regions of stability of bilayer B, cylinder C, and spherical S morphologies for dilute solutions of diblock copolymer AB in selective solvent S , in the plane of copolymer composition f_B plotted *vs.* good solvent characteristic χ_{BS} . The parameters considered for the simulation are $\chi_{AS} = 1$, $\chi_{AB} = 0.2$, $N = 100$, and $\nu = 1$. The transitions between lamellar and cylindrical periodic phases are determined using PSCF. The two formulations of SCFT, PSCF and real space implementation of SCFT (1 d code) show good agreement.

4.2 A Minimal Model of Micellization

Subsequent sections of this chapter present SCFT predictions for how the critical aggregation concentration (CAC) and micelle structure for spherical micelles vary with χ_{AS} and other parameters, for spherical micelles. Most of these results shown

later are for systems with modest values of χ_{AS} , $0.5 < \chi_{AS} < 3.0$, for which there can be significant solvent penetration of the core. Earlier work on simple models of micellization (discussed in Chapter 2) have tended to ignore this effect. Before discussing our numerical results it is thus useful to consider a highly simplified analytic treatment of micellization that allows for solvent penetration into the micelle core.

The simplest possible view of micellization is as a kind of two-phase coexistence, between a polymer-rich phase that represents the core of a micelle and solvent-rich phase that represents the solvent outside of each micelle. The conditions for coexistence requires that we equate the chemical potentials of the solvent and the polymer species in these two phases. In what follows, we approximate these chemical potentials with a simple variant of Flory-Huggins theory. The model can be used to obtain simple predictions for the volume fraction of solvent in the micelle core, and for ϕ^{CAC}, which we identify with the volume fraction of copolymer dissolved in the solvent-rich phase.

The solvent-philic block of a copolymer is immersed in a solvent-rich phase, whether the copolymer is incorporated into a micelle (in which case this block forms part of the micelle corona) or dissolved as a free molecule in the surrounding solvent. To simplify the theory as much as possible, we thus ignore the corona block, and approximate the chemical potentials for both components by those of a mixture of solvent with a homopolymer of length $N_A = f_A N$ equal to the length the solvent-phobic block of the copolymer.

Let ϕ_A and ψ_A represent the volume fractions of polymer in the solvent-rich and polymer-rich phases of this hypothetical two-phase system, respectively. Let $\phi_S =$

$1-\phi_{\rm A}$ and $\psi_{\rm S}=1-\psi_{\rm A}$ represent the corresponding solvent volume fractions. By using Flory-Huggins expressions for the chemical potentials of both components, we obtain the coexistence conditions

$$\chi_{\rm AS}N_{\rm A}\phi_{\rm S}^2-(N_{\rm A}-1)\phi_{\rm S}+\ln(\phi_{\rm A})=\chi_{\rm AS}N_{\rm A}\psi_{\rm S}^2-(N_{\rm A}-1)\psi_{\rm S}+\ln(\psi_{\rm A}) \qquad (4.2.1)$$

$$\chi_{\rm AS}\phi_{\rm A}^2+(1-\frac{1}{N_{\rm A}})\phi_{\rm A}+\ln(\phi_{\rm S})=\chi_{\rm AS}\psi_{\rm A}^2+(1-\frac{1}{N_{\rm A}})\psi_{\rm A}+\ln(\psi_{\rm S}). \qquad (4.2.2)$$

We hereafter focus on the limit $N_{\rm A}\gg 1$, in which we can ignore the terms proportional to $1/N_{\rm A}$ in Equation (4.2.2) and the terms that are independent of $N_{\rm A}$ in Equation (4.2.1). In the limit $\phi_{\rm A}\ll 1$ of a very low volume fraction of polymer in the solvent-rich phase (low $\phi^{\rm CAC}$), we may set the left side of Equation (4.2.2) to zero (thus setting the solvent chemical potential to that of pure solvent). We obtain a nonlinear equation

$$0\simeq\chi_{\rm AS}\psi_{\rm A}^2+\psi_{\rm A}+\ln(\psi_{\rm S}), \qquad (4.2.3)$$

for the volume fraction $\psi_{\rm S}$ of solvent in the micelle core as a function of $\chi_{\rm AS}$. In the same limit, the above model yields a critical aggregation concentration

$$\phi^{\rm CAC}=\psi_{\rm A}\exp\left(-f(\chi_{\rm AS})N_{\rm A}\right), \qquad (4.2.4)$$

where

$$f(\chi_{\rm AS})=\chi_{\rm AS}\,\psi_{\rm S}^2-1-\psi_{\rm S}. \qquad (4.2.5)$$

In the limit $\chi_{\rm AS}\gg 1$ in which S is a non-solvent for A, these results reduce to

$\psi_S \simeq \exp(-\chi_{AS})$ and

$$\lim_{\chi_{AS} \gg 1} \phi^{CAC} \simeq \exp[-(\chi_{AS} - 1)N_A] . \tag{4.2.6}$$

For modest values of χ_{AS}, Eq. (4.2.4) suggests that $\ln \phi^{CAC}$ should decrease approximately linearly with chain length, but with a pre-factor $f(\chi_{AS})$ that is not a simple linear function of χ_{AS}, and that (for small molecule solvents) is effected by solvent penetration into the core.

4.3 Critical Aggregation Concentration

Figure 4.3 shows numerical SCFT predictions for the variation of $\ln \phi^{CAC}$ plotted *vs.* the solvent selectivity χ_{AS} for cylindrical micelles in systems with fixed chain length $N = 100$ and composition $f_B = 0.26$, for fixed $\chi_{BS} = 0.4$ and $\chi_{AS} = 0.2$. The critical concentration drops dramatically as χ_{AS} is increased. As expected, $\ln \phi^{CAC}$ decreases as roughly $-\chi_{AS} N_A$ for sufficiently strongly selective solvent, $\chi_{AS} > 2$. A weaker dependence on χ_{AS} is seen for more weakly selective solvents, with $0.5 < \chi_{AS} < 2$, which allow significant penetration of solvent into the core.

The dotted line shows the prediction of the highly simplified theory developed in Section 4.2. This theory underestimates the absolute magnitude of ϕ^{CAC} by several orders of magnitude. It does, however, yield reasonably good predictions for the χ_{AS} dependence of $\ln \phi^{CAC}$, as characterized by the slope in the plot of $\ln \phi^{CAC}$ vs. χ_{AS}. This success suggests that the change in slope is predominantly a result of a shift in copolymer chemical potential caused by solvent penetration into the core.

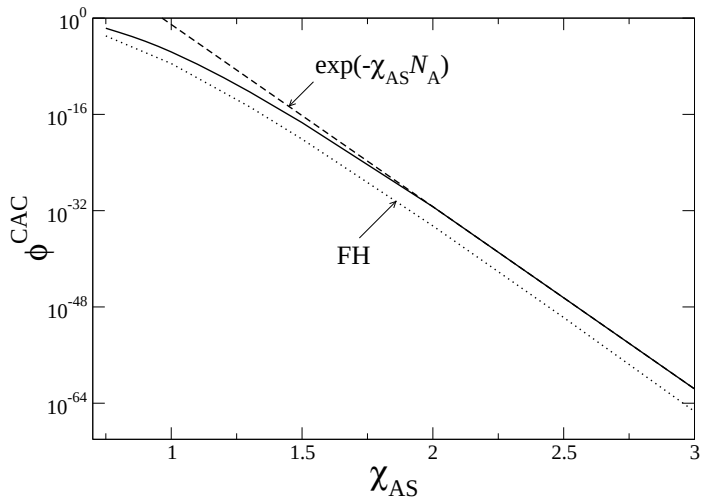

Figure 4.3: CAC (in volume fraction) of the diblock AB for a cylindrical aggregate is plotted *vs.* the selectivity of the solvent $\chi_{\rm AS}$. This data was presented earlier in Figure 3.4 (a). The dotted line represents an analytical expression (4.2.4) derived from Flory-Huggins theory mentioned in the text. The dashed line shows an exponential decrease $\phi_{\rm AB} \sim \exp(-\chi_{\rm AS} N_{\rm A})$. The calculation is carried out for $f_{\rm B} = 0.26$, $N = 100$, $\chi_{\rm BS} = 0.4$, and $\chi_{\rm AB} = 0.2$.

In the case of a polymeric solvent S, $\phi^{\rm CAC}$ is found to scale as $\sim \exp(-\chi_{\rm AS} N_{\rm A})$, where $N_{\rm A}$ is the core block length. The basis behind this scaling is that, $\chi_{\rm AS} N_{\rm A}$ represents the enthalpic cost of dissolving the solvent phobic block A in solvent S. However, the variation of $\phi^{\rm CAC}$ for a small molecule solvent S is found to be $\phi^{\rm CAC} \sim \exp(-(\alpha\chi_{\rm AS} - \beta)N_{\rm A})$ where $\alpha \rightarrow 1$ and $\beta \rightarrow 1$ gradually as one approaches the limit of $\chi_{\rm AS} >> 1$ (not shown).

Figure 4.4 shows SCFT predictions for the dependence of $\phi^{\rm CAC}$ on the core block length for systems with a fixed value of $\chi_{\rm AS} = 1$. The results shown there are for spherical micelles with $f_{\rm B} = 0.35$, $\chi_{\rm BS} = 0.4$, $\chi_{\rm AB} = 0.2$, over a range of values of N. The dashed line in this figure shows a fit of the results to a function $\phi^{\rm CAC} \propto \exp(-fN_{\rm A})$, with $f = 0.19$. This result confirms that, even for relatively

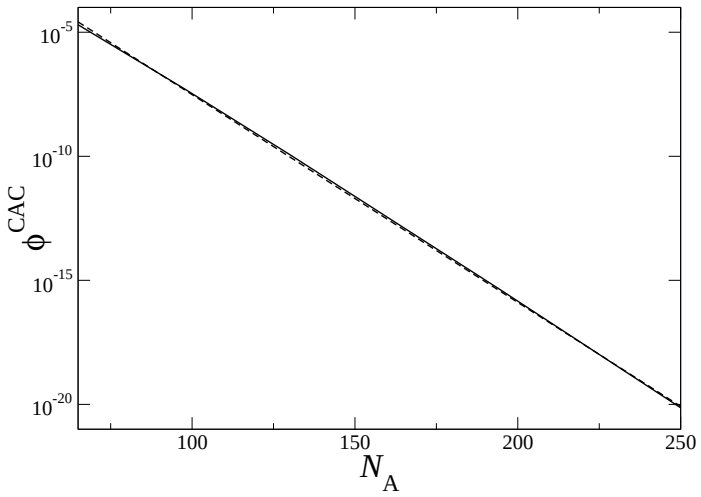

Figure 4.4: ϕ^{CAC} for the binary system AB/S is plotted *vs.* the core chain length N_{A} . The parameters used for the calculation are $f_{\mathrm{B}} = 0.35$, $\chi_{\mathrm{AS}} = 1.0$, $\chi_{\mathrm{BS}} = 0.4$, $\chi_{\mathrm{AB}} = 0.2$, and $\nu = 1$. The dotted line represents an analytical expression (4.2.4) derived from Flory-Huggins theory mentioned in the text. The dashed line represents a fit of the form $\phi^{\mathrm{CAC}} \sim \exp(-fN_{\mathrm{A}})$ with $f = 0.19$.

small value of χ_{AS} , $\ln \phi^{\mathrm{CAC}}$ decreases as $-f(\chi_{\mathrm{AS}})N$, with an almost perfectly linear dependence on N, as suggested by (4.2.4).

The simplified theory of Section 4.2, using Equations (4.2.2) and (4.2.5), predicts a value of $f = 0.22$ for $\chi_{\mathrm{AS}} = 1$, in reasonable agreement with Figure 4.4. It thus appears that this simple Flory-Huggins theory can provide a reasonable quantitative estimate of the slope $f = \mathrm{d} \ln \phi^{\mathrm{CAC}} / \mathrm{d}N_{\mathrm{A}}$ at modest values of χ_{AS} , but not for the absolute magnitude of ϕ^{CAC} .

In the example shown in Figure 4.4, the solvent volume fraction in the core of the micelle varies from 0.34 for $N_{\mathrm{A}} = 65$ to 0.32 for $N_{\mathrm{A}} = 260$. As discussed in more detail below, the solvent penetration does not vary much with N_{A} , and is mainly dependent on the value of χ_{AS} . The solubility of copolymer in solvent, or ϕ^{CAC} ,

instead varies over 15 orders of magnitude when N_{A} is increased from $N_{\mathrm{A}} = 50$ to $N_{\mathrm{A}} = 260$.

4.4 Core Composition

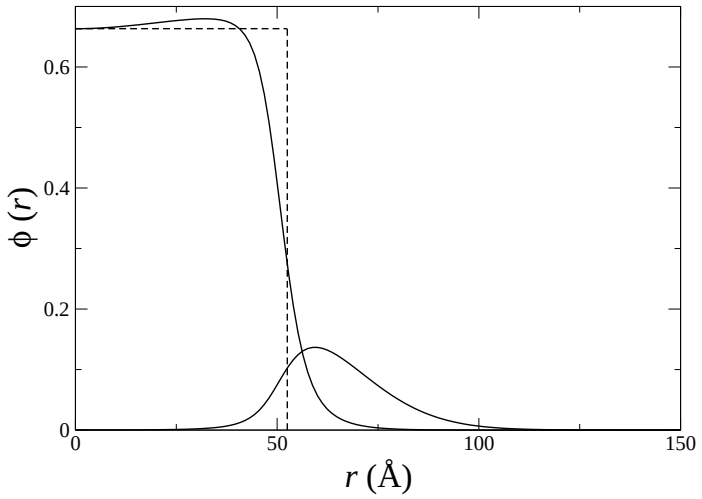

Figure 4.5: Volume fractions of A and B segments for a spherical micelle with $f_{\mathrm{B}} = 0.35$, $N = 100$, $\chi_{\mathrm{AS}} = 1$, $\chi_{\mathrm{BS}} = 0.4$. Distances are calculating using statistical segment lengths $b_{\mathrm{A}} = 6$Å, and $b_{\mathrm{B}} = 6$Å.

Figure 4.5 shows an example of the volume fraction profiles of A (core) and B (corona) monomers for a spherical micelle as functions of distance from the center of the micelle. In this and all subsequent plots of micelle structure we show the structure of a micelle that coexists with a concentration ϕ^{CAC} of dissolved unimers, as would be true whenever the total polymer concentration exceeds ϕ^{CAC}. In this example, the core-block volume fraction $\phi_{\mathrm{A}}(r)$ exhibits a reasonably well defined central region in which the volume fractions of core and solvent are almost constant, and in which the volume fraction of the corona block is negligible. This is surrounded by a narrow

interfacial region in which all three components intermix, outside of which there is a corona region containing solvent and B segments but almost no A segments, and a surrounding phase of nearly pure solvent.

The dashed lines in this figure show how we define a volume fraction $\phi_{\rm A}^{\rm core}$ for A segments in the micelle core, and a corresponding core radius $R_{\rm core}$. The volume fraction $\phi_{\rm A}^{\rm core}$ is simply defined be the value of $\phi_{\rm A}(r)$ at $r = 0$, the center of the micelle. In this example $\phi_{\rm A}^{\rm core} = 0.66$. The corresponding volume fraction of solvent at the center of the micelle is thus approximately 0.34. We define a corresponding core radius $R_{\rm core}$, also shown by the dashed line, by requiring that $\phi_{\rm A}^{\rm core}$ times the volume $4\pi R_{\rm core}^3/3$ of a sphere of radius $R_{\rm core}$ equals the integrated excess volume of A segments in the micelle, or

$$\frac{4}{3}\pi R_{\rm core}^3 \phi_{\rm A}^{\rm core} = M^{\rm ex}\, N_{\rm A}\, v, \tag{4.4.1}$$

where $M^{\rm ex}$ is the excess number of polymers in the micelle, which we refer to as the aggregation number. The dependence of $M^{\rm ex}$ and $R_{\rm core}$ upon the degree of solvent selectivity is analyzed in Section 4.5.

Figure 4.6 shows how the volume fraction $\phi_{\rm A}(r)$ of A segments varies with changes in $\chi_{\rm AS}$. Note that as $\chi_{\rm AS}$ (solvent selectivity) decreases: (i) the volume fraction $\phi_{\rm A}^{\rm core}$ decreases, (ii) the core radius decreases, and (iii) the core interface becomes broader. We define a critical value of $\chi_{\rm AS}$, or CMT, in the next section as the value at which the aggregation number extrapolates to zero. For this system, the apparent CMT occurs at $\chi_{\rm AS} = 0.72$. Over the range of values of $\chi_{\rm AS}$ shown here, we can identify the core of the micelle with the region in which $\phi_{\rm A}(r)$ is nearly constant. Very close

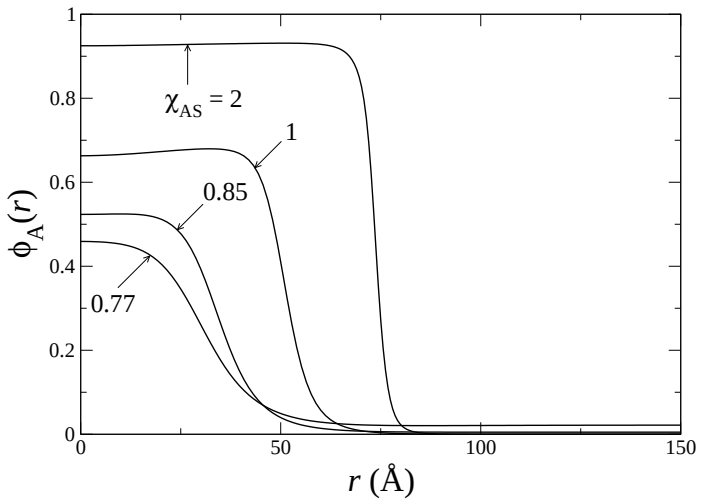

Figure 4.6: Volume fractions of A segments *vs.* radius for spherical micelle for several values of χ_{AS} . All other parameters are the same as in Figure 4.5: $f_B = 0.35$, $N = 100$, $\chi_{AS} = 1$, $\chi_{BS} = 0.4$, and $b_A = b_B = 6$Å.

to the CMT, we expect the interfacial region to begin penetrating to the center of the micelle, due to the steady decrease in core radius and the increase in interfacial width, and thus destroy the distinction between the micelle core and interfacial regions. We have, however, thus far been unable to obtain converged solutions to SCFT in this critical regime of very small, weakly segregated micelles.

Figure 4.7 shows how the volume fraction ϕ_A^{core} of solvent-phobic A monomers at the micelle center varies with changes in χ_{AS} , for micelles with the same value for all other parameters as those used in Figure 4.6. The vertical dashed line is our estimate of the critical value of χ_{AS} below which no micelles exist. The solvent penetration ϕ_S^{core} can be obtained from the incompressibility condition $\phi_S^{core} = 1 - \phi_A^{core}$, because the volume fraction of B segments is negligible in the center of the core.

The dot-dashed line in Figure 4.7 shows the prediction of the Flory-Huggins theory

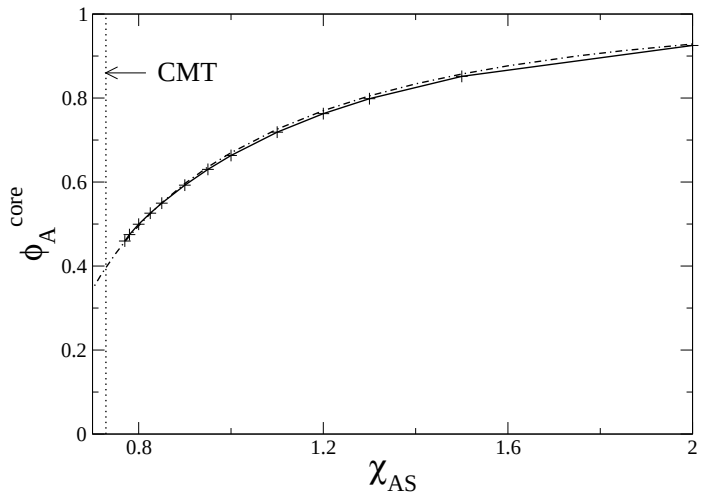

Figure 4.7: Dependence of volume fraction of the core block $\phi_{\mathrm{A}}^{\mathrm{core}}$ at the center of a spherical micelle on solvent selectivity χ_{AS} , for micelles with $\chi_{\mathrm{BS}} = 0.4$, $\chi_{\mathrm{AB}} = 0.2$, and $N = 100$. Notice significant penetration of the core by the small molecule selective solvent as χ_{AS} approaches its CMT value. Dash-dotted line is the prediction from a simple Flory-Huggins theory, Equation (4.2.2).

for $\phi_{\mathrm{A}}^{\mathrm{core}}$, as given by Equation (4.2.2). This simple analytic theory yields nearly perfect agreement with SCFT results for the core composition. The penetration of solvent into the core can thus be adequately understood by treating the core (for this purpose) as a homogeneous phase with a solvent chemical potential equal to that of the surrounding solvent. The deviations of the chains from random walk statistics thus appears to have almost no effect upon the local solvent solvent chemical potential, though it certainly certainly does effect the polymer chemical potential and CAC.

4.5 Micelle Size and Critical Micelle Temperature

Experiments on systems with weakly selective solvents have shown the existence of a critical micelle temperature (CMT) that divide temperatures for which aggregates are observed from temperatures at which surfactants dissolve as a single molecule. The micelle aggregation number has been observed to decrease rapidly with decreasing degree of selectivity near the CMT, both for pluronics in water,[46–51] and for PS-PI in dialkyl phthalates.[52] In this section, we study how M varies with $\chi_{\rm AS}$ in SCFT near the CMT, and propose an operational definition of the CMT as the value of $\chi_{\rm AS}$, or temperature, at which M extrapolates to zero. The aggregation number of a micelle is simply the excess number of polymer molecules $M_{\rm AB}^{\rm ex}$, as defined in Chapter 3, which we hereafter denote by M.

Figure 4.8 shows SCFT results for the aggregation number M as a function of $\chi_{\rm AS}$ for micelles with $f_{\rm B} = 0.35$ and $N = 100$ and the same values for other parameters as those used in previous plots. Figure 4.9 shows a corresponding plot for "hairy" micelles with $f_{\rm B} = 0.60$. The reference volume used in all calculations in this section is $\nu = 118\,\text{Å}^3$, which is approximately the volume of a four-carbon repeat unit. As in other plots of structural properties of equilibrium micelles, the value of M is defined here for equilibrium micelles that coexist with a unimer concentration $\phi^{\rm CAC}$.

We see that M varies nearly linearly with $\chi_{\rm AS}$, and seems to extrapolate to zero at a reasonably well defined value of $\chi_{\rm AS} = \chi_{\rm AS}^{\rm CMT}$. We determine a value for $\chi_{\rm AS}^{\rm CMT}$ by fitting M vs. $\chi_{\rm AS}$ to a second order polynomial and extrapolating to zero. For the crew-cut micelles shown in Figure 4.8, we obtain $\chi_{\rm AS}^{\rm CMT} = 0.73$.

We define an effective core radius $R_{\rm core}$ in Equation 4.4.1 as a simple function

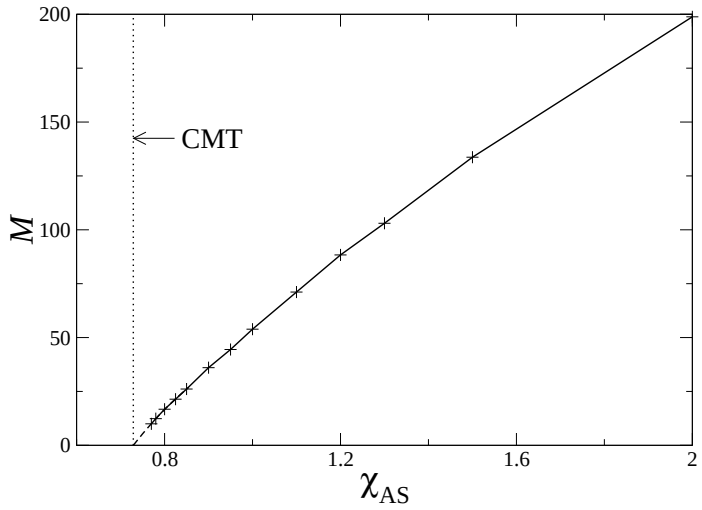

Figure 4.8: Variation of micelle aggregation number M *vs.* solvent selectivity χ_{AS} for $f_{\mathrm{B}} = 0.35$ and $N = 100$. The point at which extrapolation of M extrapolates to zero, indicated by the dashed line, goes to zero is identified as the critical micelle temperature (CMT). The simulation is carried out with $\chi_{\mathrm{BS}} = 0.4$, $\chi_{\mathrm{AB}} = 0.2$, and $N = 100$, with statistical segment lengths of 6 Å for both monomer types. The reference volume of 118Å^3.

$R_{\mathrm{core}} \propto MN_{\mathrm{A}}/\phi_{\mathrm{A}}^{\mathrm{core}}$. Because M extrapolates to zero at the CMT, either $\phi_{\mathrm{A}}^{\mathrm{core}}$ or R_{core}, or both, must extrapolate to zero at the CMT. We showed in Section 4.4 that $\phi_{\mathrm{A}}^{\mathrm{core}}$ is rather well described by Flory-Huggins theory. We actually know that this is true only over the range of value of χ_{AS} for which we have been able to obtain converged SCFT solutions for micelles, which corresponds approximately to the range of values in which there exists a well defined core region. If we extrapolate the Flory-Huggins solution down to the estimated CMT, however, the extrapolated value of the $\phi_{\mathrm{A}}^{\mathrm{core}}$ remains nonzero at the CMT. Since the core composition and core radius are related to M by Equation (4.4.1), and since M extrapolates to zero at the CMT, this implies that R_{core} must extrapolate to zero at the CMT.

Figure 4.10 shows the calculated core volume vs. χ_{AS} for crew-cut micelles, with

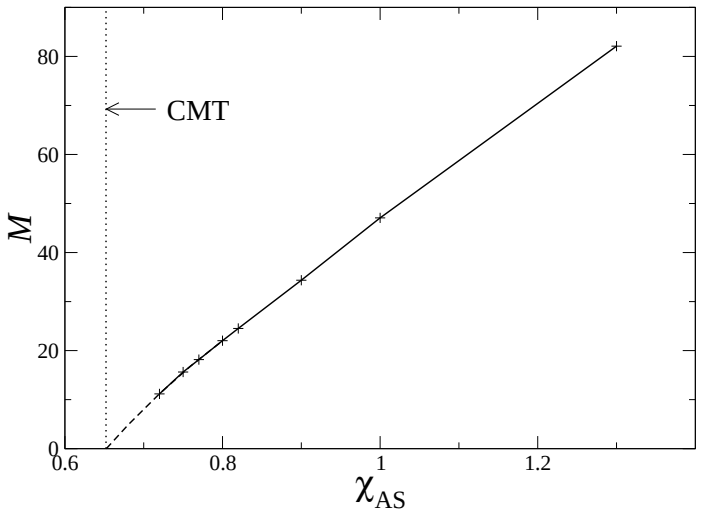

Figure 4.9: Variation of M *vs.* solvent selectivity $\chi_{\rm AS}$ for a hairy micelle, with $f_{\rm B} = 0.6$ and $N = 100$. All other parameters are the same as in Figure 4.8.

$f_{\rm B} = 0.35$. Figure 4.11 shows the corresponding behavior of the actual radius. As suggested by the above argument, the core volume extrapolates to zero at the CMT, with a slope that seems to increase rapidly with decreasing $\chi_{\rm AS}$ near the CMT.

Figure 4.12 shows how the core radius varies with changes in overall chain length at fixed values of the interaction parameters and other parameters (corresponding to fixed temperature), for a sequence of diblock copolymers with a fixed composition $f_{\rm B} = 0.35$, using $\chi_{\rm AS} = 1$. Simple random walk statistics would yield $R_{\rm core} \propto N_{\rm A}{}^{1/2}$. The strong stretching theory with a fixed interfacial tension yields $R_{\rm core} \propto N_{\rm A}{}^{2/3}$. Both more detailed theories and experiments[43,45,171] have previously yielded exponents slightly greater than 1/2. The dotted line shows a power law fit $R_{\rm core} \propto N_{\rm A}{}^{0.58}$ with an exponent in the expected range.

Figure 4.13 shows the dependence of aggregation number M vs. $\chi_{\rm AS} - \chi_{\rm AS}^{\rm CMT}$ for chains of two compositions ($f_{\rm B} = 0.35$ and $f_{\rm B} = 0.6$) and several chain lengths.

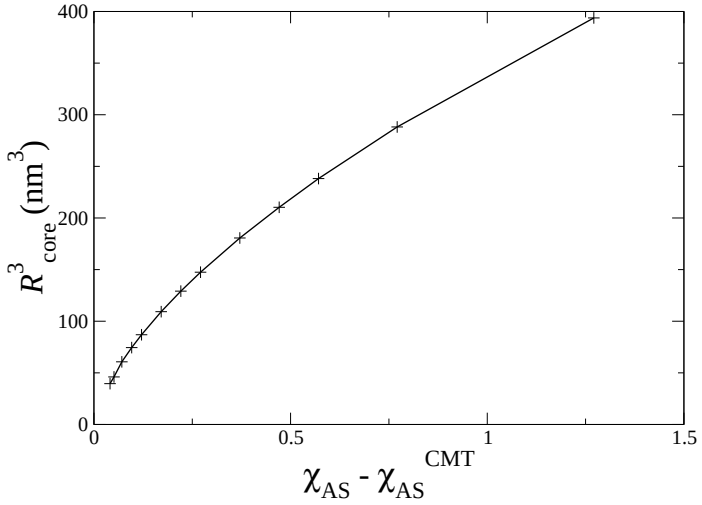

Figure 4.10: The variation of $R^3_{\rm core}$ plotted *vs.* the solvent selectivity for crew-cut micelles with $f_{\rm B} = 0.35$, $N = 100$, $\chi_{\rm BS} = 0.4$, and $\chi_{\rm AB} = 0.2$.

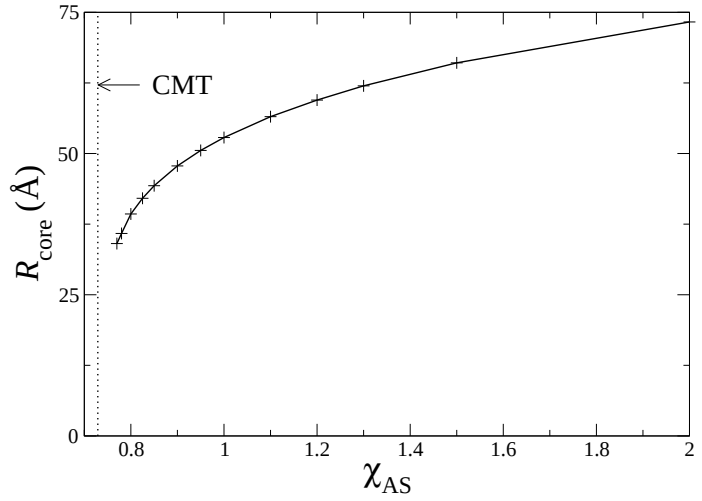

Figure 4.11: The radius of the core of a micelle $R_{\rm core}$ plotted *vs.* $\chi_{\rm AS}$ for the same parameters as in Figure 4.10.

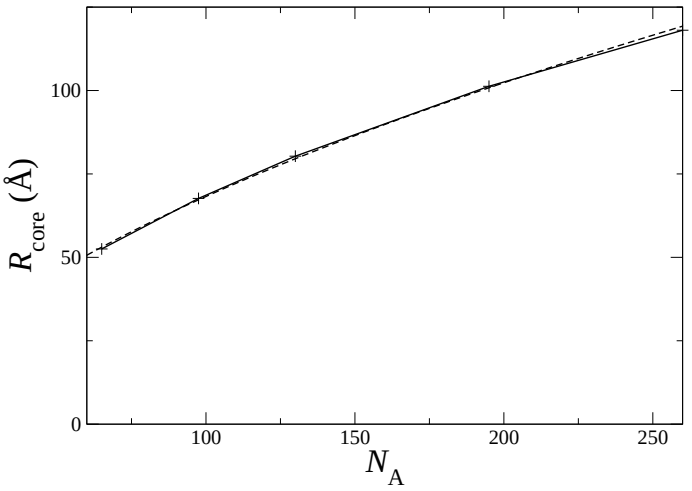

Figure 4.12: Micelle core radius $R_{\rm core}$ vs. core block length $N_{\rm A}$ for crew-cut micelles with $f_{\rm B} = 0.35$ and variable N, at fixed values of all other parameters. These simulations use $\chi_{\rm AS} = 1$, $\chi_{\rm BS} = 0.4$, $\chi_{\rm AB} = 0.2$, $N = 100$, $b_{\rm A} = 6$Å, and $b_{\rm B} = 6$Å.

For all the chain lengths, the value of $\chi_{\rm AB}\, N$ is maintained at a constant value of $\chi_{\rm AB}\, N = 20$. Other parameters are the same as in previous figures. The tendency of chains with long core blocks to have higher aggregation numbers is partly a simple geometrical effect: If we assumed that the micelle core scales with core block length as ${N_{\rm A}}^{1/2}$ (random walk statistics), and the core composition depends primarily upon $\chi_{\rm AS}$, almost independent of chain length, we would predict an aggregation number $M \propto R_{\rm core}^3 / v N_{\rm A}\, \phi_{\rm A}^{\rm core}$ that varies with $N_{\rm A}$ at each value of $\chi_{\rm AS}$ as

$$M \sim N_{\rm A}^{1/2}. \tag{4.5.1}$$

Motivated by this simple scaling argument, we rescale the y-axis in Figure 4.13 to $M/N_{\rm A}^{1/2}$, and present the results in Figure 4.14. The chain lengths for each block composition are found to nearly collapse onto a master curve, except for the shortest

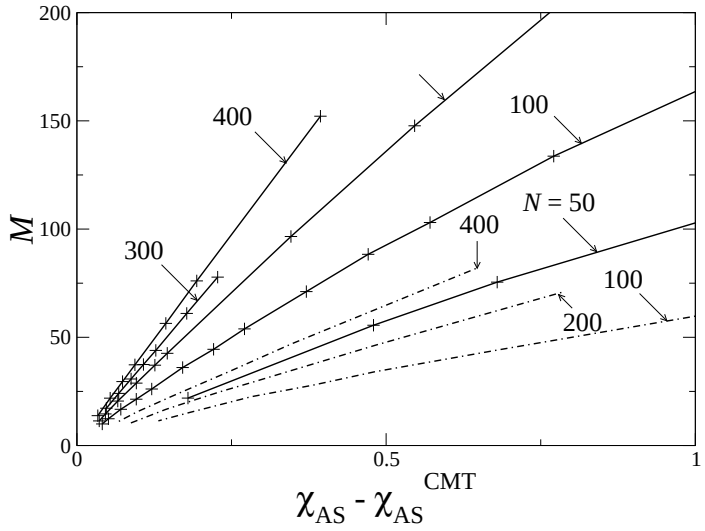

Figure 4.13: Variation of M for crew-cut ($f_{\mathrm{B}} = 0.35$) and hairy ($f_{\mathrm{B}} = 0.6$) spherical micelles with different chain lengths plotted *vs.* the difference χ_{AS} - $\chi_{\mathrm{AS}}^{\mathrm{CMT}}$, where $\chi_{\mathrm{AS}}^{\mathrm{CMT}}$ is the critical value of χ_{AS} at the CMT for each chain. Solid lines are used for chains with $f_{\mathrm{B}} = 0.35$ and dash-dotted line for chains with $f_{\mathrm{B}} = 0.6$.

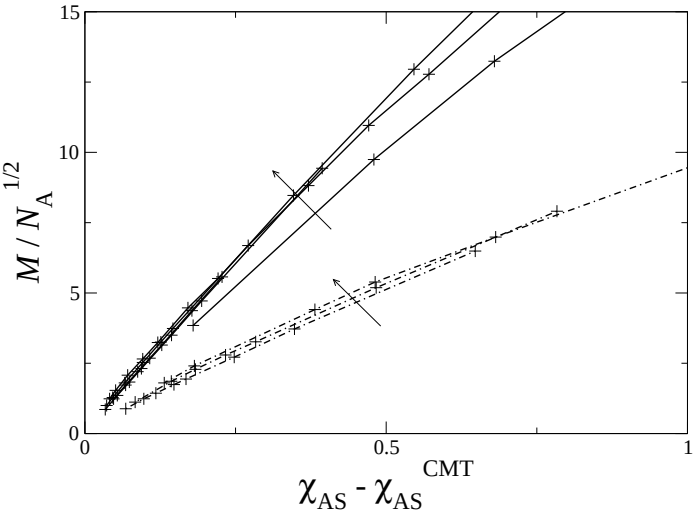

Figure 4.14: Dependence of $M/N_{\mathrm{A}}^{1/2}$ on $\chi_{\mathrm{AS}} - \chi_{\mathrm{AS}}^{\mathrm{CMT}}$ for crew-cut ($f_{\mathrm{B}} = 0.35$) and hairy ($f_{\mathrm{B}} = 0.6$) spherical micelles, for several chain lengths. The solid line represents the case of $f_{\mathrm{B}} = 0.35$, and the dash-dot line represents the case of $f_{\mathrm{B}} = 0.6$. The data presented here is the same data set presented in Figure 4.13, and the arrow indicates the direction of increasing chain length of AB N.

chain $N = 50$ for $f_B = 0.35$. Interestingly, however, the crew-cut and hairy micelles do not collapse onto the same master curve. Recall that we used the length N_A of the solvophobic block to rescale the y-axis, because we assumed that the core radius is determined primarily by the length of the core block. The fact that different compositions fall on different master curves thus implies that this assumption is false, and that the core radius actually depends significantly upon the length of the corona block. The fact that smaller values of $M/N_A{}^{1/2}$ are obtained for hairy micelles ($f_B = 0.6$) implies that the core radius decreases with increasing corona block length. This suggests that the stretching of the corona chains plays a significant role in determining the micelle size near the CMT, and that corona stretching free energy increases significantly with increasing corona block length over this range of values of f_B.

Consider a mixture of homopolymer A and solvent S, this binary system is found to phase separate at a value of $\chi_{AS} = 1/2$ (Θ temperature) for an infinitely long homopolymer A. We condense the minimum value of χ_{AS} required to form micelles χ_{AS}^{CMT} relative to core block length N_A for different chain lengths with $f_B = 0.35$ and $f_B = 0.6$ in Figure 4.15. The y-axis is rescaled to $\chi_{AS}^{CMT} - 1/2$, and the x-axis is represented as $N_A^{-1/2}$ so that the point (0, 0) on the plot represents the Θ temperature. Both block compositions are found to approach the Θ temperature with increasing N_A. The hairy micelle requires a slightly higher value of χ_{AS} in order to form micelles relative to the crew-cut micelle with the same N_A. This behavior presumably must arise from the longer corona block of the hairy micelle.

The behavior of M with respect to χ_{AS}, and χ_{AS}^{CMT} dependence on the core chain

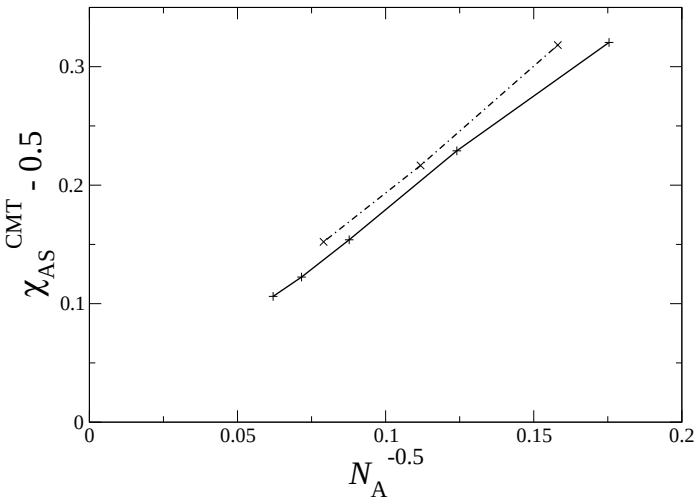

Figure 4.15: Variation of χ_{AS}^{CMT} for spherical micelles with $f_B = 0.35$ (solid line) and $f_B = 0.6$ (dash-dot line) for different values of core block length N_A . The x-axis and y-axis are normalized so that the point (0, 0) represents the Θ temperature for an infinitely long homopolymer of A.

length N_A show contrasting behaviors. The behavior $M/N_A^{1/2}$ is found to be strongly dependent on the corona block composition. Whereas, the behavior of χ_{AS}^{CMT} is found to depend strongly only on the core chain length, and is almost independent of the corona chain length.

4.6 Corona Structure

The dependence of corona concentration profiles on solvent selectivity χ_{AS} is studied in this section. Won *et al.* [172] studied the corona profile of PB-PEO in water for spherical and cylindrical micelles using SANS. They observed the solvated corona brush to collapse at the interface. To study this behavior we determine the value of solvent selectivity χ_{AS} required to completely collapse the solvated brush at the

interface. To obtain this value of χ_{AS} , the concentration profile of the brush in a lamellar phase is studied relative to χ_{AS} . The other interaction parameters are fixed at $\chi_{\mathrm{BS}} = 0.4$ and $\chi_{\mathrm{AB}} = 0.2$, with the degree of polymerization of the polymer being $N = 100$ relative to the size of the solvent.

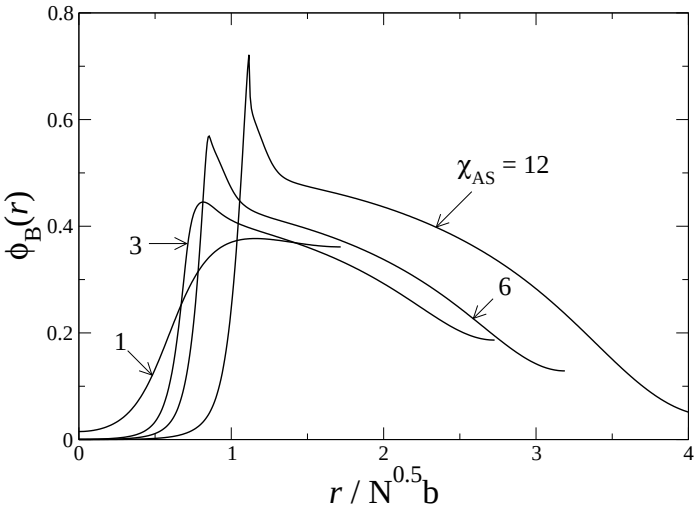

Figure 4.16: The volume fraction $\phi_{\mathrm{B}}(r)$ of the corona monomer B for various values of solvent selectivity χ_{AS} . The parameters used for the simulation are $N = 100$, $\nu = 1$, $\phi_{\mathrm{AB}} = 0.5$, $f_{\mathrm{B}} = 0.5$, $\chi_{\mathrm{BS}} = 0.4$, and $\chi_{\mathrm{AB}} = 0.2$. The calculations are carried out using a periodic formulation of SCFT.

The concentration profiles of the corona block B while varying the solvent selectivity χ_{AS} is presented in Figure 4.16. The amount of solvent which penetrates the solvent phobic A domain is directly proportional to $\exp(-\chi_{\mathrm{AS}})$. The unfavorable contact between A and S is reduced when the corona block starts piling up at the interface. Upon varying the interaction parameter between the core and the solvent χ_{AS} from 1 to 12 the corona brush collapses slowly or one needs a very high value of $\chi_{\mathrm{AS}} > 12$ in order to collapse the corona brush completely at the interface.

Won *et al.* [172] noticed collapse of the brush with $\phi_{\mathrm{B}} \approx 0.6$ at the interface. We

determined the solvent selectivity should be $\chi_{AS} \sim 6$ to achieve $\phi_B \approx 0.6$ at the interface. This value of χ_{AS} is almost twice the value for the PB-water (≈ 3.5) interaction parameter reported by Won *et al.* .[172] Even for $\chi_{AS} = 12$ we notice that the solvated brush does not collapse completely at the interface. Hence, we expect the corona to be well solvated, and do not expect collapse of the brush for the interaction parameters ($\chi_{AS} \leq 3$) considered in our study.

Leermakers *et al.* [64] studied the variation of corona profiles for a diblock of the form $A_{50}B_{200}$ by varying the interaction of the solvent and corona block from $\chi_{BS} = 0$ to $\chi_{BS} = 0.5$ with $\chi_{AB} = 0.5$, and $\chi_{AS} = 2.0$. In their case, the authors notice similar corona profiles with maximum for the corona profile being below $\phi_B < 0.35$ for the case of $\chi_{AS} = 2.0$.

4.7 Conclusions

This chapter presented SCFT predictions of the stability and structure of several types of isolated aggregates in dilute solution, over a wide range of parameters.

Predictions of the domains of stability of bilayer (B), cylinder (S), and spherical (S) aggregates are given in Section 4.1. Transitions from bilayer to cylinder (B $\rightarrow$ C) and from cylinder to sphere (C $\rightarrow$ S) can be driven by a corresponding increase in volume fraction f_B of the solvophilic block, by a corresponding increase in the quality of the solvent for this block (decreases in χ_{BS}), or by a corresponding increase in solvent selectivity (increases in χ_{AS}). Quantitative predictions for these morphological boundaries have been given for one chain length ($N = 100$).

Sections 4.3-4.4 examine how ϕ^{CAC} (the solubility of polymers in solvent) and

the solubility of solvent in the micelle core vary with changes in the degree of solvent selectivity. We find that SCFT predictions for the extent of solvent penetration into the core are extremely well matched by a simple variant of Flory-Huggins theory, described in 4.2, that describes the core as a macroscopic phase that coexists with a phase of nearly pure solvent. The extent of solvent penetration is almost independent of chain length and other parameters, but depends on χ_{AS}. SCFT predictions for the CAC are well approximated by a function of the form

$$\phi^{\mathrm{CAC}} \propto e^{-f(\chi_{\mathrm{AS}})N_{\mathrm{A}}}, \tag{4.7.1}$$

where N_{A} is the length of the solvophobic block and $f(\chi_{\mathrm{AS}})$ is a nonlinear function of χ_{AS}. In the more heavily studied case of AB diblock copolymers in a B homopolymer matrix, the function $f(\chi_{\mathrm{AS}})$ is very nearly equal to χ_{AB}, giving a critical aggregation concentration $\phi^{\mathrm{CAC}} \propto \exp(-\chi_{\mathrm{AB}} N_{\mathrm{A}})$. In this case, the argument of the exponential is simply equal to the change in standard state free energy associated with transferring the A block of the block copolymer from a core of nearly pure A into a matrix of nearly pure B. For the case of a modestly selective small molecule solvent, the minimal model of Section 4.2 yields a value for $f(\chi_{\mathrm{AS}})N_{\mathrm{A}}$ that basically is equal to the corresponding chemical potential difference for a process that transfers the N_{A} block from a core region that contains a significant amount of solvent into a region of nearly pure solvent. This minimal model also seems to provide a reasonably accurate estimate of the slope $\mathrm{d}\ln\phi^{\mathrm{CAC}}/\mathrm{d}N_{\mathrm{A}}$. This underestimates the absolute magnitude of ϕ^{CAC} by several orders of magnitude, however, because it completely neglects the free energies arising from the solvent-phobic / solvent-philic interface and chain stretching

free energies in a micelle.

The core radius for micelles in slightly selective solvent appears to scale almost as $N_A{}^{1/2}$ with changes in chain length at fixed composition f_B , as expected for the unperturbed random walk statistics. A comparison of results for crew-cut and hairy-micelles also suggests, however, that the core radius is sensitive to the length of the corona block as well as the length of the core block, and decreases with increasing corona block length. The nature and origin of this dependence on the corona block length deserves more careful study than it has been given here.

The critical value χ_{AS}^{CMT} is found to approach the $\chi_{AS}^{CMT} = 1/2$ in the limit $N_A \to \infty$, and appears to depend on N_A as

$$\chi_{AS}^{CMT} - 0.5 \propto N_A{}^{-1/2}, \tag{4.7.2}$$

reminiscent of the dependence of the critical value of χ in a polymer solution. Interestingly, $\chi_{AS}^{CMT} - 0.5$ seems to be almost independent of the length of the corona block. We do not yet have any simple physical argument for this empirical observation.

For sufficiently strongly selective solvents (such as water), SCFT calculations show that the base of the solvophilic corona can partially "collapse" in order to shield the solvent-phobic core from the solvent, as suggested by Won *et al.* .[172] In the extreme case, the corona can contain a narrow inner region with a very high concentration of B segments, with a structure of "loops" similar to that of a dense adsorbed layer, and an outer brush of extended tails. We find, however, that this phenomena becomes pronounced for polymers of length $N = 100$ in a typical good solvent only for very large values of χ_{AS} , $\chi_{AS} > 5 - 10$.

CHAPTER 5

Phase Behavior

In this chapter, I present a study of the phase behavior of non-dilute solutions of an AB diblock copolymer in a small molecule selective solvent S. Free energies and structures for various periodic ordered phases have been calculated using the pseudo-spectral implementation of SCFT described in Chapter 2.

Notation in this chapter is the same as in previous chapters: A represents the solvent-phobic block and B the solvent-philic block of the copolymer. The region of parameter space examined here is similar to that examined in the previous chapter. I focus primarily on the effects of changes in the value of the interaction parameter χ_{AS} between the solvent and solvent-phobic block, and of the copolymer composition f_{B}. Most of the systems studied here have a fixed chain length of $N = 100$, and fixed

values $\chi_{BS} = 0.4$ and $\chi_{AB} = 0.2$ for the remaining two interaction parameters.

Some aspects of the phase behavior can be anticipated by qualitative arguments. The phase behavior is known in several limits. In the limit $\phi_{AB} \rightarrow 1$, we must recover the phase behavior of a pure diblock copolymer. For $\chi_{AB} > 10.5$, this includes a well-known sequence of ordered phases. For a non-selective good solvent ($\chi_{AS} = \chi_{BS} < 0.5$), the SCFT phase behavior is reasonably well described by the dilution approximation, which predicts a phase diagram similar to that of a pure diblock copolymer with an effective interaction parameter $\chi_{AS}\,\phi_{AB}$. For a selective solvent ($\chi_{AS} > 0.5$ and $\chi_{BS} < 0.5$), in the limit $f_B \rightarrow 0$, we must recover the phase behavior of a A homopolymer in a poor solvent. When χ_{AS} exceeds a critical value slightly larger than 0.5, this binary system exhibits phase coexistence between polymer-rich and polymer-poor homogeneous phases. In the opposite limit $f_B \rightarrow 1$, with $\chi_{BS} < 0.5$, we expect a homogeneous solution of B homopolymer in solvent. For intermediate values of f_B, and sufficiently strongly selective solvent, it is possible for lamellar phase and the ordered sphere and cylinder phases in which the solvent-phobic A block forms the core domain to swell indefinitely upon addition of solvent, forming structures of essentially isolated spheres or cylinders surrounded by solvent. We thus expect SCFT to predict unbinding transitions for these phases upon decreasing ϕ_{AB}, in which the characteristic length scale of the periodic structure diverges as the volume fraction approaches a very low critical concentration. When SCFT predicts such an unbinding transition, an ordered phase is found to unbind to their corresponding isolated aggregate, where the critical aggregation concentration (CAC) is the minimum concentration required to form an isolated aggregate. We do

not, however, expect the inverted sphere cylinder, and gyroid phases, in which the solvent-philic block forms the "core" domain, to swell more than a limited amount upon addition of solvent. Instead, one might foresee that these phases can accommodate only a modest amount of solvent before expelling excess solvent into a coexisting solvent-rich phase, and should thus exhibit broad regions of two-phase coexistence. The numerical calculations presented here include all of these phenomena, as well as several others, and show how they fit together into a comprehensive picture.

The remainder of the chapter is organized as follows: Section 5.1 examines the regions of stability of the disordered phase, which are determined using the RPA. These stability limits provide a useful rough guide to the phase diagram. Section 5.2 presents phase portraits for systems with varying copolymer composition f_{B} and copolymer volume fraction, for several different sets of values of the interaction parameters, with different values of χ_{AS}. Section 5.3 presents phase portraits for several systems with fixed block lengths (fixed N and f_{B}) as functions of χ_{AS} and ϕ_{AB} for systems with several different values of copolymer composition. The resulting phase portraits are qualitatively similar to the temperature-composition phase diagrams obtained experimentally for copolymers of different composition. Section 5.5 focuses on the FCC and BCC lattices of spherical micelles, and shows how SCFT can be used to quantify pair-wise interactions between micelles in these phases.

5.1 RPA Spinodals

The regions of local stability of the disordered homogeneous phase can be easily determined using the random phase approximation (RPA). RPA calculations of the

spinodal (stability) limits for AB diblock copolymers in S have been given previously by Huang and Lodge,[88] who showed that these stability limits provide a useful rough guide to the phase diagram. Following these authors, we begin by presenting results for the RPA limits of stability as context for the phase portraits shown in subsequent sections.

The RPA spinodal (stability) limit is a line or surface in parameter space along which a homogeneous system becomes unstable to the growth of infinitesimal composition fluctuations with some wavenumber q^*. Parts of the spinodal surface along which $q^* \neq 0$ generally correspond to order-disorder transitions, along which the system undergoes a transition from a homogeneous phase to an ordered phase with a finite characteristic length scale. For the systems of interest here, parts of the spinodal surface along which $q^* = 0$ usually correspond either to regions of two-phase coexistence or to unbinding transitions. In the results presented here, we distinguish between these two types of instability. Huang and Lodge did not distinguish these two cases.

Figure 5.1 shows limits of stability of the disordered phase for several values of $\chi_{\rm AS}$, for systems with $N = 100$, $\chi_{\rm AB} = 0.2$, and $\chi_{\rm BS} = 0.4$. This choice of parameters yields $\chi_{\rm AB}\, N = 20$, which ensures the appearance of periodic phases in the pure diblock limit ($\phi_{\rm AB} = 1$). Along the line $f_{\rm B} = 0$, corresponding to a homopolymer in solvent, we expect the polymer and solvent S to exhibit macrophase separation into two homogeneous phases when $\chi_{\rm AS}$ exceeds a critical value. The critical value for the chain length $N = 100$ used here is $\chi_{\rm AS} = 0.605$.

For the lowest value of $\chi_{\rm AS}$ shown in this figure, $\chi_{\rm AS} = 0.7$, the limit of stability

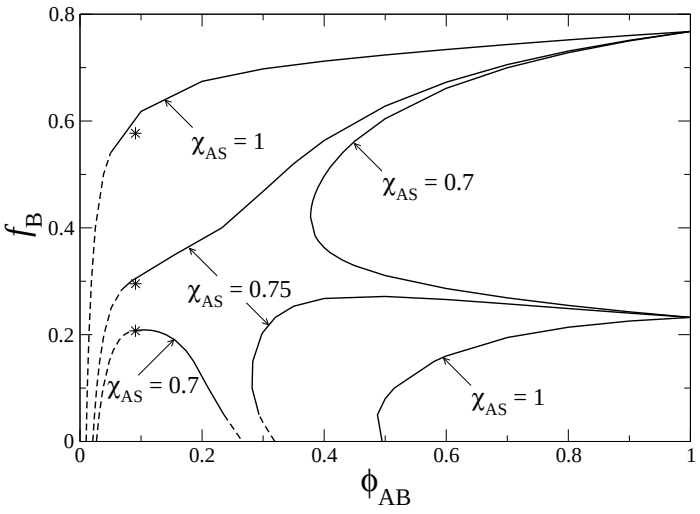

Figure 5.1: Spinodal curves of the disordered phase for AB in S calculated using RPA for various values of χ_{AS} , for systems with $\chi_{BS} = 0.4$, $\chi_{AB} = 0.2$, and $N = 100$. The star points (*) represent the critical values of ϕ_{AB} and f_B arrived at using the Flory-Huggins theory for coexistence between homogeneous phases.

line has two U-shaped branches: One branch, at high values of ϕ_{AB} , encloses a region of concentrated ordered phases, and terminates at $\phi_{AB} = 1$ at the limits of stability of the homogeneous phase of pure diblock copolymer. The instability occurs at a wavenumber $q^* \neq 0$ everywhere along this branch (as indicated by a solid line), corresponding to an order-disorder transition. The second branch, which occurs at much lower values of ϕ_{AB} and f_B, terminates at $f_B = 0$ at the Flory-Huggins spinodal for the phase separation of A homopolymer and solvent. At very low values of f_B, the instability occurs at $q^* = 0$ (dashed line) along both sides of the loop, corresponding to an instability to phase separation into two homogeneous phases. At higher values of f_B , however, the instability occurs at $q^* \neq 0$ along the polymer-rich phase side of the loop but at $q^* = 0$ along the solvent-rich side.

Upon increasing χ_{AS} only slightly, to $\chi_{AS} = 0.75$ the areas enclosed by these two

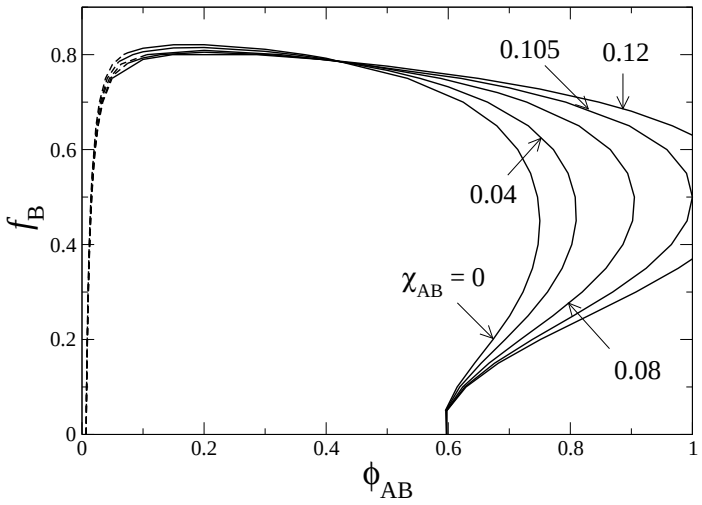

Figure 5.2: Spinodal curves of the disordered phase for AB in S calculated using RPA for various values of $\chi_{\rm AB}$ with $\chi_{\rm AS} = 1.25$, $\chi_{\rm BS} = 0.45$, and $N = 100$.

spinodal lines merge. Thereafter, the resulting topology remains unchanged as $\chi_{\rm AS}$ is increased to $\chi_{\rm AS} = 1.0$, and beyond. For values of $\chi_{\rm AS} = 0.75$ and greater, the limits of stability contain two long segments with an instability at $q^* \neq 0$, and a long nearly vertical segment at low values of $\phi_{\rm AB}$ along which the instability occurs at $q^* = 0$. We show in what follows that an unbinding transition occurs near parts of this $q^* = 0$ instability at low values of $\phi_{\rm AB}$.

The asterisks in Figure 5.1 show the critical values of $\phi_{\rm AB}$ and $f_{\rm B}$ calculated using a Flory-Huggins theory for phase separation of AB copolymer in S into homogeneous polymer-rich and solvent-rich phases. Interestingly, the $q^* = 0$ and $q^* \neq 0$ parts of the spinodal lines always meet rather close to this point. The spinodal lines shown here, however, are not the same as the spinodals of this Flory-Huggins theory, except in the limit $f_{\rm B} = 0$.

Figure 5.2 shows how the spinodal lines vary with changes in $\chi_{\rm AB}$, at a fixed

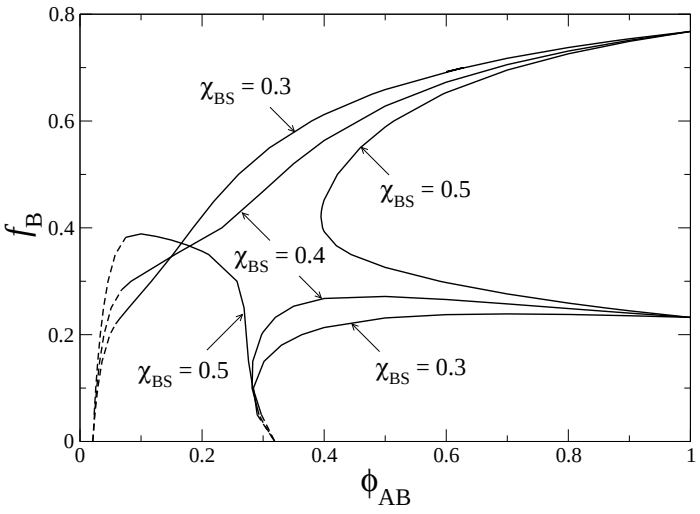

Figure 5.3: Spinodal curves of the disordered phase for AB in S calculated using RPA for various values of $\chi_{\rm BS}$ with $\chi_{\rm AS} = 0.75$, $\chi_{\rm AB} = 0.2$, and $N = 100$.

value of $\chi_{\rm AS} = 1.25$. The other parameters have constant values of $N = 100$ and $\chi_{\rm BS} = 0.45$. In this figure $\chi_{\rm AB}$ is varied from 0 to 0.12, causing $\chi_{\rm AB}\, N$ to vary from $\chi_{\rm AB}\, N = 0$ to $\chi_{\rm AB}\, N = 12$. The ODT for a pure diblock copolymer melt is found to occur at a value of $\chi_{\rm AB}\, N = 10.5$ for $f_{\rm B} = 0.5$. Hence, for values of $\chi_{\rm AB}\, N < 10.5$ the disordered phase is stable phase for all compositions at $\phi_{\rm AB} = 1$, while ordered phases appear for $\chi_{\rm AB}\, N > 10.5$. Even for $\chi_{\rm AB}\, N < 10.5$, however, most of the region enclosed by this spinodal line corresponds to regions in which ordered phases are stable. Microphase separation can thus be induced in solutions even for very low values of $\chi_{\rm AB}\, N$ by solvent selectivity. Note that the spinodal lines are almost independent of $\chi_{\rm AB}$ in the dilute limit.

Figure 5.3 show the dependence of the RPA spinodals upon the parameter $\chi_{\rm BS}$, which controls how "good" a solvent S is for the B block. Other parameters have fixed values of $N = 100$, $\chi_{\rm AB} = 0.2$, and $\chi_{\rm AS} = 0.75$. The value of $\chi_{\rm AS} = 0.75$ is very close

to the value at which the unstable regions were found to merge in Figure 5.1. Here, we see that this phenomena can be modified somewhat by changing χ_{BS}. The value of χ_{AS} at which the two unstable regions merge decreases with increasing solvent quality, or decreasing χ_{BS}.

5.2 Constant Interaction Parameters: f_{B} *vs.* ϕ_{AB}

In this section we describe phase portraits in the block composition f_{B} *vs.* the diblock volume fraction ϕ_{AB} plane for a sequence of systems with fixed interaction parameters and fixed overall chain length N. Results obtained in the previous chapter for isolated aggregates in the dilute limit are also compared to results obtained for highly swollen periodic phases.

Figures 5.4, 5.5, and 5.6 show phase portraits for a sequence of systems with increasing values of χ_{AS}, with all other parameters held fixed. Throughout this sequence $N = 100$, $\chi_{\mathrm{AB}} = 0.2$, and $\chi_{\mathrm{BS}} = 0.4$. The values of $\chi_{\mathrm{AS}} = 0.7$, 0.75, and 1.0, as well as the values of other parameters, are the same as those used for the spinodal curves shown in Figure 5.1. Note that the overall shape of the boundaries between disordered phases and ordered or two-phase regions is well anticipated by the RPA spinodal curves: Figure 5.4 shows a homogeneous phase everywhere outside of two pockets whose shapes and positions are similar to those shown in Figure 5.1 for the same value of χ_{AS}. For higher values of χ_{AS}, these two regions merge, and the size of the ordered regions steadily expands with increasing χ_{AS}.

In Figure 5.4, there is a concentration region that extends to $\phi_{\mathrm{AB}} = 1$ in which we observe the usual sequence of ordered phases for a pure diblock copolymer melt,

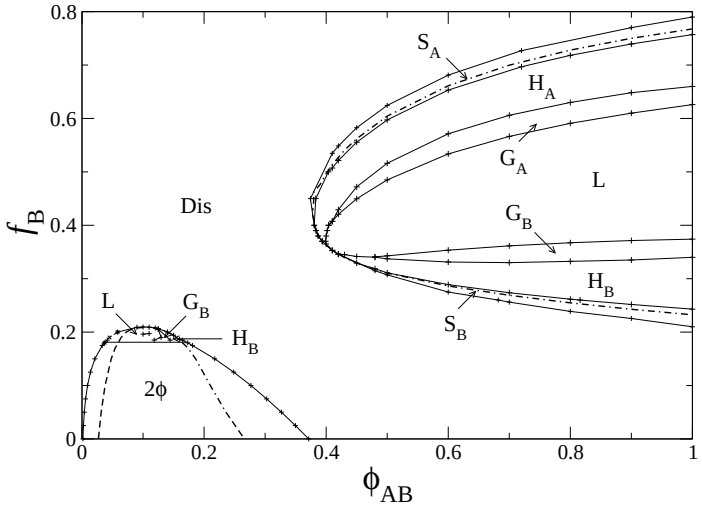

Figure 5.4: Phase diagram for AB in S in the f_{B} v/s ϕ_{AB} plane with $\chi_{\mathrm{AS}} = 0.7$, $\chi_{\mathrm{BS}} = 0.4$, $\chi_{\mathrm{AB}} = 0.2$, and $N = 100$.

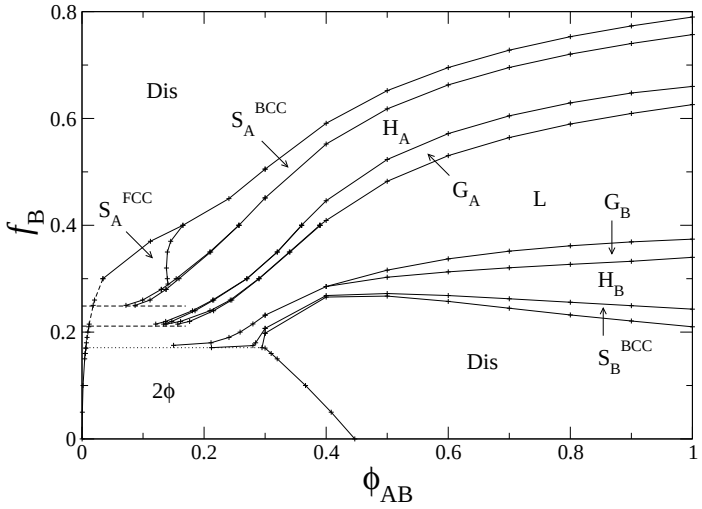

Figure 5.5: Phase portrait for AB in S with $\chi_{\mathrm{AS}} = 0.75$, $\chi_{\mathrm{BS}} = 0.4$, $\chi_{\mathrm{AB}} = 0.2$, and $N = 100$.

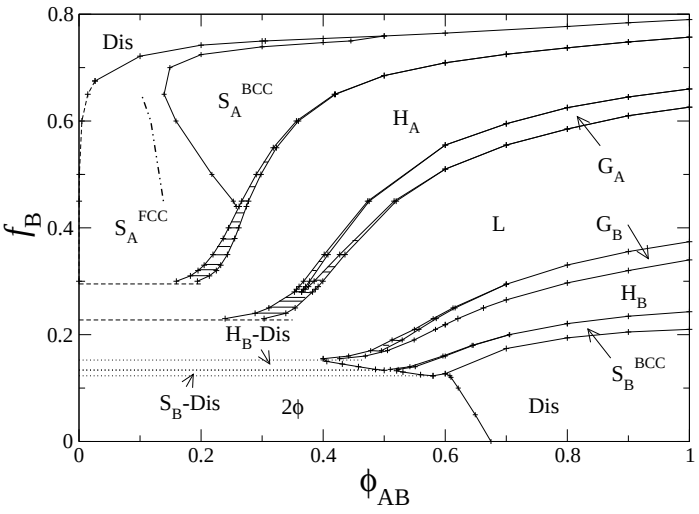

Figure 5.6: Phase portrait of AB in S with $\chi_{AS} = 1$, $\chi_{BS} = 0.4$, $\chi_{AB} = 0.2$, and $N = 100$. The double dot dash line represents the line where spherical micelles at the CAC fill space on a FCC lattice.

from $S_A^{BCC} \rightarrow H_A \rightarrow G_A \rightarrow L \rightarrow G_B \rightarrow H_B \rightarrow S_B^{BCC}$. Here and hereafter, we use the subscript to denote the type of monomer in the core of each structure in the corresponding neat diblock copolymer phase. The transition around the boundary of this region is an order-disorder transition between a disordered phase and a periodic phase with a finite period, rather than an unbinding transition. For small values of f_B , there is instead a wide region of two phase coexistence between a polymer-rich homogeneous macrophase and a solvent-rich homogeneous phase. This coexistence region can be described by the Flory-Huggins theory. The only unexpected feature in Figure 5.4 is the appearance of a pocket of ordered phases close to the critical point of the Flory-Huggins theory that describes phase separation into two homogeneous phases. Expanded versions of this region are presented in Figures 5.10 and 5.11. The phase behavior in this region is discussed in more detail later.

Figure 5.5 shows the two distinct phase regions, seen in Figure 5.4, merge as χ_{AS} is increased from $\chi_{AS} = 0.7$ to $\chi_{AS} = 0.75$. RPA spinodals predicted merging of both phase regions earlier in Figure 5.1. In Figure 5.5 and subsequent phase portraits, dashed horizontal lines represent the values of f_B at which we predict transitions between bilayers, cylindrical micelles, and spherical micelles in the limit of infinite dilution. Note that, upon decreasing ϕ_{AB} the order-order transition from $S_A^{FCC} \rightarrow H_A$ and $H_A \rightarrow L$ approach the corresponding transitions between different types of isolated aggregates in dilute solution: The $S_A^{FCC} \rightarrow H_A$ transition tends to the transition between isolated spherical and cylindrical micelles, and the $H_A \rightarrow L$ transition tends to the crossover between isolated cylinders and bilayers. The region of stability of highly swollen lamellar, hexagonal and spherical periodic faces thus match the regions in which bilayers, cylindrical micelles, and spherical micelles are predicted to be stable in dilute solution. The lamellar L, hexagonal H_A and spherical S_A^{FCC} phases thus undergo unbinding transitions, in which the domain size increases without bound as a result of dilution, as discussed in Chapter 3.

Figure 5.6 shows phase portrait for $\chi_{AS} = 1.0$. The region of ordered phases in the plot increases and is dominated by phases with core block A. The regions of two phase coexistence regimes between S_A^{FCC} and H_A, S_A^{BCC} and H_A, and H_A and L are also expanded. As for $\chi_{AS} = 0.75$, the ordered S_A^{FCC}, H_A and L phases swell indefinitely, and extrapolate to the known regions of stability of spherical, cylindrical, and bilayer aggregates in dilute solution.

We notice the unbinding transition to occur at a higher value of ϕ_{AB} for a higher value of χ_{AS}. This transition for $\chi_{AS} = 0.75$ (see Figure 5.5) is found to occur at

$\phi_{AB} \approx 0.1$, whereas the same transition for $\chi_{AS} = 1$ (see Figure 5.6) is found to occur at $\phi_{AB} \approx 0.2$. We explain this by tracking the domain size of the ordered phases. Domain size is directly proportional to selectivity of the solvent χ_{AS}. The increase in χ_{AS} corresponds to an increase in domain size for the same value of ϕ_{AB}. Hence, we expect the transition of the ordered phases to isolated aggregate morphologies to occur at a higher value of ϕ_{AB} when you increase the value of χ_{AS}.

For lower values of f_B in Figure 5.6, the inverted phases $H_B$and $S_B^{BCC}$are found to coexist with a solvent-rich (nearly pure solvent) homogeneous phase. These two-phase regions cover a wide range of concentration, but exist only within a very narrow range of values of f_B, $0.12 < f_B < 0.16$. This phase coexistence is a natural consequence of the inability of ordered phases $H_B$and $S_B^{BCC}$to absorb more than a limited amount of solvent into their solvent-philic, B-rich core domains before beginning to expel excess solvent. Zhang and Eisenberg[24] referred to such inverted structures as "compound micelles".

In all the phase portraits presented earlier and in the future, $S_A^{FCC}$is found in the dilute limit irrespective of the corona block length, or composition. In order to describe the phase transition from $S_A^{FCC} \rightarrow S_A^{BCC}$, with increasing ϕ_{AB}, the double dot-dashed line in the phase portraits are calculated. This line corresponds to the point at which a spherical micelle at the CAC, with a volume Ω_m, completely occupies the volume on a FCC lattice with a lattice parameter a. This condition can also be expressed as the volume fraction of the spherical micelles on a FCC lattice $\phi_{micelle}$ is

equal to 1, or

$$\phi_{\text{micelle}} = \frac{4\Omega_{\text{m}}}{a^3} \tag{5.2.1}$$

$$= 1. \tag{5.2.2}$$

The volume occupied by a single micelle Ω_{m} is calculated using $\Omega_{\text{m}} = (4/3)\pi r_{\text{CAC}}^3$, and we describe how we determine r_{CAC} in Section 5.5. The point at which $\phi_{\text{micelle}} = 1$ is close to the $\text{S}_{\text{A}}^{\text{FCC}} \rightarrow \text{S}_{\text{A}}^{\text{BCC}}$transition on the phase portraits, but does not quantitatively match the $\text{S}_{\text{A}}^{\text{FCC}} \rightarrow \text{S}_{\text{A}}^{\text{BCC}}$transition.

Figures 5.7, 5.8 and 5.9 examine the effect of changes in several parameters that were not varied in Figs. 5.4, 5.5, and 5.6. Figure 5.7 describes the phase behavior for a system with $\chi_{\text{AS}} = 1$ in a theta solvent ($\chi_{\text{AS}} = 0.5$) rather than the modestly good solvent ($\chi_{\text{AS}} = 0.4$) used in previous figures. Figure 5.8 shows a phase portrait for systems with $\chi_{\text{AS}} = 0.75$ but for somewhat longer chains, of $N = 150$. Figure 5.9 shows a phase portrait for a system with a reduced value of $\chi_{\text{AB}} = 0.08$, for which the product $\chi_{\text{AB}}\, N = 8$ is lower than the critical value of 10.5 necessary to form ordered phases for a pure diblock copolymer melt.

Upon comparing Figures 5.6 and 5.7 we see that effect of increasing χ_{AS} from 0.4 (good solvent) to 0.5 (theta solvent) upon the phase portrait is quite subtle. We expect the decrease in solvent quality to cause a slight decrease in the extent of chain swelling for the solvent-philic B blocks. Their is a slight decrease in the area of the spherical phases. Identical behavior is observed for the crossovers of isolated aggregates as well. The transitions from S $\rightarrow$ C $\rightarrow$ B occurs at higher f_{B} in Figure 5.7

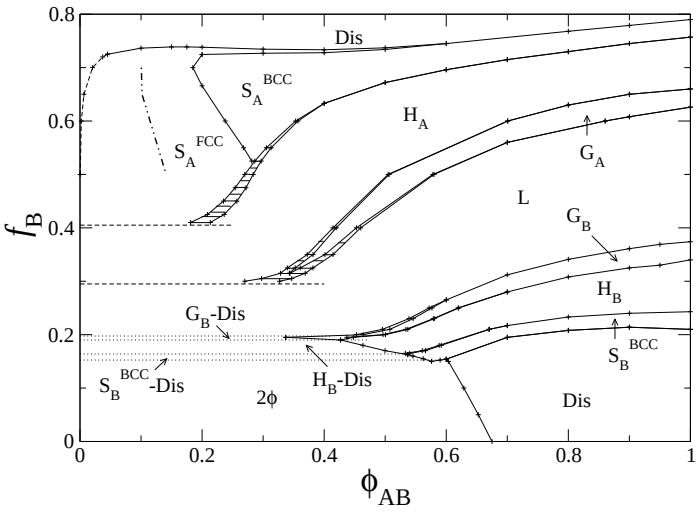

Figure 5.7: Phase portrait for AB in S with $\chi_{AS} = 1.0$ in a Θ solvent, $\chi_{BS} = 0.5$. All parameters other than χ_{BS} are the same as those in Fig. 5.6.

than the crossover values of f_B predicted in Figure 5.6. The change in solvent quality leads to the disappearance of the the gyroid phase at a lower value of ϕ_{AB} , as one approaches the C $\rightarrow$ B transition. The domain size of the $G_A$phase starts going up rapidly at the point at which it is replaced by phase coexistence of L and $H_A$for the values of χ_{AS} 0.75 and 1 studied in Figures 5.5, 5.6, 5.7 and 5.8.

Upon comparing Figure 5.8 and 5.5, we see that the effect of increasing overall chain length, at fixed values of all other parameters, is similar to that of increasing χ_{AS} : The ordered phases occupy a somewhat larger region in Figure 5.8 then in Figure 5.5. Some of the two-phase regions between ordered phases also become more evident.

All the phase portraits presented till now have had $\chi_{AB}\, N = 20$. This value of $\chi_{AB}\, N$ leads to ordered phases being present for a pure diblock copolymer melt. In Figure 5.9, we consider a value of $\chi_{AB} = 0.08$, or $\chi_{AB}\, N = 8$. This leads to a

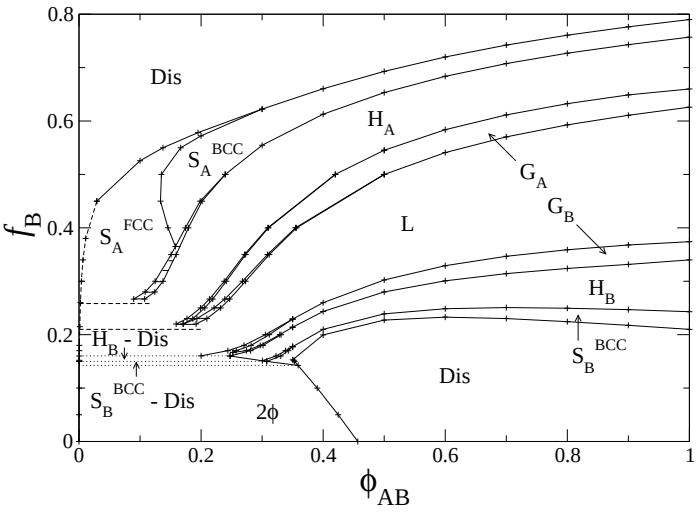

Figure 5.8: Phase portrait for AB in S with $\chi_{AS} = 0.75$, $\chi_{BS} = 0.4$, $\chi_{AB} = 0.2$, and $N = 150$. The only difference from the parameters used in Figure 5.5 is the increase in N from 100 to 150

disordered phase for a pure diblock copolymer melt. The other interaction parameters are $\chi_{AS} = 1.25$, and $\chi_{BS} = 0.45$. The rest of the parameters are unchanged. From Figure 5.9 we notice that other than the pure diblock limit being disordered, the phase behavior is similar to previous phase diagrams presented in Figures 5.5, 5.6, 5.7 and 5.8. We notice the unbinding transition of the periodic phases, where the order-order transitions tends to the crossover of isolated aggregates. For the range of block composition $0.2 < f_B < 0.14$, upon dilution of the diblock copolymer AB, we notice the formation of two phase regions of a solvent-rich macrophase coexisting with periodic phases having the solvent-philic block as the core. In the regime of concentrated diblock copolymer $\phi_{AB} \sim 1$, there is a clear order-disorder transition observed for the ordered phases. The phase behavior in Figure 5.9 is purely driven by the selectivity of solvent χ_{AS}. Hence, we observe ordered structures for the binary

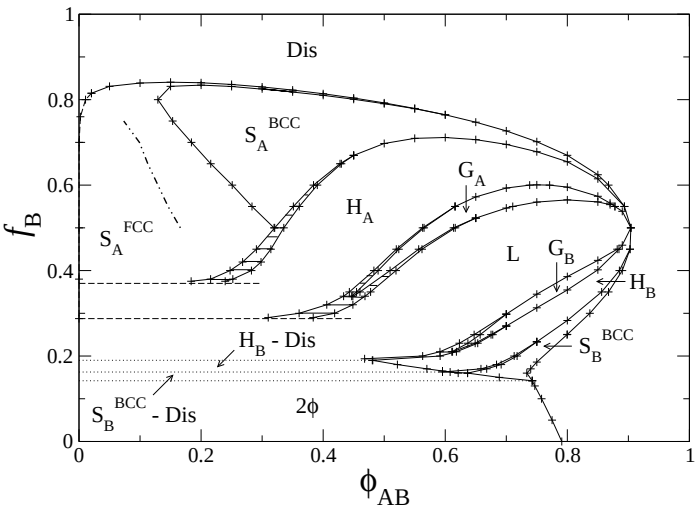

Figure 5.9: Phase diagram for AB in S with $\chi_{AS} = 1.25$, $\chi_{BS} = 0.45$, $\chi_{AB} = 0.08$, and $N = 100$. The double dot dash line represents the line where spherical micelles at CAC fill space on a FCC lattice.

system of AB/S even when the pure diblock copolymer exists in a disordered state.

We now consider the pocket of ordered phases found near the Flory-Huggins critical point for the weakly-selective solvent shown in Figure 5.10. This pocket occurs near the top of wide region of two phase coexistence between homogeneous polymer-rich and polymer-poor phases, near the expected critical point. The discovery of a pocket of ordered phases here was a surprise to us. In retrospect, however, the presence of such a pocket could be foreseen by comparing the binodal predicted by Flory-Huggins theory to the RPA spinodal and to the unbinding curve that we calculate for the lamellar phase. These features are presented in Figure 5.11. At low values of f_B the Flory-Huggins binodal lies outside both the the RPA spinodal on the polymer-rich side and outside both the spinodal and the lamellar unbinding (or CAC) on the solvent-rich side. Near the Flory-Huggins critical point, however, the

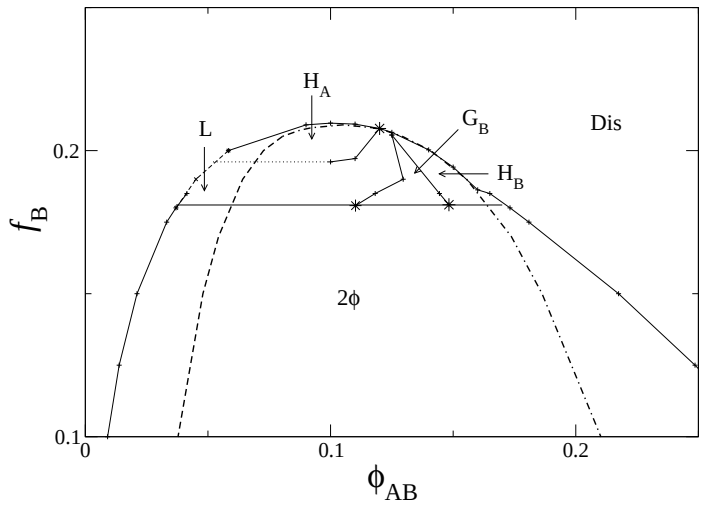

Figure 5.10: A zoomed in region of the phase diagram for AB in S in the f_{B} v/s ϕ_{AB} plane with $\chi_{\mathrm{AS}} = 0.7$, $\chi_{\mathrm{BS}} = 0.4$, $\chi_{\mathrm{AB}} = 0.2$, and $N = 100$. The phase behavior near the line in this figure that separates the ordered phases from the wide two phase region is not shown in detail, and must have a more complicated topology than that shown here (which violates the Gibbs rule if taken literally). Data points represented by $*$ are extrapolations of trends observed.

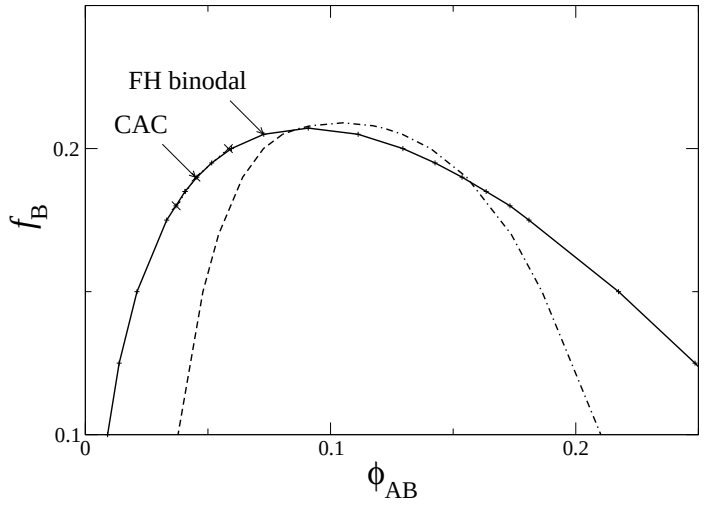

Figure 5.11: The RPA spinodal, the Flory-Huggins binodal, and the CAC for the bilayer morphology for the same parameters considered in Figure 5.10.

RPA spinodal crosses the FH binodal on the polymer-rich side of the phase dome, at $f_{\mathrm{B}} = 0.183$, and the unbinding/CAC line crosses the Flory-Huggins binodal at a very similar value of $f_{\mathrm{B}} = 0.181$. The crossover between CAC of bilayers and the Flory-Huggins binodal is indistinguishable in Figure 5.11, and is studied in more detail in Figures 5.12 (a) and 5.12 (b).

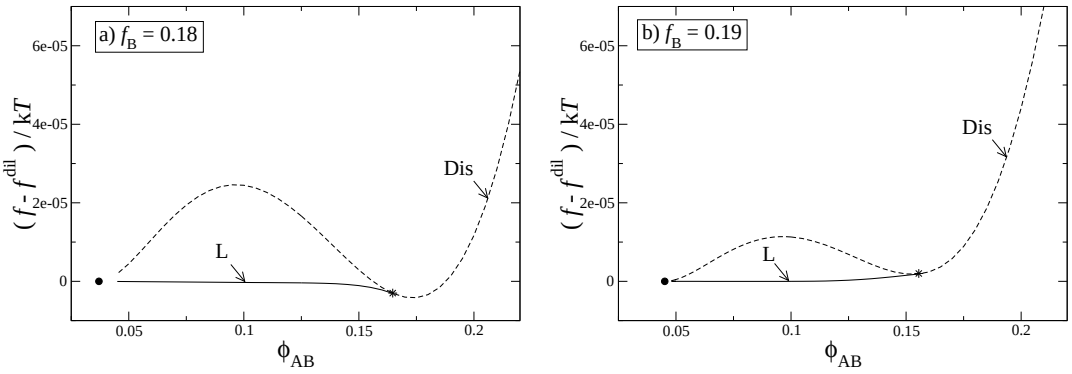

Figure 5.12: The Helmholtz free energy plotted *vs.* ϕ_{AB} to show the two different transformations occurring in plots a) $f_{\mathrm{B}} = 0.18$ and b) $f_{\mathrm{B}} = 0.19$ for $\chi_{\mathrm{AS}} = 0.7$. Macrophase separation is preferred for $f_{\mathrm{B}} = 0.18$ as the double tangent line between the two disordered phases is lower than the unbinding line, whereas it is the other way around for $f_{\mathrm{B}} = 0.19$.

The effect of the crossing of the unbinding/CAC line and the Flory-Huggins binodal line upon the free energy is shown in Figure 5.12. Figures 5.12 (a) and 5.12 (b) show the Helmholtz free energy per monomer of the L and Dis phases plotted *vs.* ϕ_{AB} . The corresponding free energy of the bilayer aggregates f^{dil} at the CAC is subtracted from free energies of both phases to allow us to show the differences in an expanded scale. As a result of this subtraction, the lamellar free energy is always horizontal near the unbinding transition, by construction. In these figures, the solid circle corresponds to the CAC for the bilayer morphology, and the $*$ represents the

spinodal point calculated using the RPA. The binodal is determined by drawing a line (not shown) between the two minima of the disordered phase free energy, which corresponds to the solvent-rich and polymer-rich homogeneous macrophases. If we draw an imaginary double tangent between these two minima in Figure 5.12, we find that the double tangent is lower than the lamellar free energy for all $f_{\mathrm{B}} < 0.181$, including the value $f_{\mathrm{B}} = 0.18$ shown on the left, but the lamellar free energy density is lower than the double tangent line for the case of all $f_{\mathrm{B}} > 0.181$, including the value $f_{\mathrm{B}} = 0.19$ shown on the right.

For $f_{\mathrm{B}} > 0.181$, the phase transition between ordered and disordered phases on the solvent-rich side of this pocket is thus an unbinding transition, along which the period of a very weakly-segregated ordered phase diverges. The relevant ordered phase is $\mathrm{H_A}$at higher values of f_{B} and lamellar at lower values. Along the polymer-rich side of the phase diagram, the transition between an ordered and disordered phase seems, to within our numerical accuracy, to closely follow the calculated RPA spinodal, and thus be either a continuous transition or an extraordinarily weakly first order transition. Plots of the evolution of the composition profile seem to show a second-order transition to a phase with a finite periodicity for all $f_{\mathrm{B}} > 0.183$ along this phase boundary. In the narrow range of composition $0.181 < f_{\mathrm{B}} < 0.183$, we believe that there must be a sequence of two phase regions connecting different ordered and disordered phases, in which some of the ordered-phases must end at eutectic points, but we have not tried to accurately map this out, because it is rather complicated behavior involving extraordinarily small differences in free energy that exists over a very small range of values of f_{B} . Our use of simple horizontal straight line to

separate the ordered phases from the region of Flory-Huggins two-phase separation should thus not be taken literally, since it flagrantly violates the Gibbs phase rule (by implying the coexistence of 5 phases in a binary system): It simply represents a narrow sequence of complex phase behavior that we have not attempted to resolve.

5.3 Constant Block Lengths: χ_{AS} *vs.* ϕ_{AB}

Phase portraits are calculated for constant block lengths $f_B\,N$ and $f_A\,N$ for the χ_{AS} *vs.* ϕ_{AB} plane. The range of values considered for χ_{AS} ranges from $\chi_{AS} = 0.4$, which makes the solvent non-selective or neutral, to $\chi_{AS} = 1.3$, which makes the solvent selective. The same phase is present throughout for all values of χ_{AS} for $\phi_{AB} = 1$ for all phase portraits presented in this section.

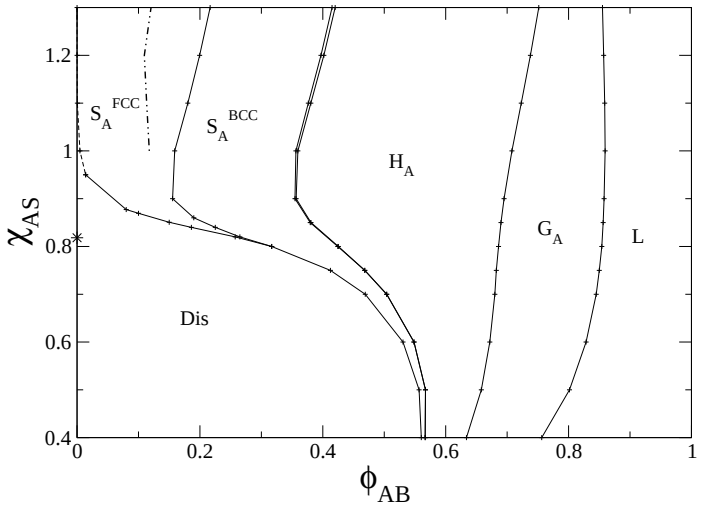

Figure 5.13: Simulating the phase portrait of AB in S with $f_B = 0.60$, $N = 100$, $\chi_{BS} = 0.4$, and $\chi_{AB} = 0.2$. The double dot dash line represents the line where spherical micelles at the CAC fill space on a FCC lattice.

Figure 5.13 shows the phase portrait for a block composition of $f_B = 0.60$ and

$N = 100$. The spherical phase $S_A^{FCC}$is the stable ordered phase in the dilute limit, which unbinds to the isolated spherical micelles (S) morphology. This transformation to S is always preceded by $S_A^{FCC}$and never by S_A^{BCC}in Figure 5.13. Even though the spheres are "hairy" ($f_B > 0.5$), in which case $S_A^{BCC}$is expected to be the stable ordered phase,[131,135,137,138,140] we notice the transition $S_A^{BCC} \rightarrow S_A^{FCC}$to occur before the spherical periodic phases transforms into isolated spherical micelles. SCFT predictions are found to differ with the mean field study carried out by Grason,[142] in which case the author predicted transitions from $S_A^{BCC} \rightarrow S_A^{FCC} \rightarrow S_A^{BCC}$with decreasing concentration of AB. The model used by Grason assumes no penetration of solvent in the core which is not the case as seen from SCFT predictions presented earlier in Chapter 4 as well as from experimental studies.[50,52] The unbinding transition occurs at higher values of ϕ_{AB} for larger values of χ_{AS} , which is also the same behavior shown by the phase transition between $S_A^{FCC}$and S_A^{BCC}. There is a small but noticeable two phase region between $S_A^{BCC}$and $H_A$at higher χ_{AS} . Other phases found in Figure 5.13 vary from $L \rightarrow G_A \rightarrow H_A \rightarrow S_A^{BCC} \rightarrow S_A^{FCC}$upon decreasing the concentration of AB. The area occupied by the ordered phases goes down as the solvent selectivity is reduced i.e., the value of χ_{AS} is reduced. We determined the critical value of χ_{AS} , defined as χ_{AS}^{CMT} earlier in Chapter 4, to be $\chi_{AS}^{CMT} = 0.82$, and is represented by $*$ on the y-axis in Figure 5.13. We notice a rapid change in phase behavior for values of χ_{AS} below 0.82 in Figure 5.13.

In Figure 5.14 we present the phase portrait for $f_B = 0.35$ and $N = 100$. Upon reducing the corona block composition to $f_B = 0.35$ the spheres are crew-cut in nature due to shorter length of the corona block. Hence, we expect $S_A^{FCC}$to occupy

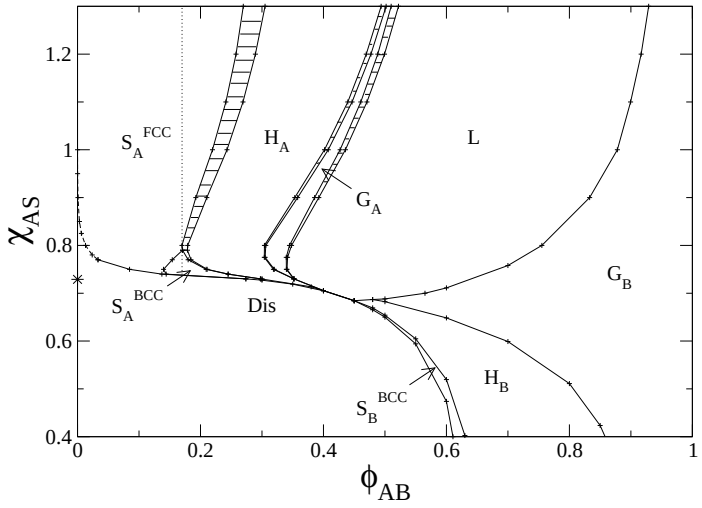

Figure 5.14: Simulating the phase portrait of AB in S with $f_B = 0.35$, $N = 100$, $\chi_{BS} = 0.4$, and $\chi_{AB} = 0.2$. The dotted line represents constant volume fraction of $\phi_{AB} = 0.17$ along which the aggregation number M of spherical micelles on the spherical lattices of $S_A^{FCC}$and $S_A^{BCC}$is studied, which is presented in Section 5.5.

more area in the phase portrait relative to the phase portrait of $f_B = 0.60$. The transition from $S_A^{BCC}$to $S_A^{FCC}$is observed in experimental studies[131,135,137,138,140] when one starts reducing the corona block length or corona block composition. That is the case as seen in figure 5.14 where $S_A^{BCC}$is reduced to a small pocket close to the order disorder transition. However, SCFT predicts $S_A^{BCC}$to transform itself into S_A^{FCC}as one increases the concentration of solvent even for $f_B = 0.60$. $S_A^{FCC}$is found to always precede the spherical micellar regime be it for a hairy corona or a crew-cut corona. The stable isolated aggregate morphology is found to be isolated spherical micelles in Figure 5.14.

I observe large regions of two phase coexistence between H_A, and S_A^{FCC}as well as between $H_A$and G_A, and also between $G_A$and L in Figure 5.14. These two phase regions are filled with solid lines to differentiate them with single phase regions in

Figure 5.14. The two phase region between ordered phases grows with increasing χ_{AS}. This corresponds well to the phase portraits described for constant solvent selectivity χ_{AS} where we notice no two phase regions for $\chi_{AS} = 0.7$, presented in Figure 5.4, but large two phase regions for $\chi_{AS} = 1$, presented in Figure 5.6.

The phase at $\phi_{AB} = 1$ is independent of χ_{AS}, and is always G_B for this block composition. Decreasing concentration of AB induces phase transition from $G_B \rightarrow L \rightarrow H_A \rightarrow S_A^{FCC}$ for high values of χ_{AS}, whereas for low values of χ_{AS} we notice the phase transition from $G_B \rightarrow H_B \rightarrow S_B^{BCC} \rightarrow$ Dis. The critical value of χ_{AS} where these phase transformations change is calculated as $\chi_{AS}^{CMT} = 0.73$, and is represented by $*$ on the y-axis in Figure 5.14.

Phase portrait for block composition of $f_B = 0.26$ and $N = 100$ is presented in Figure 5.15. In this case H_A dominates the dilute regime $\phi_{AB} << 1$ and H_B dominates the concentrated regime $\phi_{AB} \sim 1$. At high solvent selectivity $\chi_{AS} > 0.8$ we notice phase transitions to go from $H_B \rightarrow G_B \rightarrow L \rightarrow ((L + G_A) \rightarrow G_A \rightarrow (G_A + H_A))$ or $L + H_A \rightarrow H_A$, whereas for $\chi_{AS} < 0.7$ we notice phase transitions to go from $H_B \rightarrow S_B^{BCC} \rightarrow$ Dis. The gyroid phase G_A is observed to vanish with increasing solvent selectivity. G_A is replaced by a large two phase coexistence region between L, and H_A. This two phase region is filled with solid lines to differentiate them with single phase regions in Figure 5.15. Experiments conducted by Lodge *et al.* .[3,89] for PS-PI in dialkyl phthalates also predicted this behavior.

A small pocket of S_A^{FCC} is observed close to the order-disorder transition in the dilute limit. The two phase coexistence between H_A and S_A^{FCC} is found to tend towards the crossover between isolated aggregates C and S. The dashed line in Figure 5.15

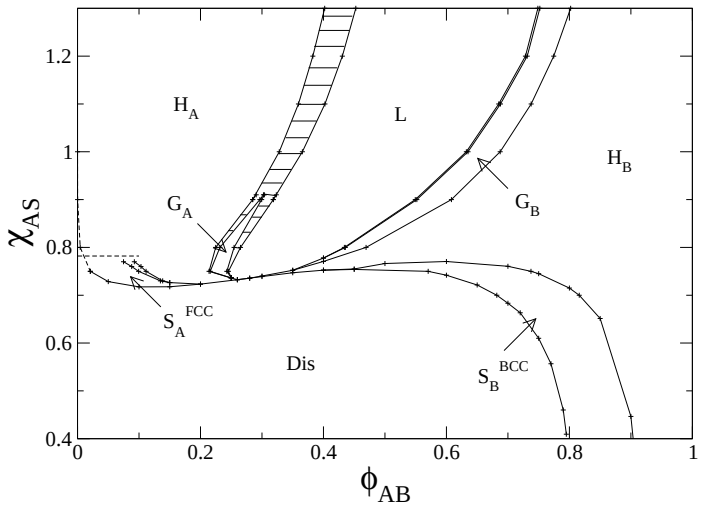

Figure 5.15: Simulating the phase portrait of AB in S with $f_B = 0.26$, $N = 100$, $\chi_{BS} = 0.4$, and $\chi_{AB} = 0.2$.

represents the unbinding transition. Notice that even for small block composition of B $f_B = 0.26$, where we expect periodic phases with solvent-philic core B to dominate the phase portrait for a pure diblock copolymer melt, instead this phase portrait is dominated by ordered phases with solvent-phobic core block A.

Figure 5.16 represents the phase portrait for block composition of $f_B = 0.19$ and $N = 100$. In this case the dilute regime is dominated by the lamellar phase and the concentrated regime is dominated by the disordered phase. The lamellar phase unbinds into bilayers at low concentrations of the diblock. Decreasing concentration of AB induces phase transition from $S_B^{BCC} \rightarrow H_B \rightarrow H_B + G_B \rightarrow G_B \rightarrow G_B + L \rightarrow L$. There is noticeable two phase region between L and G_A. This two phase region is filled with solid lines to differentiate them with single phase regions in Figure 5.16.

It is the first in the series of phase portraits where we do not notice the presence of the ordered phase with core of solvent-phobic block A S_A^{FCC}, S_A^{BCC}, H_A, and G_A,

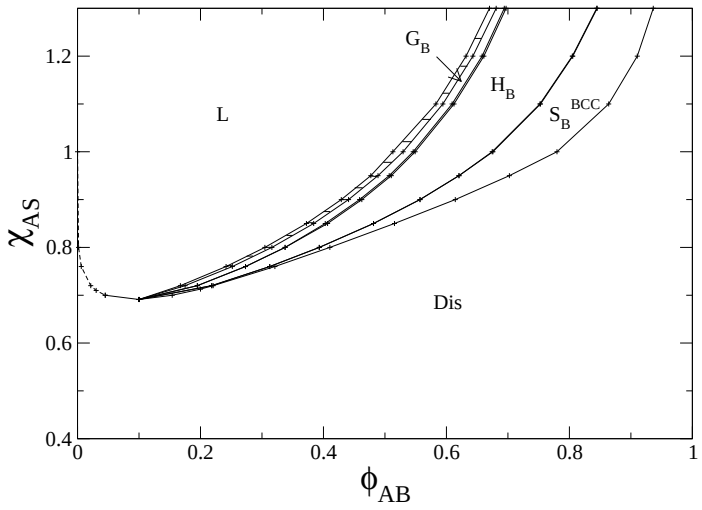

Figure 5.16: Simulating the phase portrait of AB in S with $f_{\mathrm{B}} = 0.19$, $N = 100$, $\chi_{\mathrm{BS}} = 0.4$, and $\chi_{\mathrm{AB}} = 0.2$.

and absence of ordered phase in the $\phi_{\mathrm{AB}} = 1$ limit. One needs to drive down the block composition so that you do not notice any phase with solvent-phobic block A in the core. This phase portrait is another example, refer to Figure 5.9 for an example in the f_{B} *vs.* ϕ_{AB} plane presented earlier, where solvent selectivity χ_{AS} drives the phase behavior for a diblock copolymer which is disordered in its pure form.

5.4 Comparison to Experiment: PS-PI in DBP

The phase behavior of the binary system AB/S has been studied in various systems.[3,27,87,96] Here, we attempt to compare SCFT predictions to one of the experimental phase portraits of PS-PI in dibutyl phthalate (DBP) as presented by Lodge and coworkers[3] with DBP as the selective solvent in Figure 5.18. DBP has a preference for styrene monomer. The choice of χ parameters, statistical segment lengths,

and volume of the solvent are determined from literature for the aforementioned system. The interaction parameter between styrene and isoprene blocks has been obtained from Lodge *et al.* ,[2] where order-disorder transition (ODT) values for nearly symmetric lamellar forming PS-PI melts and PS-PI in neutral solvents were used to generate a master curve. The plot was then used to determine the value of χ_{SI} as:

$$\chi_{\mathrm{SI}} = \frac{33}{T} - 0.0228 \tag{5.4.1}$$

with the reference volume as the styrene segment volume. Using Equation (5.4.1), we arrive at an ODT for SI(15-13) diblock copolymer melt as 280 °C, whereas, Lodge *et al.* [3] determined it to be 230 °C. This deviation from Equation (5.4.1) is evident in Figure 5.17, where the data point for SI(15-13) is shown by $*$. The deviation is found to be of the order of 15-20 % to the value of ODT obtained using the master curve. The ODT values for other pure nearly symmetric diblock copolymer melts[173–175] are also found to deviate from the master curve (solid line in Figure 5.17) presented in Equation (5.4.1).

Literature values for the interaction parameter $\chi_{\text{S-DBP}}$ were not found. It is determined using the empirical formula $\chi_{\text{S-DBP}} = 0.34 + (V/\mathrm{R}T)(\delta_{\mathrm{S}} - \delta_{\mathrm{DBP}})^2$ mentioned in the book Polymer Chemistry by Hiemenz and Lodge.[60] The solubility parameters were obtained from the polymer handbook.[176] However, the solubility parameters of PS and DBP are very close to each other thus yielding $\chi_{\text{S-DBP}} = 0.34$. In the SCFT simulations the solvent (DBP) volume was used as the reference volume.

The interaction parameter between isoprene and DBP had been determined by Hanley and Lodge.[177] It is estimated by determining the ratio of peak intensities for

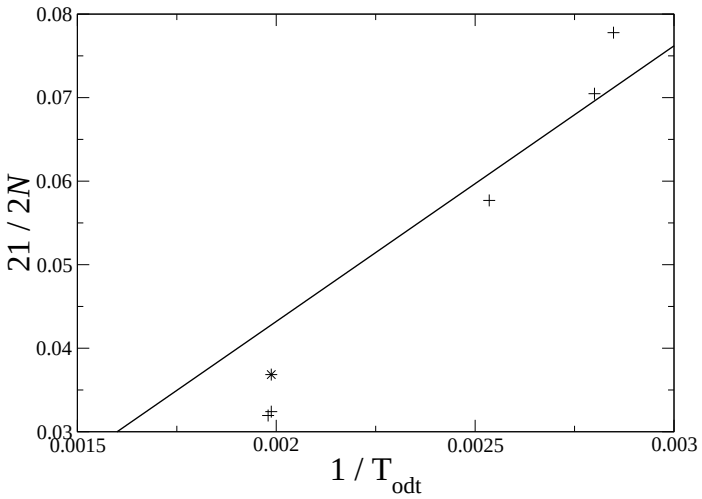

Figure 5.17: ODT of pure symmetric diblock copolymer melt of SI determined from various studies plotted in the same plot as the master curve presented in Equation (5.4.1). The data has been obtained from for lamellar forming SI solutions and melts.[2]

protonated and deutrated solvent for the lamellar phase, and comparing values of the ratio to SCFT estimates. The interaction parameter $\chi_{\text{I-DBP}}$ is used as the fitting parameter for the fitting the ratio using SCFT. The other interaction parameters were fixed at values of $\chi_{\text{SI}} = 0.08$ and $\chi_{\text{S-DBP}} = 0.3$. Two different coefficients for $1/T$ term for $\chi_{\text{I-DBP}}$ are reported in the text determined for two different PS-PI block compositions. The average of the coefficients is considered for the purpose of this section thereby using $\chi_{\text{I-DBP}} = 451/T - 0.56$. The reference volume used to calculate this interaction parameter is not mentioned in the thesis. The reference volume for this interaction parameter is taken as the DBP molecular volume from a fitting procedure we used. At $\phi_{\text{AB}} = 0.7$, we determine the ODT for a lamellar phase calculated using SCFT for this reference volume is closer to the ODT reported in the article.[3] Whereas, with styrene reference volume the ODT obtained using SCFT was

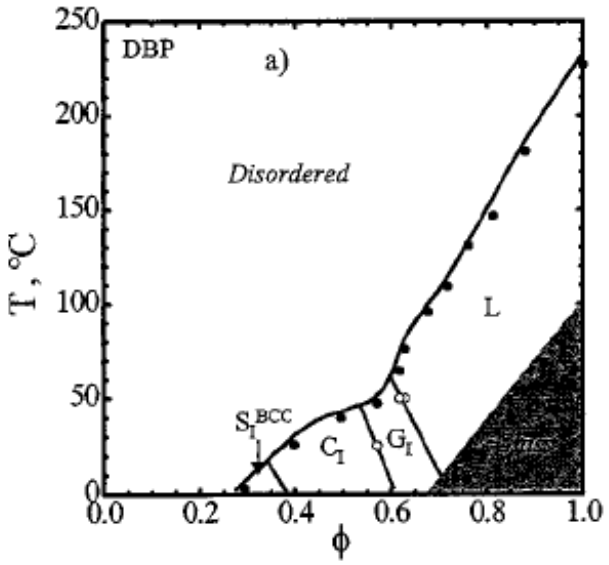

Figure 5.18: Phase portrait of polystyrene(PS)-polyisoprene(PI)(15-13) in dibutyl phthalate (DBP) which has been experimentally studied by Lodge and coworkers.[3]

found to differ by a larger margin with respect to the ODT reported in the article.[3]

The density of PS is mentioned as 1.05 g/mL and that of DBP is mentioned as 1.043 g/mL.[3] This gives us the ratio of monomer volumes as:

$$\frac{\nu_{\rm DBP}}{\nu_{\rm PS}} = \frac{M_{\rm DBP}}{M_{\rm PS}} \frac{1.05}{1.043} = 2.69, \tag{5.4.2}$$

where $M_{\rm DBP}$ and $M_{\rm PS}$ are the molecular weights of DBP and styrene respectively. The degree of polymerization for PS-PI is 285 with a reference volume as the styrene monomer volume.[3] The degree of polymerization with the solvent reference volume is 285/2.69 = 106. The ratio of statistical segment lengths[60] between PS and PI is 6.7/6.5 which has been approximated to 1.

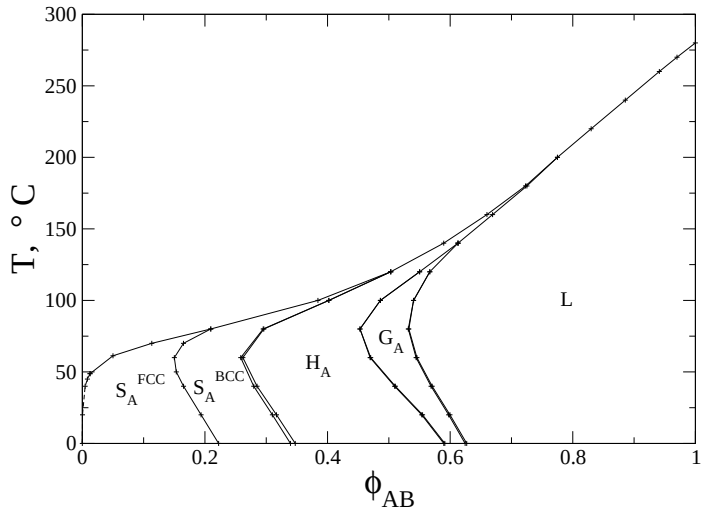

Figure 5.19: Simulating the phase portrait of polystyrene(PS)-polyisoprene(PI)(15-13) in dibutyl phthalate (DBP) which has been experimentally studied by Lodge and coworkers.[3]

The periodic phases show similar phase behavior as seen in the experimental plot (see Figure 5.18) with phase transitions: $\mathrm{L} \rightarrow \mathrm{G_A} \rightarrow \mathrm{H_A} \rightarrow \mathrm{S_A^{BCC}}$, upon dilution. We notice two phase coexistence regions for $\mathrm{H_A}$and $\mathrm{S_A^{BCC}}$, but barely noticeable in the case of other ordered phases. The ODT and critical micelle temperature (CMT) are found to match well in the case of experiments[3,52,89] where the CMT is calculated at $\phi_{\mathrm{AB}} = 0.01$ and $\phi_{\mathrm{AB}} = 0.02$, and compared with ODT at $\phi_{\mathrm{AB}} \sim 0.2$. CMT and ODT are similar in the range of $0.01 < \phi_{\mathrm{AB}} < 0.2$ according SCFT calculations presented in Figure 5.19.

The ODT at $\phi_{\mathrm{AB}} = 1$ is off by 50 °C relative to the experimental phase portrait in Figure 5.19. This corresponds to the deviation presented in Figure 5.17. The SCFT simulation predicts ODTs for $0.2 < \phi_{\mathrm{AB}} < 1$ to be much higher than those observed by the Lodge and coworkers,[3] which might be because of discrepancy in

the value of $\chi_{\text{PI-DBP}}$ interaction parameter used in simulation yielding a higher ODT. We expect SCFT to predict a higher ODT[78,80] than the ODT determined for block copolymer in solutions using experimental techniques.[2] Interaction parameters used in the calculation are also a source of the discrepancy.

5.5 Micelle Interactions in Spherical Phases

The interplay between the two spherical phases $S_A^{FCC}$and S_A^{BCC}in the dilute limit has been widely studied through experiments.[3,52,89,131,132,134–141] In this section I present a study of interactions between spherical micelles on FCC and BCC spherical lattices. This is studied using a combination of the periodic formulation of SCFT as well as the real space implementation of SCFT. Using the periodic formulation of the SCFT I calculate the nearest neighbor distance between spheres d_{nn} in $S_A^{FCC}$and S_A^{BCC}as well as the excess aggregation number M^{ex} of the spherical aggregates on the lattices of $S_A^{FCC}$and S_A^{BCC}. I determined the aggregation number of the spherical aggregate at CAC M^{CAC} , and the size of the spherical aggregate at CAC represented by its radius r_{CAC} using the real space implementation of SCFT.

The excess aggregation number M^{ex} is defined as

$$M^{\text{ex}} = \left(\phi_{\text{AB}} - \phi^{\text{CAC}}\right) \frac{a^3}{kN\nu}. \tag{5.5.1}$$

The volume fraction of copolymers present in the form of spherical aggregates on lattices $S_A^{FCC}$and $S_A^{BCC}$is proportional to $\left(\phi_{\text{AB}} - \phi^{\text{CAC}}\right)$, as ϕ^{CAC} is the volume fraction of copolymers dissolved in the solution. We expect the rest of the copolymers to be

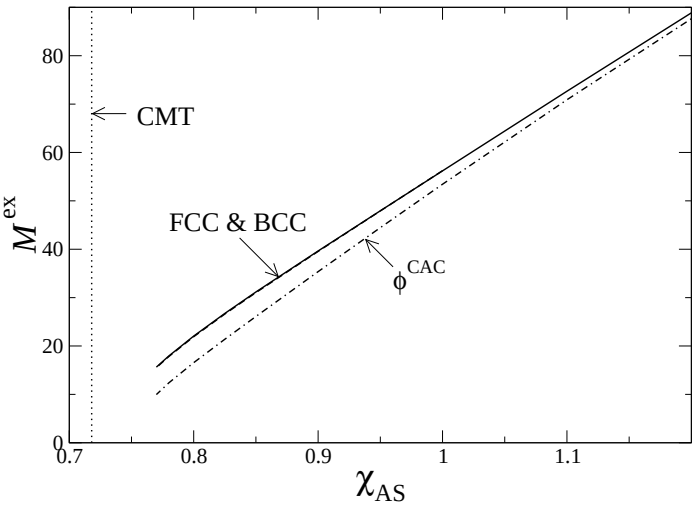

Figure 5.20: Variation of the aggregation number M^{ex} along a constant volume fraction of AB $\phi_{\text{AB}} = 0.17$, FCC represented by solid black line and BCC represented by dashed lines, with $f_{\text{B}} = 0.35$, $\chi_{\text{BS}} = 0.4$, $\chi_{\text{AB}} = 0.2$, $N = 100$, $\nu = 1$, $b_{\text{A}} = b_{\text{B}} = 6$Å, and reference volume is taken as 118Å^3. The aggregation number for FCC, and BCC are indistinguishable in this case. The dash dot line represents the aggregation number M^{CAC} at ϕ^{CAC} and the dotted line represents the critical micelle temperature(CMT).

present in the form of spherical aggregates arranged on a cubic lattice with a volume of a^3. The factor $a^3/kN\nu$ converts the volume fraction into an aggregation number. Here a represents the domain size of the cubic lattice and k represents the number of spherical aggregates present in lattices of $\text{S}_{\text{A}}^{\text{FCC}}$and $\text{S}_{\text{A}}^{\text{BCC}}$. The number of spherical aggregates in $\text{S}_{\text{A}}^{\text{FCC}}$lattice is $k = 4$, and in a $\text{S}_{\text{A}}^{\text{BCC}}$lattice is $k = 2$.

In Figure 5.20, the variation of M^{ex} relative to the solvent selectivity χ_{AS} along a constant volume fraction line $\phi_{\text{AB}} = 0.17$, which is the dotted line in Figure 5.14 is presented. Another point to note is that only χ_{AS} is varied and χ_{BS} , and χ_{AB} are kept constant so the assumption of χ_{AB} and χ_{BS} being constant in this temperature range is made in order to calculate the CMT.

The parameters used in the simulation are $f_{\mathrm{B}} = 0.35$, $N = 100$, $\chi_{\mathrm{BS}} = 0.4$, and $\chi_{\mathrm{AB}} = 0.2$. The statistical segment length of both monomers A, and B is taken as 6Å, and the reference volume is set at $\nu = 118\text{Å}^3$. The aggregation numbers for both phases $\mathrm{S_A^{FCC}}$, and $\mathrm{S_A^{BCC}}$are indistinguishable on the plot. Hence, the phase transition between $\mathrm{S_A^{FCC}}$and $\mathrm{S_A^{BCC}}$is not due to the differing values of M^{ex} for $\mathrm{S_A^{FCC}}$and $\mathrm{S_A^{BCC}}$. In Figure 5.20, M^{ex} approaches M^{CAC} as one increases the solvent selectivity χ_{AS} . This corresponds to the phenomena where unbinding occurs at a higher values of ϕ_{AB} as one increases the values of χ_{AS} .

M^{ex} can also be represented relative to the aggregation number of the spherical micellar aggregate at the CAC M^{CAC} for particular block composition f_{B} . It is given by

$$\frac{M^{\mathrm{ex}}}{M^{\mathrm{CAC}}} = \frac{\left(\phi_{\mathrm{AB}} - \phi^{\mathrm{CAC}}\right)}{\left(\phi_{\mathrm{AB}}{}' - \phi_{\mathrm{AB}}{}^{\mathrm{free}}\right)} \frac{a^3}{kV_{\mathrm{a}}} \tag{5.5.2}$$

where ϕ'_{AB} is the volume fraction of the diblock copolymer in the simulation cell, $\phi_{\mathrm{AB}}^{\mathrm{free}}$ is the volume fraction of the diblock copolymer dissolved in the solution, and V_{a} is the volume of the simulation cell for the spherical micelle. The difference $\left(\phi'_{\mathrm{AB}} - \phi_{\mathrm{AB}}^{\mathrm{free}}\right)$ gives the amount of diblock copolymer in the spherical micellar aggregate.

Utilizing the definition of M^{ex} presented in Equation (5.5.2), I would like to study dependence of M^{ex} on the concentration or volume fraction of the diblock copolymer in the system. M^{CAC} is constant for a particular block composition f_{B} considered here and will be represented by $\mathrm{M^{CAC}}$ for the constant value of f_{B} considered from here on. In Figure 5.21, the variation of M^{ex} /$\mathrm{M^{CAC}}$ relative to ϕ_{AB} for the good solvent case where $\chi_{\mathrm{BS}} = 0.4$, and $f_{\mathrm{B}} = 0.5$ is presented. We observe the aggregation number for $\phi_{\mathrm{AB}} < 0.05$ is same as the value of aggregation number at $\phi^{\mathrm{CAC}} \approx 10^{-6}$.

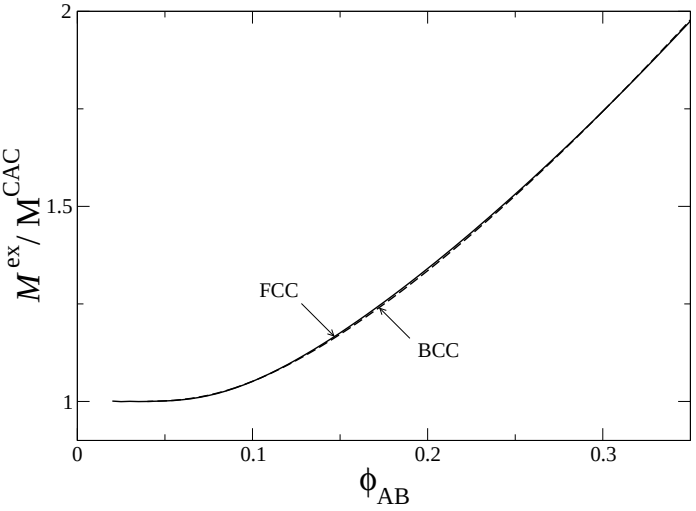

Figure 5.21: Aggregation number M^{ex}, normalized relative to the aggregation number at ϕ^{CAC} , *vs.* the volume fraction of the diblock copolymer ϕ_{AB} in the periodic phases FCC and BCC for $f_{\mathrm{B}} = 0.5$ for the good solvent with $\chi_{\mathrm{BS}} = 0.4$, $\chi_{\mathrm{AS}} = 1$, $\chi_{\mathrm{AB}} = 0.2$, and $N = 100$

Once again, M^{ex} is almost indistinguishable for both the spherical phases $\mathrm{S}_{\mathrm{A}}^{\mathrm{FCC}}$, and $\mathrm{S}_{\mathrm{A}}^{\mathrm{BCC}}$. An important feature of figure 5.21 is that M^{ex} or the aggregation number of the spherical aggregates in the cubic lattices of $\mathrm{S}_{\mathrm{A}}^{\mathrm{FCC}}$, and $\mathrm{S}_{\mathrm{A}}^{\mathrm{BCC}}$is not the same as M^{CAC} for $\phi_{\mathrm{AB}} > 0.1$. M^{ex} approaches $\mathrm{M}^{\mathrm{CAC}}$ as one gets closer to this volume fraction at which both $\mathrm{S}_{\mathrm{A}}^{\mathrm{FCC}}$, and $\mathrm{S}_{\mathrm{A}}^{\mathrm{BCC}}$unbind to form isolated spherical micelles.

We predict a monotonic increase in M^{ex} with increasing ϕ_{AB} from Figure 5.21, whereas the aggregation number determined by Grason[142] was found to have a maximum for a certain value of ϕ_{AB} . The model used by Grason is a mean field analytical model with a corresponding assumption that the selective solvent does not penetrate the core of an aggregate. Especially for a small molecule solvent the assumption of no presence of solvent in the core of a spherical micellar aggregate hardly holds true. Significant solvent presence in the core was shown previously in Figure 4.7 in

page 103 as well as observed through experiments.[49,52] SCFT predicts, for the set of parameters considered here, significant solvent presence $\phi_S \approx 0.3$ present in the core of aggregates.

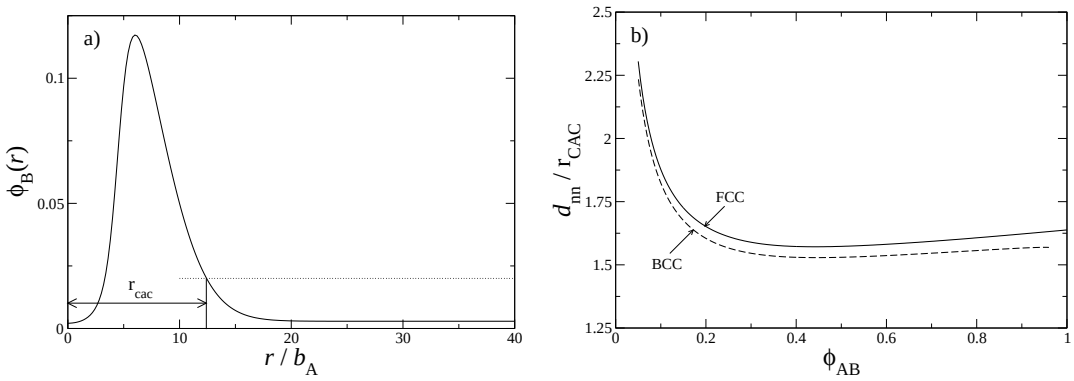

Figure 5.22: Figure (a) represents the definition of r_{CAC} . r_{CAC} is the value of r at which the volume fraction $\phi_{\mathrm{B}}(r) - \phi_{\mathrm{B}}^{\mathrm{free}} = 0.02$, where $\phi_{\mathrm{B}}^{\mathrm{free}}$ is the volume fraction of dissolved monomer of B in the solvent. Figure (b) represents the nearest neighbor distance d_{nn}, normalized relative to the radius of a micelle at CAC, *vs.* volume fraction of the diblock ϕ_{AB} for the periodic phases FCC and BCC with $f_{\mathrm{B}} = 0.6$ for a good solvent with $\chi_{\mathrm{BS}} = 0.4$, $\chi_{\mathrm{AS}} = 1$, $\chi_{\mathrm{AB}} = 0.2$, and $N = 100$.

The aggregation number M^{ex} is found to be indistinguishable for both spherical phases $\mathrm{S}_{\mathrm{A}}^{\mathrm{FCC}}$and $\mathrm{S}_{\mathrm{A}}^{\mathrm{BCC}}$, even though they have different coordination number (number of nearest neighbors), and different nearest neighbor distances, which is presented in Figure 5.22. We denote the nearest neighbor distance as d_{nn}. This behavior is found for the variation relative to both the solvent selectivity as well as different volume fractions of the diblock copolymer AB.

The interaction between the spherical aggregates on $\mathrm{S}_{\mathrm{A}}^{\mathrm{FCC}}$, and $\mathrm{S}_{\mathrm{A}}^{\mathrm{BCC}}$lattices is described in terms of a pair potential. The assumption here is that the major contri-

bution of interactions comes from the nearest neighbors on the lattice. The nearest neighbor distance for S_A^{FCC}, and $S_A^{BCC}$are given by

$$d_{nn}^{FCC} = \frac{a}{\sqrt{2}} \tag{5.5.3}$$

$$d_{nn}^{BCC} = \frac{\sqrt{3}a}{2}. \tag{5.5.4}$$

The definition of r_{CAC} is dependent on convention. The radius of the spherical aggregate at CAC r_{CAC} is defined as the distance from the center of the aggregate at which the excess volume fraction of the corona or solvent philic block of the copolymer is $\phi_B(r) = 0.02$, when $\phi_B(r)$ is corrected for amount of B monomer dissolved in the solvent S. The definition of r_{CAC} is presented in Figure 5.22 (a). In Figure 5.22 (b) the variation of d_{nn} with respect to ϕ_{AB} is presented. The parameters used to calculate d_{nn} are $f_B = 0.6$, $N = 100$, $\chi_{BS} = 0.4$, $\chi_{AS} = 1$, and $\chi_{AB} = 0.2$. We find that d_{nn} does not vary much in the region where $\phi_{AB} > 0.2$, but suddenly starts increasing around $\phi_{AB} \approx 0.2$ which represents the onset of unbinding transition from a periodic phase, either S_A^{FCC}or S_A^{BCC}, to an isolated spherical micellar morphology. Another key feature in Figure 5.22 is that d_{nn} for the S_A^{FCC}phase is greater than d_{nn} for the S_A^{BCC}phase.

The ratio of M^{ex} /M^{CAC} earlier presented relative to ϕ_{AB} in Figure 5.21 is presented in Figure 5.23 relative to d_{nn}/r_{CAC} . Figure 5.23 reiterates the behavior of $M^{ex} \rightarrow M^{CAC}$ as the spherical phases starts to unbind or as the nearest neighbor distance d_{nn} between the spherical aggregates on the lattices of S_A^{FCC}, and S_A^{BCC}increases. The nearest neighbor distance is large enough for $d_{nn}/r_{CAC} > 2.5$ due to which the

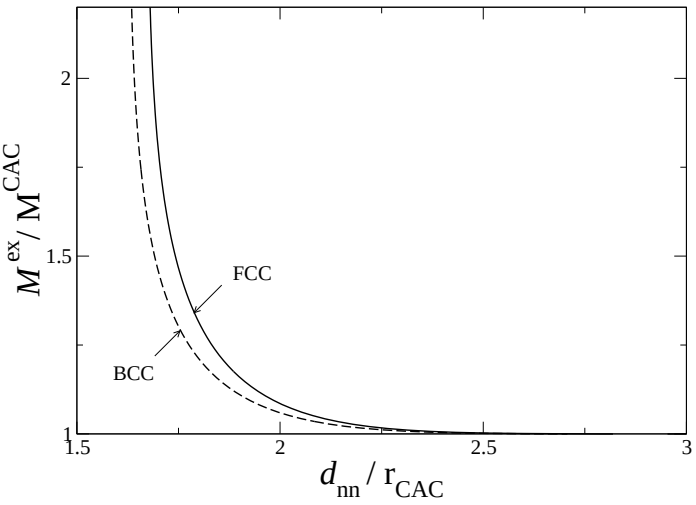

Figure 5.23: Aggregation number M^{ex} normalized relative to the aggregation number at CAC versus nearest neighbor distance d_{nn} in periodic phases of FCC and BCC with $f_{\text{B}} = 0.5$ for the good solvent with $\chi_{\text{BS}} = 0.4$, $\chi_{\text{AS}} = 1$, $\chi_{\text{AB}} = 0.2$, and $N = 100$.

aggregation number of the spherical aggregates on $\text{S}_{\text{A}}^{\text{FCC}}$and $\text{S}_{\text{A}}^{\text{BCC}}$lattices are same as M^{CAC}. This implies that the spherical aggregates on periodic lattices of $\text{S}_{\text{A}}^{\text{FCC}}$or $\text{S}_{\text{A}}^{\text{BCC}}$can be treated as isolated spherical micellar aggregates in the regime where $d_{\text{nn}}/r_{\text{CAC}} > 2.5$. The aggregation number of spherical aggregates on the lattices of $\text{S}_{\text{A}}^{\text{FCC}}$, and $\text{S}_{\text{A}}^{\text{BCC}}$is found to vary with d_{nn} or ϕ_{AB} as well as with solvent selectivity χ_{AS} .

A pair-wise interaction potential F_{pair} between the nearest neighbors in each lattice is used to quantify the interaction between the nearest neighbors on lattices of $\text{S}_{\text{A}}^{\text{FCC}}$, and $\text{S}_{\text{A}}^{\text{BCC}}$. The interaction energy between the spherical aggregates F_{int} is dependent on the coordination number z, or the number of nearest neighbors for each lattice. F_{int} is then represented in the form of pair-wise potential between nearest neighbors through the Equation (5.5.5). Here the factor 1/2 comes about in order to avoid

double counting of a pair of nearest neighbors. $F_{\rm pair}$ and $F_{\rm int}$ are related through the expression

$$F_{\rm int} = \frac{1}{2} z F_{\rm pair} \, . \tag{5.5.5}$$

In essence $F_{\rm int}$ is the excess Helmholtz free energy described relative to isolated spherical micelles at $\phi^{\rm CAC}$. $F_{\rm int}$ is given by

$$F_{\rm int} = \frac{\Omega_{\rm m}}{\nu} \left[\left(f - f^{\rm CAC} \right) - \Delta\mu^{\rm CAC} \, \left(\phi - \phi^{\rm CAC} \right) \right] \tag{5.5.6}$$

where $\Omega_{\rm m} = a^3/k$ is the volume occupied by each micelle on a lattice with a lattice parameter a, ν is the volume occupied by each monomer or a solvent molecule. The dependence of $F_{\rm pair}$ on the nearest neighbor distance $d_{\rm nn}$ is presented in Figure 5.24.

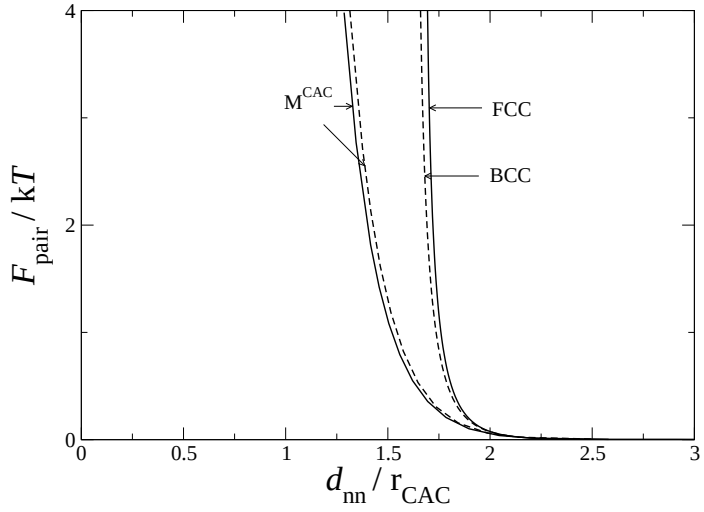

Figure 5.24: Energy of interaction per bond $F_{\rm pair}/{\rm k}T$ versus $d_{\rm nn}$, normalized relative to the radius at the CAC, for the spherical phases FCC and BCC for $f_{\rm B} = 0.5$ for the good solvent with $\chi_{\rm BS} = 0.4$, $\chi_{\rm AS} = 1$, $\chi_{\rm AB} = 0.2$, $N = 100$, and $\nu = 1$. The dashed black lines represent the BCC phase and solid black lines the FCC phase. The lines on the left represent spherical phases with a constant aggregation number of $\rm M^{CAC}$.

F_{pair} has also been calculated by maintaining a constant $M^{\text{ex}} \equiv \text{M}^{\text{CAC}}$, to distinguish from the calculations where M^{ex} varies with d_{nn} or ϕ_{AB}. In order to maintain constant $M^{\text{ex}} = \text{M}^{\text{CAC}}$, I calculate the lattice spacing a in each spherical phase to achieve the desired aggregation number. This can be determined simply by inverting the relation used to calculate M^{ex} in equation (5.5.2), which then yields

$$a = \left(\frac{\left(\phi^{'} - \phi_{\text{free}}\right) k V_{\text{m}}}{\left(\phi - \phi^{\text{CAC}}\right)} \right)^{\frac{1}{3}}. \tag{5.5.7}$$

The pair-wise interaction F_{pair} is found to be similar for $\text{S}_{\text{A}}^{\text{FCC}}$and $\text{S}_{\text{A}}^{\text{BCC}}$for both variable aggregation number as well as constant aggregation number. This behavior is similar to that noticed for excess aggregation number M^{CAC} relative to ϕ_{AB}, where even though $\text{S}_{\text{A}}^{\text{FCC}}$and $\text{S}_{\text{A}}^{\text{BCC}}$have different coordination numbers and d_{nn} their aggregation numbers are indistinguishable. The pair-wise interaction potential F_{pair} for variable M^{ex} is found be stiffer than for the F_{pair} with a constant aggregation number of M^{CAC}. This behavior is due to larger M^{ex} or larger size of spherical aggregates on the lattice for variable M^{ex} relative to $M^{\text{ex}} = \text{M}^{\text{CAC}}$.

Upon approaching the dilute limit both the phases tend to the same exchange chemical potential $\Delta\mu^{\text{CAC}}$, shown in Figure 3.8 in page 82, which should be the case as the spherical micelles are so farther apart that it does not matter if they are arranged on FCC lattice or a BCC lattice. This behavior is noticeable in the variation of M^{ex} and F_{pair} relative to d_{nn} presented in figures 5.23 and 5.24, respectively.

5.6 Conclusions

Phase behavior is analyzed in the phase cube with solvent selectivity χ_{AS}, block composition f_B, and volume fraction of the diblock ϕ_{AB} as the varying parameters. The periodic phases with a solvent-phobic core are found to swell, whereas the ones with the solvent-philic core tend to macrophase separate in the dilute regime as they can not swell indefinitely. I also relate the order-order transition lines between the periodic phases which can swell to the transformations of their respective isolated aggregate morphologies in the dilute limit. The transition between $S_A^{FCC}$and H_A, and $H_A$and L tends to the transition between spherical and cylindrical aggregates, and cylindrical and bilayer aggregates, respectively.

For the case of constant solvent selectivity or f_B *vs.* ϕ_{AB} plane RPA theory is used to analyze the binary system. Flory-Huggins theory is used to calculate the critical values of f_B and ϕ_{AB}, and also the binodals of homogeneous phases. RPA theory is used to determine the spinodal of the disordered phase, and the value of critical wave vector modulus q^* yields additional information of the order-disorder transition. If $q^* \neq 0$ implies the order-disorder transition is preceded by the presence of a periodic phase, and $q^* = 0$ might indicate the presence of isolated aggregate morphologies prior to disorder transition from an ordered phase. The critical value of ϕ_{AB} derived from Flory-Huggins theory, and the critical point derived from RPA do not vary much relative to values of χ_{AS}, or χ_{AB} in the f_B *vs.* ϕ_{AB} plane. RPA also hints towards two different regions of phase behavior present in the f_B *vs.* ϕ_{AB} plane. There is a region of phases related to the macrophase separation between a pure solvent and pure homopolymer A, which is solvent-phobic, close to $f_B = 0$, and the

second region arising from the periodic phases in the pure diblock limit $\phi_{AB} = 1$. Upon increasing the value of χ_{AS} one finds these two phase regions merge as solvent selectivity χ_{AS} drives periodic phase formation over larger area in the plane of constant solvent selectivity χ_{AS} . RPA is also used to study the variation of spinodal relative to either interaction parameter between the blocks of the diblock copolymer χ_{AB} or the good solvent characteristic χ_{BS} .

Phase portraits for constant solvent selectivity χ_{AS} or f_B *vs.* ϕ_{AB} plane are determined using SCFT. There are two detached phase regions found for $\chi_{AS} = 0.70$. One of them corresponds to phase behavior of pure diblock copolymer melt, and the other corresponds to macrophase separation between homopolymer of solvent-phobic block A and solvent S. I notice ordered phases are stable close to the critical point of macrophase separation. This observation has never been made before using SCFT. The two detached phase regions are found to merge at a certain value of χ_{AS} in the range $0.70 < \chi_{AS} < 0.75$ for the parameters considered in the simulations.

For the periodic regime one notices large two phase coexistence regimes present between the ordered phases as we decrease the volume fraction of the diblock ϕ_{AB} in the system. The gyroid phase $G_A$is replaced by two phase coexistence regimes between L and $H_A$close to the unbinding transition, and approach the crossover between isolated aggregate morphologies B and C. I predict wide phase coexistence regimes between $S_A^{FCC}$and $H_A$as well as $S_A^{BCC}$and H_A. The transformation of the spherical periodic phases $S_A^{FCC}$and $S_A^{BCC}$to isolated spherical micelles is always preceded by S_A^{FCC}. For small block composition of B block f_B and in the dilute limit a two phase region with a solvent-rich disordered macrophase and a polymer-rich disordered macrophase

is found.

Periodic phases with solvent-philic core are found to macrophase separate upon dilution in coexistence with a solvent-rich phase. The inability of the periodic phases with a core of solvent-philic block to swell indefinitely causes them to macrophase separate with a solvent-rich phase. The "compound micelles" noticed by Zhang and Eisenberg[24,92] with the solvent-philic block at the core are found in this regime to coexist with a solvent rich macrophase in aqueous solutions of polystyrene-poly(acrylic acid).

Selectivity of the solvent tends to drive phases with A as core to dominate the phase portraits. Solvent S partitions itself preferentially into solvent-philic B domains leading to this behavior. This is seen in cuts of phase portraits at constant f_{B} as well as at constant χ_{AS} . The periodic phases noticed for the pure diblock limit is controlled by $\chi_{\mathrm{AB}}\,N$. For a solvent selective enough, I notice a large region of the phase portrait where ordered phases are found to be stable, even though the diblock copolymer is disordered in its pure form ($\phi_{\mathrm{AB}} = 1$). The parameter regime considered in this chapter are for selective solvents and thus, χ_{AS} drives the phase behavior in the phase portraits presented.

We can comment on the solubility of S in AB or AB in S by studying the two phase region in the region of $f_{\mathrm{B}} \sim 0$. The solubility of the small molecule selective solvent is much higher than the solubility of the diblock copolymer in the solvent S. This distinction is due to the relatively smaller size of the solvent, which is also found to play a major role in the kinetics of micellization discussed in the next chapter.

For the case of constant block length or the plane χ_{AS} *vs.* ϕ_{AB} even for low block

compositions $f_B = 0.26$ and chain length $N = 100$ we notice the phase portrait to be dominated by phases with solvent-phobic block A as the core. The ordered phase $S_A^{FCC}$is stable in the dilute regime even for block composition as low as $f_B = 0.26$, which is generally found for a majority B block composition in a pure diblock copolymer melt. For high solvent selectivity and dilute solutions of diblock copolymer one notices large two phase regions between periodic phases. The gyroid phase $G_A$is found to be replaced by two phase coexistence between L and $H_A$upon increasing the selectivity of the solvent. The lower limit of χ_{AS} considered is the neutral solvent, where the phase behavior can be described using the dilution approximation.

SCFT is used to simulate a phase portrait determined by Lodge and coworkers[3] for PS-PI in DBP. SCFT predicts the phase transformations correctly. However, the agreement is found to be of a more qualitative nature rather than quantitative nature. This deviation might be due the inability to obtain accurate interaction parameters as well as the effect of fluctuations which is disregarded in the coarse grained theory of SCFT.

The interplay between the spherical periodic phases S_A^{FCC}, and $S_A^{BCC}$with spherical micellar aggregates is studied by combining real space implementation of SCFT as well as its periodic counterpart. The aggregation numbers of spherical micelles are found to be almost indistinguishable on FCC and BCC lattices. Whereas, they are found to differ from the value of aggregation number of these isolated spherical micelles found at ϕ^{CAC} with varying χ_{AS} and volume fraction of the diblock copolymer. This observation is striking even though FCC lattice and BCC lattice have different lattice parameters as well as different coordination numbers, but spherical micelles on these

lattices end up having indistinguishable aggregation numbers.

Pair-wise interactions between micelles are calculated and found to be similar for both lattices. Once again this observation is striking given the fact that FCC and BCC lattices are found to have different lattice parameters as well as different coordination numbers. This pair-wise interactions can be utilized in Monte-Carlo simulations, because of the prediction of the pair-wise interaction being independent of the type of lattice. This attribute can be used to develop more realistic models of interactions between spherical micelles.

We notice the transition between S_A^{FCC}, and $S_A^{BCC}$to occur close to a point where the spherical aggregates to fill space on a FCC lattice. We predict the transformation from $S_A^{FCC} \rightarrow S_A^{BCC}$to be driven by the concentration of AB in the system. Increasing the concentration of AB leads to spherical micelle micelles to condense onto a FCC lattice, and the point at which the spherical aggregates fills space on a S_A^{FCC}lattice is close to $S_A^{FCC} \rightarrow S_A^{BCC}$transformation.

There has been a previous study on the phase behavior of AB/S using SCFT by Suo *et al.* .[90] Our motivation here has been to do a comprehensive study of the system from $\phi_{AB} = 0$ to $\phi_{AB} = 1$, which includes isolated aggregates found in the dilute limit. This has not been clearly studied by Suo *et al.* .[90] Also, they have not considered the possibility of phase coexistence between the solvent rich homogeneous macrophase and ordered phases with solvent-philic core block. Their analysis of the transition between spherical ordered phases $S_A^{FCC}$and $S_A^{BCC}$is limited, and they do not correlate the phase transition with the structural properties of isolated spherical micelles.

CHAPTER 6

Kinetics of Micellization

Small molecule surfactants[178] and polymeric surfactants[24,91] are similar in many ways, and show similar morphological trends in solution. The kinetics of micellar aggregation is, however, often much slower for polymeric surfactants. Typical small surfactants form aggregates in the microsecond/millisecond range.[179] The corresponding time scale for polymeric surfactant systems cover a wide range, but are often much longer than experimentally accessible time scales.[156,158,180] Slow kinetics for polymeric systems is generally attributed to a high degree of incompatibility between the core block and the solvent or a high glass transition temperature of the core block.

Figure 6.1 depicts two different types of dynamical processes that are relevant to the formation and dissolution of micelles in solution. Stepwise growth, shown on the

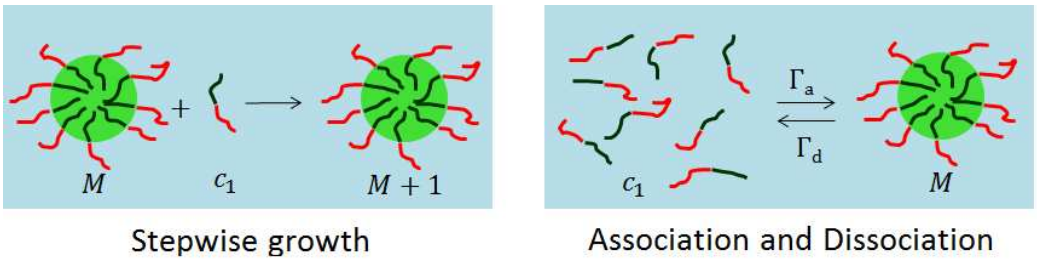

Figure 6.1: The two dynamical processes involved in kinetics of micellization.

left, is a comparatively fast process in which the number of molecules in a micelle can increase by one by absorbing a molecule from a reservoir of free surfactant molecules (unimers) dissolved in the surrounding solvent, or decrease by one by expelling one molecule into the surrounding solvent. These processes change the aggregation numbers of individual micelles, and allow exchange of molecules between micelles, but do not change the total number of micelles in a solution. Association and dissociation are slower processes that can create or destroy an entire micelle, shown on the right in Figure 6.1. We are primarily interested in this chapter in estimating timescales for spontaneous micelle association and dissociation.

Several theoretical studies have examined the dynamics of micelle association and dissociation. The classic treatment of Aniansson and Wall[181,182] assumes that association and dissociation occurs via stepwise growth. These authors, and most subsequent workers, assumed that micelle association and dissociation occur as the result of a random series of steps, in which the elementary step is the exchange of an individual surfactant molecule between a micelle and a coexisting gas of unimers. Here and hereafter, we refer to single surfactant molecules dissolved in solvent as unimers. Halperin and Alexander[183] and Nyrkova and Semenov[184] have subsequently considered fission

and fusion as alternative mechanisms, but also concluded that the stepwise growth mechanism normally dominates the rate of micelle association in polymeric systems, even when this process is very slow.

The theory of micelle association by stepwise growth is, in many ways, similar to the classical theory of nucleation and growth of a liquid droplet from a supersaturated vapor or solution. The main difference, of course, is the presence of a preferred size for micelles, which prevents micelles (unlike nuclei that appear during phase separation) to grow to only a finite size. In both theories, the size of an aggregate is assumed to undergo a biased random walk in a free energy landscape that is given by the free energy $G(M)$ as a function of an aggregation number M (i.e., the number of molecules in a micelle). The rate of micelle association is controlled by diffusion over barrier in this free energy landscape. Nyrkova and Semenov[184] stripped away some of the mathematical complexity of the original presentation by Aniansson and Wall to give a particularly clear description of micelle association and dissociation as an activated process analogous to nucleation. These authors were also the first to emphasize the fact that the relevant free energy barriers depend strongly on unimer concentration, and to explore some of the expected consequences of this fact.

The most important input to any quantitative theory of the micellization kinetics is thus a prediction of the free energy $G(M)$ of a micelle as a function of the degree of micellar aggregation M. Simple scaling theories for $G(M)$ been used to study dynamical processes in micellar solutions by Halperin and Alexander,[183] for diblock copolymers in strongly selective solvent, and by Semenov,[185] for diblock copolymers in polymeric matrix. For diblock copolymer surfactants in a polymeric matrix or

a small molecule solvent, we expect self-consistent field theory (SCFT) to provide rather accurate estimates of the barriers to micelle association and dissociation. The first such estimates were given by Semenov[185] for a polymeric matrix, who used a simple strong segregation theory (SST) to calculate these barriers at the critical micelle concentration (CMC). It was clear from Semenov's results that these barriers are quite large for typical polymeric systems. SST is expected to be quantitatively accurate, however, only for very strongly segregated micelles, with $\chi N \gg 10$.

The main goal of this chapter is to present a theory that is based upon the use of numerical SCFT to calculate the required free energy landscape for diblock copolymer surfactants in selective solvent. We consider both diblock copolymer in small molecule selective solvent and AB diblock copolymer in a matrix of homopolymer B. Quantitative estimates of rates of micelle dissociation and association are obtained from a theory that is based on Kramer's theory of activated processes, which allows us to estimate pre-exponential factors as well as free energy barriers.

We do not explicitly consider the possible role of fission or fusion here, but note that the free energy as a function of aggregation number that we calculate here would be required as an input to any of the more detailed analysis of these processes.

Recent experiments on a block copolymer in an ionic solvent, Meli *et al.* [154,155] have measured a decrease in both the average micelle size and polydispersity in a system that they have also shown to have a negligible rate of unimer exchange between micelles. This indicates an important role for some other aggregation mechanism. Mattice and coworkers,[186,187] and Dormidontova[188] have predicted that micelle fusion and fission can play a dominant role in micelle formation in solutions of strongly

amphiphilic polymeric surfactants. Mattice and coworkers used a Monte Carlo simulation employing two mechanisms: unimer insertion and expulsion, and micelle fusion and fission. They concluded micelle fusion and fission can dominate at high surfactant concentrations while unimer insertion and expulsion dominates for higher solvent selectivities. Dormidontova used scaling arguments to conclude that the micelle fusion mechanism depends on both the concentration of diblock copolymers as well as the aggregation number distribution of spherical micelles. Dormidontova's analysis has been criticized by Nyrkova and Semenov,[184] who concluded instead that the barrier to nearly equilibrium sized micelles by the fusion of two sub-critical micelles is always larger than the barrier to stepwise growth. Pool and Bolhuis[189] have shown in simulations that sufficiently large micelles (larger than the equilibrium size at the CMC) can also be unstable to fission. Fission of large micelles does not seem to be ruled out by the arguments of Nyrkova and Semenov, and might well play a role in the phenomena observed by Meli *et al.* . We do not explicitly consider the possible role of fission or fusion here, but note that the free energy as a function of aggregation number that we calculate here would be required as an input to any of the more detailed analysis of these processes.

6.1 Equilibrium Micellization

In this section I describe the model used to determine equilibrium properties of micellar solution. Consider a system of total volume V that contains micelles of various sizes and a low concentration of dissolved surfactant molecules ("unimers"). Let $N_{\mathrm{m}}(M)$ be the total number of micelles that contain exactly M surfactants, and let

$c_{\rm m}\,(M) = N_{\rm m}\,(M)/V$ be the corresponding concentration of such micelles. N_1 is the number of free unimers, and $c_1 \equiv N_1\,/V$.

The total Gibbs free energy of such a dilute solution (defined relative to that of pure solvent) is approximately

$$G = N_1\,\mu_1 + \sum_{M=2}^{\infty} N_{\rm m}\,(M)\mu_{\rm m}(M), \tag{6.1.1}$$

where $\mu_{\rm m}(M)$ and μ_1 are the chemical potentials for micelles of size M and dissolved unimers, respectively. In a dilute solution, these are given by

$$\mu_{\rm m}(M) = G_{\rm m}\,(M) + {\rm k}T\,\ln(c_{\rm m}\,(M)/c_{\rm m}^0\,) \tag{6.1.2}$$

$$\mu_1\,(M) = G_1 + {\rm k}T\,\ln(c_1\,/c_1^0\,). \tag{6.1.3}$$

In these expressions, $G_{\rm m}\,(M)$, for $M > 1$, and $G_1 \equiv G_{\rm m}\,(1)$ are standard state free energies for micelles of size $M > 1$ and unimers ($M = 1$). They are defined relative to unspecified standard state concentrations $c_{\rm m}^0$ and c_1^0.

The equilibrium concentration of micelles of size M may be obtained by minimizing the above free energy subject to a constraint on the total number of copolymer molecules, or (equivalently) by imposing the reaction equilibrium condition,

$$\mu_{\rm m}(M) = \mu_1\,M. \tag{6.1.4}$$

The resulting micelle concentrations may be written as

$$c_{\rm m}\,(M) = c_{\rm m}^{0}\, e^{-\Delta G\,(M,c_1\,)/{\rm k}T}\,, \tag{6.1.5}$$

where

$$\Delta G\,(M, c_1\,) \equiv G_{\rm m}\,(M) - \mu_1\, M, \tag{6.1.6}$$

is a grand-canonical chemical potential for the formation of a single micelle of size M.

Figure 6.2 shows the typical shape of the function $\Delta G(M)$ *vs.* aggregation number M for a micelle-forming system at concentrations near the critical micelle concentration (CMC). The curve has a minimum at a nonzero aggregation number $M_{\rm e}$, which corresponds to the most probable equilibrium micelle. The equilibrium distribution given above is peaked around $M_{\rm e}$, but includes a distribution of sizes.

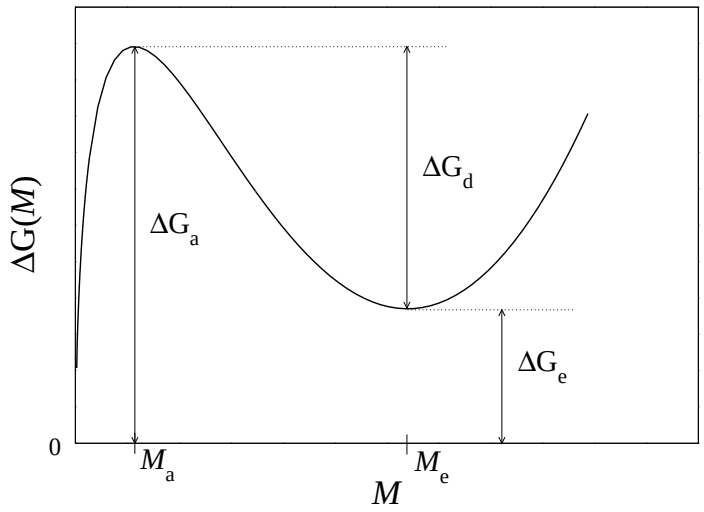

Figure 6.2: Schematic of $\Delta G\,(M)$ *vs.* M for a micelle forming system at a concentration c very slightly below the CMC. Symbols are defined in the text.

A useful simplified description of equilibrium micellization in systems with $M_e \gg 1$ may be obtained by simply ignoring the translational entropy of the micelles. This simplification approximates $\mu_m(M)$ as the internal free energy $G_m(M)$, ignoring the logarithmic dependence of $\mu_m(M)$ on $c_m(M)$ while retaining the logarithmic dependence of μ_1 on c_1. The equilibrium state of the resulting theory is obtained by minimizing the approximate free energy $G \simeq \sum_M N_m(M) G_m(M) + N_1 \mu_1$. This yields a sharp micellization transition when the total concentration c of the surfactant reaches a critical concentration c_c at which $\Delta G_e(c_c) = 0$. It predicts that no micelles are formed for $c < c_c$, and upon increasing concentration to $c_1 > c_c$ monodisperse micelles of size M_e coexists with the constant unimer concentration $c_1 = c_c$. This simplified picture becomes more accurate as M_e increases, and is adequate for describing many aspects of micellization in polymer systems with $M_e \sim 10^2 - 10^3$.

Allowing for micelle entropy modifies this picture by creating a distribution of micelle sizes peaked around M_e, and by slightly rounding the onset of micellization. The width of the equilibrium distribution $c_m(M)$ may be estimated by approximating $\exp(-\Delta G(M, c_1)/kT)$ as a Gaussian peaked at $M = M_e$. This yields a standard deviation

$$\sigma_e \equiv \langle (M - M_e)^2 \rangle^{1/2} = \left[\frac{1}{kT} \frac{\partial^2 \Delta G(M, c_1)}{\partial M^2} \right]^{-1/2}, \tag{6.1.7}$$

and a total micelle concentration (micelles per volume)

$$c_m = \sqrt{2\pi} \sigma_e \, c_m^0 \, e^{-\Delta G_e / kT}. \tag{6.1.8}$$

The apparent sharpness of the micelle transition in systems with $M_e \gg 1$ is a

result of the extreme sensitivity of $\Delta G_{\rm e}\,(c_1\,)/kT$ to changes in c_1 . If we approximate $\Delta G\,(M)$ as a continuous function of M, it is straightforward to show that

$$\frac{1}{kT}\frac{{\rm d}\Delta G_{\rm e}\,(c_1\,)}{{\rm d}\ln(c_1\,)} = -M_{\rm e}\,. \tag{6.1.9}$$

For values of c_1 near the CMC, the concentration of micelles thus changes by a factor of e when $\ln(c_1\,)$ changes by $1/M_{\rm e}$. As a result, the sharp micelle transition predicted by the simplified theory is actually "smeared" over a fractional concentration range $\Delta c_1\,/c_1 \sim 1/M$ that is typically of order one percent.

Because the onset of micellization is a rapid crossover, rather than a true phase transition, the definition of the CMC is in part a matter of convention. One convenient definition adopted here is that the equilibrium CMC is the equilibrium unimer concentration c_1 for which half of the available copolymer is in micelles, or for which

$$c_1 = c_{\rm m}\,M_{\rm e}\,, \tag{6.1.10}$$

where $M_{\rm e}$ is the average micelle size.

The concentration $c_{\rm c}$ was defined above, for mathematical convenience, as the point at which $\Delta G_{\rm e} = 0$. The ratio of $c_{\rm c}$ to the actual CMC, as defined by Eq. (6.1.10), depends on the value chosen for the micelle standard concentration $c_{\rm m}^0$, since this choice also effects the numerical values of $G_{\rm m}\,(M)$ and $\Delta G\,(M)$. To remove the explicit dependence of some of our expressions upon $c_{\rm m}^0$, it is convenient to adopt a convention in which $c_{\rm m}^0$ is chosen to be the CMC, as defined above. In a Gaussian

approximation for $c_{\rm m}\,(M)$, this this convention yields

$$c_{\rm m}^{0} \;= c_{\rm c}\,/(\sqrt{2\pi}\sigma_{\rm e}\,M_{\rm e}\,), \tag{6.1.11}$$

where $c_{\rm c}$ is the experimental CMC, and $M_{\rm e}$ and $\sigma_{\rm e}$ are the average and standard deviation of M at the CMC. The right hand side of Eq. (6.1.11) is equal to the total number concentration of micelles at the CMC. The requirement that $\Delta G\,(M_{\rm e}\,) = 0$ is true at the CMC if and only if one chooses the standard concentration $c_{\rm m}^{0}$ to be equal to the concentration of micelles at the CMC.

6.2 Free Energy Barriers

The overall goal of this chapter is to predict the rates of spontaneous micelle formation (association) and dissolution (dissociation). As described earlier, Aniansson and Wall[181,182] and most others[183,184] assume that micelle association and dissociation occur primarily by stepwise processes, via the insertion and expulsion of individual surfactant molecules ("unimers").

Following this methodology, our resulting kinetic theory is closely analogous to the classical theory of vapor phase nucleation. The most important difference is that there is a finite preferred micelle size $M_{\rm e}$, which results in some crucial differences.

Micelle formation is an activated process that we expect to occur at a rate (micelles created per volume per unit time)

$$R_{\rm a}\,(c_1\,) \simeq R_{\rm a0}\;\, e^{-\Delta G_{\rm a}\,/{\rm k}T}\,, \tag{6.2.1}$$

with a concentration-dependent activation barrier $\Delta G_{\rm a}\,(c_1\,)$ and a (thus far unspecified) prefactor $R_{\rm a0}\,(c_1\,)$. Once formed, micelles can spontaneously dissociate via a sequence of elementary reactions at a rate (per unit time)

$$R_{\rm d}\,(c_1\,) \simeq R_{\rm d0}\,e^{-\Delta G_{\rm d}\,/{\rm k}T}\,, \tag{6.2.2}$$

with an activation barrier $\Delta G_{\rm d}(c_1)$ and a prefactor $R_{\rm d0}(c_1)$. Detailed balance requires that

$$R_{\rm a}\;= R_{\rm d}\,c_{\rm m}\,, \tag{6.2.3}$$

for any unimer concentration c_1, and $c_{\rm m}\,(c_1\,)$ is the corresponding equilibrium number concentration of micelles.

The activation barrier for association and dissociation are determined from plots of $\Delta G\,(M)$ *vs* M. $\Delta G\,(M)$ has a maximum at a significantly smaller aggregation number $M_{\rm a}$ as seen from Figure 6.2 in Page 165. In what follows, we use

$$\begin{aligned}\Delta G_{\rm e}\,(c_1\,) &\equiv \Delta G\,(M_{\rm e}\,,c_1\,)\\ \Delta G_{\rm a}\,(c_1\,) &\equiv \Delta G\,(M_{\rm a}\,,c_1\,)\end{aligned} \tag{6.2.4}$$

to denote the minimum and maximum values of $\Delta G(M,c_1)$, respectively, at a specified unimer concentration c_1 .

The difference between secondary minima and maxima of $\Delta G\,(M)$ is defined as

$$\Delta G_{\rm d}\,(c_1\,) \equiv \Delta G_{\rm a}\,(c_1\,) - \Delta G_{\rm e}(c_1\,), \tag{6.2.5}$$

as indicated in Figure 6.2. In the kinetic theory, the free energies $\Delta G_{\rm a}\,(c_1\,)$ and $\Delta G_{\rm d}\,(c_1\,)$ act as barriers to micelle association and dissociation, respectively.

We show that in Section 6.5 that the prefactor $R_{\rm d0}$ is proportional to both the unimer concentration c_1 and the unimer diffusivity D_1 ,

$$R_{\rm d0} \sim c_1\, D_1\, R/\sigma_{\rm e}\sigma_{\rm a}. \tag{6.2.6}$$

In this expression, R is the micelle radius, $\sigma_{\rm e}$ is the width of the equilibrium distribution (the width of the maximum in $\exp(-\Delta G(M, c_1\,)/{\rm k}T\,)$ near $M_{\rm e}$), and $\sigma_{\rm a}$ is the width of the minimum well in $\exp(-\Delta G(M, c_1\,)/{\rm k}T\,)$ near $M_{\rm a}$.

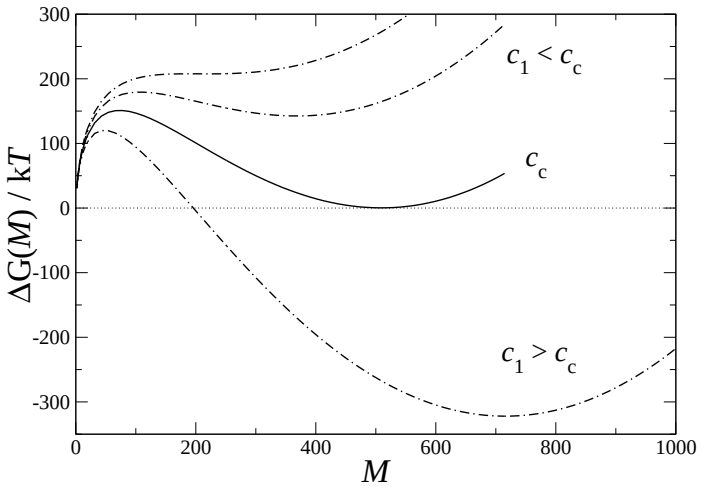

Figure 6.3: Example of how the SCFT excess free energy $\Delta G(M)$ varies with changes in unimer concentration c_1 near the CMC. Here, $c_{\rm c}$ is the concentration of the diblock copolymer at which $\Delta G_{\rm e} = 0$, which is very close to experimental CMC. These calculations were carried out for a system $f_{\rm B} = 1/2$, $\chi_{\rm AB}\, N_{\rm A} = 24$, $N = N_{\rm B} = 400$, $v = 100{\rm \AA}^3$ and $b = 6{\rm \AA}$ and $\chi_{\rm AB} = 0.12$.

Figure 6.3 shows $\Delta G(M, c_1\,)$ for a diblock copolymer AB in a matrix of homopolymer B, and how it is affected by changes in unimer concentration c_1. Resulting changes

in $\Delta G_{\rm a}(c_1)$ and $\Delta G_{\rm d}(c_1)$ can be seen. The barriers $\Delta G_{\rm a}(c_1)$ and $\Delta G_{\rm d}(c_1)$ are equal when $c_1 = c_{\rm c}$, where (by definition) $\Delta G_{\rm e}(c_1) = 0$. In the following, this barrier is represented at $c_{\rm c}$ for either reaction as

$$\Delta G_{\rm c} = \Delta G_{\rm a}(c_{\rm c}) = \Delta G_{\rm d}(c_{\rm c}). \tag{6.2.7}$$

It should be clear from Figure 6.3 that the association barrier $\Delta G_{\rm a}(c_1)$ decreases with either increasing μ_1 or c_1, while $\Delta G_{\rm d}(c_1)$ rapidly increases with increasing c_1. In subsaturated solutions, with $c_1 < c_{\rm c}$, we thus have $\Delta G_{\rm a} > \Delta G_{\rm d}$, while the reverse is true in supersaturated solutions with $c_1 > c_{\rm c}$, for which $\Delta G_{\rm a} < \Delta G_{\rm d}$.

The dependence of $\Delta G_{\rm a}(c_1)$ and $\Delta G_{\rm d}(c_1)$ upon unimer concentration can be obtained by calculating their derivatives with respect to μ_1 or $\ln c_1$. It is straightforward to show that

$$\frac{1}{{\rm k}T}\frac{{\rm d}\Delta G_{\rm a}(c_1)}{{\rm d}\ln(c_1)} = -M_{\rm a}, \tag{6.2.8}$$

$$\frac{1}{{\rm k}T}\frac{{\rm d}\Delta G_{\rm d}(c_1)}{{\rm d}\ln(c_1)} = M_{\rm e} - M_{\rm a}. \tag{6.2.9}$$

These identities immediately tell us that for large micelles, with $M_{\rm e} \gg 1$ and $M_{\rm a} \gg 1$, $\Delta G_{\rm a}(c_1)/{\rm k}T$ is a very rapidly decreasing function of c_1, and that $\Delta G_{\rm d}(c_1)/{\rm k}T$ is a very rapidly increasing function of c_1. They also imply that $\Delta G_{\rm d}$ must vary much more rapidly with concentration than $\Delta G_{\rm a}$, simply because $M_{\rm e}$ is usually significantly larger than $M_{\rm a}$: SCFT calculations for nearly symmetric diblock copolymers in homopolymer matrix of B yield $M_{\rm e}/M_{\rm a} \sim 8$ at the CMC for a wide range of parameters. This corresponds to an equilibrium core radius that is about the twice

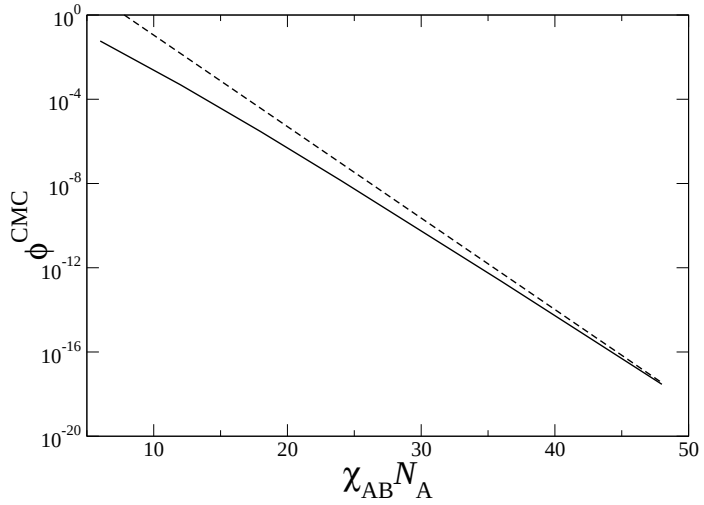

Figure 6.4: Volume fraction of the diblock copolymer at critical micelle concentration CMC $\phi^{\rm CMC}$ *vs.* $\chi_{\rm AB}\, N_{\rm A}$, for a diblock AB with $f_{\rm A} = 1/2$, $\chi_{\rm AB}\, N_{\rm A} = 24$, $N_{\rm B} = N_{\rm AB} = 200$, $v = 100 \text{Å}^3$ and $b = 6\text{Å}$. The dashed line represents values which scale as $\sim e^{-\chi_{\rm AB}\, N_{\rm A}}$.

that of the activated state.

The prefactor in the rate of association or dissociation is directly proportional to the concentration of free surfactant. Consider the case $c > c_{\rm c}$, in which under thermodynamic equilibrium c_1 is pinned at $c_{\rm c}$. From Chapter 4 we know that $c_{\rm c} \sim \exp(-\chi_{\rm AS}\, N_{\rm A})$. Hence, there are two competing exponential dependences, one from $c_{\rm c}$ and another from $\Delta G_{\rm c}$.

There are potential situations that arise where $c_{\rm c}$ is high but $\Delta G_{\rm c}$ might limit the rates of association or dissociation. Or, possibly $c_{\rm c}$ is low and the solubility of the diblock copolymer limits the rates of association or dissociation. Consequently, when studying experimental observations involving surfactants with a wide range of solubilities, or block copolymer surfactants that involve a range of core block molecular weights, it is useful to distinguish four possible situations:

(1) *Unimer solution*: In this case, sufficiently weak surfactants, or short copolymers, do not form micelles. As a rule of thumb, we may expect to see micelles of AB copolymers form in an B matrix only if the pure diblock copolymer material at the same temperature would form an ordered phase. The variation of volume fraction at the CMC as calculated for a simple polymer blend, is presented in Figure 6.4 relative to $\chi_{AB}\, N_A$ for the diblock copolymer AB in B homopolymer. This Figure 6.4 gives the amount of free copolymers we expect to be present in the system at equilibrium.

(2) *Equilibrium micellar solution*: For surfactants that are somewhat less soluble, or for fairly long copolymers, there may exist a range of experimental parameters and core block molecular lengths for which micelles form. In these systems, the barrier to creation or destruction at the CMC remains small enough for micelles to be created and destroyed over experimentally observable timescales. This is the only case in which it possible to observe a reversible CMC.

(3) *Partially equilibrated micellar solution*: A solution where the exchange of molecules between micelles, or micelles and the unimer solution remains reasonably rapid, but in which the barriers to creation and destruction of entire micelles at the CMC become so large that creation and destruction become unobservably slow at the CMC. In this case, the distribution of micelle sizes can change by unimer exchange, but the total number concentration of micelles cannot.

(4) *Frozen micelles*: In systems with negligible unimer solubility and/or glassy micelle cores, the rate of exchange of unimers between micelles can become negligible.

The dynamical model of stepwise growth and shrinkage used here is only relevant in cases 2 and 3 (fully or partially equilibrated micellar solutions). In case 1, there

are no micelles, and in case 4 the system is in a kinetically frozen state. It seems likely that most experiments on micelle-forming block copolymer surfactants in a homopolymer or a small molecule solvent matrix involve either frozen or partially equilibrated micelles.

Partial equilibration was first emphasized by Nyrkova and Semenov.[184] In the true equilibrium state of a micellar solution, the unimer concentration is that of the CMC concentration. A system will generally not be able to reach this state, even when the exchange of individual monomers remains rapid, if the barriers to the association and dissociation of whole micelles are large at the CMC, i.e., if $\Delta G_{\mathrm{c}} / \mathrm{k}T \gg 1$. This does not mean, however, that micelles can never be created or destroyed in such systems. Because the barriers $\Delta G_{\mathrm{a}}(c_1)$ and $\Delta G_{\mathrm{d}}(c_1)$ are sensitive to c_1, micelle association may proceed rapidly at unimer concentrations sufficiently far above the CMC, and micelle dissociation at concentrations somewhat below the CMC, even when both reactions are suppressed near the CMC. If the unimer concentration in such a system ever reaches a range near the CMC in which both association and dissociation are suppressed while unimer exchange remains rapid, the distribution of micelle sizes will continue to evolve without changing the total number concentration of micelles. The distribution of micelle sizes in such a system will thereafter evolve towards a state that minimizes the free energy subject to a constraint on the total number concentration of micelles. Over time, this is expected to yield a relatively narrow distribution in which the average aggregation number is history dependent and generally different from its equilibrium value.

Nyrkova and Semenov[184] have characterized this situation by defining two kinet-

ically controlled concentrations $c_{\mathrm{a}}(\tau)$ and $c_{\mathrm{d}}(\tau)$ for partially equilibrated systems conducted over a timescale τ. These define a concentration range near the CMC in which both reactions are suppressed. The "association concentration" $c_{\mathrm{a}}(\tau)$ is the concentration above which micelle association occurs with a characteristic timescale less than the experiment time τ, and below which the association rate is unobservable. Nyrkova and Semenov refer to $c_{\mathrm{a}}(\tau)$ as the "apparent CMC". The "dissociation concentration" $c_{\mathrm{d}}(\tau)$ is the concentration below which micelles dissociate with a lifetime less than τ, and above which their is no observable dissociation. Exact values of c_{c} and c_{d} do, of course, depend upon the choice of experimental timescale τ, but only logarithmically, because the underlying reaction rates are exponentially sensitive functions of concentration.

6.2.1 SCFT Methodology

In previous sections we have described equilibrium micellization, and also a kinetic theory in terms of free energy barriers. Here we would like to describe how these free energy barriers are obtained using SCFT. The goal here ultimately is to obtain kinetic information of the system by using equilibrium SCFT calculations to describe the activation barriers. The theory described below is applicable for any size of solvent i.e., S can either be a homopolymer or a small molecule solvent.

The excess Helmholtz free energy G_{m} has been defined earlier in section 3.6 from chapter 3. Here, we use M_i to represent the excess number of molecules for each species i. We will refer to M_i as the aggregation number for species i, and use $M \equiv \{M_{\mathrm{AB}}, M_{\mathrm{S}}\}$ as shorthand for the set of relevant aggregation numbers. Generally,

$M_{\mathrm{AB}} > 0$ for the surfactant AB, but $M_{\mathrm{S}} < 0$ for the matrix solvent S. Let $\mu_i^{\mathrm{m}}(M)$ denote the equilibrium chemical potential of species i for a micelle with specified values for M_i. These chemical potentials also describe the coexisting homogeneous solution background for the SCFT simulation. The equilibrium CMC occurs at a surfactant composition c_{c} for which $\Phi^{\mathrm{m}} = 0$ was earlier described in Section 3.6 from Chapter 3.

The goal here is to estimate the rate at which a micelle of size M forms spontaneously from a homogeneous solution which contain a small amount of AB surfactant dissolved in S. Let μ_i denote the chemical potential of species i in this parent solution. In order to estimate the micellization rate, an estimate of the free energy $\Delta G\left(M, \mu\right)$ is required to create a micelle with any specified set of aggregation numbers M from a solution with a specified set of chemical potentials $\mu = \{\mu_{\mathrm{AB}}, \mu_{\mathrm{S}}\}$. The free energy of micelle formation can be thought of as a reaction free energy where M diblock copolymers from a sea of unimers at chemical potential μ combine to form a micelle with aggregation number M. The free energy for this hypothetical process may be approximated as a sum

$$\Delta G\left(M, \mu\right) = G_{\mathrm{m}}\left(M\right) - \sum_i \mu_i M_i, \tag{6.2.10}$$

where $G_{\mathrm{m}}\left(M\right)$ will be acquired from the SCFT Helmholtz free energy for a micelle of a specified size.

The excess free energy that we obtain by this method is an excess Helmholtz free energy, but for systems with equal pressures, inside and outside the micelle, this is also equal to the corresponding excess Gibbs free energy. The difference in free energy

of two systems with the same total volume and the same bulk pressure is the same free energy excess.

The procedure described above is similar to that used in previous SCFT studies of the barrier to nucleation in polymer blends by Wang and coworkers.[190,191] Each SCFT simulation contains a micelle surrounded by a larger homopolymer rich region with a low concentration of dissolved copolymer unimers. The concentration of unimers in the surrounding solution is related to the size of the micelle: Micelles of different sizes yield different values for the copolymer chemical potential, and thus coexist with bulk solutions of different concentrations.

The quantity $G_{\mathrm{m}}(M)$ is different from the grand-canonical free energy Φ^{m} because the chemical potential μ_i used here is the chemical potential of species i in the parent solution, rather than the chemical potential $\mu^{\mathrm{m}}(M)$ for a micelle of the specified size. In general, a micelle of arbitrary size and composition can not coexist in local equilibrium with a parent solution of specified composition. The chemical potentials in this definition of ΔG are thus fixed parameters characteristic of the parent solution, rather than functions of the micelle size.

Because ΔG is a function of both M and μ, one can ask for what values of M for which ΔG is extremal. The extrema of ΔG with respect to M at fixed μ, or a certain concentration of AB in the parent solution, must satisfy the requirement

$$0 = \frac{\partial \Delta G}{\partial M_i} = \mu_i^{\mathrm{m}}(M) - \mu_i, \tag{6.2.11}$$

for each component i. The extrema of ΔG have different physical interpretations depending on whether or not they are minima. A minimum of ΔG with $M_{\mathrm{AB}} > 0$

corresponds to the lowest free energy micelle in the parent solution. This optimal micelle is precisely what is calculated from SCFT simulations with the specified values of μ_i^{m}. Grand-canonical SCFT theory thus automatically finds the optimal values of M. Extrema of ΔG with respect to M that are maxima or saddle-points correspond to barriers that must be overcome in order to form a micelle. These barriers control the rate of spontaneous micelle formation.

One can thus construct a plot of ΔG *vs.* M for for any specified value of the exchange chemical potential (or composition) of the parent solution. For a parent solution with a composition near the CMC, we may expect this curve to contain a minimum at the optimal micelle size and a maximum at a much lower value of M. This maximum is the barrier to formation of a micelle from that solution. The minimum corresponds to the value of M that we would obtain from a grand canonical simulation at the same chemical potential, and yields a formation free energy ΔG that, at the minimum, equals the excess grand-canonical free energy Φ^{m}. For the value of $\Delta\mu$ at the CMC, we thus expect to find $\Delta G = 0$ at this minimum, as $\Phi^{\mathrm{m}} = 0$ is the condition for determining the CMC for a system under equilibrium.

To generate the desired curve, one must first run a series of SCFT simulations of micelles of different sizes, and tabulate values of G_{m} , M and $\Delta\mu$ for each set of conditions. It is necessary to trace a stable trajectory of the SCFT solution from the equilibrium micelle size all the way down to the smaller size that corresponds to the top of the barrier, which corresponds to the critical micelle size.

6.3 Polymeric Solvent: AB in B

In this section we calculate the barriers for association and dissociation of micelles using SCFT. We consider the blend of AB surfactant with a homopolymer solvent B. In subsequent subsections we compare our SCFT predictions with strong-segregation theory.

6.3.1 Strong Segregation Theory

In this section predictions of the strong-segregation theory (SST)[37,185] is employed as a basis of comparison for the SCFT calculations which are detailed below. This theory can not be readily extended to the case of a small molecule selective solvent as discussed earlier in Chapter 2 so comparisons with AB/B blend are not possible. The micelle is split into two regions: the core, and the corona. R_{core} is the core radius and R_{m} is regarded as the micelle radius. Enforcing the incompressibility constraint leads to a relation between the aggregation number of the micelle M and R_{core} which is

$$MN_{\text{A}}v = \frac{4\pi}{3}R_{\text{core}}^3, \tag{6.3.1}$$

where v is the monomer reference volume. The block composition of the core block (monomer A) may be written as ratio of the volume occupied by the core and the total micelle volume

$$f_{\text{A}} = \left(\frac{R_{\text{core}}}{R_{\text{m}}}\right)^3. \tag{6.3.2}$$

We follow a variant of SST used by Leibler which was employed to study a dry brush. In this system, the solvent, which is a B homopolymer, does not penetrate the

corona.[37] This assumption is retained here. The internal free energy of a spherical micelle (Helmholtz or Gibbs) is given by a sum

$$G_{\rm m} \ = F_{\rm core} + F_{\rm corona} + 4\pi R_{\rm core}^2 \gamma, \tag{6.3.3}$$

where, $\gamma = \sqrt{\chi_{\rm AB}\,/6}\, b/v$ is the interfacial tension, and

$$\begin{aligned} F_{\rm core} &= \frac{3\pi^2}{80} M \frac{R_{\rm core}^2}{N_{\rm B}\, b^2}, \\ F_{\rm corona} &= \frac{1}{2}(1 - f_{\rm A}^{1/3}) M \frac{R_{\rm core}^2}{N_{\rm B}\, b^2}, \end{aligned} \tag{6.3.4}$$

are the core and corona stretching free energies, respectively . So, all the contributions to the free energy are either due to molecular stretching or interfacial tension. The CMC may be obtained by minimizing the excess free energy

$$\Delta G\,(M, \Delta\mu) = G_{\rm m}\,(M) - \Delta\mu M, \tag{6.3.5}$$

with respect to the aggregation number of the micelle M by adjusting $\Delta\mu$. As before, a single exchange chemical potential $\Delta\mu$ determines the composition of this system, which is same as the exchange chemical potential of AB aggregated in the micelle at the CMC. It is, at the CMC, found to be

$$\Delta\mu = C(f_{\rm A})(\chi_{\rm AB}\, N_{\rm A}\,)^{1/3}, \tag{6.3.6}$$

where $C(f_{\rm A}) = (4\pi/3)^{4/3}(1 + \frac{3\pi^2}{40} - f_{\rm A}^{1/3})$.

The barrier at the CMC $\Delta G_{\rm c}$, which is given by the maxima of ΔG in (6.3.5) relative to M, is calculated numerically. At the CMC of a system with $f_{\rm A} = 1/2$ (the case studied most extensively for AB in a polymeric solvent B) we find the following scaling for the barrier,

$$\frac{\Delta G_{\rm c}}{kT} = 0.4783\, \bar{N}_{\rm A}{}^{\frac{1}{2}} (\chi_{\rm AB}\, N_{\rm A}\,)^{\frac{5}{6}}. \tag{6.3.7}$$

Since the SST yields results that are simply power laws in $\chi_{\rm AB}\, N_{\rm A}$, it cannot predict a minimum value of $\chi_{\rm AB}\, N_{\rm A}$ below which micelles are not stable.

6.3.2 Nondimensionalization

The barrier and the aggregation number obtained using SCFT can be expressed in terms of nondimensionalized variables. It is straightforward to show for the case of homopolymer solvent B that non-dimensionalizing all lengths in the SCFT equations in terms of the end-to-end length of the A block $L \equiv \sqrt{N_{\rm A}}\, b$,[190] yields expressions for the excess quantities M and $G_{\rm m}\,(M)$ that must exhibit a parameter dependence of the form

$$G_{\rm m}\,(M) \;=\; {\rm k}T\, \bar{N}_{\rm A}{}^{1/2} \hat{G}(\chi_{\rm AB}\, N_{\rm A}\,, f_{\rm A}\,, \alpha), \tag{6.3.8}$$

$$M \;=\; \bar{N}_{\rm A}{}^{1/2} \hat{M}(\chi_{\rm AB}\, N_{\rm A}\,, f_{\rm A}\,, \alpha). \tag{6.3.9}$$

Here, $\alpha = N_{\rm B}/N$ where $N_{\rm B}$ is the degree of polymerization of homopolymer B, and

$$\bar{N}_{\rm A} \;\equiv N_{\rm A}\, b^6/v^2. \tag{6.3.10}$$

The quantities, $\hat{G}$ and $\hat{M}$ are dimensionless functions that can only be determined through a solution of the SCFT equations. The values of μ_1 /kT and the unimer volume fraction at the CMC are simple functions of $\chi_{AB} N_A$, f_A and α alone, and independent of $\bar{N}_A$. The above relations for $G_m(M)$ and M hold true for a small molecule solvent as well, in which case α is given by $\alpha = N_S/N$. Later in the chapter, we find ΔG_c to be sensitive to the value of α. Earlier in Chapter 4, we found that micellar aggregation number M is dependent on the solvent-philic block composition f_B for the small molecule solvent S.

The dependence of $G_m(M)$ upon $\bar{N}_A$ in equation (6.3.8) implies that the barrier height ΔG_c obtained at a given value of $\chi_{AB} N$ (or a given degree of unimer solubility) will be higher for an polymeric system with a low value of χ_{AB} and larger N_A than for a system with a larger χ_{AB} but smaller N_A. We may expect much larger micellization barriers for hydrocarbon polymers in a hydrocarbon matrix than comparable barriers in small molecule surfactants in water, even for pairs of systems with similar unimer solubilities.

Spherical micelles are also not stable at any copolymer concentration below a minimum value of $\chi_{AB} N_A$. The values of c_c that we calculate here as a function of $\chi_{AB} N_A$ as a line of points in a plane of copolymer concentration vs. $\chi_{AB} N_A$ along which SCFT predicts a vanishing free energy for an isolated spherically symmetric "defect" in an otherwise homogeneous system. This line of micellar defects terminates at a minimum value of $\chi_{AB} N_A$ at which the CMC reaches 100 % copolymer, which we will denote by $(\chi_{AB} N_A)^*$. The behavior of $\Delta G_c(\chi_{AB} N_A)$ near this termination point is expected to be somewhat different for symmetric and asymmetric copolymers.

In the special case of a symmetric diblock copolymer, SCFT predicts a continuous (second order) order-disorder transition (ODT) for the pure copolymer at $\chi_{AB}\, N = 10.5$ or (equivalently) $\chi_{AB}\, N_A = 5.25$. Near this critical point, all of the ordered phases become very weakly segregated, and have increasingly similar free energies. Similarly, we expect both the equilibrium micelle and the critical micelle (if both solutions exist down to this point) to become progressively more diffusive and more similar in free energy near this point. For symmetric copolymers, we thus expect the SCFT prediction for the free energy barrier ΔG_c to vanish continuously as $(\chi_{AB}\, N_A)$ approaches $(\chi_{AB}\, N_A)^* = 5.25$ from above.

Our expectations are informed by a previous study by Wang *et al.*[192] which considered isolated, spherically symmetric micelle-like solutions to the SCFT equations in one-component melts of asymmetric diblock copolymers. These authors found that the SCFT excess free energy for "micelles" in the melt vanishes at a critical value of $\chi_{AB}\, N_A$ that is slightly above the value predicted by SCFT for a transition to an ordered phase of spheres. (The differences reflect the fact that the phases of ordered spheres are stabilized by weakly attractive interactions between nearby micelles). This critical value corresponds to the value at which the CMC that is calculated here for a binary system reaches 100 % copolymer. It appears that $(\chi_{AB}\, N_A)^*$ depends only weakly on composition: For a copolymer with $f_A = 0.1$, Wang *et al.* find $(\chi_{AB}\, N_A)^* = 4.76$, *vs.* $(\chi_{AB}\, N_A)^* = 5.25$ for a symmetric copolymer. For highly asymmetric copolymers, however, Wang *et al.* also found that core of the micelle remains well-segregated when its excess free energy vanishes, and that the barriers to dissociation and association remain nonzero at this point. One thus expects that in

a two-component system, ΔG_c must remain nonzero as the CMC approaches 100 % copolymer, or as $\chi_{AB} N_A$ approaches $(\chi_{AB} N_A)^*$ from above.

6.3.3 SCFT Results

In this section, we present SCFT results for micelles containing copolymers with an A core block of length N_A in a B homopolymer solvent of length $N_B = 2N_A$. We focus primarily on symmetric copolymers ($f_A = 1/2$) but also present some results for $f_A = 1/4$. Throughout this section, the values of v and b used are $v = 100\text{Å}^3$ and $b = 6$Å. In all but one figure (Figure 6.12), we use the incompatibility $\chi_{AB} = 0.12$. These parameter values are fairly typical for rather strongly interacting pair of hydrocarbons, for copolymers with molecular weights of $10^4 - 10^5$ g/mol. The calculated barrier heights below would be even larger over the same range of values of $\chi_{AB} N_A$ if a smaller value for χ_{AB} is chosen with correspondingly larger values of N_A or N (and $f_A = 1/2$).

Figure 6.5 shows the calculated free energy excess $\Delta G(M)$ at $c_1 = c_c$ for several symmetric copolymers with $\chi_{AB} = 0.12$ and $\chi_{AB} N_A = 12$, 24, and 36. The barrier ΔG_c is found to be in the range of $50\ kT < \Delta G_c < 300\ kT$ for these three different lengths of AB surfactant. These barriers are significant. Figure 6.6 shows the calculated core block volume fraction $\phi_A(r)$ of the "critical" micelle ($M = M_a$) at the CMC for these blends. The core radius of the equilibrium micelle at the CMC, $M = M_e$, is approximately twice that of the corresponding critical micelle. The systems shown in this figure are all in the intermediate segregation regime, for which $\phi_A(r)$ reaches nearly unity within the core. For $\chi_{AB} N_A \leq 8$ (not shown) the core

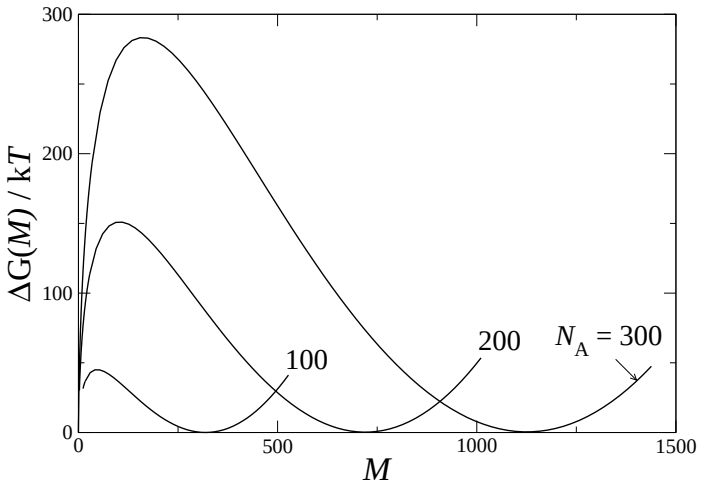

Figure 6.5: Predictions of numerical SCFT for $\Delta G\,(M)$ vs. M at $c_1 = c_c$ for symmetric copolymers ($f_A = 1/2$) with $\chi_{AB} = 0.12$ and $N_A = 100$ ($\chi_{AB}\,N_A = 12$), $N_A = 200$ ($\chi_{AB}\,N_A = 24$), and $N_A = 300$ ($\chi_{AB}\,N_A = 36$). All systems in this and all subsequent figures have $v = 100\text{Å}^3$, and $b = 6\text{Å}$.

radius for the critical nucleus becomes comparable to the interfacial width, and the core becomes less strongly segregated.

The SST and SCFT predictions for $\Delta G\,(M)$ are compared in Figure 6.7. A simple classical Gibbs nucleation theory also provides a similar estimate of M_a , and it is also shown. The cost increase of ΔG for large aggregates $M > M_e$ is clear from SST: it is the interfacial energy that initiates the nucleation of a micelle and a secondary minima arises which balances these terms (see Equation 6.3.3). The cost of stretching of the core and corona blocks then increases upon adding more unimers for $M > M_e$. A comparison of SST and SCFT indicates that SST is somewhat accurate throughout the intermediate segregation regime, and all trends are qualitatively reasonable. However, significant quantitative discrepancies exist over the entire range shown. One important theoretical distinction is that SCFT

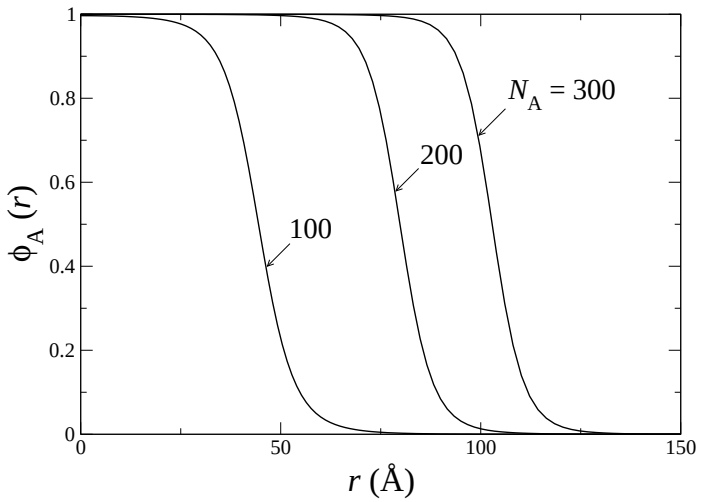

Figure 6.6: Volume fraction $\phi_{\rm A}(r)$ of A monomers *vs.* radial coordinate r for the activated state, with $M = M_{\rm a}$, at $c_1 = c_{\rm c}$ for each of the three systems considered in Figure 6.5.

also predicts a nonzero minimum value of $\chi_{\rm AB}\, N_{\rm A}$ below which micelles never form, and the absence of any such minimum value in SST. The strengths of SST lie in its qualitative explanation of the molecular origins of coexisting physical aggregates.

Figure 6.8 shows both numerical SCFT and SST results for the barrier $\Delta G_{\rm c}$ at the CMC vs. $\chi_{\rm AB}\, N_{\rm A}$, for chains of variable length with a fixed incompatibility $\chi_{\rm AB} = 0.12$. SCFT results are shown for two series of copolymers with $f_{\rm A} = 1/2$ and $f_{\rm A} = 1/4$. SST predictions are also shown, but only for $f_{\rm A} = 1/2$. Predictions for symmetric ($f_{\rm A} = 1/2$) and asymmetric ($f_{\rm A} = 1/4$) copolymers with equal core block lengths are quite similar, though the corona block lengths differ by a factor of 3. The most notable result is the large absolute magnitude of the barriers, which are of order 100 kT over most of the range shown here. The SCFT prediction for $\Delta G_{\rm c}$ falls to less than 10-15 kT, as would be required to obtain measurable rates of micelle

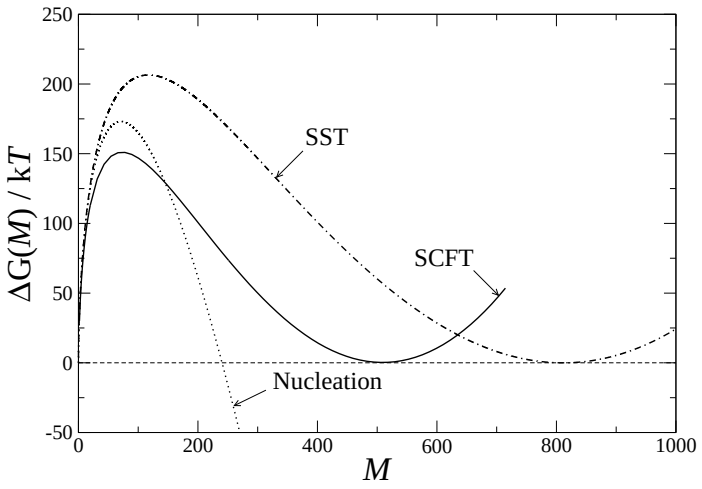

Figure 6.7: Comparison of SCFT and SST predictions for $\Delta G\,(M, c_1\,)$ at the CMC, for a diblock AB with $f_{\rm A}\ = 1/2$, $\chi_{\rm AB}\,N_{\rm A}\ = 24$, $N_{\rm B}\ = N_{\rm AB} = 400$, $v = 100\text{Å}^3$ and $b = 6\text{Å}$. The line marked nucleation theory is obtained by simply neglecting the core and corona stretching energies in the SST, which yields an expression for $\Delta G\,(M)$ of the same form as that used in classical Gibbs theory of nucleation.

association and dissociation, only for $\chi_{\rm AB}\,N_{\rm A}\ < 8$. For symmetric copolymers at the lowest value shown, $\chi_{\rm AB}\,N_{\rm A}\ = 6$, we find a CMC of 6 % copolymer and a barrier of approximately 7 kT . No results for $\Delta G_{\rm c}\,(\,\chi_{\rm AB}\,N_{\rm A}\,)$ are shown for lower values of $\chi_{\rm AB}\,N_{\rm A}$ due to weak saddle point convergence for the critical micelle in this weak segregation regime. In this regime, fluctuations are likely to dominate and complicate the picture as well.

The activation barrier $\Delta G_{\rm c}(\chi_{\rm AB}N_{\rm A})$, for symmetric copolymers seems to extrapolate to zero at a value somewhere near the bulk ODT of $\chi_{\rm AB}\,N_{\rm A}\ = 5.25$ for symmetric copolymers. This is consistent with our hypothesis in this regime presented earlier. We also find, that the barriers for symmetric and strongly asymmetric copolymers are almost indistinguishable provided their core block lengths have the same length.

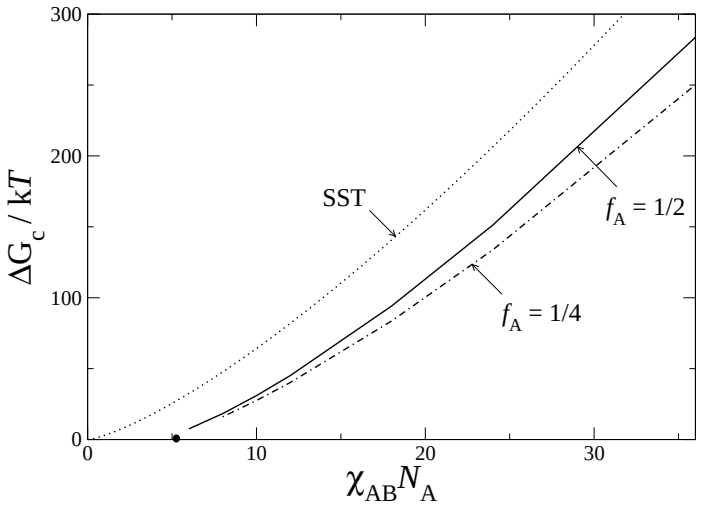

Figure 6.8: Activation barrier ΔG_c at the CMC vs. $\chi_{AB}\, N_A$, as predicted by SCFT and SST. All calculations use parameters $v = 100\text{Å}^3$, $b = 6\text{Å}$ and $\chi_{AB} = 0.12$ over a range of chain lengths. SCFT results are show for $f_A = 1/2$ (thick line) and $f_A = 1/4$ (dash dot). SST predictions are shown only for $f_A = 1/2$. The dot on the horizontal axis marks the critical point $\chi_{AB}\, N_A = 5.25$ of a symmetric diblock copolymer melt.

These results are thus consistent with the idea that the barrier for asymmetric copolymers decreases continuously to zero with decreasing $\chi_{AB}\, N_A$, which is not what one would expect on theoretical grounds.

Figure 6.9 shows radial profiles of the core block monomer A for spherical micelles for AB in B is studied close to the ODT of AB melt. The polymeric solvent B does not penetrate the core drastically as $\chi_{AB}\, N_A$ approaches ODT. Even for $\chi_{AB}\, N_A$ values as low as $\chi_{AB}\, N_A = 6$ we notice the spherical micelle to be well segregated from the polymeric matrix of B. Earlier in Chapter 4, we noticed for the case of small molecule solvent S to penetrate the core of a micelle much more significantly than the homopolymer B.

Figure 6.10 shows an example of how the barriers ΔG_a (c_1) and ΔG_d (c_1) for

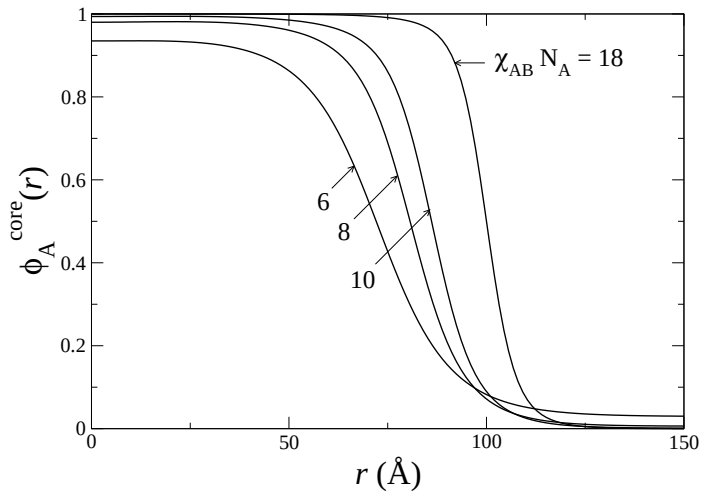

Figure 6.9: Variation of the radial profile of the core monomer A $\phi_{\rm A}^{\rm core}(r)$ for a symmetric block copolymer ($f_{\rm B}$ =0.50, $N = 200$) in homopolymer B ($N_{\rm B} = 200$) as both approach order-disorder transition (ODT). ODT for the case of AB in B is found to occur at $\chi_{\rm AB}\,N_{\rm B} = 5.25$.

symmetric copolymers vary with the unimer concentration c_1 . It was shown earlier the variation of $\Delta G_{\rm a}$ and $\Delta G_{\rm d}$ are coupled to the aggregation numbers $M_{\rm a}$ and $M_{\rm e}$ through the equations (6.2.8) and (6.2.9). The variation of the aggregation numbers $M_{\rm a}$ and $M_{\rm e}$ with respect to c_1 are presented in figure 6.11. As $M_{\rm e} > M_{\rm a}$, $\Delta G_{\rm d}$ is much more sensitive to c_1 than $\Delta G_{\rm a}$. The difference in slopes at $c_1 = c_{\rm c}$ is given by the ratio $M_{\rm e}\,/M_{\rm a} - 1 \simeq 7$. Note that dissociation barrier $\Delta G_{\rm d}\,(c_1)$ vanishes entirely below a nonzero critical concentration that is surprisingly close to the CMC: in the example shown here, $\Delta G_{\rm d} = 0$ for a concentration of $c_1 \simeq 0.7 c_{\rm c}$. The association barrier $\Delta G_{\rm a}$, however, never entirely vanishes, and only slowly approaches zero with increasing c_1 .

The persistence of the non-zero association barrier at concentrations $c_1 \gg c_{\rm c}$ is a result of the large slope of the function $G_{\rm m}\,(M)$ for small values of M. At

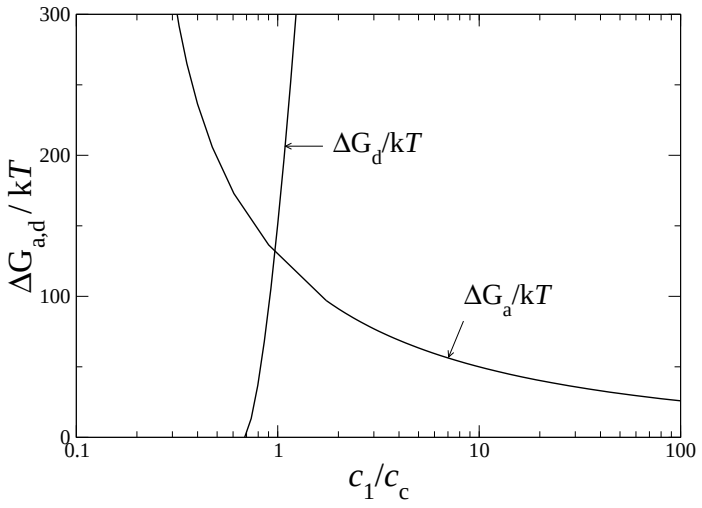

Figure 6.10: Dependence of activation barrier $\Delta G_{\rm a}$ (c_1) and dissolution barrier $\Delta G_{\rm d}$ (c_1) upon unimer concentration c_1 for a system with $f_{\rm A} = 1/2$, $\chi_{\rm AB} N_{\rm A} = 24$, $N_{\rm A} = 200$, $N_{\rm B} = 400$, $v = 100\text{Å}^3$ and $b = 6\text{Å}$ and $\chi = 0.12$.

concentrations $c_1 \gg c_{\rm c}$, $M_{\rm a}$ is driven to values much lower than its value at the CMC. The behavior seen in this regime can be understood by using the context of SST calculation. In this, $G_{\rm m}\,(M)$ is dominated for very small values of M by the contribution to the excess free energy from the interfacial tension $4\pi R_{\rm core}^2\gamma$. We expect that this will hold for micelles for which the core radius $R_{\rm core}$ is much smaller than that of the critical size at the CMC but is yet still larger than the intrinsic width of the interface between core and corona materials. This behavior of small micelles appears in both the classical theory of nucleation and the strong stretching theory of diblock copolymer micelles, and reasonably approximates to the SCFT results shown here. Because $M \propto R_{\rm core}^3$, and the interfacial contribution to the free energy scales as $G_{\rm m} \propto \gamma R_{\rm core}^2$, we find $G_{\rm m}\,(M) \propto M^{2/3}$. The unimer concentration is $\partial G_{\rm m}\,(M)/\partial M = \mu_1$, which, at the barrier yields, ${M_{\rm a}}^{-1/3} = \mu_1$. The association

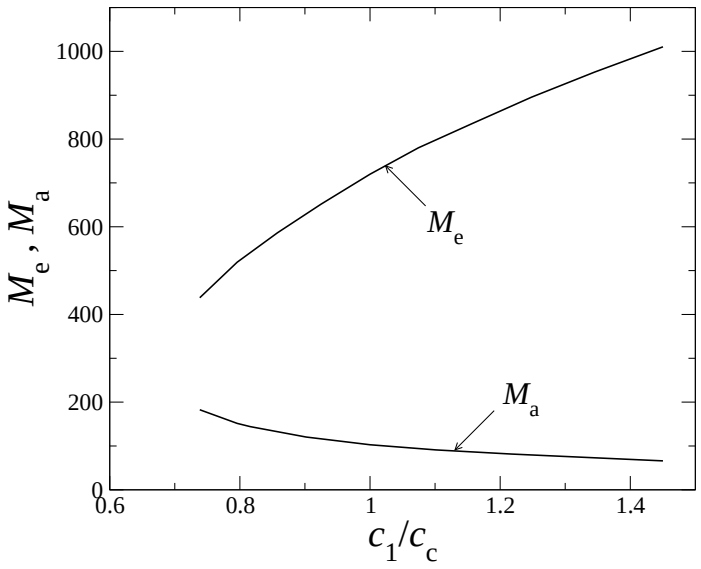

Figure 6.11: Aggregation number at the secondary minima of ΔG M_e *vs.* the unimer concentration c_1/c_c, for a diblock AB with $f_A = 1/2$, $\chi_{AB} N_A = 24$, $N_B = N_{AB} = 400$, $v = 100\text{Å}^3$ and $b = 6\text{Å}$.

barrier can then be written as

$$\Delta G_a\,(c_1\,) \sim [\mu_1\, - \mu_c\,]^{-2} \propto [\ln(c_1\,/c_c\,)]^{-2}, \tag{6.3.11}$$

and this approaches zero only logarithmically with c_1 . In systems with $\Delta G_c \gg kT$, this behavior yields a value c_a that can be several orders of magnitude larger than c_c , but a value of c_d that is only slightly less than c_c .

Figure 6.12 shows an example of how the concentrations $c_a(\tau)$ and $c_d(\tau)$ vary with $\chi_{AB}\, N_A$ for systems with large barriers, $\Delta G_c \gg \text{k}T$, at the CMC. For simplicity, c_a and c_d are defined here as the concentrations at which the barriers fall to fixed values of $\Delta G_a\,(\,c_1\,) = 15\text{k}T$ and $\Delta G_d\,(\,c_1\,) = 15\text{k}T$, rather than specifying a corresponding timescale. As already noted, the dissociation concentration is never more than a few

tens of percent below the equilibrium c_c over the range of values of $\chi_{AB} N_A$ studied here, but c_a can exceed c_c by several orders of magnitude.

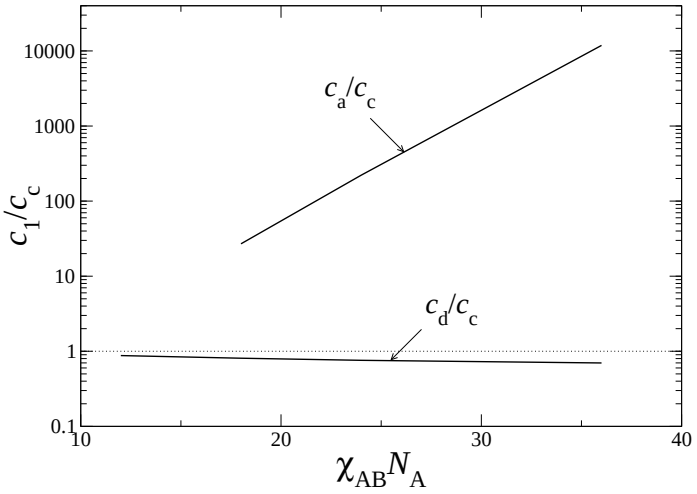

Figure 6.12: Plot of variation of the threshold concentration c_a and dissolution barrier concentration c_d with respect to χN_B, for a series of systems with $f = 1/2$, $\chi = 0.24$, $v = 100\text{Å}^3$ and $b = 6\text{Å}$.

It is also worth noting that the dependence of c_a/c_c on $\chi_{AB} N_A$ is actually weaker than the exponential dependence of c_c on $\chi_{AB} N_A$. The absolute magnitude of $c_a(\tau)$ for any fixed timescale τ (or corresponding barrier height ΔG_a) actually decreases with increasing $\chi_{AB} N_A$, though somewhat less strongly than c_c. It is thus certainly possible (and probably common in practice) to obtain an initial concentration $c_1 \gg c_a$ in a dilute solution of strongly insoluble copolymers.

6.4 Small Molecule Solvent: AB in S

The micelle kinetics of diblock AB in a small molecule solvent S is studied in this section. The reference volume used in SCFT calculations here is set to the molecular

volume of solvent. Two block compositions of spherical micelles are considered, the first one representing a crew-cut micelle, with $f_{\mathrm{B}} = 0.35$, and another representing a hairy micelle, with $f_{\mathrm{B}} = 0.60$. In all of the following the calculations $\chi_{\mathrm{AB}}\, N = 20$, and the solvent volume and bond length are $v = 118\text{Å}^3$ and $b = 6\text{Å}$, respectively.

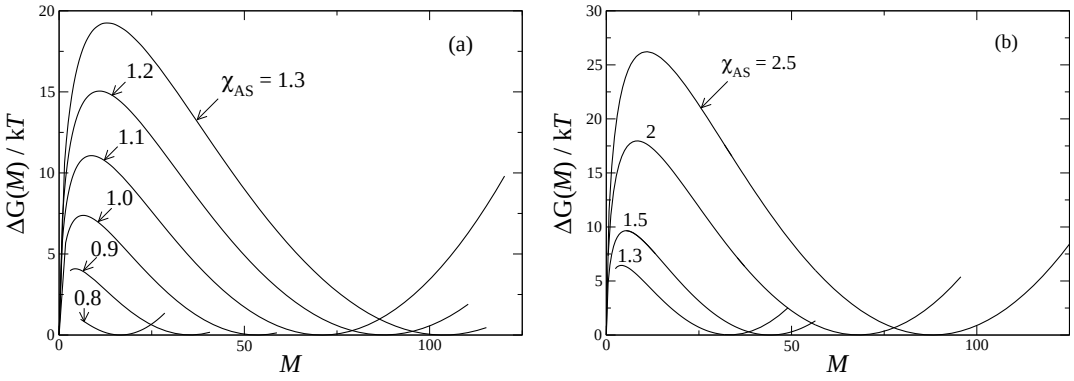

Figure 6.13: ΔG calculated for various values of solvent selectivity χ_{AS} for (a) a crew-cut spherical micelle with $f_{\mathrm{B}} = 0.35$, and (b) a hairy spherical micelle with $f_{\mathrm{B}} = 0.60$. The calculation was carried out for AB/S system with $N = 100$, $\chi_{\mathrm{BS}} = 0.4$, and $\chi_{\mathrm{AB}} = 0.2$.

The free energy of formation for micelles at the critical micelle concentration ΔG is presented for the crew-cut micelle ($f_{\mathrm{B}} = 0.35$) and for the hairy micelle ($f_{\mathrm{B}} = 0.60$) in Figure 6.13 (a) and (b), respectively. The degree of polymerization of the diblock is $N = 100$, and the solvent prefers the B block with $\chi_{\mathrm{BS}} = 0.4$. Note that the hairy micelle requires a higher degree of selectivity in order to attain similar barrier height as in the case of the crew-cut micelle of equal overall chain length. This behavior is due to the difference in block composition which results in a smaller R_{core} for the hairy micelle. The barriers for association ΔG_{a} , as previously shown for AB in B, are found to scale as $\sim \gamma R_{\mathrm{core}}^2$ which is higher for the case of crew-cut micelle as it

has a larger exposed micellar area. In general for a wide range of solvent selectivity χ_{AS} , for both kinds of micelle, the barrier to micelle formation in AB/S is roughly $10\,kT$. It is significant to note the contrast with the polymeric solvent in Figure 6.5 from Section 6.3 where the barriers are around $100\,kT$.

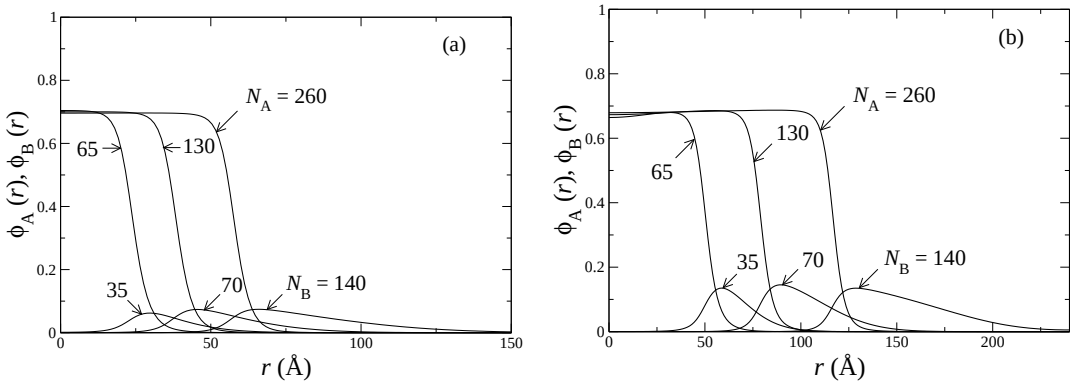

Figure 6.14: Volume fractions $\phi_A(r)$ and $\phi_B(r)$ of A and B monomers respectively, for the (a) activated state and (b) at the CMC, relative to the radial coordinate r for various values of core and corona block lengths for a crew-cut spherical micelle with $f_B = 0.35$. The calculation was carried out for AB/S system with $N = N_A + N_B$, $\chi_{AS} = 1.0$, $\chi_{BS} = 0.4$, and $\chi_{AB} = 0.1$.

The volume fraction profiles of the core $\phi_A(r)$, and the corona $\phi_B(r)$ for the activated state and at the critical micelle concentration of the crew-cut micelle are presented in Figure 6.14 (a) and Figure 6.14 (b), respectively.

In Figure 6.15 we present the dependence of $\Delta G(M)$ on the interaction parameter χ_{BS} for both block compositions, $f_B = 0.35$ and $f_B = 0.60$. A decreasing value of χ_{BS} causes the corona block to stretch more into the solvent domain. This still does not explain the behavior of the ΔG_c increasing with decrease in the value of χ_{BS} for a particular f_B , while other parameters maintained at the same value. The

behavior should be related more to interfacial cost ($\sim \gamma R_{\rm core}^2$) as $\Delta G_{\rm a}$, or maxima of ΔG , is mainly dominated by it for smaller values of M as discussed previously. As M decreases, correspondingly the barrier $\Delta G_{\rm c}$ goes down. Upon plotting the concentration profiles (not shown) at $M = M_{\rm a}$ we notice that $R_{\rm core}$ is lower for a lower value of $\chi_{\rm BS}$. Hence, lower value of $\chi_{\rm BS}$ leads to lower barrier to micelle formation or dissolution at $c_{\rm c}$.

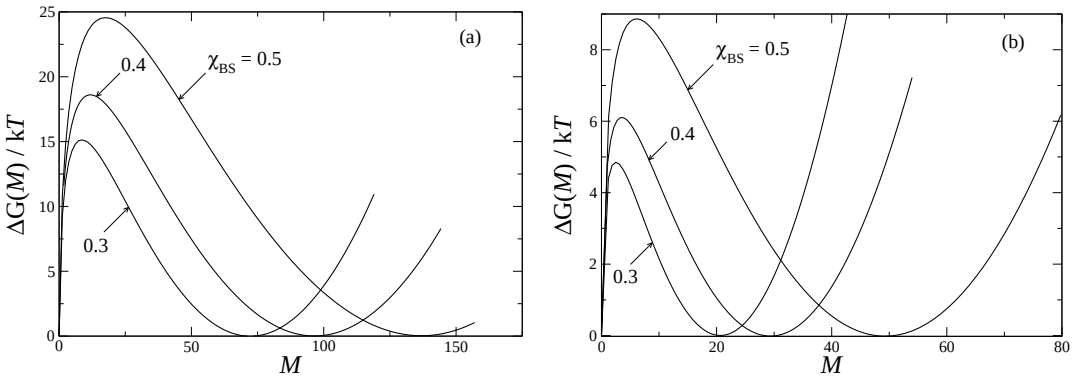

Figure 6.15: ΔG calculated for various values of good solvent interaction parameter $\chi_{\rm BS}$ for (a) crew-cut micelle with $f_{\rm B} = 0.35$ and (b) hairy spherical micelle with $f_{\rm B} = 0.60$. The calculation was carried out for AB/S system with $N = 200$, $\nu = 1$, $\chi_{\rm AS} = 1.0$, and $\chi_{\rm AB} = 0.1$.

The dependence of $\Delta G_{\rm c}$ on the solvent selectivity $\chi_{\rm AS}$ is studied in Figure 6.16. The x-axis is normalized relative to the the interaction parameter at critical micelle temperature $\chi_{\rm AS}^{\rm CMT}$ in order to display different block compositions and block lengths onto a master plot. Longer chain lengths give rise to larger barriers for a particular block composition, and the rate of increase of the barriers with $\chi_{\rm AS}$ is also higher for longer chain lengths. The barriers are still moderate when compared with barriers for AB in polymeric solvent. The polymeric solvent yields barriers which are of the

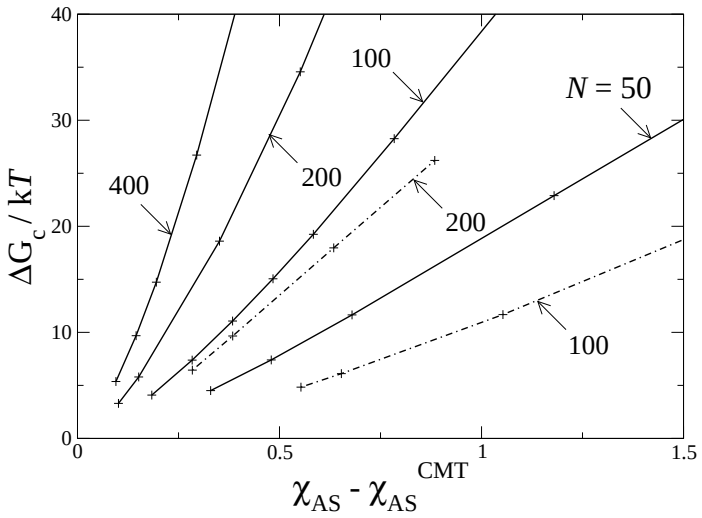

Figure 6.16: Variation of $\Delta G_{\rm c}$ for a crew-cut spherical micelle ($f_{\rm B}$ =0.35, solid line) and a hairy spherical micelle ($f_{\rm B}$ =0.6, dash-dot line) for various degrees of polymerization N of the diblock copolymer AB relative to solvent selectivity $\chi_{\rm AS}$ normalized relative to its' value at critical micelle temperature(CMT).

order of $\sim 100{\rm k}T$ presented in Figure 6.8.

The dependence of $\Delta G_{\rm c}$ on the ratio of the solvent size relative to diblock copolymer size is studied by tracking the radial profiles of the core block monomer A. In the case of small molecule solvent S, the solvent is found to penetrate the core of a spherical micelle to a much higher degree than in the case of the solvent being homopolymer B as seen from Figures 6.9 and 6.17. $\Delta G_{\rm c}$ is the maxima for ΔG when $c_1 = c_{\rm c}$, which implies the cost of interface goes up dramatically in comparison to to the free energy contribution from entropy of mixing of the solvent with increasing size of the solvent.

The variation of $\Delta G_{\rm a}$, and $\Delta G_{\rm d}$ for the crew-cut micelle $f_{\rm B} = 0.35$ and the hairy micelle $f_{\rm B} = 0.60$ is presented in Figures 6.18 and 6.19, respectively. When $c_1 = c_{\rm c}$, the barrier to formation of micelles $\Delta G_{\rm a}$ and barrier to dissolve a micelle $\Delta G_{\rm d}$ are

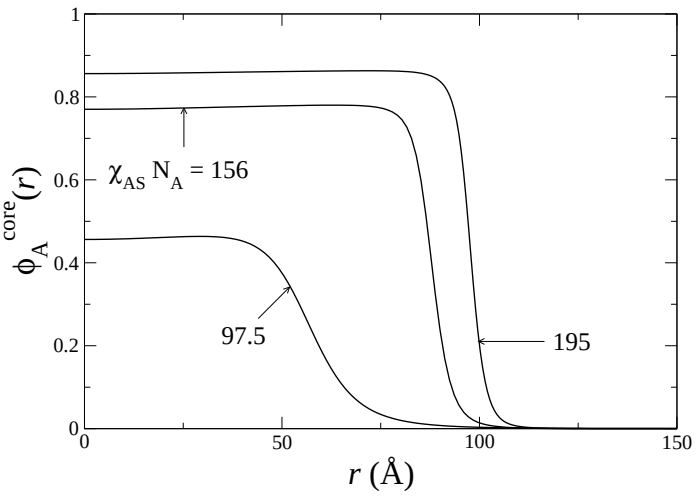

Figure 6.17: Variation of the radial profile of the core monomer A $\phi_{\rm A}^{\rm core}(r)$ for a crew-cut spherical micelle ($f_{\rm B}$ =0.35, $N = 200$) at $c_{\rm c}$ as it approaches critical micelle temperature (CMT). CMT for this case is found to occur at $\chi_{\rm AS}\, N_{\rm A} = 85$.

equal $\Delta G_{\rm a} = \Delta G_{\rm d}$. The two block compositions are compared for a similar degree of segregation with the product of solvent selectivity $\chi_{\rm AS}$ and core block length $N_{\rm A}$. For the crew-cut micelle $f_{\rm B} = 0.35$ we consider a value of $\chi_{\rm AS}\, N_{\rm A} = 130$, and for the hairy micelle $f_{\rm B} = 0.6$ we consider a value of $\chi_{\rm AS}\, N_{\rm A} = 120$. The barrier to formation of micelles $\Delta G_{\rm a}$ is found to go down much slower for $c_1 > c_{\rm c}$ than the barrier to dissolve a micelle $\Delta G_{\rm d}$ for $c_1 < c_{\rm c}$. In order to achieve observable association one needs to go above at least an order of magnitude of $c_{\rm c}$ for both block compositions of micelles. In the case of a polymeric solvent observable association is observed at c_1 about at least a few orders of magnitude above $c_{\rm c}$ as seen in Figure 6.10 from Section 6.3. This difference in behavior stems from the value of $\Delta G_{\rm c}$ being an order of magnitude larger for the polymeric solvent with respect to that of the small molecule solvent case.

The barrier to dissolve a micelle is extremely sensitive to c_1 and goes to zero at few 10s of percent below $c_{\rm c}$ for both block compositions. The barrier to dissolve a

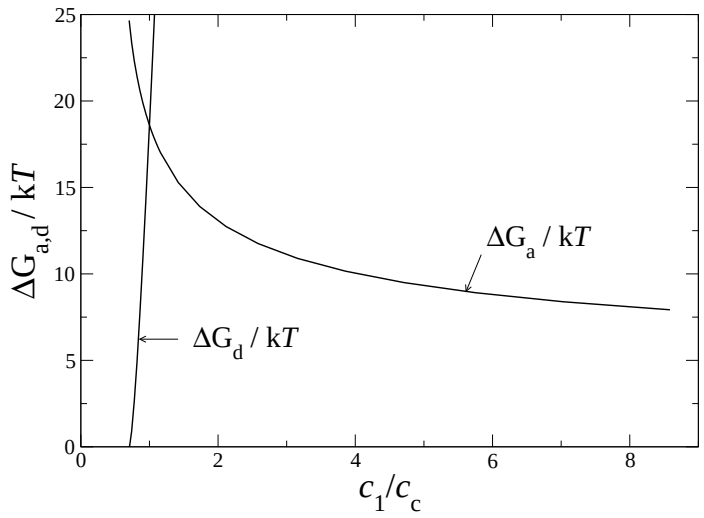

Figure 6.18: $\Delta G_{\rm a}$ and $\Delta G_{\rm d}$ calculated for various values of unimer concentration c_1 for a crew-cut spherical micelle with $f_{\rm B} = 0.35$. The calculation was carried out for AB/S system with $N = 200$, $\nu = 1$, $\chi_{\rm AS} = 1.0$, $\chi_{\rm BS} = 0.4$, and $\chi_{\rm AB} = 0.1$.

micelle $\Delta G_{\rm d}$ goes to zero at $c_1 = 0.7c_{\rm c}$ for the crew-cut micelle $f_{\rm B} = 0.35$ presented in Figure 6.18, and $\Delta G_{\rm d} = 0$ at $c_1 = 0.6c_{\rm c}$ for the hairy micelle $f_{\rm B} = 0.60$ presented in Figure 6.19. This behavior of vanishing $\Delta G_{\rm d}$ almost remains independent of the ratio of block polymer size to solvent size when you notice that $\Delta G_{\rm d} = 0$ at $c_1 = 0.7c_{\rm c}$ for the polymeric solvent presented in Figure 6.10 from Section 6.3. This is an important observation as other kinetic parameters show a remarkable sensitivity to the ratio of block copolymer size and solvent size.

The persistence of a non-zero association barrier at concentrations $c_1 \gg c_{\rm c}$ is a result of the large slope of the free energy of micelle $G_{\rm m}\,(M)$ for small values of M as seen previously in the case of AB in B. This leads to $\Delta G_{\rm a}$ approaching zero only logarithmically with c_1 . In systems with $\Delta G_{\rm c} \gg kT$, this behavior yields a value $c_{\rm a}$ that can be several orders of magnitude larger than $c_{\rm c}$, but a value of $c_{\rm d}$ that is only

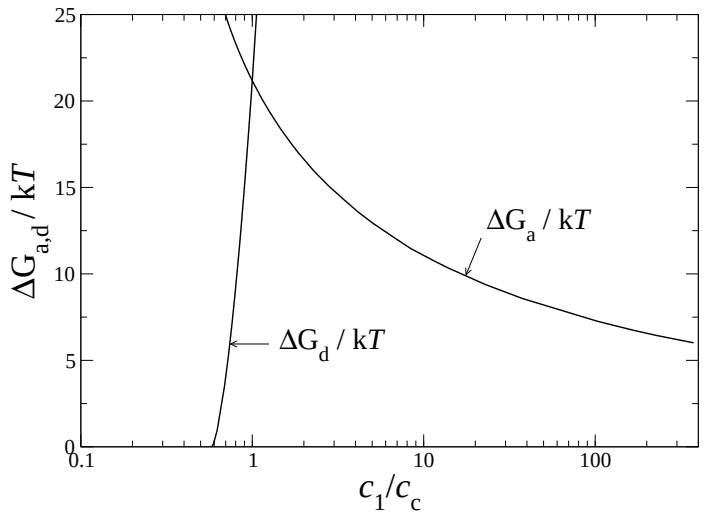

Figure 6.19: $\Delta G_{\rm a}$ and $\Delta G_{\rm d}$ calculated for various values of unimer concentration c_1 for a hairy spherical micelle with $f_{\rm B} = 0.60$. The calculation was carried out for AB/S system with $N = 200$, $\nu = 1$, $\chi_{\rm AS} = 1.5$, $\chi_{\rm BS} = 0.4$, and $\chi_{\rm AB} = 0.1$.

slightly less than $c_{\rm c}$.

Figure 6.20 shows an example of how the concentrations $c_{\rm a}\,(\tau)$ and $c_{\rm d}\,(\tau)$ vary with $\chi_{\rm AS}$ in systems with large barriers, $\Delta G_{\rm c} \gg {\rm k}T$, at the CMC. For simplicity, $c_{\rm a}$ and $c_{\rm d}$ are defined here as the concentrations at which the barriers fall to fixed values of $\Delta G_{\rm a}\,(c_1\,) = 10{\rm k}T$ and $\Delta G_{\rm d}\,(c_1\,) = 10{\rm k}T$, rather than specifying a corresponding timescale. As already noted, the dissociation concentration is never more than a few tens of percent below the equilibrium $c_{\rm c}$ over the range of values of $\chi_{\rm AS}\,N_{\rm A}$ studied here, but $c_{\rm a}$ can exceed $c_{\rm c}$ by several orders of magnitude.

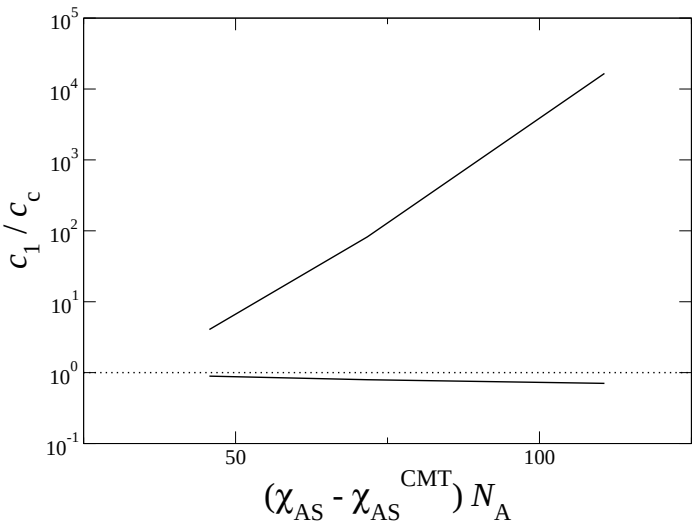

Figure 6.20: Plot of variation of the threshold concentration c_a and dissolution barrier concentration c_d for a block composition of AB of $f_B = 0.35$ and $N = 200$ with different degrees of solvent selectivity χ_{AS} plotted relative to χ_{AS} normalized relative to its' value at CMT.

6.5 Kinetic Theory

In this section, a more quantitative theory of micellar association and dissociation rates is presented. This is a necessary precursor to estimate values for the pre-exponential factors of the expressions for reaction rates given in Section 6.2. The treatment of association and dissociation is based on a dynamical model of changes in aggregation number M, which is regarded as a diffusive process. The analysis is based on Kramers' theory[193] for diffusion over a barrier.

For simplicity, the elementary reactions in which a single molecule is inserted into or expelled from a micelle are assumed to be limited only by the rates of unimer diffusion in the surrounding matrix. This approximation should yield an upper bound on the true reaction rates, and one which could be reduced either by the existence of

a barrier to insertion, or by slow dynamics within the core.

6.5.1 Kramers' Theory

In this section, we present, a stochastic model that describes random changes in the aggregation number M. The aggregation number M is assumed to change by a random sequence of elementary reactions that add or remove individual molecules diffusively.

Treating M as a continuous variable allows random fluctuations to be described by a diffusive process. This is possible if the elementary free energy difference

$$\begin{aligned} \Delta\mu(M) &\equiv G_{\rm m}\left(M+1\right) - G_{\rm m}\left(M\right) - \mu_1 \,, \\ &\simeq \frac{\partial \Delta G\left(M\right)}{\partial M} \end{aligned} \tag{6.5.1}$$

is smaller than kT in the parameter range of interest. SCFT calculations, presented is Sections 6.3 and 6.4, suggest that this condition is typically satisfied for the range of parameters considered here for all but very smallest values of M. Because SCFT is not only most reliable for larger aggregates, but also not applicable to aggregates with only a few molecules, the focus is on the calculation of the dissociation rate $R_{\rm d}$. An estimate of this rate is sensitive only to the accuracy of our model for $\Delta G(M)$ for the range $M_{\rm a} < M < M_{\rm e}$. Given an expression for $R_{\rm d}$, one may then use the detailed balance condition to calculate $R_{\rm a}$.

We consider a probability distribution $P(M,t)$ of micellar aggregates size M which

diffuses in time. It obeys a conservation equation

$$\frac{\partial P(M,t)}{\partial t} = -\frac{\partial J(M,t)}{\partial M}, \tag{6.5.2}$$

where $J(M,t)$ is a probability flux given by

$$J = D_{\mathrm{K}} \left(-\frac{1}{kT}\frac{\partial \Delta G}{\partial M} P - \frac{\partial P}{\partial M} \right). \tag{6.5.3}$$

Here, $D_{\mathrm{K}}(M)$ is an effective one-dimensional diffusivity, which can in general depend upon M. This parameter $D_{\mathrm{K}}(M)$ is derived in terms of the diffusivity of free unimers in the next subsection, but it can be treated arbitrarily here. In equilibrium, there is no flux $J(M,t) = 0$ for all M, and $P(M,t) \propto \exp(-\Delta G\,(M)/\mathrm{k}T\,)$.

The dissociation rate may be calculated by considering steady-state dynamics with a small flux $J < 0$ that is independent of both M and t. To define a steady-state, an absorbing boundary condition is introduced at a cutoff $M = a$ with $a < M_{\mathrm{a}}$, which removes micelles from the ensemble when they shrink to a sub-critical size. To compensate for this removal of micelles at $M = a$, one must assume that micelles are somehow also introduced into the system at a low rate, with initial sizes comparable to or greater than M_{e} . For small enough flux J, it can be safely assumed that the distribution of $P(M,t)$ is insensitive to the details of how micelles are injected into the system for M near M_{e} , since these new micelles will quickly explore an equilibrium ensemble of sizes, and take much longer to diffuse over the barrier.

The 1D flux $J(M,t)$ of Eq. (6.5.3) satisfies the relation

$$\frac{Je^{\Delta G\,/kT}}{D_{\rm K}} = -\frac{\partial}{\partial M}\left(e^{\Delta G\,/{\rm k}T}\,P\right). \tag{6.5.4}$$

To calculate J, both sides of the above equation are integrated from $M = a$ to an arbitrary value $b \sim M_{\rm e}$, setting $P(a) = 0$ and approximating J as a constant. We additionally assume that the normalized probability distribution $P(M)$ for a micelle with size $M \approx M_{\rm e}$ can be given by the normalized equilibrium distribution $P(M) \simeq \exp(-\Delta G\,(M)/{\rm k}T\,)/Q$. The normalization is

$$Q \equiv \int dM\; e^{-\Delta G\,(M)/{\rm k}T}, \tag{6.5.5}$$

which is the grand-canonical partition function for a single micelle. With these assumptions, one finds

$$\frac{1}{J} = Q\int dM\;\frac{e^{\Delta G\,(M)/kT}}{D_{\rm K}\,(M)}. \tag{6.5.6}$$

Since $P(M)$ is a normalized probability distribution, in this approximation i.e., $\int dMP(M) = 1$, the flux J is exactly equal to the rate of dissociation $R_{\rm d}$ for a single micelle, it's inverse lifetime. Taking the distribution $\exp(\Delta G\,(M)/{\rm k}T\,)$, in Equation (6.5.6) as a Gaussian of width $\sigma_{\rm a}$ centered around $M_{\rm a}$, approximate $D_{\rm K}\,(M)$ by its value at $M_{\rm a}$, and set $J = R_{\rm d}$, we find a simple approximation for the dissociation rate

$$\frac{1}{R_{\rm d}} \simeq \frac{Q\sqrt{2\pi}\sigma_{\rm a}\,e^{\Delta G_{\rm a}\,/{\rm k}T}}{D_{\rm K}\,(M_{\rm a}\,)}. \tag{6.5.7}$$

Similarly choosing to approximate the single micelle partition function

$\exp(-\Delta G\,(M)/\mathrm{k}T\,)$ (remember $\Delta G_{\mathrm{e}} = \Delta G_{\mathrm{a}} - \Delta G_{\mathrm{d}}$) as a Gaussian of width σ_{e} peaked around M_{e} then yields

$$R_{\mathrm{d}} \simeq \frac{D_{\mathrm{K}}\,(M_{\mathrm{a}}\,)}{2\pi\sigma_{\mathrm{a}}\,\sigma_{\mathrm{e}}} e^{-\Delta G_{\mathrm{d}}\,/\mathrm{k}T}\,. \tag{6.5.8}$$

The creation rate R_{a} may then be obtained from from R_{d} using the conditions of detailed balance (6.2.3). Writing the equilibrium concentration of micelles with a similar Gaussian approximation as $c_{\mathrm{m}} = c_{\mathrm{m}}^{0} \int dM\ \exp(-\Delta G\,(M)/\mathrm{k}T\,) = c_{\mathrm{m}}^{0}\,Q$ yields a simple expression for the association rate

$$R_{\mathrm{a}} \simeq \frac{D_{\mathrm{K}}\,(M_{\mathrm{a}}\,)}{\sqrt{2\pi}\sigma_{\mathrm{a}}} c_{\mathrm{m}}^{0}\, e^{-\Delta G_{\mathrm{a}}\,/\mathrm{k}T}\,. \tag{6.5.9}$$

The rate depends on c_{m}^{0} , the standard state micelle concentration used to define $G_{\mathrm{m}}\,(M)$. Also, $c_{\mathrm{m}}\,(\,M_{\mathrm{a}}\,) = c_{\mathrm{m}}^{0}\,\exp(-\Delta G_{\mathrm{a}}\,/\mathrm{k}T\,)$ is the equilibrium number concentration. None of the above expressions rely on our proposed use of the equilibrium concentration of micelles at the CMC as a standard state.

6.5.2 "Diffusion" of Micelle Size

In this subsection, we derive the effective diffusivity constant D_{K} in terms of physical properties such as the unimer diffusivity. This is carried out by calculating the average rate $\mathrm{d}\langle M\rangle/\mathrm{d}t$ at which a micelle with a known initial size grows or shrinks due to the diffusion of unimers into or out of the micelle. In the 1D Fokker-Planck equation, the micellar growth rate is given by average value $\mathrm{d}\langle M\rangle/\mathrm{d}t$ for a system with an initial micellar distribution that is mono-disperse, or $P(M') = \delta(M' - M)$, one that initially

is tightly localized around a value M. The drift velocity is

$$\frac{\mathrm{d}\langle M\rangle}{\mathrm{d}t} = -\frac{D_{\mathrm{K}}\left(M\right)}{\mathrm{k}T}\Delta\mu(M), \tag{6.5.10}$$

where $\Delta\mu(M)$ is the thermodynamic driving force for the elementary reaction $M \rightarrow M+1$, and $D_{\mathrm{K}}\left(M\right)/\mathrm{k}T$ is a generalized micelle size mobility.

This average growth rate $\mathrm{d}\langle M\rangle/\mathrm{d}t$ for a micelle of size M can predicted by relating the rate of diffusion of unimers into or out of a micelle with the mobility expression of Equation (6.5.10). For a micelle of size M in contact with a reservoir of unimers of macroscopic concentration c_1, we treat the micelle as a simple sphere of effective radius R surrounded by a reservoir of quasi-static concentration $c_1\left(r\right)$. This varies with distance from the micelle center, and the gradients in $c_1\left(r\right)$ create a net diffusive flux of unimers into or out of the micelle. The boundary condition at the micelle surface $r = R$ is fixed by the assumption that adsorption and desorption is rapid enough to maintain the reaction equilibrium between the micelle and the gas of monomers. This assumption is

$$\frac{\partial G_{\mathrm{m}}\left(M\right)}{\partial M} = \mu_1\left(r\right), \tag{6.5.11}$$

where $\mu_1\left(r\right)$ is the local unimer chemical potential associated with the concentration $c_1\left(r\right)$. An assumption of quasi-steady state diffusion with a monomer diffusivity D_1, paired with the above boundary condition, yields a concentration profile

$$\frac{c_1\left(r\right)}{c_1\left(\infty\right)} = 1 + (e^{(\Delta\mu(M)/\mathrm{k}T\,)} - 1)\frac{R}{r}. \tag{6.5.12}$$

The total diffusive flux is given by

$$\frac{\mathrm{d}\langle M\rangle}{\mathrm{d}t} = 4\pi D_1 \, R c_1 \, (\infty)[e^{\Delta\mu(M)/\mathrm{k}T} - 1]. \tag{6.5.13}$$

In the limit $\Delta\mu \ll \mathrm{k}T$, we may treat M as a continuous variable, and

$$\frac{\mathrm{d}\langle M\rangle}{\mathrm{d}t} \simeq 4\pi D_1 R c_1 \, \Delta\mu, \tag{6.5.14}$$

where $c_1 \; = c_1 \, (\infty)$ is the unimer concentration far from the micelle. By comparing Equations (6.5.10) and (6.5.14) we find

$$D_{\mathrm{K}} \, (M) = 4\pi D_1 \, R c_1 \, , \tag{6.5.15}$$

where c_1 is the macroscopic unimer concentration and $R(M)$ is an effective unimer capture radius for a micelle of size M.

Taken literally, the above approximations obviously ignore the existence of barriers for the adsorption or desorption of unimers. The effects of these local barriers can be mimicked, however, by choosing the effective capture radius R to be somewhat smaller than would otherwise be appropriate. If R is interpreted as the micelle core radius and, that of the junction point between A and B blocks, ignores the fact that unimers can be irreversibly "captured" by a micelle when the end of the core block wanders sufficiently far into the core. The capture radius R should thus be understood to be an effective radius of encapsulation, and one that discards the details of how unimers move in the proximity of the micelle.

6.5.3 Characteristic Timescales

In order to connect this formalism to experiment, it is convenient to express the association and dissociation rates in terms of two corresponding timescales $\tau_{\rm d}$ and $\tau_{\rm a}$. They are defined as

$$\tau_{\rm d} = \frac{1}{R_{\rm d}}, \qquad \tau_{\rm a} = \frac{c_1}{M_{\rm e}\, R_{\rm a}}. \tag{6.5.16}$$

The association time $\tau_{\rm a}$ is interpreted as the time it takes the current unimer concentration c_1 to be consumed into micelles if the current micelle creation rate continues. $\tau_{\rm d}$ is simply the micelle dissociation lifetime, and it is independent of the unimer concentration and equilibrium micelle size. By combining the above definitions with definition (6.1.10) of the experimental CMC, it follows that $\tau_{\rm d}$ and $\tau_{\rm a}$ must be equal at the CMC (though for this to be the case, CMC must be chosen to satisfy $\Delta G_{\rm e} = 0$ at the CMC).

The kinetic theory thus yields the timescales

$$\tau_{\rm d} = \tau_{\rm d0}\, e^{\Delta G_{\rm d}\,(c_1\,)/{\rm k}T}, \quad \tau_{\rm a} = \tau_{\rm a0}\, e^{\Delta G_{\rm a}\,(c_1\,)/{\rm k}T}, \tag{6.5.17}$$

with prefactors

$$\tau_{\rm d0} = \frac{\sigma_{\rm a}\,\sigma_{\rm e}}{2D_1\, R c_1}, \tag{6.5.18}$$

$$\tau_{\rm a0} = \frac{\sigma_{\rm a}}{2\sqrt{2\pi} D_1\, R M_{\rm e}\, c_{\rm m}^0}. \tag{6.5.19}$$

Here, D_1 is the tracer diffusivity of a unimer in the solvent, R is the micelle radius,

defined as an effective micellar "capture" radius of a copolymer in the Smoluchowski theory for diffusion controlled reactions. The widths σ_{e} and σ_{a} are dispersions of the equilibrium micelle distribution and the barrier. Specifically, σ_{a} is the width of the peak in the function $\exp(\Delta G\,(M)/\mathrm{k}T\,)$ near the maximum in $\Delta G\,(M)$ at $M = M_{\mathrm{a}}$.

The explicit dependence of the above expression for $\tau_{\mathrm{a}0}$ upon the standard state concentration c_{m}^{0} is a result of the fact that R_{a} is inversely proportional to the number concentration $c_{\mathrm{m}}\,(M_{\mathrm{a}}\,) = c_{\mathrm{m}}^{0}\,\exp(-\Delta G_{\mathrm{a}}\,(c_1\,)/\mathrm{k}T\,)$ of micelles of size M_{a} , expressed in terms of c_{m}^{0} . If the convention (6.1.11) is adopted for c_{m}^{0} , so that the CMC corresponds exactly to the concentration c_{c} at which $\Delta G_{\mathrm{e}} = 0$, then

$$\tau_{\mathrm{a}0} = \frac{\sigma_{\mathrm{a}}\,\sigma_{\mathrm{e}}}{2D_1\,Rc_{\mathrm{c}}}, \tag{6.5.20}$$

where σ_{e} is the equilibrium polydispersity at the CMC, and c_{c} is the experimental CMC. With this convention, it is clear that τ_{a} and τ_{d} are indeed equal at the CMC.

The fact that the prefactor $\tau_{\mathrm{a}0}$ does not depend upon the unimer concentration c_1, while $\tau_{\mathrm{d}0}$ does, is a result of the way that τ_{a} is defined: the prefactors of the underlying rates R_{a} and R_{d} are both proportional to c_1 , but the timescale $\tau_{\mathrm{a}} = c_1\,/M_{\mathrm{e}}\,R_{\mathrm{a}}$ is that required to consume all of the available unimers into an aggregate, resulting in a rate independent of c_1 .

The result for how τ_{d} depends on c_1 , D_1 and R appears to be consistent with the conclusions of Nyrkova and Semenov,[184] though this similarity is obscured by a superficial difference. Nyrkova and Semenov introduced the notion of an entropic barrier representing the cost of adding and removing a unimer from a micelle. By their arguments, the free energy cost of localizing a free surfactant in a volume of

roughly the micelle size R^3, necessary to insert it into a micelle, results in adding an additional free energy

$$\Delta G = -\mathrm{k}T\ \ln(c_1\, R^3) \tag{6.5.21}$$

to the barriers $\Delta G_{\mathrm{a}}\,(c_1\,)$ and $\Delta G_{\mathrm{d}}\,(c_1\,)$. This is given in their equation (32). Nyrkova and Semenov's discussion of this barrier stated explicitly that they were being careless about what volume should multiply c_1 inside the logarithm, but their reasoning makes it clear that this factor should be order the micelle volume R^3, as derived in Equation (6.5.21). This additional free energy resulted in a characteristic time $\tau_0 = R^2/D_1\, M_{\mathrm{e}}$, in their equation (26), one that is also independent of c_1. Combining Nyrkova and Semenov's definition of τ_0, including this entropic barrier results in an expression for τ_{d} and τ_{a} with the same dependence on D_1, c_1, and R as that obtained here.

In a system with large barriers to association and dissociation, the amount of time it takes to establish a partial equilibrium distribution of micelle sizes is roughly

$$\tau_e \sim \frac{\sigma_e^2}{D_{\mathrm{K}}} \sim \frac{\sigma_e^2}{D_1\, c_1\, R}. \tag{6.5.22}$$

This is the time required for an aggregate with an aggregation number M to diffusively explore a range of values with width σ_e. This is always comparable to the prefactor $\tau_{\mathrm{d}0}$ in the expression for τ_{d}, without the exponential term. Near the CMC, the time to establish local equilibrium is thus always much shorter than τ_{d} or τ_{a}.

Here, we would like to estimate a "typical" order of magnitude for the prefactors $\tau_{\mathrm{d}0}$ and $\tau_{\mathrm{a}0}$ for a diblock copolymer near the CMC in a polymeric matrix. This

is difficult for polymeric systems because both D_1 and c_c can vary enormously for different polymers. The diffusivities of hydrocarbon polymers of modest molecular weight ($M \sim 10^4 - 10^5$) at temperatures well away from the glass transition often fall with a wide range $D_1 \sim 10^{-13} - 10^{-9}$ cm^2/sec. The CMC can, of course, vary even more, and can also become astronomically small. To obtain a simple estimate for comparison, consider a system with a relatively high CMC of $c_c = c_1 = 10^{+17}$ cm^{-3}, which corresponds surfactant volume fraction of 10^{-3} for a diblock copolymer with $N = 10^2$ and a monomer reference volume of $v = 100\text{Å}^3$. Using typical values of $M \simeq 200$, $\sigma_e \simeq 20$, $\sigma_a \simeq 10$ and $R = 10$ nm, one then obtains a range of values

$$\tau_{d0} \simeq 10^{-4} - 10^{0} \text{ sec} \tag{6.5.23}$$

at the CMC for systems with $D_1 \sim 10^{-13} - 10^{-9}$ cm^2/sec. Because τ_{d0} varies inversely with concentration, however, this timescale can become many orders of magnitude larger for strongly amphiphilic surfactants.

The estimate given in Equation (6.5.23) suggests that it may be difficult to find diblock copolymer system that can reach true equilibrium at the CMC. The lower end of the above range would allow for micelle dissociation at timescales somewhat less than the typical experimental time of order 10^4 seconds (a few hours), but only if the barrier for micelle formation at the CMC is less than about $10\,kT$. This estimate also suggests that it would be relatively easy to find model systems that can establish partial equilibrium via unimer exchange. In the next section, we present estimates of timescales for polymeric surfactants in a polymeric matrix as well as for polymeric surfactants in a small molecule solvent.

6.6 Estimates of Timescales

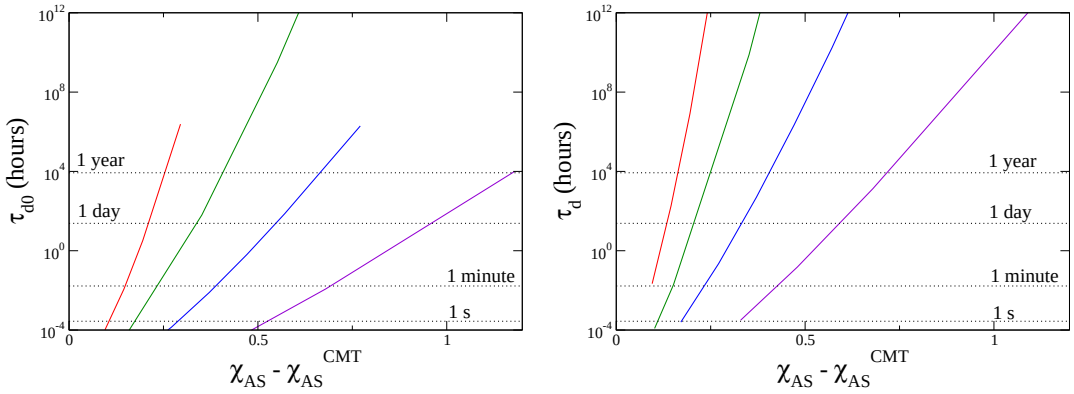

Figure 6.21: Plot of variation of the prefactor for dissociation timescale τ_{d0} (plot (a)) and dissociation timescale τ_d (plot (b)) relative to solvent selectivity χ_{AS} normalized relative to its' value at critical micelle temperature(CMT) for AB/S. A crew-cut spherical micelle (f_B =0.35) is considered for various chain lengths N of AB with $\chi_{BS} = 0.4$ and χ_{AB} $N = 20$. The color scheme used here is: violet for $N = 50$, blue for $N = 100$, green for $N = 200$, and red for $N = 400$.

Once we have the information regarding barriers to association and dissociation at the CMC, we can then estimate the rates of these processes using the theory for kinetics presented earlier. The rate of dissociation R_d for a system under thermodynamic equilibrium, which will have a unimer concentration of $c_1 = c_c$, is derived as $R_d = R_{d0} \exp(-\Delta G_c)$. The timescale for dissociation is given by $\tau_d = R_d^{-1}$, where $\tau_{d0} = R_{d0}^{-1}$ with τ_{d0} representing the prefactor for the dissociation timescale τ_d . It was earlier presented in Equation (6.5.18) that τ_{d0} is a function of c_1 which in the case of thermodynamic equilibrium is given by $c_1 = c_c$. This yields the expression $\tau_{d0} = \sigma_a \sigma_e / (2 D_1 R c_c)$, where σ_a and σ_e are the widths of the equilibrium micelle distribution and of the barrier. Using typical values of $\sigma_a = 10$, $\sigma_e = 20$, $R = 10$ nm,

and using c_c values obtained for each value of χ_{AS} for different degrees of polymerization of AB we arrive at the variation of τ_{d0} which is presented in Figure 6.21(a) for AB in small molecule solvent S. Similar calculation for the a polymeric solvent B is presented in Figure 6.22. Typical values of tracer diffusivity used are $D_1 \sim 10^{-7}\,\mathrm{cm^2 s^{-1}}$ for small molecule solvents[176] and $D_1 \sim 10^{-10}\mathrm{cm^2 s^{-1}}$ for the polymeric solvents.[194,195]

Once the prefactors of the dissociation rate have been calculated we can directly calculate the timescale of dissociation $\tau_d = R_d^{-1}$ which is related to τ_{d0} and ΔG_c through the relation $\tau_d = \tau_{d0} \exp(\Delta G_c)$ for $c_1 = c_c$, or thermodynamic equilibrium. The sensitivity of ΔG_c to the solvent size is found to be high as seen from Figures 6.8 and 6.16 presented earlier. The timescales required for dissociation for a typical diblock copolymer in a polymeric solvent is much higher than the timescales required for a diblock copolymer AB in S. The tracer diffusivity is taken as $D_1 \sim 10^{-7}\mathrm{cm^2 s^{-1}}$ for S, which is true for most of the small molecule solvents however, it can be as low as $D_1 \sim 10^{-12}\,\mathrm{cm^2 s^{-1}}$ in some cases.[176] The disparate behavior of ΔG_c as well as lower tracer diffusivity of diblock copolymer in a polymeric matrix, which is taken as $D_1 \sim 10^{-10}\,\mathrm{cm^2 s^{-1}}$ for AB in B, leads to much longer timescales for AB/B system than in the AB/S system.

To analyze which one of the two, the prefactor τ_{d0} or the barrier ΔG_c, drives the change in timescale of dissociation relative to χ_{AS} for small molecule solvent S we study the plots of τ_{d0} (see Figure 6.21 (a)) and τ_d (see Figure 6.21 (b)). The contribution of τ_{d0} and $\exp(\Delta G_c)$ are found to be of the same order of magnitude from these plots. This implies that the timescales are driven equally by solubility of diblock copolymer in the solution as well as the barriers to form or dissolve a micelle.

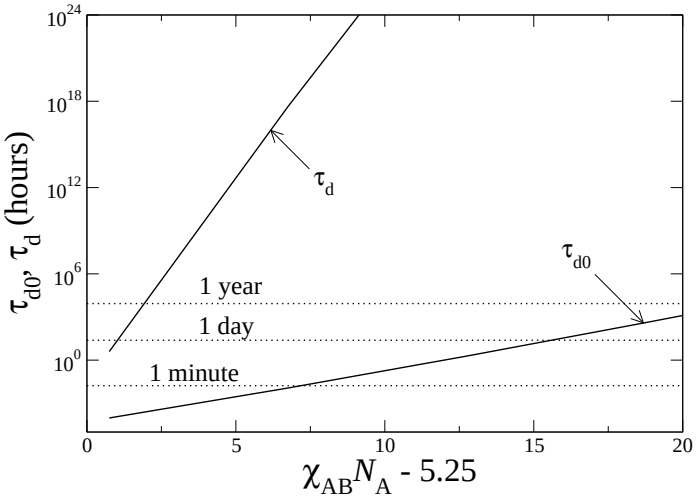

Figure 6.22: Plot of variation of the prefactor for dissociation timescale τ_{d0} and dissociation timescale τ_d relative to $\chi_{AB}\,N_A$ normalized relative to its' value at ODT for AB/B. The case of polymeric solvent B with $N = N_B = 200$ is considered here.

Another way to interpret the behavior if a diblock copolymer has significant solubility in a particular small molecule solvent this will automatically lead to small barriers to formation or dissolution of micelles.

A similar analysis for the case of polymeric solvent, presented in Figure 6.22, yields a different conclusion. We found the dissociation timescale τ_d to be dominated by the value of exp(ΔG_c), as τ_{d0} is at least an order of magnitude lower than exp(ΔG_c). Hence, in the case of the polymeric solvent ΔG_c is found to drive the exponential increase in timescales. The presence of partially equilibrated systems is a distinct possibility for the case of polymeric solvent.

6.7 Conclusions

SCFT calculations are used to predict barriers for micelle association and dissociation for a diblock AB in a small molecule solvent as well as in a polymeric solvent. The calculations yield large barriers to micelle association and dissociation at the CMC for both kind of solvents away from the CMT in the case of small molecule selective solvents or away from the ODT in the case of AB in a B homopolymer matrix.

The barrier for association and dissociation is found to increase rapidly as one increases the size of the solvent relative to the size of the diblock copolymer AB. The radial profiles close to the CMT and ODT, for the case of polymeric solvent B, point that the solvent penetration goes down due to larger size of the solvent, and in essence the micelles are found to have a larger core size as well. This thereby increases the cost of the interfacial free energy and thus, contributing to disparate free energy barriers for these two systems.

Typical values of timescales for the dissociation process using the stepwise growth mechanism are presented at the CMC. The dissociation timescale is a function of the CMC and ΔG_{c} . Once again disparate sizes of solvents considered here describe distinct behaviors. For the small molecule solvent case, c_{c} , which is directly proportional to τ_{d0} , and ΔG_{c} , which contributes to τ_{d} through $\exp(\Delta G_{\mathrm{c}})$, are found to have similar order of magnitude contributions to the dissociation timescales. Whereas, in the case of polymeric matrix it is found that the timescale is mainly driven by the value of ΔG_{c} . This leads us to hypothesize existence of parameter regimes where partially equilibrated system for a polymeric solvent can be observed.

Gibbs nucleation theory as well as SST are used to make quantitative comparisons

to SCFT predictions. Analytic theory helps us put in perspective different contributions to the free energy made by core stretching, corona stretching, and the cost of interface. The free energy of formation for micelles of smaller size are found to be dominated mainly by the free energy contribution of the interface.

In the case of diblock copolymer AB in a small molecule selective solvent S, barriers are also calculated for two kinds of spherical micelles one with a majority of the solvent-philic block $f_{\mathrm{B}} = 0.60$ and the other a minority of the solvent-philic block with $f_{\mathrm{B}} = 0.35$. Various chain lengths for these two block compositions as well as various values of interaction parameter χ_{BS} are considered. The order of magnitude of the barriers at CMC for both block compositions are similar however, the slope of the barriers at the CMC for hairy micelle with $f_{\mathrm{B}} = 0.60$ is found to be lower than that of the crew-cut micelle with $f_{\mathrm{B}} = 0.35$ for the same block copolymer degree of polymerization N. The barriers at the CMC are also found to go down as one decreases the value of χ_{BS} for the hairy micelle as well as the crew-cut micelle.

Even though SCFT predicts large barriers at the CMC one can influence the barrier height by varying the unimer concentration. The barriers to form or dissolve a micelle are found to be extremely sensitive to c_1. We can drive down the dissolution barrier by decreasing c_1 below c_{c} whereas, in order to drive down the barrier to form a micelle we have to increase c_1 above c_{c}. The sensitivity to unimer concentration is particularly striking in the case of dissociation, irrespective of the system being AB in homopolymer B or AB in small molecule solvent S. Polymeric micelles can dissociate rapidly if the unimer concentration c_1 drops below an apparent dissociation concentration c_{d} that, in the parameter regime studied here, is generally only a few

tens of percent below the CMC. To contrast, the behavior of barriers at the CMC is found to be very sensitive to the ratio of block copolymer size to the solvent size whereas c_{d} is found to be independent of this ratio. Independent of the magnitude of ΔG_{c} , the apparent concentration c_{a} is found to exceed the CMC by few orders of magnitude.

CHAPTER 7

Summary

We have studied the driving forces behind aggregate assembly in a blend of diblock copolymers AB, consisting of a solvent-philic block (B) and a solvent-phobic block (A), in a solvent S. Structural assembly in this blend is largely propelled by the selective incompatibility of the solvent, which prefers to associate with the B-block and isolate the the A-blocks into aggregates. The aggregate morphologies which result are determined by a balance of the molecular structure of the copolymer and its overall content in the blend. We have analyzed the phase behavior and micellization kinetics of this system using self-consistent field theory (SCFT). In this chapter we summarize some of the critical insights obtained from this study.

Chapter 3, described the two formulations of SCFT essential for a full investigation

of the phase behavior of the binary AB/S blend. Notably, the unbinding transitions first reported for blends of AB in homopolymer B by Matsen[33] are also observed in this analogous system of AB in S as well. By analyzing results from the real space implementation of SCFT and the pseudo-spectral implementation of SCFT we have independently verified that the ordered phases can be studied with a high degree of numerical accuracy even for low volume fractions of diblock copolymer AB in solvent S. The numerical accuracy of the pseudo-spectral formulation of SCFT used in this study is found to have very similar rate of convergence as the spectral formulation with Anderson mixing developed by Matsen.[1]

In Chapter 4 we investigated different micelle geometries subject to the solvent selectivity χ_{AS} and good solvent characteristic χ_{BS} for a wide range of block compositions. The sequence of morphologies: bilayers $\rightarrow$ cylindrical micelles $\rightarrow$ spherical micelles is found to occur with an increasing corona block composition (B), and this agrees well with previous experimental and theoretical studies. Some thermodynamic properties of AB/S have also been determined. The first is the critical aggregation concentration which is notably found to have a weaker dependence on χ_{AS} and core block length N_{A} than that of polymeric blends which scale as $\phi^{\mathrm{CAC}} \sim \exp(-\chi_{\mathrm{AS}} N_{\mathrm{A}})$. This behavior is ultimately a result of ample solvent penetration in the micellar cores. A larger CAC is required in this blend for the moderately selective solvents studied here. Secondly, we found a minimum threshold χ_{AS} (CMT) in order for isolated aggregate formation. From this, a simple estimation for the CMT using SCFT was developed. This estimation of the CMT offers a quick and reliable method, and is a novel use of SCFT. The value of CMT is also found to be largely dependent on the

core block length alone. The radius of the core and the aggregation number both approach zero as χ_{AS} approaches the CMT. Whereas, the core is well segregated, or it has significant amount of core block present in the core.

Chapter 5 is dedicated to the phase behavior of the binary blend for the phase cube of χ_{AS} , block composition f_B , and volume fraction of the diblock ϕ_{AB} . The order-order transition lines of the periodic phases were found to swell to isolated aggregate morphologies in the dilute limit. Some periodic phases, those with a core of solvent-philic block (B), could not swell indefinitely. In these cases, dilution causes macrophase separation, and coexistence with a solvent rich phase. We also observe a small pocket of ordered phases close to the critical point of the blend which typically separates into a solvent-rich homogeneous macrophase and polymer rich homogeneous macrophase. This is an altogether novel, but expected, feature in the phase portraits for AB/S. We also notice some fairly significant coexistence regimes between spherically ordered and hexagonally ordered mesophases, which have a core rich in solvent-phobic block (A). We also employ SCFT to investigate a phase portrait determined by Lodge and coworkers[3] for PS-PI in DBP and found semi-quantitative agreement for this blend. Deviations might be explained by the inability to obtain accurate interaction parameters, but also by the neglect of fluctuations in SCFT, which may be particularly significant close to the order-disorder transitions.

The interplay between the spherically ordered phases $S_A^{FCC}$and $S_A^{BCC}$with their spherical micellar counterparts is studied with two different formulations of SCFT. The aggregation numbers of individual spherical aggregates are found to be almost indistinguishable on FCC and BCC lattices. They are both, however, found to differ

from those of isolated spherical micelles. This is a striking observation. FCC and and BCC lattices have different lattice parameters and coordination numbers, but the aggregates on these lattices are indistinguishable. Pair-wise interactions between these spherical aggregates are determined, and they are found to be similar for both lattices. These pair-wise interactions could be utilized in Monte-Carlo simulations, because of their lattice independence. More realistic models of interactions between spherical micelles may be possible with these aggregate interactions. We also notice the transition between $S_A^{FCC}$and S_A^{BCC}which occurs close to the point where the spherical aggregates grow to fill the interstitial space on the FCC lattice. We thus predict the transformation from $S_A^{FCC} \rightarrow S_A^{BCC}$to be driven by the concentration of AB surfactant in the system. A further increase in the concentration of the copolymer AB condenses the aggregates onto an FCC lattice.

The barriers for micelle association and dissociation for the same diblock copolymer AB and small molecule solvent blend are predicted in Chapter 6. Polymeric solvents are also considered. Our principal conclusion in this investigation is that solutions containing polymeric micelles of hydrocarbon polymers are rarely, if ever, able to reach thermodynamic equilibrium, except close to the CMT or ODT, and should generally not exhibit a reversible micellization transition. This is notable, because of a possible explanation for the relatively constant aggregation number found over a wide temperature range, except close to the CMT for SEP diblocks in squalene as studied by Choi, Bates, and Lodge.[196] Consider the case of SI diblocks in DEP,[52] where the authors found the aggregation number to decrease as the system approaches it's CMT over a wide temperature range. The barrier also increases rapidly as one

increases the size of the solvent relative to the size of the diblock copolymer AB. Radial profiles close to the CMT and ODT indicate that, for the case of a polymeric solvent B, core solvent penetration goes down with a larger solvent size. Micelles are also found to have a larger core size as well for these solvents. This increases the interfacial free energy cost and contributes to the disparate free energies of small and large solvent blends. This effect of interfacial tension dominating the kinetics was studied by Lund and coworkers,[157–160] in PEP-PEO water/DMF mixtures, and they found that increasing the interfacial tension led to frozen micellar systems.

Even though SCFT predicts some remarkably large barriers at the CMC, one can influence the barrier height by varying the free surfactant concentration. The barriers to form or dissolve a micelle are extremely sensitive to the free surfactant concentration c_1 . This sensitivity is particularly striking in the case of dissociation, irrespective of the system the AB surfactant being in a homopolymer B matrix or a small solvent S. Zhang and Eisenberg[153] have observed morphological transformations in PS-PAA dioxane/water mixtures even in highly segregated mixtures which had greater free surfactant content.

Surfactants in a polymeric matrix have a dissociation timescale, that is very long, driven by the substantial kinetic barriers. This leads us to expect a parameter regime that describes a partially equilibrated system, but only for a polymeric solvent, and not the small molecule solvent. Partial equilibrium is a state where we expect the distribution of of micelle sizes to change by unimer exchange, but at a fixed total number concentration of micelles.

We have considered different states of aggregation in the dilute regime under

equilibrium conditions earlier in Chapter 4. The analysis of micellization kinetics presented here for spherical micelles can clearly be extended to other aggregate structures of cylinders and bilayers using similar methods. This is a research direction which could be pursued in future.

Bibliography

[1] Matsen, M. W., 2009. Fast and accurate SCFT calculations for periodic block-copolymer morphologies using the spectral method with Anderson mixing. *The European physical journal. E, Soft matter* 30:361–9.

[2] Lodge, T. P., C. Pan, X. Jin, Z. Liu, J. Zhao, W. W. Maurer, and F. S. Bates, 1995. Failure of the dilution approximation in block copolymer solutions. *Journal of Polymer Science Part B: Polymer Physics* 33:2289–2293.

[3] Lodge, T. P., B. Pudil, and K. J. Hanley, 2002. The Full Phase Behavior for Block Copolymers in Solvents of Varying Selectivity. *Macromolecules* 35:4707–4717.

[4] Sadron, C., and B. Gallot, 1973. Heterophases in block-copolymer/solvent systems in the liquid and in the solid state. *Die Makromolekulare Chemie* 164:301–332.

[5] Gast, A. P., 1997. Polymeric micelles. *Current Opinion in Colloid & Interface Science* 2:258–263.

[6] Allen, C., D. Maysinger, and A. Eisenberg, 1999. Nano-engineering block copolymer aggregates for drug delivery. *Colloids and Surfaces B: Biointerfaces* 16:3–27.

[7] Fredrickson, G. H., V. Ganesan, and F. Drolet, 2002. Field-Theoretic Computer Simulation Methods for Polymers and Complex Fluids. *Macromolecules* 35:16–39.

[8] Lodge, T. P., 2003. Block Copolymers: Past Successes and Future Challenges. *Macromolecular Chemistry and Physics* 204:265–273.

[9] Riess, G., 2003. Micellization of block copolymers. *Progress in Polymer Science* 28:1107–1170.

[10] Gohy, J.-f., 2005. Block Copolymer Micelles. *Advances in Polymer Science* 190:65–136.

[11] Binder, K., B. Mognetti, W. Paul, P. Virnau, and L. Yelash, 2011. Computer Simulations and Coarse-Grained Molecular Models Predicting the Equation of State of Polymer Solutions. *Advances in Polymer Science* 238:329–387.

[12] Binder, K., M. Müller, and R. L. C. Vink, 2011. Phase Behavior of Polymer-Containing Systems: Recent Advances Through Computer Simulation. *Macromolecular Theory and Simulations* 20:600–613.

[13] Borisov, O. V., E. B. Zhulina, F. A. M. Leermakers, and A. H. E. Müller, 2011. Self-Assembled Structures of Amphiphilic Ionic Block Copolymers : Theory , Self-Consistent Field Modeling and Experiment. *Advances in Polymer Science* 241:57–129.

[14] Nagarajan, R., 2011. Amphiphilic Surfactants and Amphiphilic Polymers : Principles of Molecular Assembly. American Chemical Society.

[15] Moughton, A. O., M. a. Hillmyer, and T. P. Lodge, 2012. Multicompartment Block Polymer Micelles. *Macromolecules* 45:2–19.

[16] Shibayama, M., T. Hashimoto, H. Hasegawa, and H. Kawai, 1983. Ordered structure in block polymer solutions. 3. concentration dependence of microdomains in nonselective solvents. *Macromolecules* 16:1427–1433.

[17] Molau, G. E., 1970. Block Copolymers. Plenum Press.

[18] Fredrickson, F. S. B. . G. H., 1990. Block copolymer thermodynamics: Theory and experiment. *Annu. Rev. Phys. Chem.* 41:525–557.

[19] Helfand, E., and Y. Tagami, 1972. Theory of the interface between immiscible polymers. ii. *Journal of Chemical Physics* 56:3592–3601.

[20] Helfand, E., and Z. R. Wasserman, 1976. Approximation, Block Copolymer Theory. 4. Narrow Interphase. *Macromolecules* 9:879–888.

[21] Helfand, E., and Z. R. Wasserman, 1978. Block copolymer theory. 5. spherical domains. *Macromolecules* 11:960–966.

[22] Leibler, L., 1980. Theory of microphase separation in block copolymers. *Macromolecules* 13:1602–1617.

[23] de Gennes, P.-G., 1979. Scaling concepts in polymer physics. CORNELL UNIVERSITY PRESS.

[24] Lifeng Zhang and Adi Eisenberg, 1995. Multiple Morphologies of "Crew-Cut" Aggregates of Polystyrene-b-poly (acrylic acid) Block Copolymers. *Science* 268:1728–1731.

[25] Bates, S. J. F. S., 2003. On the origins of morphological complexity in aqueous dispersions of block copolymer surfactants. *Science* 300:460–464.

[26] Hongwei Shen and, A. E., 2000. Block Length Dependence of Morphological Phase Diagrams of the Ternary System of PS-b-PAA/Dioxane/H2O. *Macromolecules* 33:2561–2572.

[27] Choucair, A., and A. Eisenberg, 2003. Control of amphiphilic block copolymer morphologies using solution conditions. *European Physical Journal E – Soft Matter* 10:37 – 44.

[28] Leibler, L., H. Orland, and J. C. Wheeler, 1983. Theory of critical micelle concentration for solutions of block copolymers. *The Journal of Chemical Physics* 79:3550.

[29] Whitmore, M. D., and J. Noolandi, 1985. Theory of Micelle Formation in Block Copolymer-Homopolymer Blends. *Macromolecules* 18:657–665.

[30] Noolandi, J., and K. M. Hong, 1983. Theory of block copolymer micelles in solution. *Macromolecules* 16:1443–1448.

[31] Mayes, A. M., and M. Olvera de la Cruz, 1988. Cylindrical versus spherical micelle formation in block copolymer/homopolymer blends. *Macromolecules* 21:2543–2547.

[32] Hurter, P. N., J. M. H. M. Scheutjens, and T. A. Hatton, 1993. Molecular modeling of micelle formation and solubilization in block copolymer micelles. 1. a self-consistent mean-field lattice theory. *Macromolecules* 26:5592–5601.

[33] Matsen, M., 1995. Phase behavior of block copolymer/homopolymer blends. *Macromolecules* 28:5765–5773.

[34] Janert, P., and M. Schick, 1997. Phase behavior of ternary homopolymer/diblock blends: Influence of relative chain lengths. *Macromolecules* 30:137–144.

[35] Janert, P., and M. Schick, 1998. Phase behavior of binary homopolymer/diblock blends: Temperature and chain length dependence. *Macromolecules* 31:1109–1113.

[36] Greenall, M. J., D. M. a. Buzza, and T. C. B. McLeish, 2009. Micelle shape transitions in block copolymer/homopolymer blends: comparison of self-consistent field theory with experiment. *The Journal of chemical physics* 131:34904.

[37] Leibler, L., 1988. Emulsifying effects of block copolymers in incompatible polymer blends. *Makromol. Chem., Macromol. Symp.* 16:1.

[38] Munch, M. R., and A. P. Gast, 1988. Block copolymers at interfaces. 1. Micelle formation. *Macromolecules* 21:1360–1366.

[39] Greenall, M. J., D. M. a. Buzza, and T. C. B. McLeish, 2009. Micelle Formation in Block Copolymer/Homopolymer Blends: Comparison of Self-Consistent Field Theory with Experiment and Scaling Theory. *Macromolecules* 42:5873–5880.

[40] Helfand, E., and Y. Tagami, 1971. Theory of the interface between immiscible polymers. *Journal of Polymer Science Part B: Polymer Letters* 9:741–746.

[41] Semenov, A. N., 1985. Contribution to the Theory of Microphase Layering in Block-Copolymer Melts. *Soviet Physics JETP* 61:733–742.

[42] Daoud, M., and J. P. Cotton, 1982. Star shaped polymers : a model for the conformation and its concentration dependence. *Journal Physique* 43:531–538.

[43] Selb, J., P. Marie, A. Rameau, R. Duplessix, and Y. Gallot, 1983. Study of the structure of block copolymer-homopolymer blends using small angle neutron scattering. *Polymer Bulletin* 10:444–451.

[44] Hong, K. M., and J. Noolandi, 1981. Theory of Inhomogeneous Multicomponent Polymer Systems. *Macromolecules* 14:727–736.

[45] Pletsil, J., and J. Baldrian, 1975. Determination of the Structure Parameters of Styrene / Butadiene Block Copolymer in Heptane by Means of Small-Angle X-Ray Scattering. *Die Makromolekulare Chemie* 176:1009–1028.

[46] Mortensen, K., and J. S. Pedersen, 1993. Structural Study on the Micelle Formation of Poly(ethy1ene oxide)-Poly(propy1ene oxide)-Poly(ethy1ene oxide) Triblock Copolymer in Aqueous Solution. *Macromolecules* 26:805–812.

[47] Goldmints, I., F. K. V. Gottberg, K. A. Smith, and T. A. Hatton, 1997. Small-Angle Neutron Scattering Study of PEO-PPO-PEO Micelle Structure in the Unimer-to-Micelle Transition Region. *Langmuir* 13:3659–3664.

[48] Goldmints, I., G.-e. Yu, C. Booth, K. A. Smith, and T. A. Hatton, 1999. Structure of (Deuterated PEO) - (PPO) - (Deuterated PEO) Block Copolymer Micelles As Determined by Small Angle Neutron Scattering. *Langmuir* 15:1651–1656.

[49] Yang, L., P. Alexandridis, D. C. Steytler, M. J. Kositza, and J. F. Holzwarth, 2000. Small-Angle Neutron Scattering Investigation of the Temperature-Dependent Aggregation Behavior of the Block Copolymer Pluronic L64 in Aqueous Solution. *Langmuir* 16:8555–8561.

[50] Alexandridis, P., and L. Yang, 2000. SANS Investigation of Polyether Block Copolymer Micelle Structure in Mixed Solvents of Water and Formamide , Ethanol , or Glycerol. *Macromolecules* 33:5574–5587.

[51] Alexandridis, P., and L. Yang, 2000. Micellization of Polyoxyalkylene Block Copolymers in Formamide. *Macromolecules* 33:3382–3391.

[52] Bang, J., K. Viswanathan, T. P. Lodge, M. J. Park, and K. Char, 2004. Temperature-dependent micellar structures in poly(styrene-b-isoprene) diblock copolymer solutions near the critical micelle temperature. *The Journal of chemical physics* 121:11489–500.

[53] LaRue, I., M. Adam, E. B. Zhulina, M. Rubinstein, M. Pitsikalis, N. Hadjichristidis, D. A. Ivanov, R. I. Gearba, D. V. Anokhin, and S. S. Sheiko, 2008. Effect of the Soluble Block Size on Spherical Diblock Copolymer Micelles. *Macromolecules* 41:6555–6563.

[54] Nagarajan, R., and K. Ganesh, 1989. Block copolymer self-assembly in selective solvents: Spherical micelles with segregated cores. *The Journal of Chemical Physics* 90:5843.

[55] Halperin, A., 1987. Polymeric Micelles: A Star Model. *Macromolecules* 20:2943–2946.

[56] Birshtein, T. M., and E. B. Zhulina, 1989. Scaling theory of supermolecular structures in block copolymer-solvent systems: 1. Model of micellar structures. *Polymer* 30:170–177.

[57] Zhulina, E. B., M. Adam, I. LaRue, S. S. Sheiko, and M. Rubinstein, 2005. Diblock Copolymer Micelles in a Dilute Solution. *Macromolecules* 38:5330–5351.

[58] Lund, R., V. Pipich, L. Willner, A. Radulescu, J. Colmenero, and D. Richter, 2011. Structural and thermodynamic aspects of the cylinder-to-sphere transition in amphiphilic diblock copolymer micelles. *Soft Matter* 7:1491.

[59] Jensen, G. V., Q. Shi, G. R. Deen, K. Almdal, and J. S. Pedersen, 2012. Structures of PEP-PEO Block Copolymer Micelles: Effects of Changing Solvent and PEO Length and Comparison to a Thermodynamic Model. *Macromolecules* 45:430–440.

[60] Hiemenz, P. C., and T. P. Lodge, 2007. Polymer Chemistry. CRC Press.

[61] Leermakers, F. A. M., and J. M. H. M. Scheutjens, 1989. Statistical thermodynamics of association colloids. i. lipid bilayer membranes. *The Journal of Chemical Physics* 89:3264–3274.

[62] Leermakers, F. A. M., and J. M. H. M. Scheutjens, 1989. Statistical thermodynamics of association colloids . 2 . lipid vesicles. *Journal of Physical Chemistry* 93:7417–7426.

[63] Leermakers, F. A. M., and J. M. H. M. Scheutjens, 1989. Statistical thermodynamics of association colloids: V. critical micelle concentration, micellar size and shape. *Journal of Colloid and Interface Science* 136:231–241.

[64] Leermakers, M., C. M. Wijmans, and G. J. Fleer, 1995. On the structure of polymeric micelles: Self-consistent-field theory and universal properties for volume fraction profiles. *Polymer* 28:3434–3443.

[65] Scheutjens, J. M. H. M., and G. J. Fleer, 1979. Statistical theory of the adsorption of interacting chain molecules. 1. partition function, segment density distribution, and adsorption isotherms. *Journal of Physical Chemistry* 83:1619–1635.

[66] Linse, P., 1993. Phase Behavior of Poly(ethylene oxide)-Poly(propylene oxide) Block Copolymers in Aqueous Solution. *Journal of Physical Chemistry* 97:13896–13902.

[67] Linse, P., 1993. Micellization of Poly(ethylene oxide)-Poly(propylene oxide) Block Copolymers in Aqueous Solution. *Macromolecules* 26:4437–4449.

[68] Linse, P., and M. Malmsten, 1992. Temperature-Dependent Micellization in Aqueous Block Copolymer Solutions. *Macromolecules* 25:5434–5439.

[69] Hurter, P. N., J. M. H. M. Scheutjens, and T. A. Hatton, 1993. Molecular modeling of micelle formation and solubilization in block copolymer micelles. 2. lattice theory for monomers with internal degrees of freedom. *Macromolecules* 26:5030–5040.

[70] Kinning, D. J., E. L. Thomas, and L. J. Fetters, 1991. Morphological Studies of Micelle Formation in Block Copolymer / Homopolymer Blends. Comparison with Theory. *Macromolecules* 24:3893–3900.

[71] Zhou, J., and A.-C. Shi, 2011. Critical Micelle Concentration of Micelles with Different Geometries in Diblock Copolymer/Homopolymer Blends. *Macromolecular Theory and Simulations* 20:690–699.

[72] Yuan, X.-F., A. J. Masters, and C. Price, 1992. Self-consistent Field Theory of Micelle Formation by Block Copolymers. *Macromolecules* 25:6876–6884.

[73] Matsen, M., and F. Bates, 1996. Unifying weak- and strong-segregation block copolymer theories. *Macromolecules* 29:1091–1098.

[74] Fredrickson, G. H., and L. Leibler, 1989. Theory of block copolymer solutions: nonselective good solvents. *Macromolecules* 22:1238–1250.

[75] Fredrickson, G. H., and E. Helfand, 1987. Fluctuation effects in the theory of microphase separation in block copolymers. *The Journal of Chemical Physics* 87:697–705.

[76] de la Cruz, M., 1989. Theory of microphase separation in block copolymer solutions. *The Journal of Chemical Physics* 90:1995.

[77] Whitmore, M. D., and J. Noolandi, 1990. Self-consistent theory of block copolymer blends: Neutral solvent. *The Journal of Chemical Physics* 93:2946–2955.

[78] Banaszak, M., and M. D. Whitmore, 1992. Self-consistent theory of block copolymer blends: selective solvent. *Macromolecules* 25:3406–3412.

[79] Lodge, T., K. Hanley, B. Pudil, and V. Alahapperuma, 2003. Phase behavior of block copolymers in a neutral solvent. *Macromolecules* 36:816–822.

[80] Naughton, J., and M. Matsen, 2002. Limitations of the dilution approximation for concentrated block copolymer/solvent mixtures. *Macromolecules* 35:5688–5696.

[81] Noolandi, J., and K. M. Hong, 1982. Theory of polymeric alloys. *Polymer Bulletin* 7:561–566.

[82] Hong, K. M., and J. Noolandi, 1983. Theory of phase equilibriums in systems containing block copolymers. *Macromolecules* 16:1083–1093.

[83] Noolandi, J., A.-c. Shi, and P. Linse, 1996. Theory of Phase Behavior of Poly(oxyethylene)-Poly(oxypropylene)-Poly(oxyethylene) Triblock Copolymers in Aqueous Solutions. *Macromolecules* 29:5907–5919.

[84] Alexandridis, P., U. Olsson, and B. Lindman, 1995. Self-Assembly of Amphiphilic Block Copolymers. *Macromolecules* 28:7700–7710.

[85] Zhang, K., and A. Khan, 1995. Phase Behavior of Poly(ethylene oxide)-Poly(propy1ene oxide)-Poly(ethy1ene oxide) Triblock Copolymers in Water. *Macromolecules* 28:3807–3812.

[86] Linse, M. S. P. A. P., 1999. Phase behavior and microstructure in binary block copolymer/selective solvent systems: Experiments and theory. *Macromolecules* 32:637–645.

[87] Svensson, M., P. Alexandridis, and P. Linse, 1999. Modeling of the phase behavior in ternary triblock copolymer/water/oil systems. *Macromolecules* 32:5435–5443.

[88] Huang, C.-i., and T. P. Lodge, 1998. Self-Consistent Calculations of Block Copolymer Solution Phase Behavior. *Macromolecules* 31:3556–3565.

[89] Hanley, K. J., T. P. Lodge, and C.-I. Huang, 2000. Phase Behavior of a Block Copolymer in Solvents of Varying Selectivity. *Macromolecules* 33:5918–5931.

[90] Tongchuan Suo; Dadong Yan; Shuang Yang and An-Chang Shi, 2009. A theoretical study of phase behaviors for diblock copolymers in selective solvents. *Macromolecules* 42:6791–6798.

[91] Bang, J., S. Jain, Z. Li, T. Lodge, J. Pedersen, E. Kesselman, and Y. Talmon, 2006. Sphere, cylinder, and vesicle nanoaggregates in poly(styrene-b-isoprene) diblock copolymer solutions. *Macromolecules* 39:1199–1208.

[92] Zhang, L., and A. Eisenberg, 1996. Multiple morphologies and characteristics of "crew-cut" micelle-like aggregates of polystyrene-b-poly(acrylic acid) diblock copolymers in aqueous solutions. *Journal of the American Chemical Society* 118:3168–3181.

[93] Hongwei Shen and, A. E., 1999. Morphological Phase Diagram for a Ternary System of Block Copolymer PS310-b-PAA52/Dioxane/H2O. *The Journal of Physical Chemistry B* 103:9473–9487.

[94] Won, Y., H. T. Davis, and F. S. Bates, 1999. Giant Wormlike Rubber Micelles. *Science* 283:960–963.

[95] Bates, Y.-Y. W. A. K. B. H. T. D. F. S., 2002. Cryogenic transmission electron microscopy (cryo-tem) of micelles and vesicles formed in water by poly(ethylene oxide)-based block copolymers. *J. Phys. Chem. B* 106:3354–3364.

[96] Jain, S., X. Gong, L. E. Scriven, and F. S. Bates, 2006. Disordered network state in hydrated block-copolymer surfactants. *Physical Review Letters* 96:138304.

[97] LaRue, I., M. Adam, M. Silva, S. S. Sheiko, and M. Rubinstein, 2004. Wormlike Micelles of Block Copolymers : Measuring the Linear Density by AFM and Light Scattering. *Macromolecules* 37:5002–5005.

[98] Khougaz, K., X. F. Zhong, and A. Eisenberg, 1996. Aggregation and Critical Micelle Concentrations of Polystyrene-b-poly (sodium acrylate) and Polystyrene-b-poly (acrylic acid) Micelles in Organic Media. *Macromolecules* 29:3937–3949.

[99] Kelarakis, A., V. Havredaki, G.-e. Yu, L. Derici, and C. Booth, 1998. Temperature Dependences of the Critical Micelle Concentrations of Diblock Oxyethylene/Oxybutylene Copolymers. A Case of Athermal Micellization. *Macromolecules* 31:944–946.

[100] Crothers, M., D. Attwood, J. H. Collett, M. Manchester, Z. Yang, C. Booth, P. Taboada, V. Mosquera, N. M. P. S. Ricardo, and L. G. A. Martini, 2002. Micellization and Gelation of Diblock Copolymers of Ethylene Oxide and Styrene Oxide in Aqueous Solution. *Langmuir* 18:8685–8691.

[101] Booth, C., D. Attwood, and C. Price, 2006. Self-association of block copoly(oxyalkylene)s in aqueous solution. Effects of composition, block length and block architecture. *Physical chemistry chemical physics* 8:3612–22.

[102] Attwood, D., C. Booth, S. G. Yeates, C. Chaibundit, and N. M. P. S. Ricardo, 2007. Block copolymers for drug solubilisation: relative hydrophobicities of polyether and polyester micelle-core-forming blocks. *International journal of pharmaceutics* 345:35–41.

[103] Cambón, A., M. Alatorre-Meda, J. Juárez, A. Topete, D. Mistry, D. Attwood, S. Barbosa, P. Taboada, and V. Mosquera, 2011. Micellisation of triblock copolymers of ethylene oxide and 1,2-butylene oxide: effect of B-block length. *Journal of colloid and interface science* 361:154–158.

[104] Astafieva, I., X. F. Zhong, and A. Eisenberg, 1993. Critical micellization phenomena in block polyelectrolyte solutions. *Macromolecules* 26:7339–7352.

[105] Khougaz, K., Z. Gao, and A. Eisenberg, 1994. Determination of the Critical Micelle Concentration of Block Copolymer Micelles by Static Light Scattering. *Macromolecules* 27:6341–6346.

[106] Moffitt, M., K. Khougaz, and A. Eisenberg, 1996. Micellization of Ionic Block Copolymers. *Accounts of Chemical Research* 29:95–102.

[107] Michelle, M. M., R. Thiagarajan, D. C. Morse, and T. P. Lodge, 2012. Apparent Critical Micelle Concentrations (CMCs) in Block Copolymer/Ionic Liquid Systems: Remarkably Weak Dependence on Solvophobic Block Molecular Weight. *Macromolecules* .

[108] Nace, V. M., 1996. Nonionic Surfactant Series: Polyoxyalkylene Block Copolymers. Dekker, USA.

[109] Chu, B., 1996. Structure and Dynamics of Block Copolymer Colloids. *Langmuir* 11:414–421.

[110] Shibayama, M., T. Hashimoto, and H. Kawai, 1983. Ordered structure in block polymer solutions. 1. selective solvents. *Macromolecules* 16:16–28.

[111] Hashimoto, T., M. Shibayama, H. Kawai, H. Watanabe, and T. Kotaka, 1983. Ordered structure in block polymer solutions. 2. its effect on rheological behavior. *Macromolecules* 16:361–371.

[112] Hashimoto, T., M. Shibayama, and H. Kawai, 1983. Ordered structure in block polymer solutions. 4. scaling rules on size of fluctuations with block molecular weight, concentration, and temperature in segregation and homogeneous regimes. *Macromolecules* 16:1093–1101.

[113] Shibayama, M., T. Hashimoto, and H. Kawai, 1983. Ordered structure in block polymer solutions. 5. equilibrium and nonequilibrium aspects of microdomain formation. *Macromolecules* 16:1434–1443.

[114] Mori, K., H. Hasegawa, and T. Hashimoto, 1990. Ordered structure in block polymer solutions: 6. possible non-equilibrium effects on growth of self-assembling structures. *Polymer* 31:2368–2376.

[115] Noolandi, J., and K. M. Hong, 1980. Theory of inhomogeneous polymers in presence of solvent. *Ferroelectrics* 30:117–123.

[116] Hashimoto, T., M. Shibayama, and H. Kawai, 1980. Domain-boundary structure of styrene-isoprene block copolymer films cast from solution. 4. molecular-weight dependence of lamellar microdomains. *Macromolecules* 13:1237–1247.

[117] Hanley, K. J., and T. P. Lodge, 1998. Effect of dilution on a block copolymer in the complex phase window. *Journal of Polymer Science Part B: Polymer Physics* 36:3101–3113.

[118] Wanka, G., H. Hoffmann, and W. Ulbricht, 1994. Phase Diagrams and Aggregation Behavior of Poly (oxyethylene)-Poly (oxypropylene) -Poly(oxyet hylene) Triblock Copolymers in Aqueous Solutions. *Macromolecules* 27:4145–4159.

[119] Alexandridis, P., D. Zhou, and A. Khan, 1996. Lyotropic liquid crystallinity in amphiphilic block copolymers: Temperature effects on phase behavior and structure for poly(ethylene oxide)-b-poly(propylene oxide)-b-poly(ethylene oxide) copolymers of different composition. *Langmuir* 12:2690–2700.

[120] Alexandridis, P., 1998. Structural Polymorphism of Poly(ethylene oxide)-Poly(propylene oxide) Block Copolymers in Nonaqueous Polar Solvents. *Macromolecules* 31:6935–6942.

[121] Hajduk, D. A., M. B. Kossuth, M. A. Hillmyer, and F. S. Bates, 1998. Complex phase behavior in aqueous solutions of poly(ethylene oxide)-poly(ethylethylene) block copolymers. *J. Phys. Chem. B* 102:4269–4276.

[122] Jain, S., and F. Bates, 2004. Consequences of nonergodicity in aqueous binary peo-pb micellar dispersions. *Macromolecules* 37:1511–1523.

[123] Balsara, N. P., D. Perahia, C. R. Safinya, M. Tirrell, and T. P. Lodge, 1992. Birefringence detection of the order-to-disorder transition in block copolymer liquids. *Macromolecules* 25:3896–3901.

[124] He, Y., Z. Li, P. Simone, and T. P. Lodge, 2006. Self-assembly of block copolymer micelles in an ionic liquid. *Journal of the American Chemical Society* 128:2745–50.

[125] Simone, P. M., and T. P. Lodge, 2008. Lyotropic Phase Behavior of PolybutadienePoly(ethylene oxide) Diblock Copolymers in Ionic Liquids. *Macromolecules* 41:1753–1759.

[126] Simone, P. M., and T. P. Lodge, 2009. Phase behavior and ionic conductivity of concentrated solutions of polystyrene-poly(ethylene oxide) diblock copolymers in an ionic liquid. *ACS applied materials & interfaces* 1:2812–2820.

[127] Virgili, J. M., A. Hexemer, J. a. Pople, N. P. Balsara, and R. a. Segalman, 2009. Phase Behavior of Polystyrene- block -poly(2-vinylpyridine) Copolymers in a Selective Ionic Liquid Solvent. *Macromolecules* 42:4604–4613.

[128] Virgili, J. M., M. L. Hoarfrost, and R. a. Segalman, 2010. Effect of an Ionic Liquid Solvent on the Phase Behavior of Block Copolymers. *Macromolecules* 43:5417–5423.

[129] Virgili, J. M., A. J. Nedoma, R. a. Segalman, and N. P. Balsara, 2010. Ionic Liquid Distribution in Ordered Block Copolymer Solutions. *Macromolecules* 43:3750–3756.

[130] Seddon, K. R., 1997. Ionic Liquids for Clean Technology. *Journal of Chemical Technology & Biotechnology* 68:351–356.

[131] McConnell, G. A., A. P. Gast, J. S. Huang, and S. D. Smith, 1993. Disorder-order transitions in soft sphere polymer micelles. *Phys. Rev. Lett.* 71:2102–2105.

[132] McConnell, G. A., E. K. Lin, A. P. Gast, J. S. Huang, M. Y. Lin, and S. D. Smith, 1994. Structure and interactions in tethered-chain systems. *Faraday Discussions* 98:121.

[133] Gast, A. P., 1996. Structure, Interactions, and Dynamics in Tethered Chain Systems. *Langmuir* 12:4060–4067.

[134] McConnell, G. A., and A. P. Gast, 1996. Predicting disorder-order phase transitions in polymeric micelles. *Physical review. E, Statistical physics, plasmas, fluids, and related interdisciplinary topics* 54:5447–5455.

[135] McConnell, G., and A. Gast, 1997. Melting of ordered arrays and shape transitions in highly concentrated diblock copolymer solutions. *Macromolecules* 30:435–444.

[136] Pople, J. A., I. W. Hamley, J. P. A. Fairclough, A. J. Ryan, B. U. Komanschek, A. J. Gleeson, G.-E. Yu, and C. Booth, 1997. Ordered Phases in Aqueous Solutions of Diblock Oxyethylene / Oxybutylene Copolymers Investigated by Simultaneous Small-Angle X-ray Scattering and Rheology. *Macromolecules* 30:5721–5728.

[137] Hamley, I. W., J. A. Pople, and O. Diat, 1998. A thermally induced transition from a body-centred to a face-centred cubic lattice in a diblock copolymer gel. *Colloid & Polymer Science* 276:446–450.

[138] Hamley, I. W., C. Daniel, W. Mingvanish, S.-m. Mai, C. Booth, L. Messe, and A. J. Ryan, 2000. From Hard Spheres to Soft Spheres : The Effect of Copolymer Composition on the Structure of Micellar Cubic Phases Formed by Diblock Copolymers in Aqueous Solution. *Langmuir* 16:2508–2514.

[139] Bang, J., T. P. Lodge, X. Wang, K. L. Brinker, and W. R. Burghardt, 2002. Thermoreversible, epitaxial $fcc \leftrightarrow bcc$ transitions in block copolymer solutions. *Phys. Rev. Lett.* 89:215505.

[140] Lodge, T. P., J. Bang, M. J. Park, and K. Char, 2004. Origin of the thermoreversible fcc-bcc transition in block copolymer solutions. *Phys. Rev. Lett.* 92:145501.

[141] Bang, J., and T. P. Lodge, 2004. Long-lived metastable bcc phase during ordering of micelles. *Phys. Rev. Lett.* 93:245701.

[142] Grason, G. M., 2007. Ordered phases of diblock copolymers in selective solvent. *The Journal of chemical physics* 126:114904.

[143] Likos, C. N., H. Löwen, M. Watzlawek, B. Abbas, O. Jucknischke, J. Allgaier, and D. Richter, 1998. Star Polymers Viewed as Ultrasoft Colloidal Particles. *Physical Review Letters* 80:4450–4453.

[144] Bednar, B., K. Edwards, M. Almgren, S. Tormod, and Z. Tuzar, 1988. Rates of association and dissociation of block copolymer micelles: Light-scattering stopped-flow measurements. *Makromolecular Chemistry, Rapid Communication* 9:785–790.

[145] Prochazka, K., B. Bednar, E. Mukhtar, P. Svoboda, J. Trnena, and M. Almgren, 1991. Nonradiative energy transfer studies of block copolymers in selective solvents. *Journal of Physical Chemistry* 95:4563–4568.

[146] Hecht, E., and H. Hoffmann, 1995. Kinetic and calorimetric investigations on micelle formation of block copolymers of the poloxamer type. *Colloids and Surfaces A* 96:181–197.

[147] Ge, Z., Y. Cai, J. Yin, Z. Zhu, J. Rao, and S. Liu, 2007. Synthesis and "schizophrenic" micellization of double hydrophilic AB4 miktoarm star and AB diblock copolymers: structure and kinetics of micellization. *Langmuir* 23:1114–22.

[148] Zhang, Y., T. Wu, and S. Liu, 2007. Micellization Kinetics of a Novel Multi-Responsive Double Hydrophilic Diblock Copolymer Studied by Stopped-Flow pH and Temperature Jump. *Macromolecular Chemistry and Physics* 208:2492–2501.

[149] Wang, Y., C. M. Kausch, M. Chun, R. P. Quirk, and W. L. Mattice, 1995. Exchange of Chains between Micelles of Labeled Polystyrene-block-poly (oxyethy1ene) As Monitored by Nonradiative Singlet Energy Transfer. *Macromolecules* 28:904–911.

[150] Michels, B., G. Waton, and R. Zana, 1997. Dynamics of Micelles of Poly (ethylene oxide) -Poly (propylene oxide) -Poly (ethylene oxide) Block Copolymers in Aqueous Solutions. *Langmuir* 13:3111–3118.

[151] Alexandridis, P., J. F. Holzwarth, and T. A. Hatton, 1994. Micellization of Poly (ethy1ene oxide) -Poly (propy1ene oxide) -Poly (ethy1ene oxide)

Triblock Copolymers in Aqueous Solutions : Thermodynamics of Copolymer Association. *Macromolecules* 27:2414–2425.

[152] Chen, L., H. Shen, and A. Eisenberg, 1999. Kinetics and Mechanism of the Rod-to-Vesicle Transition of Block Copolymer Aggregates in Dilute Solution. *The Journal of Physical Chemistry B* 103:9488–9497.

[153] Zhang, L., and A. Eisenberg, 1999. Thermodynamic vs Kinetic Aspects in the Formation and Morphological Transitions of Crew-Cut Aggregates Produced by Self-Assembly of Polystyrene-b-poly (acrylic acid) Block Copolymers in Dilute Solution. *Macromolecules* 32:2239–2249.

[154] Meli, L., and T. P. Lodge, 2009. Equilibrium vs metastability: High-temperature annealing of spherical block copolymer micelles in an ionic liquid. *Macromolecules* 42:580–583.

[155] Meli, L., J. M. Santiago, and T. P. Lodge, 2010. Path-dependent morphology and relaxation kinetics of highly amphiphilic dilbock copolymer micelles in ionic liquids. *Macromolecules* 43:2018–2027.

[156] Willner, L., A. Poppe, J. Alligaier, M. Monkenbusch, and D. Richter, 2001. Time-resolved SANS for the determination of unimer exchange kinetics in block copolymer micelles Time-resolved SANS for the determination of unimer exchange kinetics in block copolymer micelles. *Europhysics Letters* 55:667–673.

[157] Lund, R., L. Willner, J. Stellbrink, P. Lindner, and D. Richter, 2006. Logarithmic Chain-Exchange Kinetics of Diblock Copolymer Micelles. *Physical Review Letters* 96:1–4.

[158] Lund, R., L. Willner, D. Richter, and E. E. Dormidontova, 2006. Equilibrium Chain Exchange Kinetics of Diblock Copolymer Micelles: Tuning and Logarithmic Relaxation. *Macromolecules* 39:4566–4575.

[159] Lund, R., L. Willner, D. Richter, H. Iatrou, N. Hadjichristidis, and P. Lindner, 2007. Unraveling the equilibrium chain exchange kinetics of polymeric micelles using small-angle neutron scattering - architectural and topological effects. *Journal of Applied Crystallography* 40:327–331.

[160] Lund, R., L. Willner, M. Monkenbusch, P. Panine, T. Narayanan, J. Colmenero, and D. Richter, 2009. Structural observation and kinetic pathway in the formation of polymeric micelles. *Phys. Rev. Lett.* 102:188301.

[161] Iyama, K., and T. Nose, 1998. Kinetics of Micelle Formation with Change of Micelle Shape in a Dilute Solution of Diblock Copolymers. *Macromolecules* 31:7356–7364.

[162] Tyler, C. A., 2005. Linear elasticity and phase behavior of block copolymer melts by self consistent field theory. Ph.D. thesis, University of Minnesota.

[163] Tyler, C. A., and D. C. Morse, 2003. Stress in self-consistent-field theory. *Macromolecules* 36:8184–8188.

[164] Qin, J., 2009. Studies of Block Copolymer Melts by Field Theory and Molecular Simulation. Ph.D. thesis, University of Minnesota.

[165] Matsen, M. W., and M. Schick, 1994. Stable and unstable phases of a diblock copolymer melt. *Phys. Rev. Lett.* 72:2660–2663.

[166] Rasmussen, K. A., and G. Kalosakas, 2002. Improved numerical algorithm for exploring block copolymer mesophases. *Journal of Polymer Science Part B: Polymer Physics* 40:1777–1783.

[167] Chang, K., and D. Morse, 2006. Diblock copolymer surfactants in immiscible homopolymer blends: Interfacial bending elasticity. *Macromolecules* 39:7397–7406.

[168] Chang, K., and D. C. Morse, 2006. Diblock Copolymer Surfactants in Immiscible Homopolymer Blends: Swollen Micelles and Interfacial Tension. *Macromolecules* 39:7746–7756.

[169] Cochran, E. W., D. C. Morse, and F. S. Bates, 2003. Design of ABC Triblock Copolymers near the ODT with the Random Phase Approximation. *Macromolecules* 36:782–792.

[170] Milner, S. T., M.-d. Lacasse, and W. W. Graessley, 2009. Why Is Seldom Zero for Polymer-Solvent Mixtures. *Macromolecules* 42:876–886.

[171] Bahadur, P., N. V. Sastry, M. S, and G. Riess, 1985. Micellar behaviour of styreneisoprene block copolymers in selective solvents. *Colloids and Surfaces* 16:337–346.

[172] Won, Y.-y., H. T. Davis, F. S. Bates, M. Agamalian, and G. D. Wignall, 2000. Segment Distribution of the Micellar Brushes of Poly(ethylene oxide) via Small-Angle Neutron Scattering. *The Journal of Physical Chemistry B* 104:7134–7143.

[173] Garetz, B. a., M. C. Newstein, H. J. Dai, S. V. Jonnalagadda, and N. P. Balsara, 1993. Birefringence and diffraction of light in ordered block copolymer materials. *Macromolecules* 26:3151–3155.

[174] Forster, S., A. K. Khandpur, J. Zhao, F. S. Bates, I. W. Hamley, and A. J. Ryan, 1994. Complex Phase Behavior of Polyisporene-Polystyrene Diblock Copolymers Near the Order-Disorder Transition. *Macromolecules* 27:6922–6935.

[175] Lin, C. C., S. V. Jonnalagadda, P. K. Kesani, H. J. Dai, and N. P. Balsara, 1994. Effect of Molecular Structure on the Thermodynamics of Block Copolymer Melts. *Macromolecules* 27:7769–7780.

[176] Brandrup, J., E. H. Immergut, E. A. Grulke, A. Abe, and D. R. Bloch, 2005. Polymer Handbook. John Wiley & Sons.

[177] Hanley, K. J., 2001. Block Copolymers : Phase Behavior in Neutral and Selective solvents. Ph.D. thesis, University of Minnesota.

[178] Israelachvili, J., 1991. Intermolecular & Surface Forces. Academic Press, USA.

[179] Wennerström, H., and L. Björn, 1979. MICELLES. PHYSICAL CHEMISTRY SURFACTANT ASSOCIATION OF. *Physics Reports* 52:1–86.

[180] Won, Y., H. Davis, and F. Bates, 2003. Molecular exchange in PEO-PB micelles in water. *Macromolecules* 36:953–955.

[181] Aniansson, E. A. G., and S. N. Wall, 1974. Kinetics of step-wise micelle association. *The Journal of Physical Chemistry* 78:1024–1030.

[182] Aniansson, E. A. G., S. N. Wall, M. Almgren, H. Hoffmann, K. I., U. W., Z. R., J. Lang, and C. Tondre, 1976. Theory of the kinetics of micellar equilibria and quantitative interpretation of chemical relaxation studies of micellar solutions of ionic surfactants. *The Journal of Physical Chemistry* 80:905–922.

[183] Halperin, A., and S. Alexander, 1989. Polymeric micelles: Their relaxation kinetics. *Macromolecules* 22:2403–2412.

[184] Nyrkova, I. A., and A. N. Semenov, 2005. On the theory of micellization kinetics. *Macromolecular Theory and Simulations* 14:569–585.

[185] Semenov, A. N., 1992. Theory of diblock-copolymer segregation to the interface and free surface of a homopolymer layer. *Macromolecules* 25:4967–4977.

[186] Halilolu, T., and W. L. Mattice, 1994. Lattice Simulation of the Interchange of Chains between Micelles of Diblock Copolymers. *Chemical Engineering Science* 49:2851–2857.

[187] Halilolu, T., I. Bahar, B. Erman, and W. L. Mattice, 1996. Mechanisms of the Exchange of Diblock Copolymers between Micelles at Dynamic Equilibrium. *Macromolecules* 29:4764–4771.

[188] Dormidontova, E. E., 1999. Micellization kinetics in block copolymer solutions: Scaling model. *Macromolecules* 32:7630–7644.

[189] Pool, R., and P. Bolhuis, 2006. Prediction of an autocatalytic replication mechanism for micelle formation. *Physical Review Letters* 97:018302.

[190] Wood, S., and Z.-G. Wang, 2002. Nucleation in binary polymer blends: A self-consistent field study. *The Journal of Chemical Physics* 116:2289.

[191] Wang, M., Jiafang. Mueller, and Z.-G. Wang, 2009. Nucleation in A/B/AB blends: Interplay between microphase assembly and macrophase separation. *The Journal of Chemical Physics* 130:154902.

[192] Wang, J., Z.-G. Wang, and Y. Yang, 2005. Nature of Disordered Micelles in Sphere-Forming Block Copolymer Melts. *Macromolecules* 38:1979.

[193] Kramers, H. A., 1940. Brownian motion in a field of force and the diffusion model of chemical reactions. *Physica* 7:284 – 304.

[194] Cavicchi, K. a., and T. P. Lodge, 2003. Self-Diffusion and Tracer Diffusion in Sphere-Forming Block Copolymers. *Macromolecules* 36:7158–7164.

[195] Chang, K., 2005. Block Copolymer Surfactants in Immiscible Polymer Blends. Ph.D. thesis, University of Minnesota.

[196] Choi, S.-H., F. S. Bates, and T. P. Lodge, 2009. Structure of poly(styrene-b-ethylene-alt-propylene) diblock copolymer micelles in squalane. *The journal of physical chemistry. B* 113:13840–13848.